

# **Investigation of the actin-membrane interaction at the leading edge and its influence on membrane diffusion**

Ireen König

This thesis is submitted to the University of Glasgow towards the degree of Doctor of Philosophy

Faculty of Medicine  
Division of Cancer Sciences and Molecular Pathology

Thesis work performed at:  
The Beaton Institute for Cancer Research  
Glasgow, G61 1BD

October 2009

## Abstract

Actin polymerisation is a highly dynamic process which drives many cellular events, including endocytosis and cell motility. It is known that actin monomers are added to the filaments at the leading edge of a migrating cell and that this polymerisation is the driving force of protrusion. Much is known about the activation and regulation of this dynamic actin remodelling, but many questions about the exact nature of the interaction between the actin filaments and the plasma membrane remain. Weisswange et al (Weisswange et al., 2005) found that the leading edge of protruding fish keratocytes functions as a diffusion barrier for lipid dyes.

The aim of the here presented thesis was to continue this project and to study the actin-membrane interaction at the leading edge, using the diffusion barrier as an initial read-out method. First it was investigated whether this diffusion barrier is present in other cell types and could therefore be seen as a general feature of protrusion. Using Fluorescence Recovery After Photo-bleaching (FRAP) in B16 F1 cells, it could be shown that the diffusion of membrane anchored GFP (GFP-F) is significantly inhibited at the leading edge compared to lamellar regions. No reduction in diffusion could be observed after destruction of the actin meshwork or at non-protruding sites of the lamellipodial periphery, showing that the diffusion barrier depends on active protrusion. The diffusion of cytoplasmic GFP was not altered near the leading edge compared to in the lamellipodium, indicating that only membrane bound proteins are affected. After showing that the diffusion barrier is a general feature of protrusion, the exact nature of the actin-membrane interaction causing this phenomenon was investigated. No direct interaction between actin and the membrane could be observed using FLIM-FRET, but FRAP experiments on fixed cells and a correlation between the strength of the diffusion barrier with the speed of protrusion indicate that the reason for the reduction in diffusion around the leading edge is the force created by the actin filaments pushing against the membrane. Further FRAP experiments indicate that actin regulating proteins such as IRSp53 are influenced by the restricted diffusion zone at the leading edge. We propose that the lipid diffusion barrier traps regulatory proteins at the leading edge and can therefore be seen as a positive feedback mechanism for actin polymerisation.

## Table of contents

Abstract.....	2
Table of Content.....	3
List of Figures.....	5
List of accompanying material.....	7
Acknowledgement.....	8
Author's declaration.....	9
Abbreviations.....	10
<b>1 Introduction .....</b>	<b>11</b>
1.1 Cell motility .....	11
1.1.1 Actin-based cell motility .....	12
1.1.1.1 model systems.....	15
1.1.1.2 Regulation of actin polymerisation at the leading edge.....	21
1.1.1.3 Force production through actin-polymerisation .....	33
1.2 Membrane diffusion .....	40
1.2.1 Lipid rafts.....	41
1.2.2 Membrane fence models .....	43
1.2.3 Examples of diffusion barriers .....	45
1.2.3.1 Tight junctions in epithelial cells .....	45
1.2.3.2 Axon Initial segment in Neurons.....	46
1.2.3.3 diffusion barrier at the leading edge of fish keratocytes .....	47
1.2.3.4 Other examples of diffusion barriers .....	52
1.3 A brief introduction into imaging methods relevant for this thesis .....	53
1.3.1 History and types of microscopy .....	53
1.3.2 Total Internal Reflection Fluorescence Microscopy.....	58
1.3.3 Fluorescence Recovery after Photobleaching.....	64
1.3.4 FLIM-FRET.....	67
1.4 Aims .....	71
<b>2 Methods and Materials.....</b>	<b>72</b>
2.1 Cells.....	72
2.1.1 B16 F1 .....	72
2.1.2 Fish keratocytes .....	74
2.1.3 Dictyostelium discoideum.....	77
2.2 Plasmids .....	78
2.3 Drugs .....	79
2.4 Other techniques .....	80
2.5 Solutions.....	85
<b>3 Evaluation of fish keratocytes as a model system .....</b>	<b>87</b>
3.1 Fish comparison .....	87
3.1.1 Fish keratocytes preparation .....	87
3.1.2 Keratocytes quality .....	89
3.2 Protein expression in fish keratocytes .....	90
3.3 Summary and conclusions .....	94

<b>4</b>	<b>The diffusion barrier at the leading edge is a universal feature of protrusion .....</b>	<b>96</b>
4.1	FLOID.....	96
4.2	Photo-bleaching and Photo-activation in TIRF .....	100
4.3	FRAP of membrane probes .....	104
4.3.1	FRAP acquisition and analysis .....	104
4.3.2	FRAP of Dil labelled fish keratocytes.....	110
4.3.3	FRAP of Dil labelled B16 F1 cells.....	113
4.3.4	FRAP of GFP-F transfected B16 F1 cells .....	116
4.3.4.1	FRAP of cytoplasmic GFP in B16 cells .....	121
4.4	Summary and conclusions .....	122
<b>5</b>	<b>Investigations into the physical basis of the leading edge lipid diffusion barrier.....</b>	<b>124</b>
5.1	FRAP approaches.....	125
5.1.1	Influence of the speed of protrusion on the leading edge diffusion barrier	125
5.1.2	Membrane recovery in fixed cells .....	127
5.1.3	Membrane diffusion under “actin-waves” .....	130
5.2	FLIM-FRET approaches .....	133
5.2.1	Influences on lifetime measurements.....	134
5.2.1.1	Fluorophore environment.....	134
5.2.1.2	Photo-bleaching.....	136
5.2.2	Interaction between actin and the plasma membrane.....	137
5.2.3	Investigation of the involvement of actin regulating proteins in linking the actin to the membrane .....	139
5.3	Summary .....	148
<b>6</b>	<b>Consequence of the diffusion barrier for the actin polymerisation at the leading edge .....</b>	<b>149</b>
6.1	Localisation and diffusion of actin-regulating proteins.....	149
6.2	FRAP on IRSp53 mutants .....	154
6.3	FRAP on CP mutants .....	159
6.4	Summary and conclusions .....	162
<b>7</b>	<b>Summary and conclusions .....</b>	<b>165</b>
	References.....	168
	Appendices.....	178

## List of figures

Figure 1-1: the structure of an actin monomer and actin filament .....	13
Figure 1-2: actin tails .....	17
Figure 1-3: fish keratocytes .....	18
Figure 1-4: Dictyostelium discoideum .....	19
Figure 1-5: B16 F1 cell .....	21
Figure 1-6: dendritic nucleation treadmilling model .....	22
Figure 1-7: schematic structure of IRSp53 (isoform1) .....	28
Figure 1-8: F-actin- and PIP <sub>2</sub> -binding sites of the IMD domain. ....	32
Figure 1-9: actin-gel force generation theories.....	35
Figure 1-10: ratchet force models .....	36
Figure 1-11: The “Lock, Load & Fire” model.....	38
Figure 1-12: plasma-membrane structure and composition .....	41
Figure 1-13: “membrane skeleton” and “anchored-protein picket” fence models .....	44
Figure 1-14: Focal Labelling and Observation of Initial Diffusion (FLOID).....	48
Figure 1-15: FLOID analysis of migrating keratocytes.....	49
Figure 1-16: finite and infinity-corrected optical light paths .....	54
Figure 1-17: Fluorescence .....	55
Figure 1-18: epi-fluorescence, confocal and multi-photon .....	57
Figure 1-19: comparison between epi and evanescence wave illumination.....	59
Figure 1-20: TIRF techniques .....	60
Figure 1-21: schematical light-path setup of epi-fluorescence and TIRF.....	61
Figure 1-22: applications of the Beatson TIRF setup.....	62
Figure 1-23: TIRF test sample.....	63
Figure 1-24: FRAP recovery .....	64
Figure 1-25: FRAP analysis by Mullineaux method.....	66
Figure 1-26: Fluorescence Resonance Energy Transfer .....	67
Figure 1-27: fluorescence lifetime detection methods.....	69
Figure 1-28: application of the Beatson FLIM-TIRF .....	70
Figure 2-1: keratocytes preparation .....	75
Figure 3-1: growing fish keratocyte layer.....	88
Figure 3-2: size and leading edge comparison of fish keratocytes .....	90

Figure 3-3: transfection of fish keratocytes.....	92
Figure 3-4: microinjection of GFP-F and GFP-actin into zebra fish keratocytes .	93
Figure 4-1: Plasma membrane labelling of B16 cell using DiI C12 dye. ....	97
Figure 4-2: Analysis of dye spreading.....	99
Figure 4-3: photo-bleaching in TIRF .....	101
Figure 4-4: analysis of photo-activation in TIRF .....	102
Figure 4-5: positioning of the region for targeted bleaching (ROI).....	105
Figure 4-6: Mullineaux analysis.....	106
Figure 4-7: exponential curve fit analysis .....	107
Figure 4-8: FRAP on DiI labelled fish keratocytes .....	111
Figure 4-9: FRAP of DiI C12 labelled B16 F1 cells .....	114
Figure 4-10: FRAP of GFP-F transfected B16 F1 cells.....	117
Figure 4-11: FRAP positions .....	120
Figure 4-12: FRAP of GFP transfected B16 cells .....	121
Figure 5-1: protrusion rate influences lipid diffusion around the leading edge.	126
Figure 5-2: fixation of membrane probes.....	128
Figure 5-3: FRAP on fixed DiI C12 labelled fish keratocytes.....	129
Figure 5-4: membrane FRAP beneath a polymerising actin wave.....	131
Figure 5-5: Dictyostelium membrane FRAP corrections and results .....	132
Figure 5-6: environmental influence of GFP lifetime .....	135
Figure 5-7: effect of photo-bleaching on GFP lifetime .....	136
Figure 5-8: lifetime measurements, - shifts and their statistical significance..	138
Figure 5-9: FLIM results of IRSp53 and membrane.....	141
Figure 5-10: FLIM results of IRSp53-IMDmut and IRSp53- $\Delta$ SH3 and membrane .	144
Figure 5-11: FLIM results of CP and actin.....	147
Figure 6-1: localisation of actin regulating proteins .....	150
Figure 6-2: diffusion constants of actin regulating proteins.....	151
Figure 6-3: Localisation of wild-type and mutants GFP-IRSp53 .....	155
Figure 6-4: diffusion constants of GFP-IRSp53 wild-type and mutants.....	156
Figure 6-5: localisation of GFP fusion of wild-type CP and two mutations.....	159
Figure 6-6: diffusion rates of GFP-fusions of CP wild-type and mutants .....	160
Figure 7-1: model of the leading edge diffusion barrier.....	167

## List of accompanying material

- Publication list
- Fluorescence lifetime imaging: association of cortical actin with a PIP3-rich membrane compartment.  
König I, Schwarz JP, Anderson KI.  
Eur J Cell Biol. 2008 Sep;87(8-9):735-41. Epub 2008 Mar 28.
- The multi-FERM-domain-containing protein FrmA is required for turnover of paxillin-adhesion sites during cell migration of Dictyostelium.  
Patel H, König I, Tsujioka M, Frame MC, Anderson KI, Brunton VG.  
J Cell Sci. 2008 Apr 15;121(Pt 8):1159-64. Epub 2008 Mar 18.
- Neuropilin-1/GIPC1 signaling regulates alpha5beta1 integrin traffic and function in endothelial cells.  
Valdembri D, Caswell PT, Anderson KI, Schwarz JP, König I, Astanina E, Caccavari F, Norman JC, Humphries MJ, Bussolino F, Serini G.  
PLoS Biol. 2009 Jan 27;7(1):e25.
- MST kinases monitor actin cytoskeletal integrity and signal via JNK stress-activated kinase to regulate p21Waf1/Cip1 stability.  
Ruth Densham†, Eric O'Neill\*, June Munro, Ireen König, Kurt Anderson, Walter Kolch, Michael F. Olson\*  
Mol Cell Biol. 2009 Dec; 29(24):6380-90. Epub 2009 Oct 12.
- The actin bundling protein fascin stabilizes actin invadopodia and potentiates protrusive invasion.  
Ang Li, John C. Dawson, Manuel Forero, Heather J. Spence, Xinzi Yu, Ireen König, Kurt Anderson and Laura M. Machesky  
Current Biology, in press  
Abstract only

## Acknowledgements

First and foremost, I would like to thank my supervisor Kurt Anderson. He not only gave me the opportunity to come to the Beatson to undertake this PhD project and guided me through both the experimental and writing phases, but he also introduced me to the joys of microscopy, which will stay with me for a very long time.

I also want to thank my adviser Margaret Frame, as well as any other group leader at the Beatson who took some of their time to discuss my project.

Many thanks to all members of R19 and BAIR, as well as everyone else at the Beatson who not only helped me in my research but also made my time here a memorable experience.

Last, but in no means least, I want to thank my family for their support and encouragement throughout my studies. Special thanks to my brother Sten, who stood by me during the last weeks of finishing this thesis.

*I would like to dedicate this thesis to my grandfather, Lothar Hennig, as he was and is always highly interested in the progress of my work and even thinks about the research of his grandchildren during his daily newspaper read.*

*(Ich möchte diese Doktorarbeit meinem Grossvater Lothar Hennig widmen, da er immer hochinteressiert an meiner Arbeit war und ist und sogar beim täglichen Zeitungslernen an die Forschung seiner Enkel denkt.)*

## **Author's declaration**

I declare that this thesis represents my own work except where acknowledge to others. No part of this work has been submitted for consideration as part of any other degree.

## Abbreviations

ADP	<i>Adenosine diphosphate</i>
ATP	<i>Adenosine triphosphate</i>
ConA	<i>Concanavalin A</i>
CytD	<i>Cytochalasin D</i>
Dil	<i>1,1'-didodecyl-3,3,3',3'-tetramethylindocarbocyanine perchlorate</i>
DMEM	<i>Dulbecco's Modified Eagles Medium</i>
DMSO	<i>Dimethyl sulphoxide</i>
FLIM	<i>Fluorescence Lifetime Imaging Microscopy</i>
FRET	<i>Fluorescence Resonance Energy Transfer</i>
HEPES	<i>4-(2-hydroxyethyl)-1-piperazineethane-sulfonic acid</i>
kDa	<i>kilodalton</i>
KK2	<i>Phosphate buffer</i>
KRB	<i>Keratocytes running buffer</i>
LatA	<i>Latrunculin A</i>
PBS	<i>Phosphate buffered saline</i>
PMA	<i>Phorbol 13-myristate 12-acetate</i>
TIRF	<i>Total Internal Reflection Fluorescence</i>
WT	<i>Wild type</i>

# 1 Introduction

## 1.1 Cell motility

The ability to move is often considered one criterion for the definition of life. Single cell organisms mainly have to move in order to find food and although multicellular life forms such as mammalian organism have specialised limbs to move, their individual cells still have to migrate. Cell migration is important during embryonic development, immune response, wound healing and many more processes crucial to ensure the wellbeing of an organism. However, cell movement can also have negative consequences, as in the case of cancer. Cancer cells can detach from the primary tumour, migrate to and through blood or lymph vessels, leave the vessels and invade into new tissue to form metastases. As the formation of these secondary tumours is one of the main factors of cancer related death, preventing the migration of cancer cells would be a possible treatment to save many lives. In order to specifically stop cancer cells and not to affect migration of other cells within the patient's body, a detailed understanding of the exact mechanism of cell motility is crucial. Likewise, the study of cell movement could also benefit other medical areas, such as faster wound healing or directed immune response.

Many theories have been proposed over the years on how individual cells are able to move. Early explanations included limb-comparable organs, surface tension and Sol-Gel transformation (reviewed in:(De Bruyn, 1947)). Today, actin-based motility is a widely accepted mechanism used by many different cell types (see section 1.1.2). Other forms of cell movement, using an actin-independent mechanism are for example bacterial movements using flagella or cilia. As this thesis investigates the interaction between actin and the plasma membrane during actin-based cell motility, the term motility or movement will therefore always refer to an actin-based mechanism.

### **1.1.1 Actin-based cell motility**

The actin cytoskeleton is crucial for cell shape, stability and internal transport. A major part of this cytoskeletal meshwork is the 42-kDa ubiquitous protein actin. One specialised part of the actin cytoskeleton is the lamellipodium. This thin (around 150-200nm) cell extension is densely packed with actin filaments and spatially excludes other cell organelles and can be seen as the “organelle of motility” (Abercrombie et al., 1970b). The within this lamellipodium arranged actin filaments undergo dynamic polymerisations and depolymerisations. This rearrangement of the actin meshwork is the foundation of actin-based cell motility (see below). Actin-based motility in cells can be classified into three steps: protrusion, adhesion and retraction (Alberts et al., 2008, Small et al., 1996). Briefly, during protrusion parts of the cell spread into new areas; during adhesion these parts form contacts with the substrate and during retraction the cell body is shifted in the direction of movement along with the detachment of underlying older adhesions. The coordination between these processes influences the efficiency of cell migration. For example, slow detachment of the rear of the cell can antagonise the force created during protrusion and cells may adopt a “stop-and-go” motility. It may also occur that a cell forms protrusions in two opposing directions, resulting in very inefficient final displacement. This thesis project concentrates on protrusion and therefore only this first step of the actin-based cell motility will be discussed in more detail.

Today it is widely accepted that actin polymerisation drives cell protrusion (reviews: (Pollard, 2007, Le Clainche and Carlier, 2008)). But initially actin was found in connection with myosin, responsible for muscle contraction (review: (Szent-Gyorgyi, 2004)). The identification of the role of the polymerisation of thin actin filaments in protrusion was closely linked to advances in microscopy. Early evidence for a finer fibre network than the previously known stress-fibres was given by Buckley and Porter (Buckley and Porter, 1967). In 1969 the group of Howard Holtzer identified stressfibers and the thinner fibres as myosin binding structures and showed for the first time that actin is present in non-muscle cells (Ishikawa et al., 1969). Some years later, it was shown that protrusion depends on these thin actin filaments (Spooner et al., 1971). The termination of migration following Cytochalasin B treatment led the authors to the conclusion

that “the microfilament network is...indispensible for locomotion”. Models started to emerge on how this protein may be able to push a cell forward. In 1975, Tilney described two systems of motility; one based on the rapid polymerisation of actin and the second based on the rearrangement of actin filament packing (Tilney, 1975). Today, many different hypotheses on the mechanism of force production remain, some of which are explained in section 1.1.1.3.

The building block of actin filaments is the monomeric form of the 375aa protein: G-actin (Figure 1-1 left). It consists of 4 structural domains and shows a central cleft with a binding site for nucleotides (ATP, ADP). Binding of a nucleotide is crucial for the stability of the monomeric actin (Kasai et al., 1965, De La Cruz and Pollard, 1995).

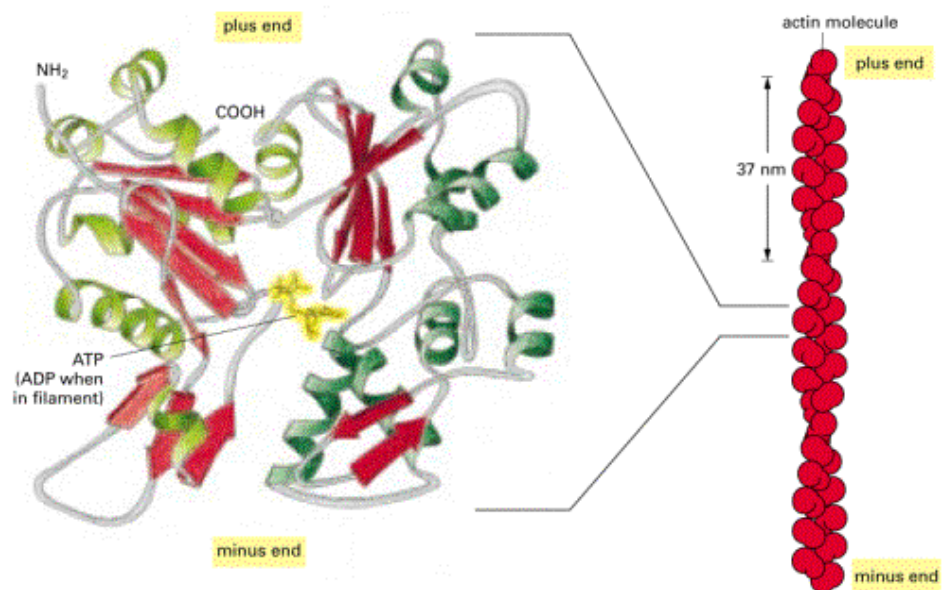


**Figure 1-1: the structure of an actin monomer and actin filament**

A nucleotide (either ATP or ADP) is bound within a cleft in the centre of an actin monomer (left). At the right is a schematic representation of an actin filament. Two strands are wound around each other with a twist every 37nm. The filament ends are biochemically different and are called + and – ends. (figure taken from Molecular Biology of the Cell, 4<sup>th</sup> edition)

Polymerisation starts when three G-actin molecules form an initial oligomer, which acts as the basis for further monomer addition. This nucleation step is the rate-limiting step in the formation of the actin filament (Alberts et al., 2008). As it happens very rarely and randomly, the cell possesses different proteins which can facilitate this process (actin nucleators) and which can be directed to

certain cellular locations (see section 1.1.1.2). Provided that monomer concentration is high enough, the further addition of monomers to the existing oligomer occurs rapidly (see below). The polymerisation of ATP-G-actin is accompanied by the hydrolysis of ATP to ADP+Pi, followed by the later release of the phosphate group. This change from ATP-actin to ADP-actin within the filament (“aging” of the filament) is responsible for a variation of the opposite ends of the filament and creates a polarity of the filament. The resulting two different ends are called +end (barbed) and -end (pointed). As the actin subunits on one end (the older end, -end) have ADP bound, whereas the subunits on the other end are bound to ATP, the two ends possess different biochemical behaviour. These differences are crucial for the directed polymerisation. If both ends were biochemically equal, they both would have the same probability of further monomer addition. This polymerisation ability depends on the concentration of free monomers. The minimal required concentration of G-actin to drive polymerisation is called critical concentration ( $c_{crit}$ ). If the real monomer concentration ( $c_{G-actin}$ ) is smaller than  $c_{crit}$ , the filament will depolymerise, if more actin monomers are present polymerisation occurs. Due to the biochemical differences between both filament ends, the critical monomer concentration needed to add G-actin is different on both ends. The critical concentration of ATP-G-actin is smaller at the +end compared to the -end ( $c_{crit(+)} < c_{crit(-)}$ ), meaning ATP-G-actin has a higher affinity for the +end and the addition of ATP-G-actin to the + end of the filaments is favoured (Pollard and Mooseker, 1981). Theoretically, if the free G-actin concentration,  $c_{G-actin}$ , is lower than both,  $c_{crit(+)}$  and  $c_{crit(-)}$ , depolymerisation will occur at both ends. Vica versa, if  $c_{G-actin}$  is higher than both critical concentrations, monomers will be polymerised to both filament ends. Practically (in vitro experiments as well as under physiological cell conditions), the concentration of ATP-G-actin ( $c_{G-actin}$ ) lies between the two critical concentrations:  $c_{crit(-)} > c_{G-actin} > c_{crit(+)}$ , which leads to polymerisation at the +ends and depolymerisation at the -ends (Kondo and Ishiwata, 1976). This process is called treadmilling. In a steady state, the rates of polymerisation and depolymerisation are equal and the overall length of the filament does not change. The completion of this process within cells requires the involvement of many other components and tight regulation, which is explained briefly in section 1.1.1.2.

One of the first indications that this treadmilling process occurs in the lamellipodium of migrating cells was the observation that the +ends of the actin filaments are directed towards the protruding (leading) edge of the cell and the -ends were located further behind (Small et al., 1978). Given this filament orientation, the treadmilling process would lead to the elongation of the filaments towards the leading edge membrane, possibly pushing this membrane outwards, forming protrusions. This treadmilling theory was further supported by direct observation of actin dynamics using fluorescently tagged actin (Bretscher, 1985). Microinjection of labelled actin led to a visible lamellipodial actin meshwork, allowing Yu-Li Wang to bleach a small area of this meshwork without interrupting its dynamics. He observed, that this bleached area moved towards the centre of the cell, leading to his conclusions that new unbleached actin monomers are predominantly incorporated at the membrane-associated end of actin filaments and that filament subunits are constantly moving backwards. Forscher and Smith (Forscher and Smith, 1988) provided further evidence for the treadmilling theory by observing actin recovery after Cytochalasin treatment. They used Cyt B to destroy an existing actin meshwork in growth cones and observed, that a new lamellar actin structure started growing from the cell edge after washout of the drug. Nowadays the treadmilling mechanism in lamellipodia is widely accepted: actin monomers are added to filaments at the leading edge and depolymerised at the rear of the lamellipodium.

### **1.1.1.1 model systems**

There are many model systems used in the study of actin-based motility and their suitability often depends on the chosen experimental setup or the investigated question. Some model systems are briefly introduced below, including the ones which have been used in this thesis to study the interaction between the actin meshwork and the leading edge plasma membrane.

## “Rocketing motility” of bacteria

Some pathogens (bacteria as well as viruses) are able to use actin from the invaded host cell for their own movement in order to invade neighbouring cells. Examples of bacteria using this form of motility are *Listeria monocytogenes*, *Shigella flexneri* or *Rickettsia conorii* (Gouin et al., 1999). The actin comet tails responsible for the movement are initiated by a bacterial specific protein located at their surface (Act A for *Listeria*, IcsA for *Shigella*). This bacterial protein is able to stimulate actin-regulating proteins from the host cell, making it unnecessary for the bacterium to produce such proteins by itself. ActA from *Listeria* cannot influence actin polymerisation in vitro, but in combination with Arp2/3 it is able to catalyse filament nucleation (Welch et al., 1998). *Shigella* protein IcsA (or VirG) has been shown to interact with N-WASP, an Arp2/3 activator (Suzuki et al., 1998). Although the polymerisation of all of these tails is driven by treadmilling, the detailed structure of the tails varies between the bacteria species (Gouin et al., 1999). *Shigella* and *Listeria* tails show a meshwork-like structure, with short filaments and a high filament density at the bacterial surface. *Rickettsia* shows a more bundle-like tail, with long parallel filaments. As one of the simplest model systems for actin-based motility, the “rocketing motility” of pathogens is useful to study the basics of this mechanism. *Listeria* for example was used to identify key components of actin-based cell motility (Loisel et al., 1999). By adding pure proteins into a buffer solution containing bacteria, it could be investigated which proteins are essential, which accelerate motility and which hinder the bacterial movement. These motility assays showed that movement could be achieved by F-actin, Arp2/3, ADF and CP and the addition of profilin,  $\alpha$ -actinin and VASP created a more efficient motility. These experiments could also be reproduced with N-WASP or ActA coated artificial particles such as beads or rods (Carrier et al., 2003). An additional important aspect of actin-based cell motility which emerged from the study of the “rocketing motility” is the attachment of the tail to the bacterial surface. Gerbal et al showed that the actin tail was strongly associated with the bacterium by performing optical laser tweezer experiments to separate the tail from the pathogen (Gerbal et al., 2000b).

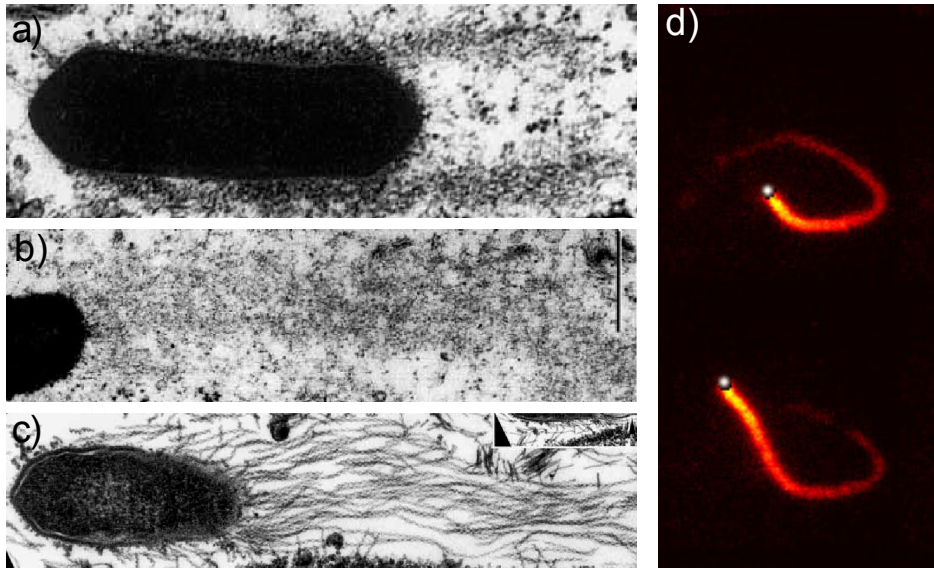


**Figure 1-2: actin tails**

Electron microscopy images of actin tails: a) *Listeria*, b) *Shigella*, c) *Rickettsia*. The actin tails of *Listeria* and *Shigella* consist of short, crosslinked filaments, which in the case of *Listeria* grow from the side of the bacterium (a) and in *Shigella* from the bacterial back (b). *Rickettsia* shows much longer filaments arranged in a parallel fashion (c). In d), a polystyrene bead coated with ActA is propelled by a fluorescent actin “comet tail”. (images a-b were taken from (Gouin et al., 1999), d from Theriot lab webpage)

However, this bacterial regulation of actin polymerisation does not represent all aspects of cellular protrusion. As the actin tail is situated outside the bacteria, these model systems lack the complexity of the leading edge situation.

### Fish keratocytes

Fish keratocytes are terminally differentiated, epidermal cells which can be found on the outside of fish scales. Their purpose is to form a protective cell layer around the fish and seal wounds as fast as possible to avoid infections. Fish keratocytes have been observed in culture from as early as 1914 (Osowski, 1914, Dederer, 1921). In 1924, H. Goodrich characterised their movement behaviour (Goodrich, 1924) and he described the typical shape of these cells with “the curious fan shaped projections” as “canoe-like” (Figure 1-3a) and measured their average rate of motion with  $6.3 \mu\text{m}/\text{min}$ . This is faster than most other cells in culture (e.g. fibroblast  $1 \mu\text{m}/\text{min}$  (Abercrombie et al., 1970a)). Viewed from above (Figure 1-3a), it can be seen that their lamellipodium comprises most of the cells surface. The cell body is confined to a rather small area at the rear of the cell. In contrast, the side view (Figure 1-3c) shows that the lamellipodium is

a very thin organelle compared to the voluminous cell body. The lamellipodium is nearly exclusively filled with a very dense meshwork of actin filaments (figure 1-2d). Besides their speed, fish keratocytes also show a very smooth, gliding movement, with only small changes in size and form of the cell. This is due to their very effective coordination of the three steps for cell motility (protrusion, adhesion, retraction) and their weak close contacts, which allow faster disassembly and therefore continuous movement (Kolega et al., 1982, Anderson and Cross, 2000). These cells are a very good model system to study all processes of cell motility. However, one substantial limitation is that these cells cannot be maintained in culture. They must be prepared freshly as primary explant cultures. As they are terminally differentiated and not able to divide anymore, the use of molecular biology techniques such as transfection is also restricted.

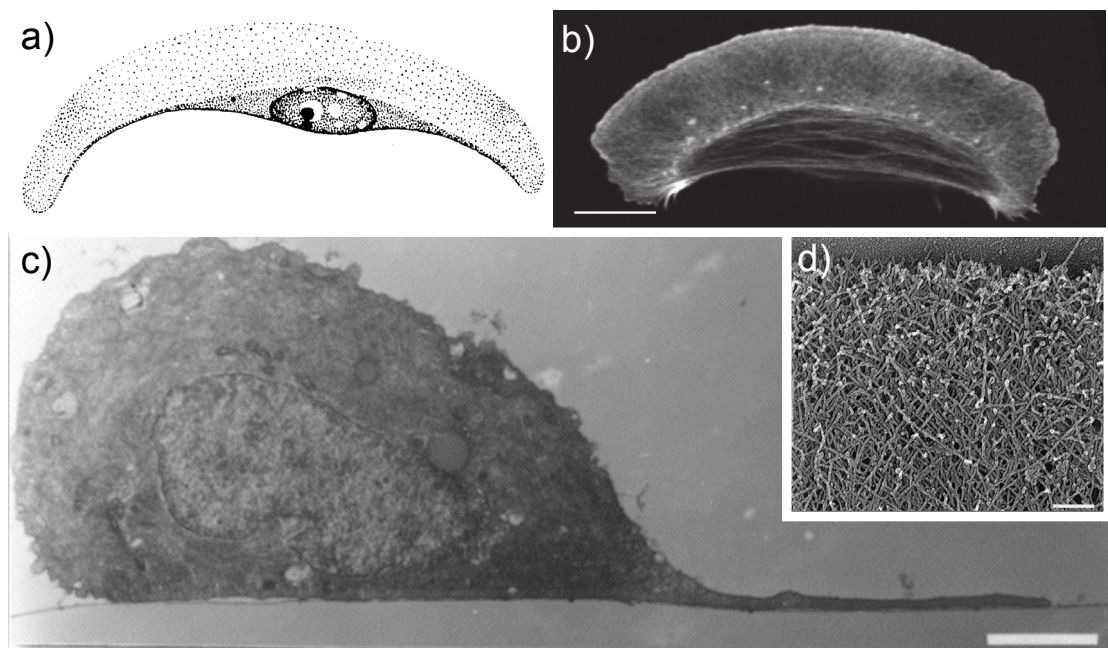


**Figure 1-3: fish keratocytes**

One of the first representations of a fish keratocyte, adopting the typical canoe-like shape (a, taken from (Goodrich, 1924)). Electron microscopy image of a slice through a fish keratocyte shows the thin protrusion (lamellipodium) and a rather voluminous cell body (b, taken from PhD thesis of Dr. Kurt I. Anderson, scalebar  $2\mu\text{m}$ ). Phalloidin staining (b, scale bar =  $10\mu\text{m}$ ) and high magnification EM of the actin within the lamellipodium (c, taken from Small et al 1999, scalebar  $200\text{nm}$ ) shows a very dense meshwork of filaments

## *Dictyostelium discoideum*

The amoebae *Dictyostelium discoideum* is a simple eukaryotic microorganism that lives in soil and feeds on bacteria. An interesting aspect of this single cell organism is its ability to aggregate with up to 100000 other *Dictyostelium* cells. This aggregation is triggered by starvation and achieved by chemotaxis towards cAMP. Aggregated cells form a slug at first, and then after migrating towards the surface, a fruiting body with spores (Figure 1-4a). These spores can survive periods of unfavourable conditions. For the study of cell migration *Dictyostelium* are mostly used in their undeveloped, vegetative stage, sometimes under starved conditions with or without a chemoattractant. A *Dictyostelium* cell has to move in order to find and engulf bacteria. This is accomplished by the formation of actin mediated pseudopodia. As their pseudopodia rapidly change direction, retract or split into two, the movement of *Dictyostelium* cells is less smooth compared to the gliding movement of fish keratocyte. The latter show great directional persistence due to their stable cell shape, whereas the cell shape of *Dictyostelium* is changed constantly. This rapid and spontaneous behaviour can be unfavourable for experiments involving complicated imaging setups (FRAP, FLIM), but is highly advantageous to study reorganisation of the actin cytoskeleton as well as signalling processes involved in cell migration.

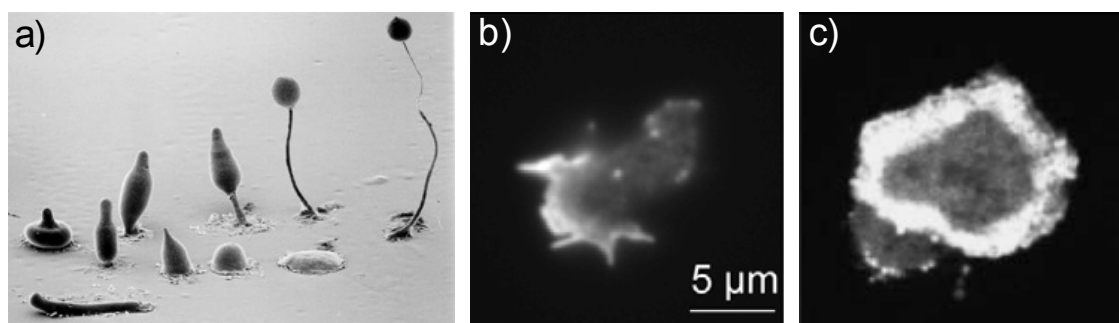


**Figure 1-4: *Dictyostelium discoideum***

The life-cycle of *Dictyostelium* cells (a) consists of several stages. Upon starvation individual cells can aggregate and form slugs and later a fruiting body, which enables the cell collective to survive in unfavourable conditions. The actin meshwork of *Dictyostelium* in its normal distribution (b, taken from (Patel et al., 2008), acquired by Ireen König) and forming a moving actin-wave (c, taken from (Gerisch et al., 2004)).

An interesting aspect with regards to this thesis is the ability of *Dictyostelium* to form moving actin meshworks within the cell (Figure 1-4c, (Gerisch et al., 2004, Bretschneider et al., 2004)). Formation of these networks is random and infrequent in wild-type cells, but occurs more frequently during the reorganisation of the actin cytoskeleton after washout of Latrunculin treatment. These “actin-waves” resemble lamellipodial meshworks and travel on the planar basal cell membrane. Within the cell, they travel without a preceding membrane fold, but if they hit the cell edge, these actin waves are able to push the membrane forward like in normal lamellipodial protrusion. The initiation of actin polymerisation in *Dictyostelium* therefore seems to be separated from protrusion. This phenomenon is interesting with respect to localising aspects as well as force production of actin polymerisation.

### **B16-F1 cells**

The B16-F1 mouse melanoma cell line was derived by injecting tumour cells into mice and then harvesting the cells from newly formed metastases (Fidler, 1975). Compared to B16-F10, where the injection-and-harvesting procedure had been repeated 10 times, the B16-F1 cell line is less invasive (Nakamura et al., 2002). Despite their low invasiveness, B16-F1's are a good model system for 2D migration. They are able to produce a big lamellipodium (Figure 1-5), which facilitates the study of actin polymerisation at the leading edge. In comparison with fish keratocytes, B16 F1 cells are less persistent in their movement (time- and direction-wise) and periods of consistent movement are disrupted by cell body retraction or standstill. In culture, only a low percentage of cells are generally engaged in rapid, persistent movement at a given time, but lamellipodia formation can be stimulated by PMA (Phorbol 12-myristate 13-acetate) treatment (Ballestrem et al., 2000).

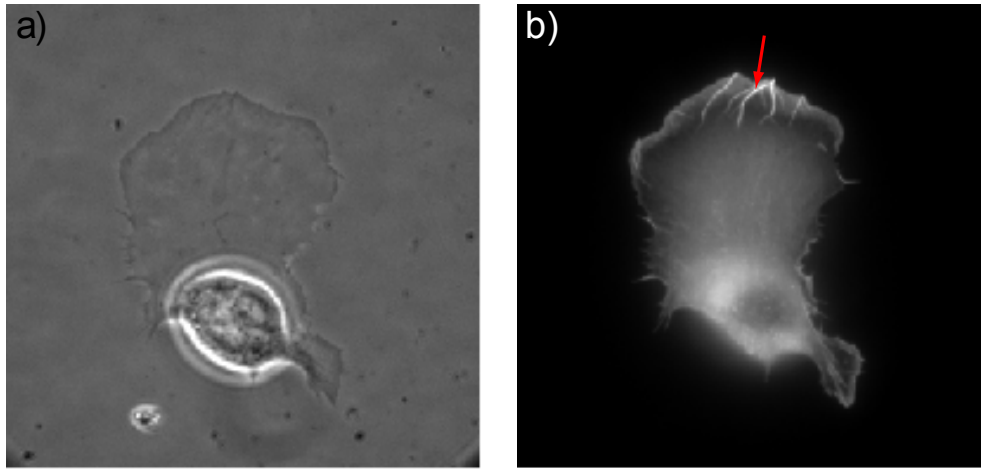


**Figure 1-5: B16 F1 cell**

A migrating B16 F1 cell in phase contrast (a) and its actin cytoskeleton, as achieved by overexpression of mRFP-actin (b). In contrast to fish keratocytes, the actin cytoskeleton within the lamellipodium of B16 cells also shows other structures than a branched meshwork, for example microspikes (arrow)

### 1.1.1.2 Regulation of actin polymerisation at the leading edge

The coupling of actin treadmilling to cell migration requires tight regulation. Cells have to coordinate protrusion as the first step of cell migration with adhesion and retraction in order to perform efficient displacement. Sometimes, the actin machinery has to respond fast to arriving external signals. This involves the correct localisation of actin polymerisation to sites of required protrusion. Termination of polymerisation within non-required areas is necessary for fast and directed movement. To optimally use the given resources within a cell, rapid depolymerisation at the filament -ends provides new free actin monomers. A rough overview of these processes at the leading edge is shown in Figure 1-6 (figure and legend taken from: (Pollard and Borisy, 2003)).

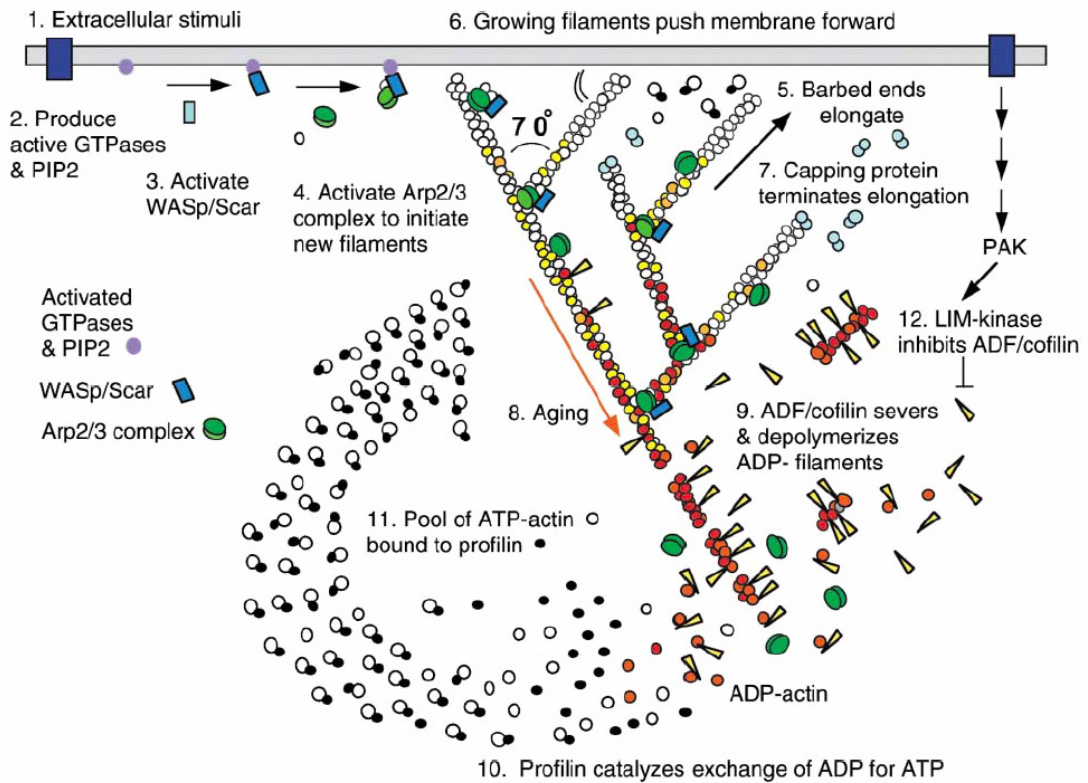


**Figure 1-6: dendritic nucleation treadmilling model**

(1) Extracellular signals activate receptors. (2) The associated signal transduction pathways produce active Rho-family GTPases and PIP<sub>2</sub> that (3) activate WASp/Scar proteins. (4) WASp/Scar proteins bring together Arp2/3 complex and an actin monomer on the side of a preexisting filament to form a branch. (5) Rapid growth at the barbed end of the new branch (6) pushes the membrane forward. (7) Capping protein terminates growth within a second or two. (8) Filaments age by hydrolysis of ATP bound to each actin subunit (white subunits turn yellow) followed by dissociation of the phosphate (subunits turn red). (9) ADF/cofilin promotes phosphate dissociation, severs ADP-actin filaments and promotes dissociation of ADP-actin from filament ends. (10) Profilin catalyzes the exchange of ADP for ATP (turning the subunits white), returning subunits to (11) the pool of ATP-actin bound to profilin, ready to elongate barbed ends as they become available. (12) Rho-family GTPases also activate PAK and LIM kinase, which phosphorylates ADF/cofilin. This tends to slow down the turnover of the filaments. (taken from (Pollard and Borisy, 2003)).

In a simplified view, extracellular signals activate members of the WASp/scar family through Rho-family GTPases. Active WASp/Scar proteins stimulate the Arp2/3 complex, which initiates the formation of new daughter filaments on the side of existing filaments. New filaments are polymerised rapidly until they are capped by CP, preventing further monomer addition. Only free, polymerising filaments can push the membrane forward. ATP hydrolysis within the filament as well as the dissociation of phosphate determines the age of the filament and older parts are favoured for severing by ADF/cofilin. This results in depolymerisation and release of ADP-G-actin into the cytoplasm. These free actin-monomers are then, catalysed by profilin, converted back to ATP-G-actin

by nucleotide exchange. The ATP-G-actin/profilin complex is then ready to be added to new barbed ends at the leading edge.

Many essential key components of actin-based cell motility were identified in motility assays using purified proteins. In 1999 the group of Marie-France Carlier was able to show, that the use of actin, Arp2/3, ADF/cofilin and CP was enough to propel a *Listeria* bacterium, which itself expressed the Arp2/3 activator ActA on its surface (Loisel et al., 1999). The movement was observed to be more efficient with additional profilin,  $\alpha$ -actinin and VASP. These experiments were reproduced using ActA coated beads instead of bacteria (Carlier et al., 2003). In contrast to the actin-tails used to propel bacteria or beads, the actin system in eukaryotic cells is far more complicated. New actin regulating proteins are discovered all the time and the understanding of the actin machinery in cells is getting more and more complex. In the following subchapters I will concentrate on some of the essential proteins involved and some which will be important for the understanding of this thesis.

### **Arp2/3 complex**

The Arp2/3 complex is a nucleator for actin polymerisation and in lamellipodial actin meshworks it is the most significant of these crucial components within the actin regulation. Arp2/3 was identified in 1994 as 7 individual proteins with the ability to bind to profilin (Machesky et al., 1994). As they were co-precipitated through many steps of purification, the authors suggested they form a rather stable complex. Two of the seven proteins were actin-related proteins, giving the complex its name. These two subunits are proposed to mimic an actin monomer each (Kiselar et al., 2007, Nolen and Pollard, 2008) and through the recruitment of one additional actin monomer (Boczkowska et al., 2008), a stable nucleus for further actin polymerisation is formed. The other subunits are probably involved in binding the complex to an existing filament, which also acts as a coactivator (Machesky et al., 1999). Due to the way in which the Arp2/3 complex associates with the existing filament, new filaments are formed in a 70° branch of the mother filament (Schaus et al., 2007). It is debated in literature whether new branches are formed at the side of an existing branch

(Amann and Pollard, 2001) or starting from the barbed end (Pantaloni et al., 2000). Regardless of which theory is accurate, the result is a dendritic actin meshwork, which promotes a higher density of actin filament +ends at the leading edge compared to regions further away from the site of protrusion. The Arp2/3 complex itself is not able to start a new filament, it needs to be activated. An Arp2/3 activator and ATP are needed to create a conformational change and bring subunits arp2 and arp3 closer together (Kiselar et al., 2007). Proteins of the WASP family are known Arp2/3 activators and are discussed in the next section.

### Arp2/3 activators

Members of the Wiskott-Aldrich syndrome protein (WASP) family were identified to be capable of activating Arp2/3 (Machesky and Insall, 1998). Today, there are 8 members of the family: WASP, N-WASP (isoform from WASP initially found in brain tissue), three isoforms of WAVE (WASP family verprolin homologous protein, also called Scar), WASH (WASP and Scar homolog), WHAMM (WASP homolog associated with actin, membrane and microtubules) and JMY (a p53 cofactor). WHAMM, WASH and JMY are relatively recent members of this family (WHAMM-2008 (Campellone et al., 2008), WASH - 2007 (Linardopoulou et al., 2007), JMY - 2009 (Zuchero et al., 2009)) and not much is known yet about their involvement in actin regulation.

A shared feature between proteins of the WASP family is the VCA domain, which can be divided into three smaller domains: one (or in the case of N-WASP two) Verprolin homology domain, a short central or Cofilin homology region and an Acidic region (Stradal et al 2004). The V domain, also called WH2 (WASP homology domain) can be found in many actin binding proteins and is able to bind monomeric actin (Miki and Takenawa, 1998, Paunola et al., 2002). The acidic domain interacts with the Arp2/3 complex (Machesky and Insall, 1998). Through the combination of these domains, the proteins are able to activate Arp2/3 and provide an extra actin monomer for the formation of an “actin-trimer” needed for the start of the polymerisation of a new filament. The double WH2 domain in N-WASP gives this protein a higher Arp2/3 activity

(Yamaguchi et al., 2000), but the other members are effective activators as well. The members of the WASP family also share a Proline-rich region adjacent to the VCA domain. This Proline-rich region is a possible interacting site for SH3 domain containing proteins such as IRSp53, cortactin, Abi2 (Pollitt and Insall, 2009). The N-terminus of the WASP family members is different and primarily regulates the activity of the VCA domain by interacting with upstream signals or releasing auto-inhibitory configurations. While WASP and N-WASP contain a WH1 (WASP homology 1, also called Ena/VASP homology 1) domain and a GBD (GTPase binding domain, also called CRIB), all three WAVE proteins possess a WHD (WAVE homology domain) (Stradal et al., 2004).

These variations in the domain composition of WASP family members results in specific recruitment to diverse actin structures. N-WASP can be released from its auto-inhibitory form by Cdc42 and PIP<sub>2</sub> binding (Rohatgi et al., 2000, Kim et al., 2000) and is mainly associated with endocytosis (clathrin coated pits, (Benesch et al., 2005)), podosomes (Mizutani et al., 2002) and intracellular vesicle transport (Taunton et al., 2000). WAVE proteins are present in vivo in a five-member complex (one of the WAVE isoforms, Abi, Nap1, PIR121, HSPC300), which is highly conserved throughout species, suggesting a specific and complicated interplay between all complex members. The GTPase Rac1 has been shown to activate the WAVE complex, but different mechanisms have been suggested. One suggestion is the direct binding of Rac1 to PIR121 (also called Sra1) (Kobayashi et al., 1998, Kunda et al., 2003), another suggested possibility is a IRSp53 mediated indirect binding of Rac1 and WAVE2 (Miki and Takenawa, 2002, Abou-Kheir et al., 2008). WAVE2 has been shown to localise at the leading edge and is mainly associated with lamellipodium and membrane ruffle formation (Hahne et al., 2001, Miki and Takenawa, 1998) and therefore the interaction between Rac1-IRSp53-WAVE2 is an important feature for the interpretation of results shown in this thesis (see chapters 5 and 6). Although the exact mechanism of WAVE complex regulation is not yet understood, it is thought that the complex is initially inactive and Rac1 causes a conformational change resulting in an active WAVE complex (Ismail et al., 2009). Due to the intricacy of the WAVE complex, it is very likely that it controls many actin processes. Besides the involvement in lamellipodia (see above), it has, for

example, been suggested to play a role in cell-cell adhesions (Yamazaki et al., 2007) and filopodia formation (Yang et al., 2007).

### Capping Protein (CP)

Capping Protein (CP) is a  $\alpha\beta$  heterodimer with a size of just over 60kDa. It is able to cap the +end of actin filament and thereby prevent new monomer addition as well as the dissociation of actin subunits (Wear and Cooper, 2004). In high concentrations, this protein has been shown to prevent motility of *Listeria* in vitro, but in lower concentrations it is one of the essential four proteins for actin-based motility (Loisel et al., 1999). In vivo, it is crucial for rapid, directed actin polymerisation. By capping a large fraction of actin filament +ends, it regulates the availability of free actin filament ends for polymerisation, which indirectly controls the concentration of free actin monomers. A high G-actin concentration allows faster growth of the free, uncapped actin filaments. Actin polymerisation without CP would result in slower, less targeted protrusion (Pantaloni et al., 2001). Although there is not much sequential similarity between the  $\alpha$  and  $\beta$  subunits, their crystal structures superimpose well (Yamashita et al., 2003), suggesting similar functions of both subunits. Indeed, mutational analysis indicated that the C-terminal domains of both subunits are crucial for actin binding (Hug et al., 1992). Having two equally strong actin binding domains in the heterodimer would explain CPs specific binding to the end of a double-helical actin filament instead of just actin monomers. The C-terminal domains are also thought to be the main interacting domains between the subunits, leading to a robust heterodimer (Casella and Torres 1994). Regulation of CP in vivo might involve phosphatidylinositol (4,5)-biphosphate (PIP<sub>2</sub>), which can bind directly to CP and is able not only to inhibit CP function (Huang et al., 2006, Kim et al., 2007) but also to uncap +ends (Schafer et al., 1996). PIP<sub>2</sub> within the membrane could then play an important factor in localising efficient actin polymerisation by selectively unblock capped +ends, enabling them to be elongated. PIP<sub>2</sub> might control the speed of polymerisation and an increase in its activity could perhaps be a first signal to stop polymerisation at certain locations by blocking a majority of filaments from monomer addition.

The constructs used for this thesis encoded the  $\beta$ 2-subunit from human CP. We obtained the GFP-CP, GFP-CP<sub>ppmut</sub> and GFP-CP $\Delta$ 7 constructs from Laura Machesky, but they were originally from Dorothy Schafer. The mutations are described in more detail below.

#### CP<sub>ppmut</sub> - actin binding mutant

Sequence analysis showed that the amino acid at position 262 was changed from leucine to arginine. Leucine 262 is probably the most important amino acid for actin binding and its mutation greatly reduced CPs ability to bind actin filaments (Barron-Casella et al., 1995). Chicken  $\beta$  subunits with mutations at this position were still able to form heterodimers, suggesting that the amino acid exchange did not cause disruption in protein folding or structure.

#### CP $\Delta$ 7 - actin binding and dimerisation mutant

The name of this mutation suggested the lack of 7 amino acids, but sequence analysis revealed that the construct lacked 12 aa on its N-terminal site and 7 (stops at aa 265) at the C-terminal site. Leucine 266 is the second most important amino acid for actin binding (Barron-Casella et al., 1995). The C-terminus is also important for the interaction between  $\alpha$  and  $\beta$  subunits (Casella and Torres, 1994), suggesting that partial deletion could result in dimerisation problems. The N-terminus may be important for dimer formation *in vivo* (Sizonenko et al., 1996), which could explain the double deletion within the CP $\Delta$ 7 construct.

## IRSp53

The 53-kDa insulin receptor substrate protein (IRSp53) was first identified by Yeh et al. in a screen for tyrosine phosphoproteins during overexpression of the insulin receptor (Yeh et al., 1996). It is also known as brain-specific angiogenesis inhibitor 1 associated protein (BAIAP2). There are several splice variants of IRSp53, namely isoforms 1-4. They are equal in aa 1-511 and differ in their length and sequence of the C-terminus. Isoform 1 (also called variant S) possesses 10 distinct aa after position 511, isoform 2 (L) has 41aa, isoform 3 (T) has 9aa and isoform 4 (M) shows 23 distinct aa. All isoforms share the main functional domains: IMD, RCB, Proline-rich and SH3 (Figure 1-7).

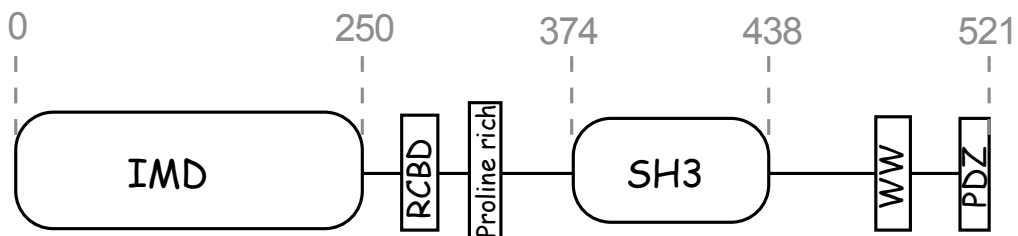


**Figure 1-7: schematic structure of IRSp53 (isoform1)**

The 521aa containing IRSp53 protein possesses two large (IMD and SH3) and several small functional domains. Isoforms 1-4 only differ in their C-terminal sequence, after aa 511. The function of the different domains is explained within the text.

The IMD (IRSp53 and missing-in-metastasis domain) is the main feature of this protein and also defines the IMD-containing protein family. The IMD belongs to the larger family of BAR (Bin-amphipysin-Rvs167) domains, whose proteins can bind and deform membranes (Peter 2004). The IM-domain can be classified as an inverse BAR domain (I-BAR), as its crystal structure shows an inverse curvature compared to the other BAR domain subclasses (N-BAR, F-BAR). Whereas the latter ones are often associated with endocytosis, the different structural curvature of the IMD domain indicates the ability to induce membrane protrusions rather than invaginations (Mattila et al., 2007, Scita et al., 2008). In 2004 IMD was described as a novel actin bundling domain, important for filopodia formation (Yamagishi et al., 2004). Since then, precise binding sites for actin filaments (Millard et al., 2005) as well as membrane phospholipids have been shown and it was implied that IMD has the ability to form membrane tubules without creating actin bundles as seen in filopodia (Mattila et al., 2007). Within the IMD also lies a binding domain for Rac (RCB), which is able to link this

small GTPase to WAVE2 (Miki and Takenawa, 2002). Another important feature of IMD is its dimerisation, which has been demonstrated *in vitro* as well *in vivo* (Yamagishi et al., 2004).

Close to the IMD is a Rac-and Cdc42-binding domain (RCBD, also called CRIB (Cdc42 and Rac interaction binding) domain), which can directly bind Cdc42 (Krugmann et al., 2001), allowing possible interactions of IRSp53 with actin-regulating proteins such as Mena (Krugmann et al., 2001), Eps8 (Funato et al., 2004) and mDia (Fujiwara et al., 2000). These interactions are all known to lead to the formation of filopodia.

Another binding domain of IRSp53 is a proline-rich domain, which may be recognised by many proteins, especially ones containing SH3 domains. It may also be involved in the autoinhibition of IRSp53, which has been proposed to take place between the N-terminal region (aa 1-178) and the central region (aa 180-317) containing the proline-rich domain. Somewhere in this central region, close to the RCBD, the exchange factor Tiam1 can bind to IRSp53 and it may enhance the signalling specificity towards Rac (Connolly et al., 2005) and therefore lamellipodia (see below).

The next important domain in the sequence of IRSp53 is a SH3 domain, located between amino acids 374 and 438. This domain allows binding of proteins containing a proline-rich sequence. The SH3 domain itself is non-specific in its binding and needs signalling molecules such as Cdc42 or Rac to link it to specific interacting partners (see above for Cdc42 related protein binding). WAVE2 was identified as a direct interacting partner with the SH3 domain of IRSp53 in conjunction with Rac1 (Miki and Takenawa, 2002). WAVE2 is associated with the formation of lamellipodia (Hahne et al., 2001) and its activity has been suggested to be regulated by IRSp53 in the presence of not only activated Rac but also PIP3 (Suetsugu et al., 2006), suggesting an important role in localising actin polymerisation to protrusion sites.

As mentioned before, the C-terminus varies among the different isoforms of IRSp53. The tryptophan-tryptophan binding domain (WW) is known for its affinity for proline-rich ligands and regulates the link between the extracellular matrix and the cytoskeleton (Ilsley et al., 2002). Isoform 1 possesses a PDZ domain

(named after the proteins it has first been identified: PSD-95, Dlg, ZO-1) which can bind the carboxyl-terminal sequence of proteins (Nourry et al., 2003), but its relevance for actin dynamics is unclear. Instead of a PDZ domain, isoforms 2 and 4 of IRSp53 possess a WH2 and WH2-like domain, respectively. The Wasp Homology domain-2 domain is very common among cytoskeletal actin-binding proteins, which are involved in the rapid turnover of actin filaments. The WH2 domain binds most likely to actin-monomers and its exact function depends on the protein it is part of, such as Thymosin  $\beta$ 4, ciboulot, Verprolin and WASP and WAVEs (Paunola et al., 2002). Isoform 3, which has neither the PDZ nor the WH2-like domain, was found to be expressed in the human breast cancer cell line MCF7, suggesting the importance of these C-terminal domains in normal, non-cancerous cell function (Okamura-Oho et al., 2001).

To summarise, IRSp53 is a protein capable of linking the actin-cytoskeleton to the membrane, especially the curved membrane of protrusion structures. Its interaction with the actin-machinery is multifunctional, leading to at least two different actin-structures: filopodia and lamellipodia. Our focus mainly lies in lamellipodia, where IRSp53 may link Rac to WAVE2 and therefore might enable the activation of the Arp2/3 complex. With its membrane deforming abilities IRSp53 is an ideal candidate to not only transfer the GTPase signal but also to create the leading edge membrane fold and maybe link the actin-cytoskeleton to the membrane.

#### IRSp53-IMDmut - membrane binding mutant

This mutant was provided by Laura Machesky and is cited in Millard et al 2005 (Millard et al., 2005). Our sequence analysis confirmed that the construct consist of full-length IRSp53 (isoform 1) with 4 point mutations within the IMD domain. Amino acids 142, 143, 146 and 147 were changed from lysine to glutamic acid. These residues are positioned at the extreme ends of the IMD domain (Figure1-8a) and are well conserved between mammalian IMDs (Millard et al., 2005). The distance between basic patches of the IMD domain correlates with the distance between F-actin fibres, as shown by electron microscopy (Yamagishi et al., 2004). Moreover, the highly acidic surface charge of F-actin fibres suggests that

basic areas of the IMD domain may be the interacting regions. A single site mutation within the Lys142-Lys147 cluster did not show visible effects, whereas the mutation of all 4 amino acids changed the behaviour of the protein enormously (Millard et al., 2005). In detailed analysis using only the mutated IMD domain, Millard et al found that the actin-bundling activity is disrupted. Unmutated IMD was able to bundle fluorescently labelled actin, whereas the IMD mutant failed to do so. They also showed that the IMDmut folded and dimerised normally, and that filopodia formation was greatly reduced when cells were transfected with IMDmut. This led Millard et al to the conclusion that Lys 142, 143, 146 and 147 function as actin-binding sites for the actin-bundling function of the IMD domain of IRSp53.

In 2007 Mattila et al (Mattila et al., 2007) showed the membrane deforming ability of the IMD domain of MIM. Besides the interaction with membrane components (PIP<sub>2</sub>) they also showed the ability of the IMD of MIM to induce tubular structures in membrane vesicles. An extensive list of MIM-IMD mutants was studied to find actin- and PIP<sub>2</sub>-binding sites. The actin-binding site mutants showed lower affinity to F-actin but none of the single or double mutants resulted in a complete loss of F-actin binding. In contrast, some double mutants showed a hugely impaired PIP<sub>2</sub>-binding. A crystal map of the mutated residues is shown in (Figure 1-8c). Interestingly, in terms of the function of our IRSp53-IMDmut, the residues with strong actin- and PIP<sub>2</sub> binding (shown in red) overlap not only with each other but also with the mutations of Millard et al (Figure 1-8a). A closer comparison of the involved sequences involved is shown in Figure 1-8d.

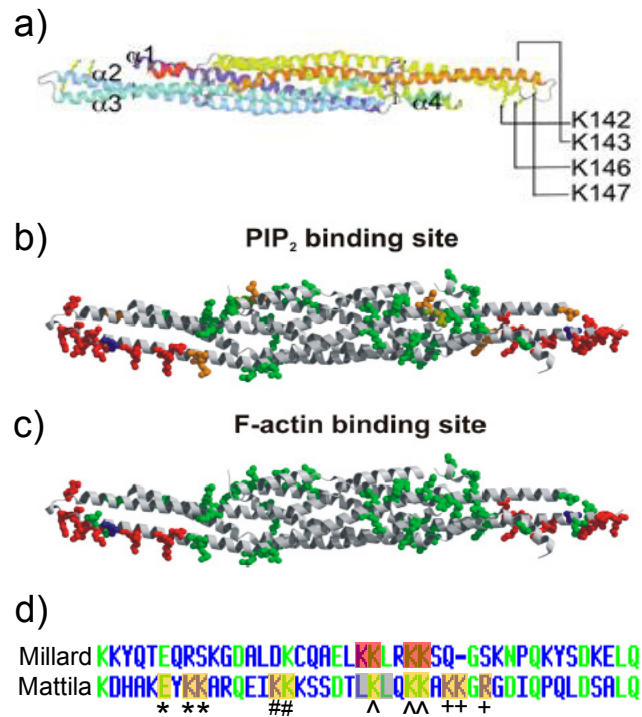


**Figure 1-8: F-actin- and PIP<sub>2</sub>-binding sites of the IMD domain.**

Locations of F-actin (a and c) and PIP<sub>2</sub> (b) binding sites in the structure of the IMD domain of IRSp53 (a) and MIM (b and c). A sequence comparison of the region around the for us interesting residues is shown in d. In red are the four mutation sites of IRSp53 described in Millard et al and used for this thesis. The lower sequence shows mutations investigated by Mattila et al. Marked in yellow are mutations which reduce actin- and even more severely PIP<sub>2</sub>-binding (residues with the same black symbol (\*#^+) were changed in one mutation). In grey are the changed residues for one mutation which showed highly reduced PIP-binding without affecting the F-actin-binding ability.

The positions of the residues shown to reduce PIP<sub>2</sub>-binding in MIM-IMD overlap with the mutated positions of IRSp53-IMDmut. The three yellow Lysine-residues in the Mattila sequence marked with ^ showed reduced F-actin as well as reduced PIP<sub>2</sub>-binding. The grey Leucine-residues reduced PIP<sub>2</sub>-binding without affecting F-actin-binding. All mutations from Millard correspond to mutations from Mattila, where it has been shown that their PIP<sub>2</sub>-binding ability is even more reduced than their actin-binding ability. Giorgio Scita et al summarises the amino acids for lipid-binding in a recent review as 108, 130, 171, 142, 143, 145 and 147 (Scita et al., 2008). Three of these positions match the mutated sites in IRSp53-IMDmut. For the experiments described within this thesis, I therefore consider the IRSp53-IMD mutation primarily as a membrane binding mutation and only secondary as a mutation with a reduced F-actin-bundling activity.

### IRSp53- $\Delta$ SH3 - WAVE2-binding mutant

This construct is described in Heung et al (Heung et al., 2008) and was provided by Laura Machesky. IRSp53 (isoform 1) was cut off at residue 374, deleting the SH3 domain as well as WW and PDZ binding motifs. The original study tested the influence of mutations on insulin-responsive tyrosine phosphorylation and IRSp53- $\Delta$ SH3 was found not to affect this process. Miki et al showed in 2000 that a mutant lacking the SH3 domain markedly reduced the ability of IRSp53 to bind WAVE2 (Miki et al., 2000). Although that mutant lacks 10 additional amino acids relative to the one used in this thesis, it is very likely that the SH3 domain is the cause for the loss of WAVE2-binding. Through disruption of WAVE2-binding to IRSp53, the IRSp53 $\Delta$ SH3 mutant should have a significantly weaker association with the actin meshwork. It is not able to activate WAVE2, which then does not interact with Arp2/3 which is essential for actin meshwork formation. If this mutant is expressed in the background of functional wild-type IRSp53, the formation of an actin meshwork should not be impaired, but the IRSp53 $\Delta$ SH3 mutant should not be part of the normal actin regulating machinery, as it cannot fulfil its function and bind to WAVE2.

#### **1.1.1.3 Force production through actin-polymerisation**

The previous subchapter explained the biochemical aspect of actin-based cell motility, i.e. the processes involved in polymerisation of actin filaments and the regulation of this highly dynamic system. The following subchapter will discuss more biophysical aspects, i.e. how this process is thought to produce the necessary force.

Force producing systems in biology somehow have to relate their basic chemical structure or changes within this structure into mechanic forces. The field of mechanochemistry investigates how this is possible. Molecular motors, such as myosin, use the energy derived from ATP hydrolysis to create a conformational change in their structure. The structural change in one part of the molecules (in myosin the head) forces a displacement in respect to other filament parts (tail section for myosin). In the case of myosin, this displacement results in the

binding of the myosin head to a new, further away subunit of the actin filament, allowing the myosin molecule to pull itself along this filament (Alberts et al., 2008). Supermolecular springs, as for example used by *Vorticella*, can store energy within their structures and release this energy upon stimulation by external factors. *Vorticella* is thought to store electrostatic repulsion between charged filaments in its rod-like, helical, filamentous organelle, the spasmoneme. In the presence of calcium this charged state is neutralised, resulting in collapse of the elongated spasmoneme, leading to fast and powerful retraction (Mahadevan and Matsudaira, 2000).

Many different mechanisms have been proposed to explain force generation by actin polymerisation, and how such force is translated into movement. They vary, for example, in their scale of the approach, in their structural detail and in the function of ATP hydrolysis.

Some models of force production apply a more macroscopic view, where a pool of actin filaments is regarded as a compact unit rather than individual filaments. This unit as a whole is considered to be the force creating structure. The purpose of these large-scale models is to consider the interaction between the many single actin filaments involved. Gerbal et al suggest that a so-called actin gel surrounds the end of a bacterium, which is moved as a result of the forces applied from the gel onto the bacterium (Figure 1-9 a). The actin gel is elongated at the sides of the bacterium, where it is also attached to the surface (Gerbal 2000). This attachment creates a friction force ( $F_{\text{fric}}$ , Figure 1-9 a) applied to the bacterium and in constant interplay with the force created due to exerted stress by the gel on the back of the bacterium ( $F_{\text{mot2}}$ , Figure 1-9 a) (Gerbal et al., 2000a). A more refined version of this model was proposed following the observation that the actin-gel-tail deforms lipid vesicles (Figure 1-9b, c; (Upadhyaya et al., 2003). Lipid vesicles were coated with ActA and used in an *in vitro* motility assay. Deformation of the vesicles was used to estimate forces exerted on the vesicle surface. The gel is thought to be bound to the initially round vesicle and constant forces at the sides of the vesicles as well as at the back elongate the vesicle. The forces at the back act retractile, the ones at the side propulsive. Depending on the shape of the vesicle, one or the other force will be dominant. If the overall stress on the vesicle becomes too high, the actin-vesicle bond ruptures, leaving the vesicles to jump forward and retake its

initial shape. This interplay between the forces repeats itself periodically, as the rupture only happens locally, leaving enough actin attached to the vesicle at all times (Upadhyaya et al., 2003). Although ATP is needed for the motility assays, its function is not mentioned within the models, as events on a filament scale are not part of the more macroscopic view.

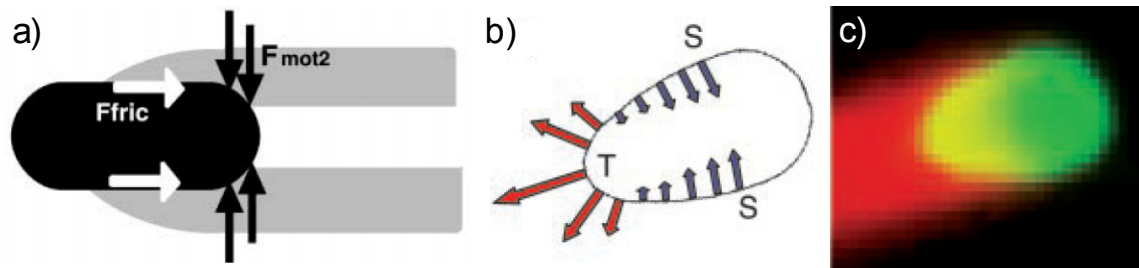


**Figure 1-9: actin-gel force generation theories**

Forces applied from the actin-gel tail to a bacterium (a).  $F_{fric}$  is a friction force due to the connection of the gel to the bacterial surface;  $F_{mot2}$  is exerted on the back hemisphere of the bacterium. Schematic representation of stress exerted on a lipid vesicle (b). Red arrows indicate retractile forces and blue arrows propulsive forces. A typical teardrop shape of an ActA coated, fluorescent lipid vesicle (c), with Rhodamin actin (red tail) and Oregon green labelled vesicle. (a taken from (Gerbal et al., 2000a), b and c from (Upadhyaya et al., 2003))

These models might well explain the movement of *Listeria*, where a step-wise progress has been observed (Kuo and McGrath, 2000), but it is more difficult to apply such models in the geometry of a protruding lamellipodium. A bacterium is squeezed by the surrounding actin-gel, which exerts forces all around the sides of the bacterium. The geometry is reversed at the leading edge. Inside the lamellipodium, the actin-gel could not squeeze the membrane, as it is between two membrane sheets and not on the outside as in the case of bacteria.

Although the macroscopic force production models might be correct on their scale, but they cannot relate the biochemistry of individual filament polymerisation to force production.

Microscopic models which consider each filament as an individual unit capable of producing force are therefore more relevant for this thesis and will be explained in more detail. Although some of them are based on the movement of the bacterium *Listeria monocytogenes*, their principles can be applied to lamellipodia. The main difference among the microscopic models is the manner in which each model approaches the insertion of new monomers to the +end of

filaments close to or even attached to the membrane and associates this insertion with force production.

One of the earliest models, the “Brownian ratchet” model, suggested that the load (bacterium) temporarily shifts away from the rigid actin polymer due to thermally influenced Brownian motion. This fluctuation creates a gap where actin monomers can intercalate and be added to the filament +end (figure 1-10a; (Peskin et al., 1993)). One prediction of this model is that the bacterial velocity should depend on the size of the load. However, experiments demonstrated that *Listeria* and *Shigella* move with similar speed (Goldberg and Theriot, 1995), despite their size difference. The original model was altered to an “elastic Brownian ratchet” mechanism (Mogilner and Oster, 1996), in which the gap is created by the thermal bending of the flexible filament and the elastic force of the elongated polymer pushes the bacteria (Figure 1-10b).

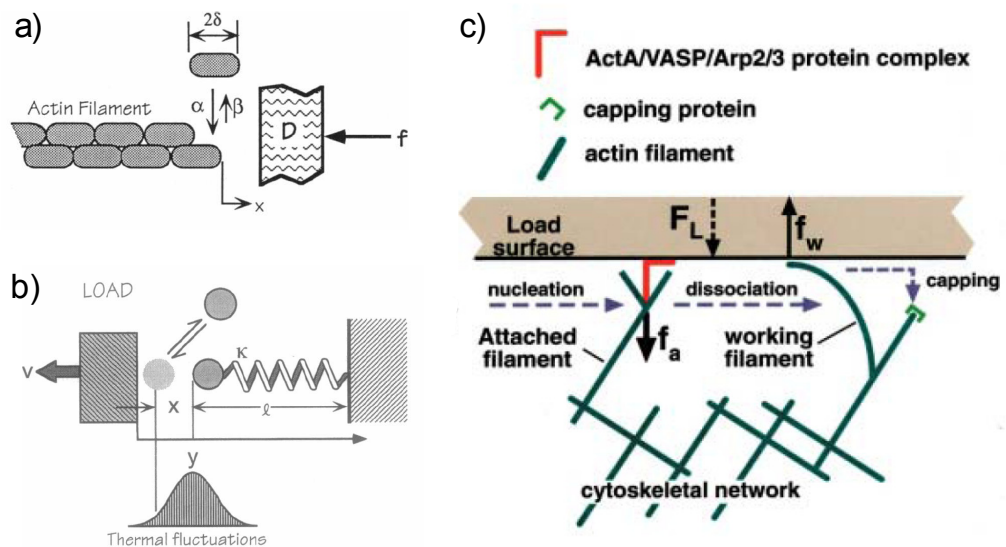


**Figure 1-10: ratchet force models**

The initial model (“Brownian ratchet”, a) assumed the insertion gap for monomers was created through thermal fluctuations of the load, whereas the actin filaments were stiff. In the “elastic Brownian ratchet” model, the gap was created by fluctuations of the elastic, spring-like filament (b). The “elastic ratchet and tethered” model (c) assumes the existence of two populations of filaments: attached and working (free) filaments. During nucleation (initiated by ActA/VASP/Arp2/3) the filaments are attached to the load surface, but they detach shortly after and are then polymerised according to the “elastic Brownian” model. (a taken from (Peskin et al., 1993), b from (Mogilner and Oster, 1996) and c from (Mogilner and Oster, 2003))

The latest version of this model considers attachment of the filaments to the bacterial surface and is called the “elastic ratchet and tethered filament model” ((Mogilner and Oster, 2003); figure 1-10c). Using optical tweezers, Gerbal et al

showed that the actin tail of *Listeria* is firmly attached to the bacterium (Gerbal et al., 2000b). The previous model (“elastic Brownian ratchet”) relied on the existence of a gap between the filament +ends and the load in order to generate force. The revised model (“elastic ratchet and tethered filament model”) considers the transient attachment of filaments and predicts the simultaneous existence of two types of actin filaments: attached or tethered filaments and detached or working filaments. Attachment between the bacterium and the actin meshwork is thought to occur during filament nucleation, when ActA binds to VASP and Arp2/3 and activates the latter. Shortly after nucleation the filaments detach from the load and exert force according to the “elastic Brownian model”. Thus free filaments are in compression and generate force, while the attached filaments are under tension and keep the contact to the bacteria. A free filament is only a “working” filament if it exerts force on the load. Filaments which are capped and do not polymerise, filaments which are oriented in the wrong direction and therefore not in contact with the load, or filaments which become crosslinked to other filaments and are therefore part of a rather stiff network are not considered working filaments. Through the use of biochemical data such as nucleation rate, capping rate, polymerisation rate, thermal energy etc the model predicts a ratio of 1:6 between tethered and working filaments.

To evaluate this model for lamellipodia, the authors calculated a theoretical pushing force (800pN/ $\mu\text{m}$ ) and compared it to experimental data from Dai and Sheetz (Dai and Sheetz, 1999). Both forces were in the same range and Mogilner and Oster concluded that their model is suitable for lamellipodial protrusion. This may be correct, but the force measured from Dai and Sheetz is the force needed to separate the cell membrane from the actin cortex in the case of blebbing. The actin cortex is different from the actin meshwork at the leading edge and it is likely that a different range of force is produced by it.

In all the ratchet models, the energy released by ATP hydrolysis is not directly used to generate force, but it drives the direction of polymerisation (Mahadevan and Matsudaira, 2000). Once a monomer is added to the filament, conformational change during ATP hydrolysis prevents depolymerisation, which only happens after phosphate release at the -end. The fact that elongated filaments stay elongated stops the load from moving back.

A model based on the permanent attachment of actin filaments to the membrane is the “Clamped-Filament Elongation” model by Dickinson and Purich ((Dickinson and Purich, 2002), Figure 1-11). The tip of each filament is assumed to be locked into a surface bound clamp, which recognised the terminal ATP subunit due to its energy difference (see figure 1-11b). The architecture of the clamp provides space to allow addition of two new actin-ATP monomers at a time. ATP hydrolysis provides energy to release the clamp, which recognises the energy signature of the newly added actin-ATP-subunits and moves to lock its position in the new place. In contrast to the Brownian motion models, this “Clamped-Filament Elongation Model” mechanism uses the energy of the ATP hydrolysis to generate force. This model can also explain the observation that *Listeria* moves in 5.4nm steps, corresponding to the subunit periodicity of actin filaments (Kuo and McGrath, 2000).

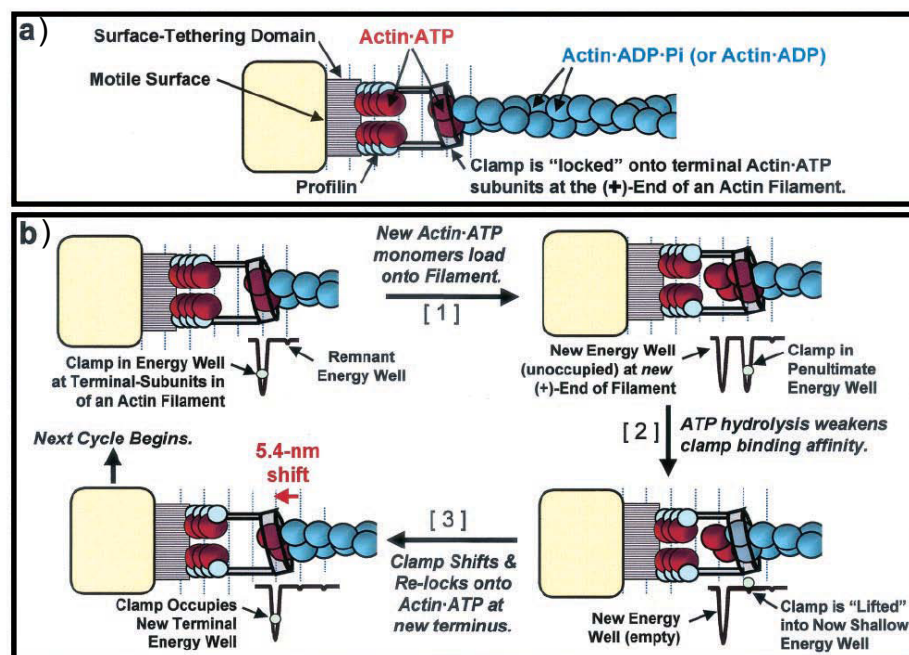


**Figure 1-11: The “Clamped-Filament Elongation” model**

Schematic representation of the clamp model (a). The step cycle of the “Lock, Load & Fire” mechanism used in the Clamped-Filament Elongation model (b): The reaction begins with a clamped filament, whose energy status is low (green circle in black energy well). The addition of new ATP-containing monomers (red) onto the filament end (“Load”, 1) creates a new, empty energy well. ATP hydrolysis attenuates clamp-binding affinity, as indicated by the conversion of a deep energy well to a shallow energy well (“Fire”, 2). The clamp then shifts its position by 5.4nm to the newly added monomers, resulting again in a low energy state, which is locked and functions as start position for the next cycle. (taken from (Dickinson and Purich, 2002))

Another possibility to create force out of a polymerising actin tail was proposed to be “buckling”. The model is based on equations for an elastic rod simulating

the actin tail and observations made with single actin filaments in TIRF (Berro et al., 2007). If the filament were attached to a surface by an actin nucleator (e.g. formin) on the barbed end site and another protein (e.g. myosin) at the pointed end, then the continuous elongation could result in a filament loop, which can act as a spring and release force. This model could run into problems in the environment of a dense lamellipodial actin meshwork, as individual filaments would not have enough space to form big buckles.

All microscopic models assume the attachment of the filaments to the load, be it temporarily or permanent. In *Listeria*, the bacterial specific Arp2/3 activating protein ActA is thought to link the bacterial membrane with the actin filaments with the aid of VASP (Laurent et al., 1999). Until today, no single molecule has been identified to perform the role of ActA in mammalian cells. VASP is present in both bacterial and eukaryotic systems, but probably cannot link actin to the membrane on its own. The Arp2/3 activator N-WASP has been shown to interact with the membrane through PIP<sub>2</sub> (Rohatgi et al., 1999) and to create actin tails when coated on beads (Yarar et al., 1999). But it is thought to regulate predominately vesicle transport, endocytosis and podosome formation rather than lamellipodial actin protrusion (Pollitt and Insall, 2009). Due to its membrane deforming ability, IRSp53 is a suitable candidate to link the actin meshwork to the pushed membrane, but as it's a rather new addition to the candidate list, this protein has not yet been incorporated into force generation models.

All of the mechanisms described above are theoretical models and largely based on biochemical data mostly obtained from rocketing motility assays. What is missing are experiments which can investigate the link between actin polymerisation and force production within a protruding lamellipodium. The ability to study this dynamic and tightly regulated process in its normal environment would be a great opportunity to experimentally test these models. However, polymerisation at the leading edge is a very rapid and delicate process, which can be unintentionally altered by the experiment itself. It is therefore difficult to investigate force generation at the leading edge of migrating cells without interrupting protrusion. In 2006, Prass et al measured the protrusive force of a migrating fish keratocyte by placing an atomic force

microscope cantilever in the path of a protruding cell (Prass et al., 2006). Based on the measured force-velocity curve they concluded that none of the existing models represents reality, although the “clamp” model matches most closely. One concern with their experimental approach is the use of a physical obstacle (the cantilever) against the leading edge. Although a pushing force could be measured, it may be that this does not represent the force generated under free movement of the leading edge. *In vivo* cells will always have a neighbour or something else they have to push against, so the experimental approach of Prass et al would represent natural condition. However, to understand the complex mechanisms involved in *in vivo* migration, we first have to understand the basics. Experimental approaches are therefore needed to investigate polymerisation at the leading edge membrane without any external influences.

Previous work from the Anderson group hypothesised that membrane diffusion could be used as an indirect readout of processes involved in protrusion at the leading edge. Lipids are globally free to diffuse laterally within the membrane (see section 1.2), but this diffusion can be altered from within the cell (fence models, see section 1.2.2). The behaviour of lipid diffusion at or around the leading edge was therefore thought to give insight into what is happening at the edge of a lamellipodium. Such experiments resulted in the detection of a lipid diffusion barrier at the leading edge ((Weisswange et al., 2005), see section 1.2.3.3) and proved to be an interesting experimental approach to further study the interaction of actin filaments with the leading edge membrane.

## 1.2 Membrane diffusion

The plasma membrane defines the boundary of a cell and separates the cytosol from the extracellular environment. It is built by two layers of lipid molecules, which are arranged with their polar, hydrophilic head groups at the outer sides and their non-polar, hydrophobic tails on the inside (see Figure 1-12). The molecules are held together mainly by noncovalent interactions among the tails. This continuous bilayer performs the function of a relatively impermeable barrier for water-soluble molecules. Membrane-incorporated-proteins

(transmembrane proteins) are located within the bilayer in order to accomplish the transport of molecules through the membrane. Transmembrane proteins are also involved in connecting a cell to the substrate or another cell as well as detection and transduction of signals from the outside environment.

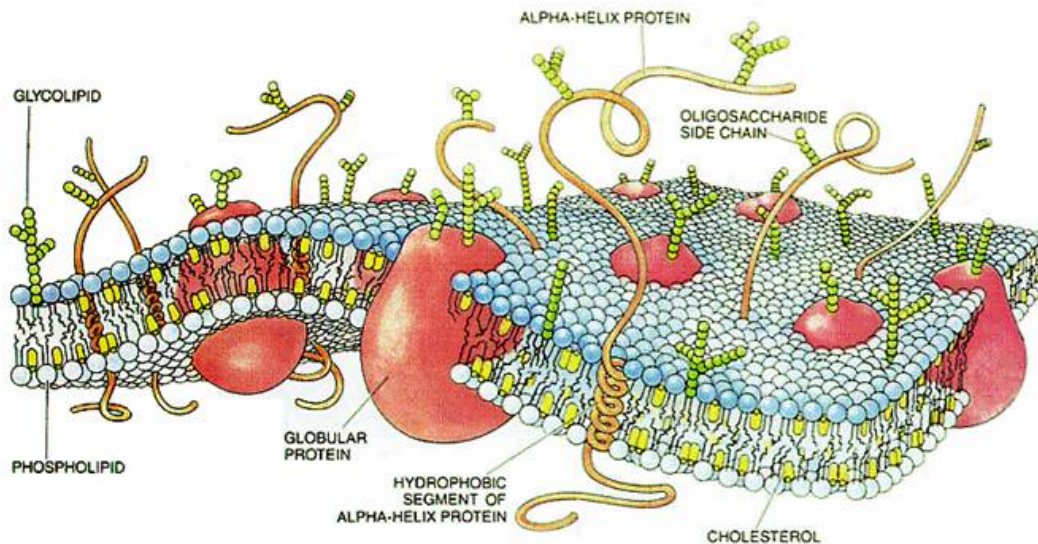


**Figure 1-12: plasma-membrane structure and composition**

This schematic representation of a membrane (taken from (Bretscher, 1973)) shows the lipid bilayer (light blue heads with black tails), different transmembrane proteins (red and brown structures), glycolipids (green) and cholesterol (yellow). The lipid bilayer behaves like a liquid, meaning the other components (as well as the lipids themselves) can diffuse within the membrane.

When it was realised that individual lipid molecules are able to diffuse freely within synthetic bilayers, the “fluid-mosaic” model was postulated (Singer and Nicolson, 1972). The authors suggested the membrane bilayer can be considered as a two-dimensional liquid. This view has later been modified to include possible restraints on membrane diffusion, some of which are described below.

### **1.2.1 Lipid rafts**

If all lipids were able to move freely within each lipid layer of the membrane, a random distribution of different kinds of lipids would be expected. When an asymmetrical distribution of lipid species was observed (laterally as well as between exoplasmic and cytoplasmic membrane leaflets), it was suggested that membranes are more organised in their lateral dimension than previously

thought (Simons and Ikonen, 1997). Liquid-ordered domains called rafts are more tightly packed than their surrounding disordered membrane phase and are thought to float within the fluid membrane monolayer. The raft model proposes that cholesterol molecules lie in between neighbouring sphingolipids, resulting in a more tightly packed, stiffer membrane domain. Raft-lipids also consist of more saturated tails and bigger head groups. Due to the latter, rafts are expected to be found preferably in the outer membrane layer. Rafts are thought to be dynamic, allowing protein and lipid exchange with their surroundings, but diffusion within a raft is slower due to the tighter packing. Molecules within a raft move more as a unit as compared to free individual movement outside a raft domain. No minimal or maximal size limit for rafts has been defined yet, as it has been very hard to visualise these, for microscopically resolution rather small, domains within live, dynamic cell membranes.

Rafts could play an important role in signalling processes, as clustering of receptors is often needed to initiate signal transduction. Other proposed areas of raft involvements are: caveolae-mediated endocytosis, polarised membrane trafficking and virus budding (Rajendran and Simons, 2005). A possible explanation of how micro-domains in the outer membrane layer can also influence the cytoplasmic, inner membrane is provided by the transbilayer coupling idea (Gingell and Owens, 1992). A changed order of the exoplasmic membrane leaflet (e.g. formation of rafts) would cause an rearrangement of lipids within the cytoplasmic leaflet due to spatial restrictions or repulsion/attraction of involved lipid tails. The existence of lipid microdomains has been indicated by qualitative (Harder et al., 1998) and quantitative (Pyenta et al., 2001) colocalisation as well as inter-raft FRET (Zacharias et al., 2002, Konig et al., 2008). But, controversy in relation to the rafts remains. For example: do rafts trap certain proteins? Is the trapping caused by rafts essential for the proteins function? Or can proteins cause a change in lipid composition and create a rafts as a consequence? The latter was shown for example by Hubbell, through the generation of a lipid asymmetry caused by the presence of bipolar proteins (Hubbell, 1990).

Actin polymerisation has been proposed to influence membrane dynamics. The actin cytoskeleton can create barriers for lipid diffusion (see section 1.2.3) and even trigger rearrangement of membrane components, i.e. initiate raft

formation (Liu and Fletcher, 2006). In order to use membrane diffusion as a readout for actin dynamics at the leading edge, we have to know whether changes within the measured lipid diffusion occur as a consequence of actin polymerisation or if changes within the membrane structure triggers actin polymerisation. The following section will explain possible restraints of membrane diffusion and their involvement with the actin cytoskeleton.

### **1.2.2 Membrane fence models**

By studying the movement of gold particle-labelled transferrin receptor within the membrane, the group of Akihiro Kusumi noticed an unexpected diffusion pattern (Sako and Kusumi, 1994). Single molecule techniques allowed them to follow the diffusion tracks of individual gold particles, i.e. of the transferrin receptor. The tracks showed rapid diffusion within small areas and sudden bigger jumps to other areas, where again a rapid but spatially restricted diffusion could be observed (see mimicked colored tracks in Figure 1-13).

Analysis of the many trajectories suggested a non-Brownian diffusion pattern. The authors postulated that the transferrin receptor is restricted in its movement by compartmentalisation of the plasma membrane: a molecule diffuses freely within one compartment for some seconds and then jumps into the next compartment. Such observations have been made possible by single molecule techniques, as the observation of multiple molecules at one time would mask single, time-wise randomly distributed jumping events.

Compartmentalised diffusion within the membrane can explain the long standing discrepancy between membrane diffusion in cell membranes and artificial membranes. Experimentally measured membrane protein diffusion rates in cell membranes are much smaller ( $0.01\mu\text{m}^2/\text{s}$ ) than in artificial membranes ( $5\text{-}10\mu\text{m}^2/\text{s}$ ). Sako et al showed that the diffusion rate of transferrin receptor within individual compartments is about  $10\mu\text{m}^2/\text{s}$ , as fast as in reconstituted membranes (Sako and Kusumi, 1995). However, this rapid movement is not correctly measured during macroscopic determination of diffusion coefficients using methods such as FRAP, because the compartment size is too small for these methods. A molecule stays within a compartment for around 29s and the

compartment size is approximately  $\approx 0.25\mu\text{m}^2$ . Distances measured during determination of diffusion rates with macroscopic methods are typically much bigger than individual compartments. The estimation of molecular mobility is therefore limited by the jumps between compartments rather than the rate of free diffusion. Thus, the movement between compartments may be seen as the reason for slower overall diffusion rates.

To explain what causes the boundaries between the membrane compartments, Kusumi's group proposed the "membrane skeleton fence" model (Figure 1-13a). According to this model, the membrane-associated portion of the cytoskeleton creates a fine mesh, where transmembrane proteins are trapped. The actin filaments act as fences that membrane proteins have to jump across in order to change compartments (Kusumi and Sako, 1996).

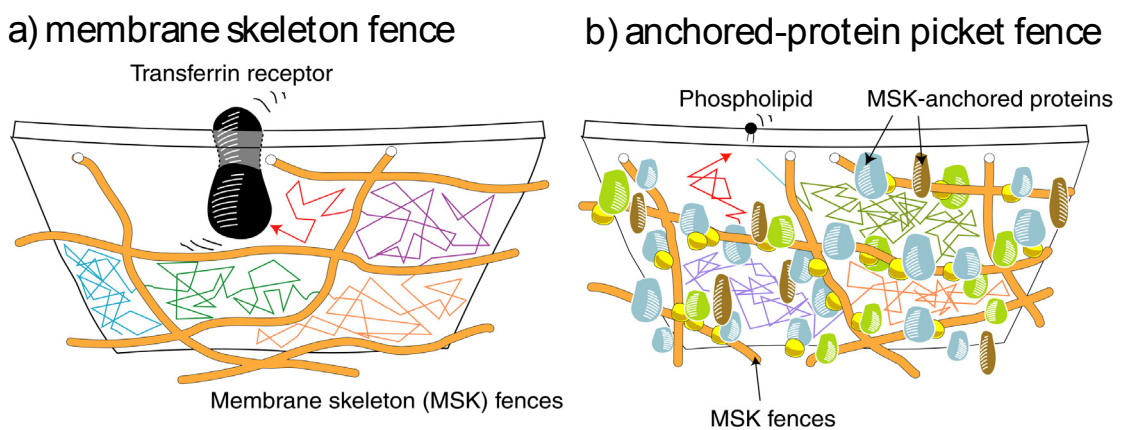


**Figure 1-13: Membrane Skeleton Fence and Anchored-Protein Picket Fence Models**

The initial "membrane skeleton fence" model (a) assumed that actin filaments (brown) create a barrier for transmembrane proteins (transferrin receptor – black). The revised "anchored-protein picket" model (b) adds some stationary proteins which act as pickets within the fence. This enables the fence to influence membrane diffusion in the outer membrane layer as well as in the inner one. The colored tracks in both schematics represent the diffusion pattern of single molecules. (figures taken from Kusumi online lab presentation)

Subsequent single molecule diffusion experiments using a labelled phospholipid (DOPE) in the outer membrane layer revealed similar trajectories as for the transferrin receptor which is located in the inner membrane layer. These observations could not be explained by the "membrane skeleton fence" model because this fence was thought to only influence membrane diffusion within the inner membrane bi-layer. Therefore, the "membrane skeleton fence" model was altered to the "anchored membrane-protein picket" model (Figure 1-13b; Fujiwara 2002). In this model the cortical membrane skeleton still serves as the

basis of the fence, but additional transmembrane proteins anchored to the actin filaments operate as pickets. Phospholipid trapping in the outer membrane leaflet is thought to be mediated by these pickets. According to this model, free diffusion of phospholipids is affected by steric hindrance as well as hydrodynamic-like friction events caused by the immobilised anchored protein pickets. This can explain why small phospholipids within the outer membrane layer are hindered in their diffusion. Possible physiological roles for such restricted diffusion include the localisation of signalling molecules to a specific region within the membrane, influencing situations such as chemotaxis, cytoskeletal reorganisation or protrusion.

### ***1.2.3 Examples of diffusion barriers***

The raft and fence models described above are possible explanations for restricted diffusion within membranes and are proposed to have implications for cellular processes such as polarisation and signalling. Diffusion barriers in general and more specifically barriers mediated by the actin cytoskeleton may regulate the protein composition of the membrane and influence the regulation of cellular processes. Such membrane influenced regulation may be important in the localisation of specific cell functions to certain cell regions.

To provide additional context for my work, the following subchapters will show some examples for diffusion barriers found in different cell systems.

#### **1.2.3.1 Tight junctions in epithelial cells**

Epithelial cells possess a rather obvious diffusion barrier: the tight junctions between neighbouring cells. The hindered diffusion of membrane components across these tight junctions was identified as early as the 1980s. Dragsten et al showed that fluorescent probes move freely within the outer layer of either the apical or the basolateral membrane, but are slowed down when diffusing along the side membranes where the tight junctions are (Dragsten et al., 1981). Flip-

flopping between the bilayers of the membrane could circumvent this barrier. It has subsequently been shown that the diffusion barrier in tight junctions depends on the presence of occludin (Balda et al., 1996). Expression of a C-terminally truncated version of this integral plasma-membrane protein specific to tight junctions was found to abolish the hindered diffusion of fluorescent lipids between the apical and basolateral membrane surface.

Selective transport of proteins to apical and basolateral membrane is thought to create the polarisation of epithelial cells. The apical and basolateral membrane are separate membrane compartments which possess very distinct features and properties, determined by the different proteins localised to each membrane area. Proteins destined for one or the other membrane surface possess specific targeting domains, which are recognised by the trans-Golgi network, which sorts the proteins into distinct vesicle populations (Winckler and Mellman, 1999). However, this selective transport alone is not enough and the tight junction diffusion barrier is needed for maintaining the polarisation of epithelial cell. Without a diffusion barrier, these proteins would become randomly distributed despite ongoing selective transport and no functional polarisation would be possible.

### **1.2.3.2 Axon Initial segment in Neurons**

Neurons are highly polarised cells. The somato-dendritic part (cell body and dendrites) receive and integrate signals, whereas the axon emits the output signal. These two domains are separated by a region called axon initial segment (AIS), which is the closest part of the axon to the cell body. Both domains contain different, specific molecules. This distribution is thought to be generated by selective transport, which is responsible to deliver the right molecules to the right domain (Kandel et al., 2000). However, this selective transport alone may not be sufficient as a mechanism to explain the highly polarised state of neurons. It does not, for example, explain why selectively transported proteins remain within their respective domains rather than mixing randomly. Several studies have investigated whether the initial segment separates protein populations by restricting their diffusion. Although some

findings concluded the non-existence of a lipid diffusion barrier in neurons (Futerman et al., 1993, Winckler and Poo, 1996), other experiments resulted in evidence supporting the existence of a diffusion barrier (Kobayashi et al., 1992, Winckler et al., 1999).

Winckler et al. initially found that the small lipid membrane dye, Dil, is able to freely diffuse between the different neuronal domains (Winckler and Poo, 1996), but later realised that this is not the case for membrane proteins (Winckler et al., 1999). The movement of different membrane associated proteins was measured using optical tweezers and antibody-coupled beads. It was not possible to drag the beads across the axon's initial segment. This AIS diffusion barrier was disrupted by treatment with the actin-depolymerising drug LatA, suggesting a direct or indirect tethering to the underlying cytoskeleton caused the diffusion barrier at the axial initial segment. This explanation would correlate with the membrane fence models (see section 1.2.2). The Kusumi lab confirmed the existence of a diffusion barrier at the AIS in 2003 using single molecule tracking and also showed a possible explanation for previous inconclusive results (Nakada et al., 2003). They found that the diffusion barrier is only formed between day 7 to 10 of cells in culture. Before, diffusion of the phospholipid DOPE was similarly fast in all neuronal compartments, but from day 7 a considerably slower diffusion rate across the initial segment could be observed. The authors conclude that the accumulation of membrane proteins anchored to the underlying cytoskeleton creates a picket fence which hinders the diffusion of membrane proteins. The accumulation happens successively during the formation of the axon and the final polarisation, which explains why the diffusion barrier cannot be seen in young cells (Futerman et al., 1993). Earlier controversy about the existence of an AIS diffusion barrier can therefore be explained by the probe used for diffusion measurements, the experimental method and by the age of the cells.

### **1.2.3.3 diffusion barrier at the leading edge of fish keratocytes**

Following the hypothesis of the Anderson lab, that membrane diffusion might be affected by actin-membrane interactions during lamellipodial protrusion, it was

shown that lipid diffusion within the membrane is hindered in its movement around the leading edge of protruding fish keratocytes. As these results form the starting point for my work, the following subchapter will explain in detail the findings of the publication “The leading edge is a lipid diffusion barrier” (Weisswange et al., 2005) and describe the unique technique used.

Actin polymerisation at the leading edge is a difficult process to study, in part due to its fast dynamics restricted to such a small space. An investigation of the membrane diffusion was thought to give an insight into processes involved in polymerisation and force production without interfering. The method of Focal Labelling and Observation of Initial diffusion (FLOID) was developed for this purpose and is shown schematically in Figure 1-14 (taken from (Weisswange et al., 2005)) below.

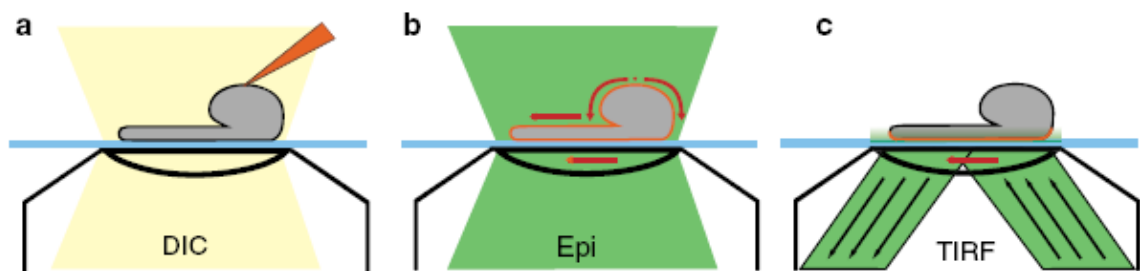


**Figure 1-14: Focal Labelling and Observation of Initial Diffusion (FLOID)**

Schematic diagram of focal labeling and observation of initial diffusion (FLOID). (a) The cell body is lightly touched by a micro-needle containing carbocyanine dye. (b) Epi illumination shows dye spreading in both dorsal and ventral cell membranes. The shortest diffusion path from the labeling point to the leading edge is via the dorsal membrane. (c) TIRF illumination shows only the ventral cell membrane (taken from (Weisswange et al., 2005))

In a FLOID experiment a migrating fish keratocyte was labeled locally with Dil C12 at the highest point of the cell body through contact with a dye coated needle (Figure 1-14a) and sequential TIRF and epi-fluorescence time-lapse images were recorded to observe spreading of the dye. Whereas epi-fluorescence excites dye molecules located in the dorsal and ventral cell membrane, the evanescent wave illumination of TIRF only excites fluorophores in the ventral membrane. Analysis of the dye fluorescence in TIRF and epi image sequences could therefore be used to investigate the diffusion of the dye around the leading edge during protrusion. It was observed that the dye always reached the leading edge first via the dorsal membrane, which is due to a path length difference (figure 4-2). However, spreading of the dye across the ventral surface

(i.e. in the recorded TIRF sequence) could result in two distinct intensity profiles (Figure 1-15c and d).

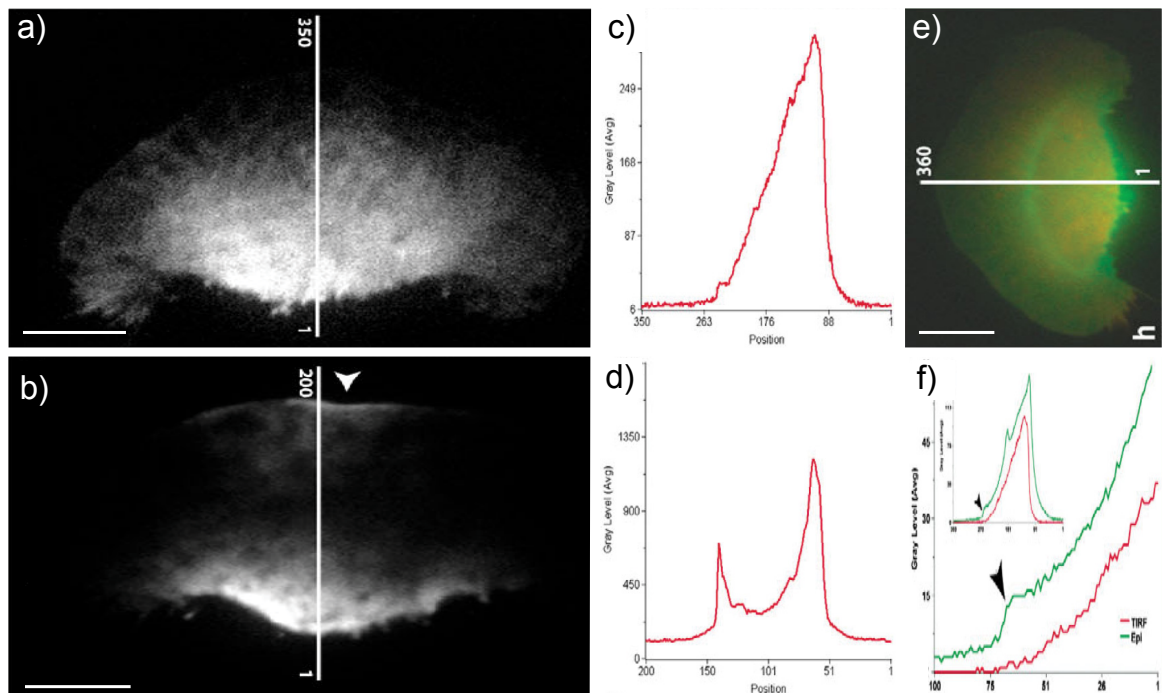


**Figure 1-15: FLOID analysis of migrating keratocytes**

The intensity scan of TIRF images (a and b) resulted in two different intensity profiles of dye fluorescence: single-peak profile (c) or double-peak profile (d). Comparison of TIRF and epi intensity profiles (f, resulting from line scan in image e) showed dye accumulation at the leading edge (black arrow head at green (epi) curve in f).

A single peak intensity profile (Figure 1-15a, c) represents dye spreading from the dorsal to the ventral surface via the rear of the cell body only. The main intensity is therefore at the back of the cell and falls off towards the front of the cell. In contrast, if the dye reaches the ventral surface by diffusing from the dorsal surface via both the front and the rear of the cell, the intensity profile will show a double peak (Figure 1-15b, d). The two peaks represent dye intensity at the ventral surface edges, whereas a much lower intensity is observed between the peaks, indicating that the dye has not reached the middle of the cell yet. In time, the dye will completely label the plasma membrane and the TIRF intensity profile of both cases will look similar. The classification of cells according to the intensity profile was therefore done at an initial stage of dye spreading, before the complete labeling of the cell.

For the single peak profile it was crucial to be certain that the dye diffusing in the dorsal membrane had reached the leading edge. As shown in Figure 1-15f, a

step function within the intensity curve indicated accumulation of dye at the leading edge. This accumulation of dye on the dorsal surface without spreading to the ventral surface could be observed for up to 7sec. The single peak situation therefore represented a blocked lipid diffusion around the leading edge. After analysis of a total of 138 cells, this profile was observed in 86% of cells. The other 14% of cells showed a double peak profile. Interestingly, it could be observed that these cells often possessed retracting leading edge regions. These results suggest that the protruding leading edge is a barrier for lateral diffusion of Dil C12.

Weisswange et al further studied the dependence of this diffusion barrier on the existence of free, polymerization competent and force producing actin filament plus ends by treating cells with Cytochalasin B (CytB). As this drug causes a loss of lamellipodium (Anderson et al., 1996) cells were pre-treated with Concanavalin A (ConA) in order to preserve the cell morphology necessary for diffusion analysis. ConA treatment alone stopped cell movement but introduced centripetal flow of actin filaments within the lamellipodium. FLOID analysis of these cells revealed that 51% of ConA immobilized cells had a single peak profile and a diffusion constant of  $3.9 \times 10^{-8} \text{cm}^2/\text{s}$  was measured for the dye spreading. In contrast, only 4% of ConA and CytB treated cells showed a single peak profile, leading Weisswange et al to the conclusion that the existence of a leading edge lipid diffusion barrier depends on actin polymerisation. This was also observed using Cytochalasin D (CytD) instead of CytB.

The authors next tested whether this inhibition of Dil C12 diffusion involved lipid microdomains. Dil C18, a carbocyanine dye with longer acyl chain than Dil C12, showed an equal inhibition in diffusion around the leading edge. Neither of the dyes, as well as an ordered phase marker cholera toxin was enriched in or excluded from any locations within the cell membrane, suggesting a rather homogeneous, non micro domain influenced diffusion. In a second approach cholesterol was extracted to disrupt membrane domain organisation. FLOID analysis resulted in 75% of cells showing a diffusion barrier at the leading edge, compared to 86% in untreated cells. If the diffusion barrier were dependent on microdomains, cholesterol extraction would be expected to abolish the diffusion barrier. It was also observed that the cholesterol extraction reduced the intensity of phalloidin staining by 25%, suggesting that the lower percentage of

cells with diffusion barrier could be due to the reduction of actin filament density. All these results led to the conclusion that the lipid diffusion barrier at the leading edge does not depend on lipid microdomains.

Weisswange et al proposed that the leading edge lipid diffusion barrier might be caused by protein density or force produced by actin polymerization. Based on actin filament density estimates (Abraham et al., 1999, Small et al., 1995), the authors conclude, that the density of actin filaments at the leading edge alone is too sparse to hinder the diffusion of sub-nanometer lipid molecules. In contrast, a high density of membrane-associated proteins at the leading edge would be sufficient to block dye diffusion. In the case of trans-membrane proteins it is easy to imagine how these proteins can occupy large amounts of membrane space and therefore leave little space for the dye to diffuse around them. If actin filaments were linked to these transmembrane proteins (temporary or permanently), a fence-like structure could be created.

Another possible explanation would be that the force produced by actin polymerisation creates the lipid diffusion barrier. Force induced changes within the inner membrane layer could then be mediated to the outer membrane layer via bilayer coupling between the membrane lipid acyl chains. Such influence of actin polymerisation on membrane domain formation was later shown by Liu and Fletcher (Liu and Fletcher, 2006) and could be involved at the leading edge.

Finally, Weisswange et al speculated that the leading edge lipid diffusion barrier could function as a trap for actin regulating factors at the leading edge and therefore represent a positive feedback loop for actin polymerisation. Following an initial signal to start actin polymerisation at the leading edge, the force generated by the polymerisation would then create the lipid diffusion barrier and in this way guarantee the presence of enough actin-regulating proteins to further promote polymerisation. This mechanism would therefore only rely on a short initial start signal, as compared to a constantly present initiator of actin polymerisation.

#### 1.2.3.4 Other examples of diffusion barriers

In addition to the above examples of diffusion barriers presented in detail, below are some further examples to show the wide-spread influence of such phenomena.

- ❖ sperm head: There is a diffusion barrier for large complexes between the postacrosome and the equatorial segment. Individual DiI16 molecules were able to diffuse between the two departments, but large particle clusters were not. The hypothesis include the disassembly of large complexes at the postacrosomal side, diffusing over the barrier and reassembly in the equatorial segment, where the newly formed complex would be hindered by the diffusion barrier from moving back to the postacrosome (James et al., 2004). The analysis were done using techniques such as FRAP and FLIP and diffusion coefficients for DiI12 were similar to the ones shown in this thesis ( $D_{\text{James-midpiece region}} = 0.91\mu\text{m}^2/\text{s}$ ;  $D_{\text{fish keratocytes}} = 1.09\mu\text{m}^2$ ).
- ❖ node of ranvier: Junctions between the paranodal glial and the axon promote the transition in sodium channel subtypes (Nav1.2 to Nav1.6) and provides a lateral diffusion barrier. This is essential for integrity of voltage-gated channel domains, needed for impulse propagation. These experiments were done studying node development in Caspr (an integral junction component) mutant mice. (Rios et al., 2003)
- ❖ budding yeast: IST2 encoding mRNA is transported to the bud tip by an acto-myosin-based process and this concentration of mRNA results in a higher IST2 protein concentration within the bud (compared to the mother cell). This enriched localisation of this plasma membrane protein is maintained by a diffusion barrier at the mother-bud neck. A temperature sensitive mutation in the septin gene revealed that septin is crucial for the function of this diffusion barrier. Due to the highly efficient diffusion barrier, these experiments could be performed by localisation studies of fluorescently tagged IST2 protein (Takizawa et al., 2000).

## **1.3 A brief introduction into imaging methods relevant for this thesis**

A major goal of this thesis was to investigate the interaction between actin and the membrane at the leading edge, using advanced imaging techniques in order to capture but not influence the very dynamic and delicate process of protrusion. This part of the introduction chapter will give a short overview of microscopy in general and a closer insight into the used microscope techniques.

### ***1.3.1 History and types of microscopy***

Some of the principles necessary for modern microscopy were already used more than 2000 years ago. According to a legend, Archimedes (Greece, 287-212 BC) used mirrors to divert and focus sunrays onto roman ships, causing them to burn. And although “burning” and “magnifying glasses” are mentioned in writings of many other philosophers, it was not until the 10th century before written theories about the function of these devices appeared. Ibn Sahl, a Baghdadi mathematician, formulated the first geometric theory for lenses and postulated the shape of a perfectly focusing lens (anaclastic) (Salih et al., 2005). He also discovered the sine law of refraction, nowadays known as Snells law. The 11<sup>th</sup> century Arab physicist Alhasan Ibn Haitham revolutionised the ideas of light by stating that it travels in straight lines and has a finite speed. His experiments and conclusions on refraction and reflection of light as well as his study of the properties of lenses were recorded in his “book of optics”, which can be seen as one of the most influential books in physics.

Although single lenses were used as magnifying eye glasses (spectacles, Salvino D’Armate), it was only in the late 16<sup>th</sup> and early 17<sup>th</sup> century that people realised that objects could be further magnified by arranging several lenses together (Z. and H. Janssen, Galileo) (Salih et al., 2005). The arrangement of several lenses is nowadays called a compound microscope, whereas a one-lens microscope is called simple microscope. Anton Van Leeuwenhoek’s was one of the first scientists to use a microscope for his studies. Although he only used a

simple microscope, he achieved a magnification of up to 270 times, mainly due to his skills at grinding lenses. This was enough to observe, amongst other things, bacteria, yeast plants and living organisms in a water drop. The design of the microscope was steadily improved, and by further understanding of the underlying physics, initial problems like chromatic aberrations could be corrected and many powerful microscopes for specific applications were created. Nowadays, microscopy can be divided into three types: optical (or light), scanning and electron microscopy. All techniques used in this thesis fall into the first category and I will focus my brief introduction on this group.

Wide-field transmission microscopy describes the classic approach to optical microscopy, where the entire field of view is illuminated and the illumination light passes through the sample. Early compound microscopes consisted of two lenses: one objective and one eyepiece lens (Figure 1-16a). The final magnification results from the multiplication of the individual magnification of both lenses and commonly ranges between 40-1000 times. The introduction of any additional pieces into this arrangement would disturb the light path and change the position of the intermediate image. As the eyepiece lens is focused on this intermediate image, a displacement of this image would result in a poor final image. The development of an infinity-corrected light path through the addition of an extra lens (Figure 1-16b) was therefore an important step in order to expand the use of wide field microscopy to techniques like DIC (differential interference contrast) and fluorescence, which require additional elements between objective and eyepiece.

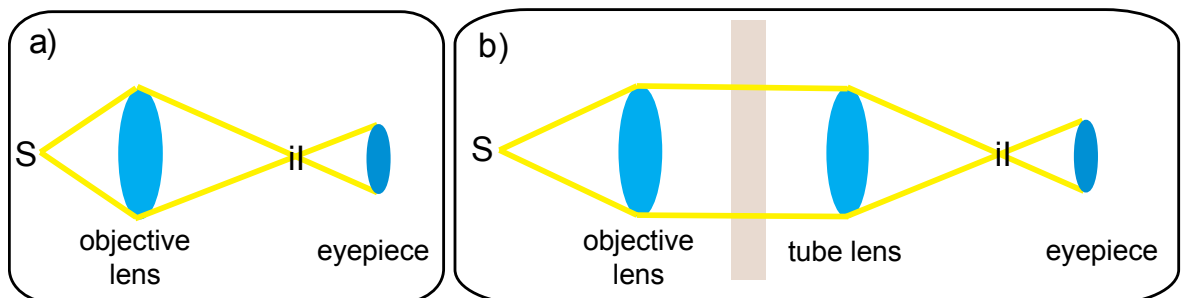


**Figure 1-16: finite and infinity-corrected optical light paths**

In a finite optical system (a) the objective lens forms an intermediate image (II) of the specimen (S), which is then observed by the eyepiece lens. The addition of an extra lens (infinity-corrected light path, shown in b) creates a parallel light beam between the objective and the tube lens. This is advantageous because the position of the intermediate image stays equal even after moving the objective lens (to focus on different planes) or introducing inserts (light brown plate in image) into the light path.

Fluorescence is a property of certain defined chemical structures which are able to absorb and emit light. A photon with the right energy is able to lift an electron from the ground (lowest-energy state, naturally preferred by molecules) to the excited state. The electron will stay for a while in this state of higher energy and then fall back to the ground state while emitting light, which, due to the loss of energy through vibrations or heat, is commonly of lower energy (i.e. higher wavelength) than the excitation light. The difference in excitation wavelength and emission wavelength is called the Stokes shift and the bigger this difference is, the easier it is to separate both excitation and emission lights using optical filters. A fluorophore can be excited by light of different wavelengths within a certain range. This range is represented by the excitation spectra (Figure 1-17a) and the highest efficiency in excitation will be at the peak wavelength. The emitted light also shows a range of wavelengths with maximal emission intensity at a certain wavelength. A general property of fluorescence is that the emission spectrum is in most cases independent of the excitation wavelength. A fluorophore may be excited with light of different wavelengths, but the emission can be measured within the same range every time.

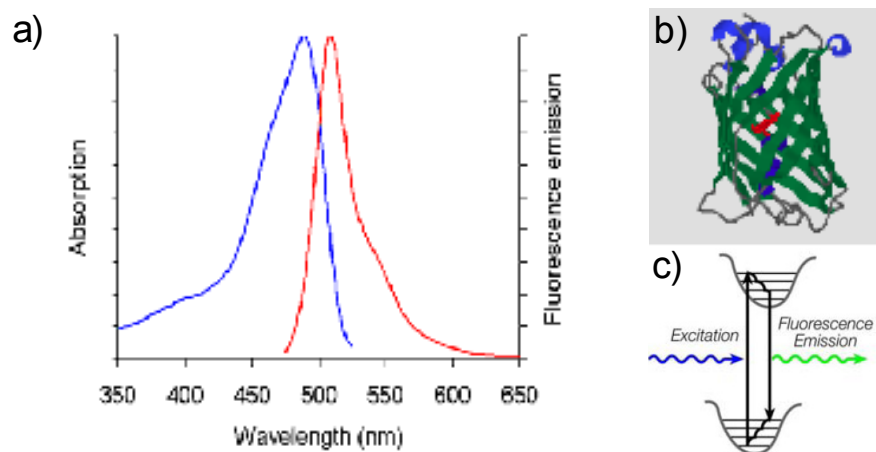


**Figure 1-17: Fluorescence**

The absorption (blue) and emission (red) spectra of GFP (a), its structure (b) and a Jablonski diagram (c). The absorption of a photon causes an electron to rise from the energetic ground state to the excited state. After some time within this higher energy state, the electron falls back to the ground state and emits a photon with a higher wavelength (lower energy).

Many natural substances have the ability to absorb and emit light. One of the first materials in which this phenomenon was observed was a solution of quinine sulphate and the optical phenomenon it displayed was described as followed: “Though perfectly transparent and colorless,....., it yet exhibits in certain

aspects, and under certain incidences of the light, an extremely vivid and beautiful celestial blue color...” (Herschel 1845, referenced in (Lakowicz, 2006). Many other substances were found to possess this property of changing the wavelength of light when illuminated with a specific wavelength and in 1962 a green fluorescent protein was discovered in the jellyfish *Aequorea* (Shimomura et al., 1962). Initially only observed as a side product during the purification of the bioluminescent protein Aequorin, this green fluorescent protein (GFP) proved to be invaluable for biological science. The important breakthrough came in 1994, when the group of Douglas C. Prasher showed that this protein could be expressed in other organisms and its fluorescence can be used to mark the expression of other genes (Chalfie et al., 1994). This discovery has allowed scientists to label proteins of interest and observe their behaviour in live cells.

The setup of a fluorescent microscope is slightly different from the setup of a transmitted light microscope described earlier. An epi illumination setup is used, where the excitation light comes through the objective, i.e. from the same side of the sample as where the detector is placed (Figure 1-18a). The very intense excitation light is passing through the sample and does not reach the detector or the eyepiece. Only emitted light from the sample can reach the detector. A combination of appropriate excitation and emission filter and dichroic mirrors are added to the light path in order to select the desired wavelength and direct the light into the right direction within the microscope. One problem with wide-field fluorescence microscopy is the illumination and imaging of the fluorescence of the whole sample. An image of a thick sample with lots of fluorescence will look blurred with little contrast, which makes it difficult to clearly see small structures. Several techniques have been invented to introduce optical sectioning, and therefore more contrast, into fluorescent microscopy, some commonly used ones are: confocal microscopy, multiphoton microscopy and Total internal reflection microscopy (TIRF). The latter one will be explained in detail in section 1.3.2.

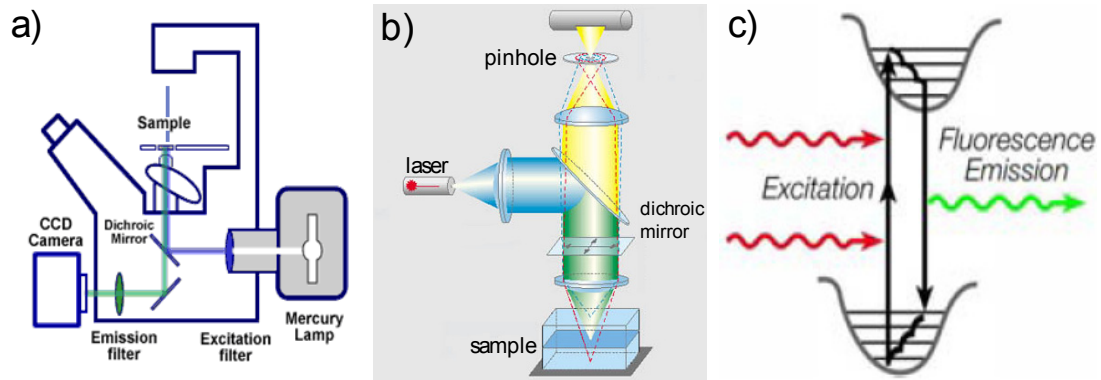


**Figure 1-18: epi-fluorescence, confocal and multi-photon**

In a), a representation of an epi-fluorescence microscope is shown. The excitation light is directed towards the sample by a dichroic mirror, where the emitted light passes through due to its altered wavelength. The main intensity of the excitation light passes through the sample, avoiding the detector and eyepiece, where only emitted light arrives. The confocal setup is shown in b). A similar setup as for epi is used, but, besides having a scanning laser, a pinhole is added in front of the detector. This pinhole cuts off emitted light from out-of-focus areas of the sample (light blue). The Jablonski diagram in c) shows the excitation principle of multi-photon microscopy. Two photons with half the normal excitation energy (around twice the wavelength) have to hit the fluorophore simultaneously in order to bring an electron from the ground state into the excited state. Emission will then occur in the normal, fluorophore dependent wavelength.

Confocal microscopy creates sectioning by introducing an aperture, also called pinhole, in front of the detector, where only light coming from the focal position of the objective can pass through (Figure 1-18b). Out of focus light, emitted from fluorophores outside the focal plane, will be blocked by the pinhole. Changing the diameter of the pinhole opening influences the thickness of the imaged section, the smallest one normally being around 350nm. The pinhole only affects emitted light, which means that the excitation light path is equivalent to that in wide-field fluorescence microscopy. One difference is the use of a focused laser beam which scans the image point by point instead of illuminating it at once. The laser passes through the whole sample, which may cause photo-damage, but as the beam is focused on the one focal plane at a time, its intensity outside this focal plane is less, reducing the possible damage. One great advantage of a confocal is the acquisition of multiple z-stacks through one sample, leading to a 3-D representation.

Multi-photon microscopy creates the optical sectioning by selective illumination. It is based on the use of light having a wavelength around twice the normal excitation wavelength and therefore carrying only half the energy per photon. Consequently, two photons are required to hit the fluorophore at the same time in order to lift an electron to the excited state (Figure 1-18c). A pulsed laser is

used to increase the intensity of photons. The density of the photon beam is the highest in the focal plane, which therefore has the highest probability of two photons exciting the same fluorophore at the same time. Outside the focal plane, the photon density is much lower and fluorophores outside the focal plane will not be excited and do therefore not emit light. As a result of selective illumination, multi-photon microscopy creates less photo-damage than confocal microscopy. Due to the higher wavelength it can also penetrate deeper into tissue, as longer wavelengths are less affected by scattering. The typical optical sectioning achieved by multi-photon microscopy is around 500nm.

### ***1.3.2 Total Internal Reflection Fluorescence Microscopy***

At the interface between two media with different refractive indices, light changes its direction of travel and is both refracted and reflected. If light passes from a medium with higher refractive index (i.e. glass=1.52) to a medium with lower refractive index (i.e. water=1.33), the exit angle for refraction is bigger than the initial incident angle of the light. By increasing the angle of incident, a critical angle is reached where the light beam is completely reflected back into the first medium. At the site of such total internal reflection, an evanescent wave is created, which penetrates into the second medium with exponentially decreasing intensity. The use of this evanescent field illumination was first described as surface contact microscopy by Ambrose (Ambrose, 1956), who used this technique to study cell adhesion. In the early 1980s Daniel Axelrod expanded the application of the evanescent field illumination to fluorescence (Axelrod, 1981, Axelrod et al., 1983), and established a new technique for optical sectioning - Total Internal Reflection Fluorescence (TIRF) Microscopy. The interface for reflection is between glass ( $n \approx 1.5$ ) and the sample, which has to be in an aqueous solution or possess a refractive index similar to water (1.33). By bringing collimated laser light to the critical angle where total reflection occurs, an evanescent wave is formed (Figure 1-19b). An important property of this wave is, that its intensity exhibits an exponential decay from the glass-water interface, and is only able to penetrate around 150-200nm into the sample. The penetration depth is also called evanescent field. The fluorophores

within the evanescent field are excited, whereas fluorescent molecules outside this depth, i.e. further away from the glass interface, cannot be excited by the evanescent wave.

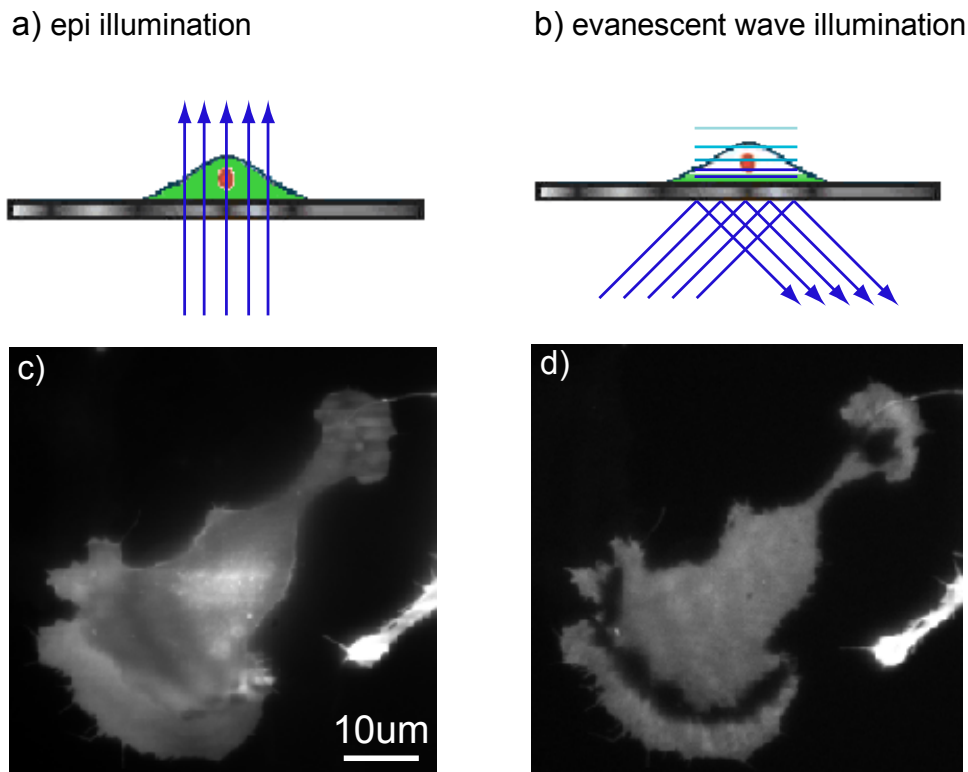


**Figure 1-19: comparison between epi and evanescent wave illumination.**

If the incident angle of the laser is  $90^\circ$  and the excitation light passes straight through the sample. All fluorophores in the sample will be excited (a and c). In total Internal Reflection Fluorescence microscopy, the laser beam impinges on the glass-sample interface with an angle higher than the critical angle, where the beam will be totally reflected (typically  $c_{crit}$  is around  $61^\circ$ ). This reflection results in the creation of an evanescent wave propagating into the low refractive index medium. Due to its exponential decrease in intensity, the evanescent wave extends into the sample only for a short distance and only fluorophores within 100-200nm will be excited (b and d). Fluorophores above this area will not be excited and do not contribute to the recorded emission, resulting in an intensity image of the basal fluorophores only.

In normal epi fluorescence microscopy, molecular structures and features close to the basal membrane cannot be observed clearly, as their signal is overpowered by fluorescence from other sections within the cell (Figure 1-19c). The selective excitation of fluorophores close to the glass-sample interface results in a much improved contrast (Figure 1-19d) and TIRF microscopy is widely used to study processes such as adhesion, endo- and exocytosis and membrane diffusion. In comparison to a confocal setup, where the images also represent fluorescence from sections of the cell, TIRF microscopy results in thinner slices. Whereas confocal sections are around 350nm, the TIRF section is roughly 150nm.

Another advantage of the selective illumination is the reduction of photo-damage in the cell.

Evanescent field illumination is commonly achieved by two different methods: prism-type or objective type (Figure 1-20).

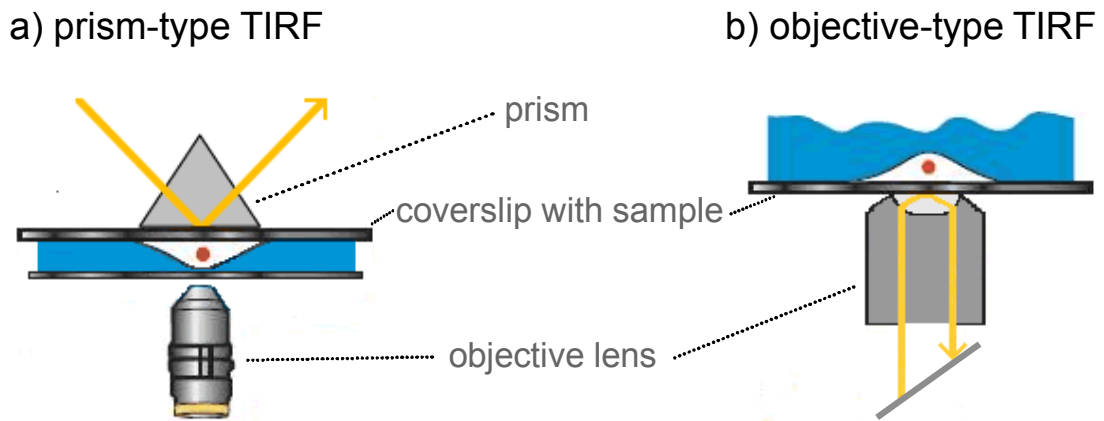


**Figure 1-20: TIRF techniques**

The Total Internal Reflection of a laser beam at the glass-sample surface can be achieved in two different ways. Historically the prism-method was used first, as it could be performed using standard NA objectives. An external collimated laser beam is directed through a glass prism positioned on the glass-sample interface, where the beam will be totally reflected. The emission of the illuminated fluorophores will be captured by the objective of the microscope (b). The glass prism with an numerical aperture identical to the glass used for sample preparation is necessary to prevent the beam from being refracted before reaching the glass-sample interface. The use of a high numerical objective ( $NA > 1.40$ ) allows excitation and emission through the objective (b). The sample can therefore be positioned right-side-up.

The initial prism-type TIRF method (Axelrod, 1981) uses normal (low NA) objectives, as used for other microscope techniques. The total internal reflection is created by a collimated laser beam passing through the glass prism or cube which is in contact with the coverslip containing the sample. A collimated parallel laser beam is necessary to assure that all light rays are hitting the glass-water interface at the same angle. The emitted light in this prism-type setup is observed using the normal optical arrangements of a microscope. Disadvantages of this method are that the sample is squeezed between prism and objective and is upside-down if using an inverted microscope (Figure 1-20a). The use of an upright microscope allows the application of cells in a petridish, but only in conjunction with a dipping lens and more complicated technical arrangements (prism and external laser are below the sample). The second type of TIRF microscopes uses illumination through the objective to

create the evanescent wave. This was made possible by the creation of high numerical aperture (NA) objective lenses. Lower NA objective did not allow a high enough angle of illumination light in order to achieve total internal reflection. The new high NA objectives allowed this and the illumination light could be brought to the critical angle (Figure 1-20b). This enabled the observation of live cells in dishes under evanescent field illumination. The setup of an objective-type based TIRF illumination requires small modifications to an existing epi fluorescence microscope. To achieve a parallel light beam leaving the objective, an additional lens is introduced in an attached TIRF condenser (Figure 1-21). In this arrangement the illumination angle is controlled by the position of the light source, generally an optical laser fibre (red arrow in Figure 1-21b).

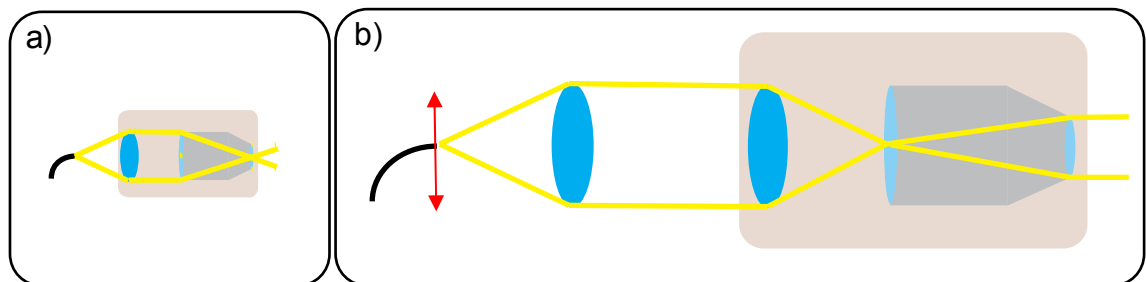


**Figure 1-21: schematical light-path setup of epi-fluorescence and TIRF**

In an epi-fluorescence microscope the laser beam is focused in the objectives focal plane (a), whereas TIRF requires focusing at the back-focal plane of the objective. This results in parallel light at the objective exit. The angle of this parallel light beam can then be adjusted for evanescent field illumination by moving the optical laser fibre output (red arrow)

Several commercial TIRF microscopes are available, but they are not ideally setup for multi-colour TIRF imaging. In most of them, multiple laser lines are combined through one fibre which dictates the same incident angle for all illumination wavelengths. However, the angle of refraction (and therefore also the critical angle for internal reflection) depends on the wavelength, as each wavelength possesses a different velocity in materials. Therefore, ideally, individual critical angles for each wavelength are needed to achieve optimal total internal reflection. Commercial TIRF microscopes with a single laser output do not allow individual critical angle adjustments, which means a compromise in evanescent illumination quality has to be made. The TIRF setup at the Beatson (described with technical details in Material and Methods section 2.4) was setup to allow individual illumination angle adjustments for 3 different laser lines

(405, 473, 561). One disadvantage of the Beatson setup is the weak epi illumination, which results from inefficient light collection due to the distant placement of the Xenon lamp in the illumination pathway. As a result, the epi illumination quality is rather poor and we tend to use laser illumination for epi instead of the Xenon lamp. However, this means that sequential epi and TIRF images for one fluorophore cannot be achieved in an ideal quality. But, with the three individually adjustable laser beams, we can perform many combinations of dual-colour TIRF or one colour TRIF and one colour laser-epi fluorescence. We are also able to use the 405 laser for photo-bleaching or -activation in evanescent field illumination. In short, our TIRF microscope provides great evanescent field illumination combined with flexibility to choose different angle positions and combinations of laser lines. This microscope has been intensively used by other research groups at the Beatson with our help, resulting in several collaborative publications. Figure 1-22 shows data from some collaborative projects.

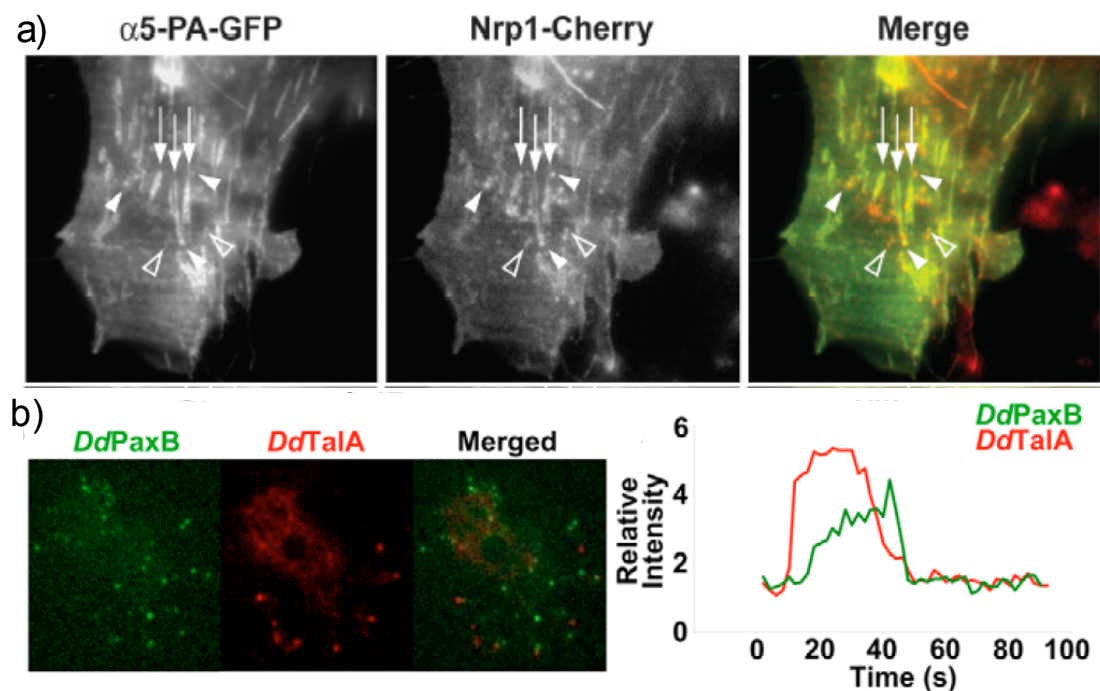


**Figure 1-22: applications of the Beatson TIRF setup**

a) NiH 3T3 cells were transfected with mNrp1-cherry and a5-PA-GFP. Latter was photoactivated with evanescent field illumination and observed in time-lapse epifluorescence microscopy, whereas mNro1-cherry was observed using TIRF. These data are part of the following publication: (Valdembri et al., 2009) (see appendix)

b) A distyostelium cell was transfected with Paxilin-GFP and Talin-RFP and their appearance and disappearance was measured (results shown in graph). These data are published in: (Patel et al., 2008) (see appendix).

In order to optimise the performance of our TIRF microscope, we developed a test sample (Figure 1-23a). Fluorescent beads were attached to a glass bottom petridish, the same type we used for experiments with cells. Then, a Fluorescein solution was added. This combination mimics the *in cellulo* situation of dim features within a high fluorescent cytoplasmic background. An estimation of image contrast (ICE) was calculated by comparing bead to background intensities and this value was calculated for different incident angles. This ratio increased hugely when the critical angle was reached. This sample allowed us to test different TIRF-objectives and assess their quality (Figure 1-23b). Although the 1.49NA Nikon objective gave a wider range of illumination angles in TIRF, better contrast was achieved with the lower NA (1.45) Nikon objective. This sample is generally useful for quality control of TIRF systems, as it provides numbers which can be compared over time as well as among different systems (manuscript in preparation, see appendix - list of publications)

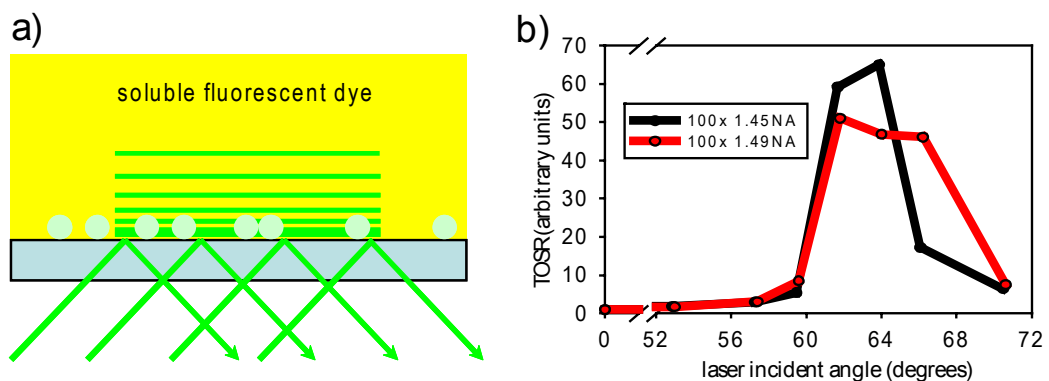


**Figure 1-23: TIRF test sample**

The TIRF test sample (a) consist of fluorescent beads attached to the glass coverslip and a fluorescent solution. The ration between bead intensity and background intensity provides an estimation of image contrast (ICE) for epi and different TIRF angles and the ration between the epi ICE and each TIRF ICE provides a TIRF optical sectioning ratio (TOSR) value, which can be used to compared different objectives (b) and other system parameters such as laser intensity. Whereas the TOSR is low in epi illumination, a sharp increase can be observed when the incident angle exceeds the critical angle and evanescent field illumination is exciting the sample ( $> 61^\circ$ ). For our system, it could be shown that an objective with a numerical aperture (NA) of 1.45 gives a higher TIRF contrast than an objective with higher NA (1.49), but the latter one allows to keep a good contrast for shallower angels than the lower NA objective.

### 1.3.3 Fluorescence Recovery after Photobleaching

Fluorescence Recovery after Photobleaching (FRAP) is a method to determine the mobility of molecules within a cellular environment. A defined region of fluorescent molecules is bleached with high laser intensity in order to destroy their ability to emit fluorescence (Figure 1-24a). Through recording a timelapse, the exchange of non-fluorescent molecules with fluorescent molecules from other, non-bleached regions can be quantified. A typical recovery curve of FRAP measurements is schematically shown in Figure 1-24b.

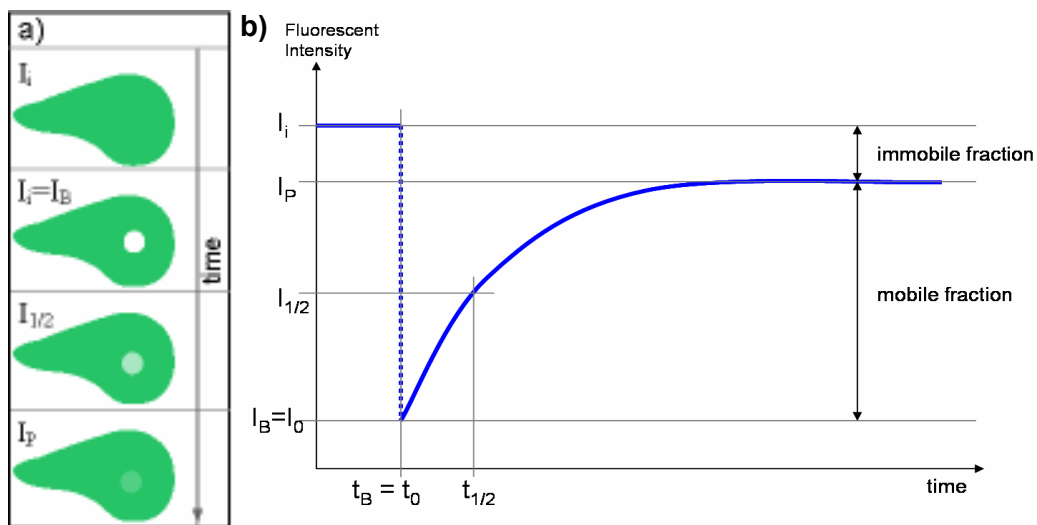


**Figure 1-24: FRAP recovery**

A FRAP experiment consists of a sequence of intensity images before and after the targeted bleaching event (a). The intensities within a region of interest (ROI) can be displayed graphically over time (b). At the beginning the initial Intensity ( $I_i$ ) is determined, which then drops rapidly to  $I_0$  during the targeted bleach event and then rises back up to a certain level of Intensity ( $I_P$ ), where a plateau effect occurs. In the case of ideal, single component diffusion a recovery curve (from  $I_0$  to  $I_P$ ) can be approximated by an exponential rise function.  $T_{1/2}$  can be extracted from this part of the curve, by finding the time point correlated to half of the final intensity ( $I_{1/2} = I_P/2$ ). To obtain the mobile/immobile fraction, the intensity values before the bleach, directly after the bleach and at the reached plateau are needed. The immobile fraction represent the amount of bleached molecules trapped in the bleached area and can be calculated using the following formula:  $(I_P - I_0)/(I_P - I_0)$ .

This curve provides two main parameters: halftime of recovery ( $t_{1/2}$ ) and mobile/immobile fraction.  $T_{1/2}$  is defined by the time at which the recovered intensity has reached half of the final plateau intensity ( $I_P$ ). The mobile fraction represents the percentage of molecules which can be exchanged with new fluorescent molecules. Respectively, the immobile fraction equals the amount of molecules trapped in the bleached area. The half-time of recovery can be composed of many different processes, such as diffusion, endo- and exocytosis

and binding events. To distinguish between these events is complicated but may be achieved through combination with other microscope techniques (e.g. photo-activation), sophisticated mathematical analysis and mathematical modelling of the process. Most commonly, FRAP is used to compare the recovery of molecules undergoing similar processes or to measure simple diffusion. The latter case was first described by Axelrod in 1976 (Axelrod et al., 1976), who introduced the fluorescence photo-bleaching recovery (FRP) as a method. He also derived theoretical, mathematical equations to describe different recovery situations. Practically, one has to extract  $t_{1/2}$  by finding the time point where half of the plateau intensity has been reached. With the use of curve fitting programmes this point can be found by fitting an “exponential rise to maximum” equation on the data:  $I = I_0 + a(1 - \exp(-bx))$ , where the parameter  $b$  is used to calculate  $t_{1/2}$  using the following equation:  $t_{1/2} = \frac{\ln 2}{b}$ . In the case of pure diffusion  $t_{1/2}$  is not a suitable parameter to compare different experimental results, as it is influenced by factors like the size of the bleached region. For diffusion scenarios it is therefore better to calculate the diffusion constant  $D$ . Axelrod presented the following equation:  $D = \gamma_D * \frac{w^2}{4 * t_{1/2}}$ , where  $\gamma_D$  is a constant depending on the shape of the laser beam and the amount of bleach, and  $w$  is the radius of the bleached circle.

Another approach (compared to the exponential curve fit) to determine the diffusion constant from FRAP experiment data is to compare the profile across the bleached area at different time points. This method was described by Conrad W. Mullineaux and colleagues and I will refer to this method as “Mullineaux method”. This method was originally used for one-dimensional FRAP measurements of the membrane of cyanobacteria. By bleaching a horizontal line through the bacteria (Figure 1-25a), the membrane marker could only recover by the vertical exchange of fluorophores. An intensity profile along a vertical line through the bleach-spot was extracted from the fluorescent images of each time point (Figure 1-25b).

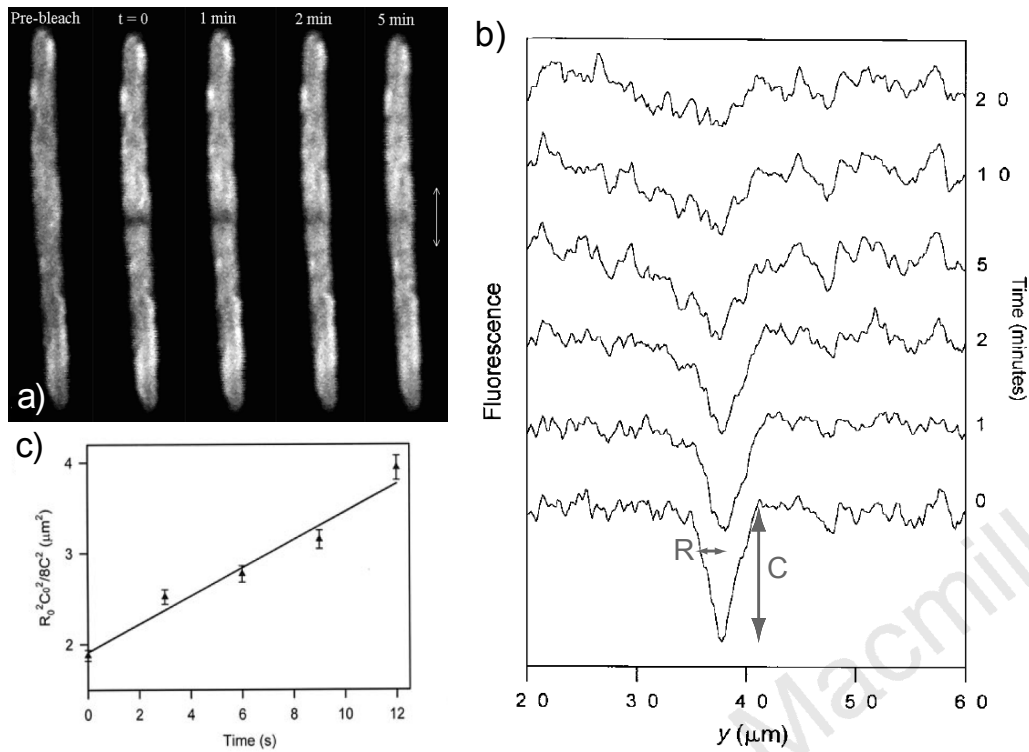


**Figure 1-25: FRAP analysis by Mullineaux method**

A sequence of fluorescent images before and after the bleach is recorded (a). A vertical intensity profile (along the arrow bar in a) is plotted for each time point after the bleach (b). A fitted Gaussian curve is used to provide the depth (C) and the half-width (R) of each profile. Finally, a function of  $R_0^2 C_0^2 / 8C^2$  is plotted against time, where the slope equals D. Figure adapted from (Mullineaux et al., 1997, Mullineaux, 2004).

The solution for a one-dimensional diffusion equation under the assumption that the cell is long in comparison to the width of the bleach, is:

$Ct = C_0 R_0 (R_0^2 + 8Dt)^{-1/2} \exp\left[-2y^2 / (R_0^2 + 8Dt)\right]$  where C is the concentration of the bleached fluorophore at different time points, R equals the half-width of the bleach and y is the distance along the vertical axis of the cell. The fit of a Gaussian profile into the intensity profiles provides the parameters C (concentration=depth of profile) and R. By plotting  $R_0^2 C_0^2 / 8C^2$  against time, a straight line should be obtained. The slope of this line equals the diffusion coefficient D.

Both methods were tried for analysis of our FRAP data, as described in section 4.3.1.

### 1.3.4 FLIM-FRET

Fluorescence resonance energy transfer (FRET, also called Förster resonance energy transfer) is a process which involves the radiation-less transfer of energy from a donor molecule to an acceptor molecule. FRET can occur when the emission spectrum of the donor significantly overlaps the excitation spectrum of the acceptor, and the dipoles of the two molecules are in favourable orientation. The efficiency of the energy transfer decreases steeply in dependence of the distance between the donor and the acceptor (FRET efficiency  $\sim 1/r^6$ ,  $r$ =distance). The maximal distance over which the energy transfer can occur is roughly 10nm. This method can therefore be used to detect close interaction between two proteins (Figure 1-26). If proteins are fused to appropriate donor and acceptor molecules, detection of FRET between the fluorophores indicates an interaction between their conjugated proteins.

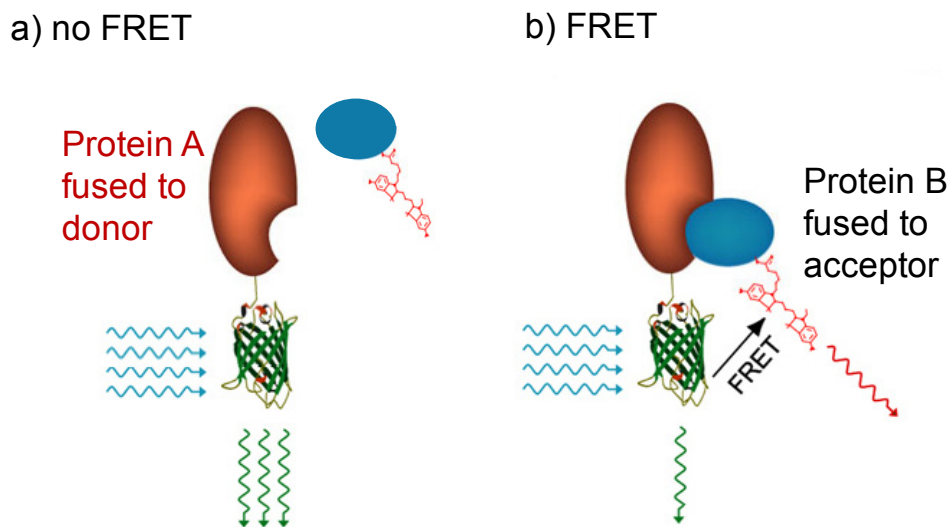


**Figure 1-26: Fluorescence Resonance Energy Transfer**

In a non-FRET situation (a) excitation of a donor fluorophore results in the emission of a donor specific wavelength, whereas if a suitable acceptor is in close proximity, an energy transfer from donor to acceptor may occur, leading to emission of the acceptor specific wavelength (b). The emission of the donor will be reduced, as some of the energy released during the fall of an electron from the excited state to the ground state is transferred to the acceptor instead of emitting a photon. By fusing proteins to donor and acceptor, the interactions between the proteins can be studied. Figure adapted from (Wouters et al., 2001).

Whether or not an energy transfer occurs can be measured using various microscope techniques and a common classification is to distinguish between intensity-based and lifetime-based methods. One way to use fluorescence

intensity to quantify FRET is to measure the initial donor emission intensity and compare it with the emission intensity after photo-bleaching of the acceptor. Photo-bleaching of the acceptor will disrupt the energy transfer from donor to acceptor, resulting in an unquenched, higher donor emission. An apparent energy transfer efficiency can be calculated using the ratio between the fluorescent intensities of the donor before and after acceptor bleaching. Another approach is to measure the acceptor emission. If no FRET situation is present, no acceptor emission should be detected. These intensity-based methods are very susceptible to fluorescent bleed-through, imaging dependent photo-bleaching and concentrations of the fluorophores and correct interpretation can be difficult (Berney and Danuser, 2003).

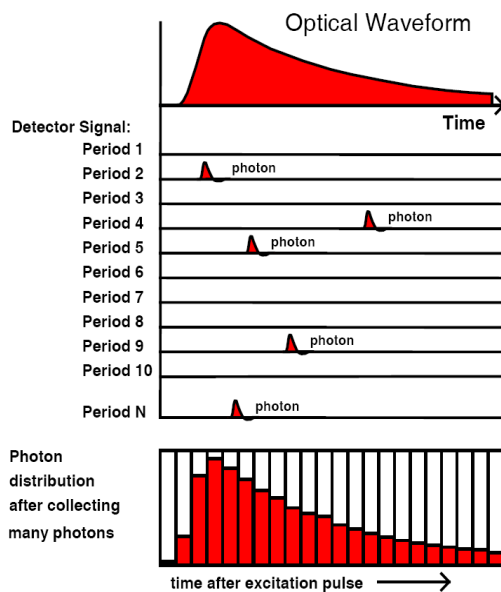
Lifetime-based methods are less dependent on these influences. The fluorescent lifetime of a fluorophore ( $\tau$ ) represents the time an electron remains in the excited state before falling back to the ground state while emitting a photon. This time is characteristic for every fluorophore but can be altered by the local environment of the fluorophore. Changes in pH, ion concentrations and interaction with other fluorescent molecules (i.e. FRET) result in different lifetimes of the observed fluorophore and can be studied using Fluorescent Lifetime Imaging Microscopy (FLIM). FRET decreases the lifetime of a donor. By comparing the lifetime of a donor alone (control) with the lifetime of a donor+acceptor situation (experiment) it can be shown whether an energy transfer occurred between the two molecules. If so, the ratio of  $\tau_{\text{donor}}/\tau_{\text{donor+acceptor}}$  can be used to calculate the FRET efficiency.

There are two common methods to measure fluorescence lifetimes: time-domain and frequency-domain (Figure 1-27). In the time-domain method the sample is illuminated by a sequence of short and fast laser pulses. Fluorescence decay curves are obtained by measuring the emitted intensity using different time windows (gates) of acquisition or by single photon counting. The system at the Beatson is a time-correlated single photon counting (TCSPC) from Becker and Hickl combined with a Multi-photon laser controlled by a Leica confocal.

Short multi-photon pulses (150fs) hit the sample at approximately 12.5ns intervals and the detector registers the time at which single photons arrive. A signal when exactly the pulse occurred is transferred to the detector, which

then correlates any arriving photon to the corresponding pulse. Over time, a typical decay curve will be built up (Figure 1-27a). Due to the low probability of two excitation photons hitting a fluorophore at the same time, many pulses will not result in the creation of an emission photon. Therefore, the cycle of laser pulse and detection has to be repeated for many times in order to achieve a high enough number of photon counts. In order to obtain a lifetime-pixel-map of the measured sample, not only the time but also the information where the photon came from (i.e. where the laser pulse hit the sample) is recorded. Due to the near-perfect counting efficiency of this method it can achieve an optimal signal-to-noise ratio. A disadvantage is the relatively long acquisition times in order to obtain enough signal (i.e. photon counts), which are in the range of 30s. With many systems it is also difficult to control the multi-photon laser intensity and sometimes no compromise between low counts or photo-damage can be found.

### a) time-domain



### b) frequency-domain

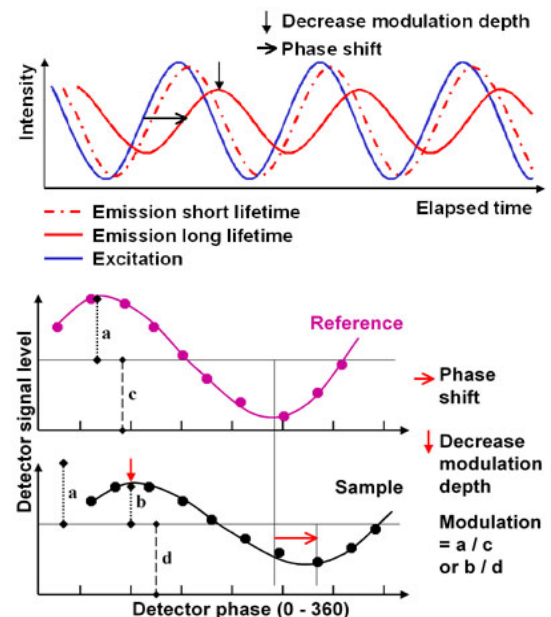


**Figure 1-27: fluorescence lifetime detection methods**

In a) (taken from Becker and Hickl TCSPC manual) the principle of time-correlated single photon counting, an example of time-domain FLIM measurement is presented. Following multiple fast laser pulses, the detector is active for short periods, where it detects a maximum of one photon at a time. The number of photons within the same time frame is counted and will build up the decay curve of the excited fluorophore, which provides the lifetime. The frequency-domain method (b, taken from Lambert instruments webpage) is based on the ability of the fluorophores to change phase and depth of the wave of a modulated light source (upper panel). By comparing the resulting wave with the one of a reference with known lifetime, an absolute value for the lifetime of the fluorophore can be calculated.

The frequency-based method to measure fluorescence lifetime is based on the change of modulated light wave properties of the emitted wave compared to the wave used for excitation. The excitation light is intensity modulated, in our systems between 10-100MHz. By exciting a fluorophore with a modulated light source, the emitted fluorescence will be modulated too, but will have a phase and a depth difference compared to the initial wave (Figure 1-27b upper panel). In order to extract these differences, the sensitivity of the image intensifier in front of the CCD camera is modulated with the same frequency as the excitation wave. A series of (typically around 12) different phase steps of the image intensifier are used for one measurements. The resulting overall differences in phase and modulation are compared with a control sample with known lifetime (reference) (Figure 1-27b lower panel), imaged under the same conditions and the final fluorophore lifetime is calculated. This method uses wide-field illumination and is therefore much faster (around 2s) than TCSPC, but gives less spatial resolution. In order to create more contrast, the frequency domain setup can easily be combined with techniques such as TIRF, spinning disc etc. One of our frequency domain systems is a FLIM-TIRF, which is used from researchers within and outside the Beatson institute. An example of a collaboration using this specialised system is shown below.

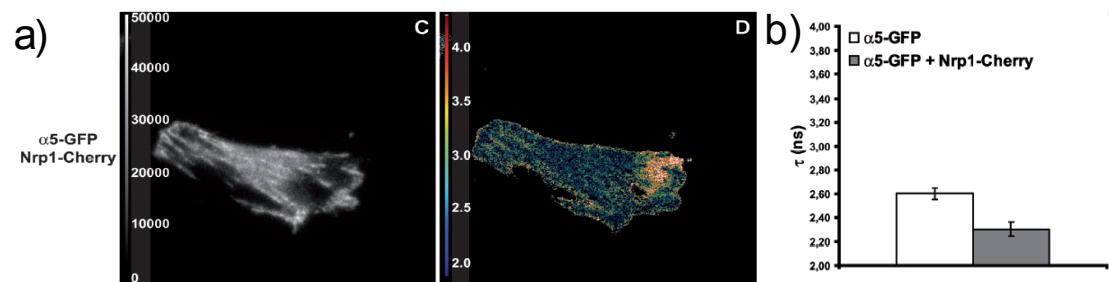


**Figure 1-28: application of the Beatson FLIM-TIRF**

TIRF-FLIM analysis of FRET between  $\alpha 5$ -GFP and mNrp1-Cherry. NIH 3T3 fibroblasts were transfected with either  $\alpha 5$ -GFP alone (not shown) or cotransfected with  $\alpha 5$ -GFP and mNrp1-Cherry (a, left TIRF intensity image, right color coded fluorescence lifetime image). In comparison with cells transfected with  $\alpha 5$ -GFP alone, the donor lifetime is decreased (from 2.6 to 2.3ns) in adhesion sites of cells expressing both  $\alpha 5$ -GFP and mNrp1-Cherry ( $P < 0.001$ ). (Valdembri et al., 2009) (see appendix)

## 1.4 Aims

The aim of this thesis was to study the actin-membrane interaction at the leading edge of migrating cells. The existence of the newly found lipid diffusion barrier at the leading edge (Weisswange et al., 2005) formed the basis of this project and was used as a read-out method for actin-membrane interactions. This phenomenon was observed in fish keratocytes and the first objective of my project was to establish whether this leading edge diffusion barrier could be found in other cell-types and therefore maybe present a general feature of protrusion. The second aim was to investigate the physical basis of this diffusion barrier in order to get a closer insight into the actin-membrane interactions. Although many theoretical models about the force generation of actin polymerisation at the leading edge exist, experimental data are sparse. With the use of different microscope techniques, we wanted to study the dynamic interface between actin-filament tips and the plasma membrane. The final objective of this thesis was to investigate the role of the leading edge diffusion barrier during regulation or localisation of actin polymerisation and establish whether actin-regulating proteins are influenced in their diffusion.

## 2 Methods and Materials

The following chapter explains experimental procedures, including the technical specification of the microscope systems used within this thesis. The supplier of technical equipment and laboratory reagents is mentioned within the text. The more exact recipes for some reagents are attached at the end of the chapter.

### 2.1 Cells

#### 2.1.1 B16 F1

##### Culture

B16 F1 mouse melanoma cells, kindly provided by Klemens Rottner (Braunschweig, Germany) were cultured in high Glucose DMEM without Pyruvate (GIBCO 41965-039) supplemented with 10% Foetal Bovine Serum (PAA laboratories A11-043-1) and 1% Glutamine (GIBCO, 25030-240). Cells were replated every 2 days when they reached around 90% confluency. After incubation in 3 ml 0.02% Trypsin (2.5% stock solution, GIBCO 15090-046), 7 ml media were added and 10% as well as 5% of the resulting solution were transferred in two separate falcon tubes, where they were centrifuged. After four minutes at 100 rpm the supernatant was removed and cells in each tube were resuspended in 10 ml media and placed in new petridishes. Incubation conditions were 37° Celsius and 5% CO<sub>2</sub>. The cells were cultured in 10 cm Corning dishes (Fischer Scientific, TKV-160-049F). To freeze cells down, the content of one nearly confluent plate was resuspended in 3 ml ice cold media containing 10% DMSO. Each cryotube was filled with 1 ml cell solution and kept at -80° Celsius for up to two weeks before transferring into liquid Nitrogen for long term storage. For reuse of the frozen cells, one vial was briefly kept in a 37° Celsius water bath until defrosted and then added to 10 ml ice cold medium, centrifuged for 4 minutes and resuspended in 10 ml warm media followed by transfer to a 10 cm culture dish.

## Transfections

To transfect B16 F1 mouse melanoma cells with plasmid DNA, 1% of the cells within a 90% confluent 10cm plate were transferred to a new 3cm dish and cultured normally for around 24h. The manufacturer's protocol for transfections with Superfect (Quiagen 301305) was followed, but volumes were changed for this cell type. The superfect-DNA complex was made in 300 $\mu$ l DMEM using 6 $\mu$ l Superfect and 1 $\mu$ g of plasmid DNA. After 15-30min this complex was mixed with 2.5ml of full medium and added to the cells for overnight incubation.

## Preparation for microscopy

A 3cm glass bottom petridish from MatTek (MatTeck corporation P35G-0-10-C) was coated for 1h with 25 $\mu$ g/ml Laminin (stock solution from Sigma L2020). Transfected cells were trypsinised with 1ml 0.02% Trypsin and after addition of 3ml medium, 15-25% were reseeded and allowed to attach for a minimum of 2h. About 1h prior to use, the normal media was changed with Microscope media, containing less phenolred and additional HEPES (GIBCO 21765) to be less autofluorescent and maintain the pH in the absence of CO<sub>2</sub>. All cells were treated with PMA (see section 2.3) to stimulate the formation of big lamellipodia. Additional drug treatment was performed as needed for experiments. For the majority of the drug treatment, a 1ml of a 3 times concentrated drug solution was prepared and added to the 2ml microscope medium on the cells, resulting in the chosen final concentration. Sometimes 3ml with the final drug concentration were directly added to the cell dish containing no medium. The following final concentrations and incubation times were used: PMA at 200ng/ml permanently, ConA at 1mg/ml for 20 minutes, CytD at 10 $\mu$ g/ml for 15 minutes or permanently (depending on experiment) and LatA at 1.26mg/ml permanently.

## 2.1.2 Fish keratocytes

### Preparation

The protocol for the preparation of fish keratocytes was adapted from Anderson and Small 1998 (Anderson and Small, 1998). Fish keratocytes can be obtained from scales of many different fish types, for the work described here zebrafish (*Brachydanio rerio*), rainbow trout (*Oncorhynchus mykiss*) or swordtail (*Xiphophorus Helligeri*) were used. After sacrificing the fish by anaesthetizing it in a 0.01% solution of benzocain (Ethyl-4-aminobenzoat, Sigma), followed by severing of the spinal cord with a scalpel cut, its scales were carefully removed one by one under a dissecting microscope. Fish were killed by Glasgow university staff and transported back to the Beatson. For transport the fish was wrapped in an aluminium foil pocket containing medium and kept on ice until use. The fish was kept moist at all times and harvested scales were temporarily stored in a petridish of full fish media. In order to help loosen debris and slime from the scales, they were rinsed several times slightly rigorously with media. Through the use of the dissecting microscope, scales were chosen and two were placed on each coverslip (typically 22mm of diameter) preferably oriented with the tissue layer facing upwards (Figure 2-1a). Seven of these coverslips had previously been positioned in a 10cm plastic petridish. To provide the pressure needed for the tissue to move from the scale to the coverslip, a smaller coverslip (19mm) was carefully placed on top of the one containing the two scales in one drop of media. To prevent the liquid from drying, which would lead to the death of the keratocytes, a moist chamber was created by adding a media soaked filterpaper to the lid of the 10cm plastic dish and closing the gap between bottom and lid using parafilm. After an initial phase of attachment (around 2 hours) the amount of liquid between the two coverslips was topped up by adding a drop of media. To avoid damaging the cells through friction, care was taken not to touch the upper coverslip while adding the media. After 6-8 hours the space between the two coverslips was filled up with media (Figure 2-1b).

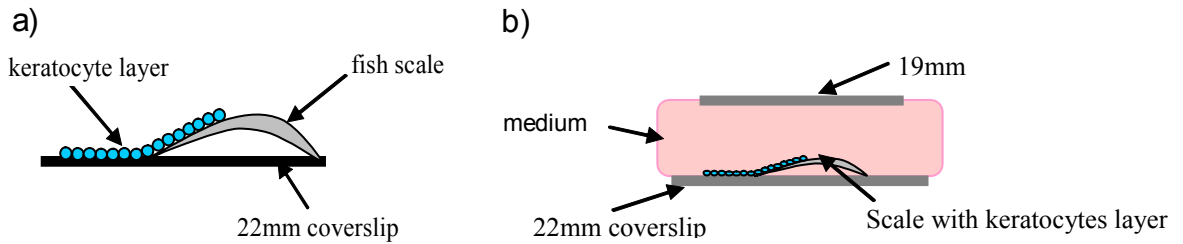


**Figure 2-1: keratocytes preparation**

The fish scale was positioned on a 22mm glass coverslip, preferably with the keratocytes layer on top (a). To force the scale into contact with the bottom coverslip, a smaller coverslip was added on top of the scale. Initially only a small amount of liquid was positioned in between them, but over night more medium was added to prevent keratocytes from dying (b).

This enabled the cells to survive overnight and finish their movement from the scale to the coverslip. The optimal temperature for the cells depend on the fish, most can be done at room temperature. The following morning the coverslips were carefully separated and the ones with an attached layer of keratocytes were washed in PBS and placed with the layer facing up in individual dishes filled with fish media (see section 2.5). In this form the cells could be kept for around 3 days.

## Transfections

Transfections of fish keratocytes with plasmid DNA were performed using Fugene, GeneJammer or Superfect. The protocols for Fugene transfections were based on the manufacturer's protocol as well as adaptations described in Jurado et al (Jurado et al., 2005). Complex formation between 3 $\mu$ l Fugene and 1 $\mu$ g of plasmid DNA was done in 96 $\mu$ l of serum free media at either 38 $^{\circ}$ C or room temperature and left for 15min at the same temperature as the media. After addition of the complex to the cells and a 5h incubation time at room temperature, the complex was replaced with either serum free or normal medium. For GeneJammer the same quantities were used as for Fugene, but serum free media was replaced with DMEM, the complex was allowed to form in 30min and the final incubation time was overnight. Keratocyte transfections using Superfect followed the same protocol as described for B16 F1 cells. All quantities for keratocyte transfections are for one 19 or 22mm coverslip of cells. The following 8 protocoll were performed on keratocytes:

- A. After a formation time of 15min at 38° Celsius, a reagent-DNA complex of 96µl serumfree medium pre-warmed to 38° C, 3µl Fugene and 1µg GFP-actin plasmid DNA was added to cells pre-treated in 2ml serum free medium and left for 5h at room temperature before replacement with serum free media and overnight incubation.
- B. The same protocol as described in A was used, but complex formation was done at room temperature with non pre-warmed serum free medium.
- C. Protocol A was followed, but pre-treatment and final overnight incubation was done in full media (with serum).
- D. Protocol A was altered by changing pre-treatment and final overnight incubation medium to full medium and the temperature of the complex formation from 38° C to room temperature
- E. A mixture of 300µl DMEM, 6µl Superfect and 1µg GFP-actin plasmid DNA was incubated for 20min at room temperature and then combined with 3ml full medium before adding it to the cells and left for incubation overnight.
- F. The same protocol as described in E was used, but cells were pre-treated in serum free medium and the complex was added to 3ml of serum free medium.
- G. A complex of 97µl DMEM, 3µl GeneJammer and 1µ GFP-Actin plasmid DNA, which had been allowed to form for 30 min, was added to the cells with 2ml full medium already present .
- H. Protocol G was changed by replacing full medium with serum free medium.

### **Preparation for microscopy**

To separate cells from the monolayer, the normal medium was replaced with a low calcium medium (Keratocyte Running Buffer - KRB) for up to 3h prior to microscopy. If cells failed to individualise, a short (1-5min) incubation in PBS

was added. For high resolution imaging, coverslips were attached to specially prepared 35mm plastic dishes with a 19mm hole in the bottom. First, a continuous bead of high viscous silicon vacuum grease (Bayer silicone) was drawn around the edge of the hole at the outside of the dish. Then, the 22mm coverslip containing the scales and the cell layers was attached with the cells facing inside the dish. By pressing the edges of the coverslip onto the dish it was assured that the seal would be water-tight.

### **2.1.3 *Dictyostelium discoideum***

#### **Cell culture and preparation for microscopy**

*Dictyostelium discoideum* AX2 cells were obtained from Rob Insall and grown in 10ml HL-5 with Glucose (from Formedium) at 22° C in 90 mm petridishes. If cell density was near confluent, cells were washed off with medium and an appropriate amount of cells were reseeded into a new dish (normally 10%). Stable expressing cells were cultured in the presence of the appropriate antibiotic ( $c_{\text{final}}=10\mu\text{g}/\text{ml}$ ). For experiments the required amount of cells was transferred into a 35mm glass bottom petridish and left to settle down for 10-20min. The medium was then replaced with  $\text{KK}_2$  buffer.

#### **Transfection**

Transfection of *Dictyostelium* cells was performed by a protocol from Michael Carnell. One third of a nearly confluent dish was used per electroporation. After resuspension of the cells in 400 $\mu\text{l}$  ice cold electroporation buffer, 10 $\mu\text{g}$  plasmid DNA was added and mixture was transferred into an electroporation cuvette. Electroporation was done at 0.4-0.6V using a BioRad gene pulser. After 10min incubation on ice, 2 $\mu\text{l}$  healing buffer was added, followed by a further

incubation of 15min at 22 °C before adding HL-5 medium. Antibiotics for selection were added 24h after electroporation.

### **Actin wave formation**

Prior to the experiment, cells were incubated for a minimum of 30min in KK2 buffer. In order to stimulate the formation of travelling actin waves the cells were treated on the microscope with 5 $\mu$ M LatA solution (stock solution from Sigma). The effect of the drug was observed by eye and LatA was replaced with KK2 buffer when cells showed a completely depolymerised actin meshwork. This normally occurred within 5-15min. Experiments were performed as long as travelling actin waves could be observed.

## **2.2 Plasmids**

The following plasmids are Clontech constructs: pEGFP- $\beta$ -actin, pAcGFP-MEM, pDsRed-F, pDs-Red-MEM. The plasmid encoding mRFP- $\beta$ -actin was provided by Klemens Rottner and is described in Pacholsky et al 2004 (Pacholsky et al., 2004). The pEGFP-mRFP fusion was provided by Joan Grindlay, who inserted mRFP within the multiple cloning site using bglII, leaving a 15bp linker between the two fluorophores. Plasmids for EGFP fused to the farnesylation site of Ras (pEGFP-F) and the pleckstrin homology domain from PLCdelta1 (pEGFP-PH-PLC) were a gift from Pascale Zimmermann (Zimmermann et al., 2002), whereas EGFP fused to the pleckstrin homology domain of Akt (pEGFP-PH-Akt) was provided by Tamas Balla (Varnai et al., 2005). pcherry-F was made by Juliana Schwarz by replacing EGFP from pEGFP-C1 (Clontech) with a cherry-F PCR product using NheI/XhoI as restriction enzymes. The Dictyostelium vectors GFP-CAR and mRFP-lim $\Delta$ cc were gifts from Rob Insall and Anette Müller-Taubenberger respectively. Laura Machesky provided the following constructs: GFP-N-WASP, GFP-WAVE2, GFP-CP, GFP-CP $\Delta$ 7, GFP-CPpmut, FLAG-IRSp53, myc-IRSp53-IMDmut and myc-

IRSp53- $\Delta$ SH3. The mentioned CP constructs were originally from Dorothy Schafer. The IRSp53 sequences were cut from their FLAG or myc vectors using BamH1/EcoR1 and ligated into a BglII/EcoR1 opened pEGFP-C1 vector. A more detailed description of the proteins function as well as the mutants can be found in the introduction section (1.1.1.2 Regulation of actin polymerisation at the leading edge).

## 2.3 Drugs

### PMA

Phorbol 12-myristate 13-acetate (PMA, also called 12-O-Tetradecanoylphorbol-13-acetate (TPA)) is a phorbol diester and a potent tumor promoter. It activates the signal transduction enzyme protein kinase C (PKC), as its structure is similar to one of PKCs natural activators diacylglycerol. PKCs control protein function through the phosphorylation of amino acids (mainly serine and threonine) and their functions are widely spread. It has been described that PMA induces rapid reorganisation of actin in cells (Downey et al., 1992, Schliwa et al., 1984). It has been used in B16 cells by Ballestrem (Ballestrem et al., 2000). A final concentration of 200ng/ml was used by diluting a 1mg/ml stock solution (in DMSO) with Microscope medium. Effects were visible from around 10 min onwards.

### ConA

Concanavalin A (ConA, ordered from Sigma) is a lectin originally extracted from jack-bean. Lectins are proteins capable of reacting with specific sugar residues. ConA clusters receptors on the cell surface, which can activate their function. Pre-treatment of cells with ConA immobilised the cells and maintained cell morphology including the lamellipodium during treatment with actin

depolymerising drugs such as CytD or LatA. A stock solution of 25mg/ml was obtained by dissolving the solid powder with PBS. Small aliquots were frozen at -20°C and diluted with KRB or MM to 1mg/ml before use. The final solution was left on the cells for 15min before wash out (effect was permanent).

### **CytD**

Cytochalasins block the +end of actin filaments and prevent further monomer addition. This leads to depolymerisation of the actin meshwork by cellular mechanisms. If cells are treated with Cytochalasins, they rapidly lose their lamellipodium (Anderson et al., 1996). A 1mg/ml stock solution of Cytochalasin D (CytD, ordered from Sigma) extracted from *zygospore mansonii* was prepared by addition of DMSO. Final concentration for cell treatment was 10µg/ml (in KRB or MM).

### **LatA**

Latrunculin A (ordered from Sigma) belongs to the family of Latrunculins, toxins produced by certain sponges. It binds actin monomers in a 1:1 stoichiometry and renders them incapable of polymerisation (Yarmola et al., 2000). A 1mM stock solution (powder ordered from Sigma and solved in DMSO) was diluted with MM or KRB to a final concentration of 3µM. Cells were treated with this solution during the whole experiment, as its effect was rapidly reversed after washout.

## **2.4 Other techniques**

### **Microinjection**

Microinjection of plasmid DNA was done using a Zeiss Axiovert 100 microscope equipped with a 40x LD Achromatic objective and an Eppendorf Transjector 5246

for pressure creation with either an automated (Eppendorf 5171) or a manual micromanipulator (Leica microsystems) for needle handling. A Femptotip II was filled with around 2 $\mu$ l of a mixture of 60ng/ $\mu$ l DNA solution and 0.5mg/ml Alexa 594 dextran (Invitrogen), which had been centrifuged for 15 minutes to avoid clogging of the needle. A background pressure (of 40-80hPa) was used to obtain a constant flow out of the needle and to inject the cells. The needle was slowly inserted into the cell nucleus until a slight expansion of cell volume was observed, following which the needle was removed from the cell. After injection, which was done under transmitted light, epifluorescence was used to check the amount of dextran positive cells and their general condition.

### **Focal labelling and Observation of Initial Diffusion**

Focal Labelling and Observation of Initial Diffusion (FLOID) was previously used to find the diffusion barrier in fish keratocytes (Weisswange et al., 2005) and was therefore the first choice of methods to further investigate this read-out for the actin-membrane interactions at the leading edge. FLOID is performed on single moving cells (keratocytes in KRB, B16 cells plated at 1/100). A microinjection needle (Femtotips II, Eppendorf) was filled with a 100 $\mu$ g/ml Dil C12 solution (ordered from Invitrogen, dissolved in Ethanol) using microinjection needle filler pipette tips. The filled needle was then placed in a needle holder and attached to a manual micromanipulator (Leica) placed on a microinjection stand (MT-75 Tall gantry micromanipulator stand from Intracel). To provide pressure an air-filled 30ml syringe was attached to the back end of the needle holder via a flexible tube. After placing the cell containing dish onto the microscope, the needle was lowered to be close to the focal plane of the cells. The needle tip was moved away from the cell in order to avoid premature labelling and a small amount of dye was pushed out of the needle by applying manual pressure to the syringe. This resulted in a fine cloud of dye crystals and the tip of the needle was placed into this cloud to allow the dye crystals to attach around the needle tip. The chosen cell was then labelled by gently bringing the dye surrounded needle tip in contact with the cell body. The microscope optics were then switched from visual transmitted light illumination to camera fluorescence detection, allowing the start of a time-lapse series of

sequential TIRF and epi fluorescence images to follow the spreading of the dye in the membrane from the initial contact point around the whole cell. These experiments were done using our custom made TIRF microscope and detailed specifications of this setup can be found in a separate section.

### **Fixation and phalloiding labelling**

To fix cells and stain for the actin cytoskeleton, fish keratocytes were dispersed from the cell layer by incubation in KRB or PBS diluted medium (50/50). B16F1 cells were seeded at around 5-10% of a nearly confluent plate and left overnight to grow. Treatment with drugs such as CytD, LatA or ConA was performed directly before fixation. The first step of fixation was a 45sec incubation in a 1% Glutaraldehyde solution, followed by 20min in a 3% Paraformaldehyde solution. If staining was required, cells were permeabilised for 60sec with 0.5% Triton, followed by overnight incubation with a 1:3000 dilution of a 200Units per ml solution of Alexa 488 or Alexa 555 Phalloidin (from Invitrogen).

### **Total internal reflection microscopy**

Total internal reflection fluorescence (TIRF) experiments were performed on a Nikon Eclipse TE 2000-U microscope equipped with 60x and 100x 1.45 NA Nikon TIRF oil immersion objectives. The Nikon Epi-fluorescence condenser was replaced with a custom condenser in which laser light was introduced into the illumination pathway directly from the optical fibre output oriented parallel to the optical axis of the microscope. The light sources for evanescent wave illumination were a 473 nm diode laser, a 561 laser, or a 405 diode laser (all from Omicron). Each laser line was coupled into the condenser separately in order to allow individual TIRF angle adjustments. Each laser was controlled separately by a DAC 2000 card or a uniblitz shutter operated by MetaMorph (Molecular Devices). Depending on the application, different filters for excitation and emission were used. A green/red dual filterblock (ET-GFP/mcherry from AHF Analysentechnik, Germany) was used for dual color (473

and 561) excitation. A Multi-Spec dual emission splitter (Optical Insights, NM) with a 595nm dichroic and two bandpass filters (510-565 for green and 605-655nm for red) was used to separate both emissions. For photo bleaching or photo activation using the 405 laser, an E480SPX excitation filter, a FF 495 dichroic mirror and an ET 525/50M emission filter were chosen. This allowed bleaching or activation as well as imaging of the green emission. For single colour GFP images, a filter block consisting of a Z 473/10 excitation filter, a 488 RDC dichroic mirror and a ET 525/50M emission filter were used and the Multi-Spec dual emission splitter was switched to bypass mode. All imaging was performed with a Cascade 512F EMCCD camera (Photometrics UK).

### **Fluorescence Lifetime Imaging Microscopy (FLIM)**

All FLIM-FRET measurements were performed using a Becker and Hickl timecorrelated single-photon counting system (SPC 730) fitted to a Leica SP2 laser scanning confocal microscope (63xHCX PL-APO objective, 1.32NA oil) with a 5-W Spectra-Physics Mai-Tai pulsed infrared laser for multiphoton excitation and a Becker and Hickl PMC-100/DC100 detector. Excitation wavelength was 843nm and a 525/50 emission filter was positioned in front of the detector. Cells were kept at 37° degree Celsius by either the use of an incubator box attached to the microscope or a small heating chamber mounted on the stage. Acquisition parameters include an ADC resolution of 64 or 256, image size of 128\*128 or 256\*256, 400Hz line-scanning rate, and 30 s collection time. Images were analyzed using SPCImage software (version 2.83) with 1 component analysis, bin of 4 (counts above 100, better around 1000) and free scatter and shift parameters. Photo-bleaching was observed by comparing the instantaneous rate of photon detection at the beginning and end of image acquisition. Only data with a photo-bleaching within 20% of the average bleaching for this particular probe were used for the final lifetime average. Resulting Fluorescence lifetime shifts were tested for significance using an unpaired two-tailed Student's t-test. Equal variance of the data was confirmed using Lavene's F-test. Where used in the text, "significant" always refers to p-values below 0.05.

## Fluorescence Recovery after Photo-bleaching (FRAP)

### Using TIRF microscopy

Bleaching of the ventral cell membrane was using evanescent field illumination was performed on the TIRF microscope described above. After stimulation with the 405 laser adjusted to total internal reflection mode, a timelapse with sequential TIRF and epi images was started. Analyses were performed by linescan intensity measurements in MethaMorph.

### Using confocal microscopy

To determine diffusion constants of GFP-fused proteins and membrane dyes, FRAP experiments were performed on an Olympus FV1000 confocal, using a UplanS Apo 60x 1.3oil objective. A separate SIM scanner controlling an independent 405 laser enabled the bleaching to occur simultaneously with the imaging scan. Cells were kept at 37° Celsius in a heating chamber placed on the stage. Acquisition was done using the Olympus Fluoview software. Scan parameters for imaging included an image size of 256x256 Pixels, bidirectional fast scan at 0.065s per frame and a zoom of 6. Excitation and emission parameters were preset in the software dye settings, namely EGFP or Dil. The Region of interest for the bleach was created with the tornado tool at a size between 16-20 pixel. Image analyses were done in Image J after importing the saved Olympus *oib* files using the bioformat importer plugin. After creation of a circular region fitting the bleached area, the use of the “intensity versus time” plugin produced the recovery curve. Each curve was later fitted in SigmaPlot using the following exponential equation:  $I = I_0 + a(1 - \exp(-bx))$ . The resulting

parameter b was extracted to calculate the diffusion constant:  $D = \frac{b * w^2}{4 * \ln 2}$ , with w being the radius of the analysed area and b being the parameter from the SigmaPlot curve fit.

## 2.5 Solutions

### B16 media

#### Culture medium:

- 450ml DMEM (high Glucose, +L-Glutamine, -Pyruvate; Gibco)
- 50ml Foetal Bovine Serum (PAA laboratories)
- 5ml of 200mM L-Glutamine solution (Invitogen)

#### Microscope medium:

- 427ml F-12 Ham (+ Glutamine, -HEPES, low phenolred; Gibco)
- 50ml Foetal Bovine Serum
- 12.5ml of 1M HEPES
- 5ml L-Glutamine (200mM)

### Fish-media

	Start medium	Keratocytes Running Buffer (KRB)
<i>component</i>	<i>c(end)</i>	<i>c(end)</i>
NaCl	84mM	100mM
KCl	1,5mM	20mM
CaCl <sub>2</sub>	1mM	0.05mM
Ca(NO <sub>3</sub> ) <sub>2</sub>	0,05mM	0,05mM
MgSO <sub>4</sub>	0.1mM	0.8mM
NaHCO <sub>3</sub>	1.67mM	1mM

PIPES	2mM	2mM
DMEM	20%	none
Pen/Strep	1%	
Chicken serum	1%	none

The autoclaved salt solutions were mixed together and DMEM (Invitrogen, high Glucose), antibiotics and serum were added and filled up to a final volume of 500ml or 1000ml. Aliquots of 50ml were stored at  $-20^{\circ}\text{C}$ .

### **Dictyostelium solution**

KK2 buffer: 15.5mM  $\text{KH}_2\text{PO}_4$ , 3.8mM  $\text{K}_2\text{HPO}_4$  at PH 6.1

Electrophoration buffer: 10mM potassium phosphate buffer PH 6.1, 50nM sucrose

Healing buffer: 100mM  $\text{CaCl}_2$ , 100mM  $\text{MgCl}_2$

## **3 Evaluation of fish keratocytes as a model system**

Previous experiments examining the leading edge lipid diffusion barrier were performed on fish keratocytes, which are a suitable model for the method of Focal Labelling and observation of initial diffusion (FLOID) (see introduction section 1.2.3.3). In this method, dye is applied to the outer membrane layer and its spreading analysed through the use of sequential TIRF and epi illumination. To study the nature of the actin-membrane interaction responsible for the diffusion barrier it may be of advantage to investigate this connection from inside the cell. Being terminally differentiated, fish keratocytes may not be suitable for bio-molecular methods such as transfections or knockdowns and it was therefore necessary to evaluate whether fish keratocytes remain the best model system to use.

### **3.1 Fish comparison**

Fish keratocytes can be obtained from many different fish types, and they differ in their properties. The following subchapter shows the comparison of three different fish types: swordtail (*Xiphophorus Helleri*), rainbow trout (*Oncorhynchus mykiss*) and zebra fish (*Brachydanio rerio*). Swordtail was chosen because of its availability, trout and zebra fish because they had been used in previous work (Small et al., 1995, Weisswange et al., 2005). To establish their suitability for future experiments, the fish keratocytes were compared in terms of simplicity and yield of the preparation, as well as their quality.

#### **3.1.1 Fish keratocytes preparation**

All types of fish keratocytes were prepared according to the same preparation protocol, adapted from (Anderson and Small 1998, see Material and Methods section 2.1.2). The preparations were evaluated on the basis of subjective

criteria such as preparation time, efficiency, cell yield and survival. Several separate preparations for each fish type were performed to exclude the influence of variables like fish health, lab temperature and transport damage. Preparations of rainbow trout resulted in a very low yield of cells. Only few of the ~70 scales used during one preparation were surrounded by keratocyte layers attached to the coverslip (Figure 3-1). The formed layers were not very big and did not contain enough cells for experiments. The quantity of keratocytes from rainbow trout could be slightly increased if the scales were washed intensively before being placed on the coverslips. The overall yield, however, was still not sufficient. In contrast, preparations of Swordtail scales generated a high number of large keratocytes layers on the coverslips. Nearly each scale was surrounded by a cell layer, and they mostly appeared after a very short incubation time of 2h. The swordtail preparation was therefore generally easier compared to the preparation of rainbow trout keratocytes. The results of the zebra fish preparation lay somewhere in the middle. Preparation was generally easy and resulted in considerably more cell layers relative to rainbow trout. Compared to swordtail, however, zebra fish scales generated fewer cell layers and sometimes the layers only formed after over-night incubation.

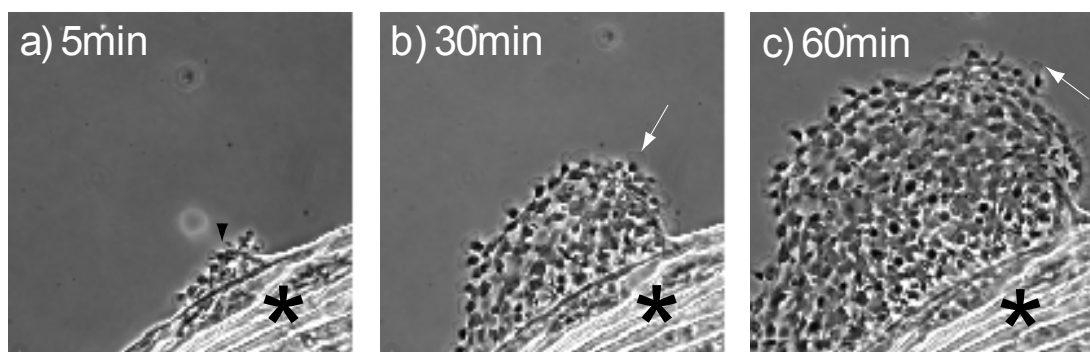


**Figure 3-1: growing fish keratocyte layer**

Under the right preparation condition the first keratocytes started to appear rapidly after placing the scale onto the coverslip (black arrowhead in a). The cells then keep moving from the scale (\*) onto the coverslip (b, c) and single keratocytes lamellipodia are visible at the edges of the cell layer (white arrowhead).

In summary, fish keratocytes could be most easily gained in high quantity from swordtail, followed by zebra fish and lastly trout.

### **3.1.2 Keratocytes quality**

Beside the simplicity and the yield of the preparation and cultivation of the fish keratocytes, it is important that the obtained cells are of suitable quality for our experiments. Quality criteria included cell size and shape, especially the shape of the leading edge. The total cell size does not influence the movement, but can be disadvantageous for methods like microinjection and FLOID. The desired cell shape is canoe-like, where the lamellipodium engages the majority of the total cell size. The canoe-like shape is the result of consistent movement in one direction. It can only be achieved by an equilibrium state of protrusion and adhesion and allows the cell to move in a most efficient way, a quality that rationalises the use of fish keratocytes as a model system for cell migration (see introduction section 1.1.1.1). A crucial criterion for this study was the condition of the leading edge. As the project goal was to investigate the actin-membrane interaction at the leading edge during active actin polymerisation by studying the diffusion of lipids and proteins in the membrane around the leading edge, it had to be excluded that this diffusion is altered by variations within the leading edge. An optimal even leading edge is evidence of equal protrusion rate at all points along the leading edge, whereas the presence of indentations indicates local regions of non-protrusion or even retraction of the actin network.

An initial control of quality was performed by eye during preparation of the cells and it was observed that individual swordtail keratocytes were smaller than trout cells. It was also noticed that swordtail keratocytes seemed to attach less strongly to the coverslip, but they interestingly seemed to possess stronger cell-cell bonds, as it was harder to break the cell layers into individual cells in low Calcium medium. More detailed assessments of the keratocytes quality were performed on fixed cells. By comparing single keratocytes from all three fish types, it was possible to demonstrate more accurately that there was indeed a size difference between the three types of keratocytes (Figure 3-2). The size (width) average for swordtail keratocytes was  $39\mu\text{m}$  ( $n=27$ ), followed by  $43\mu\text{m}$  for zebra fish ( $n=40$ ). Rainbow trout keratocytes were considerably bigger with an average of  $58\mu\text{m}$  ( $n=40$ ).

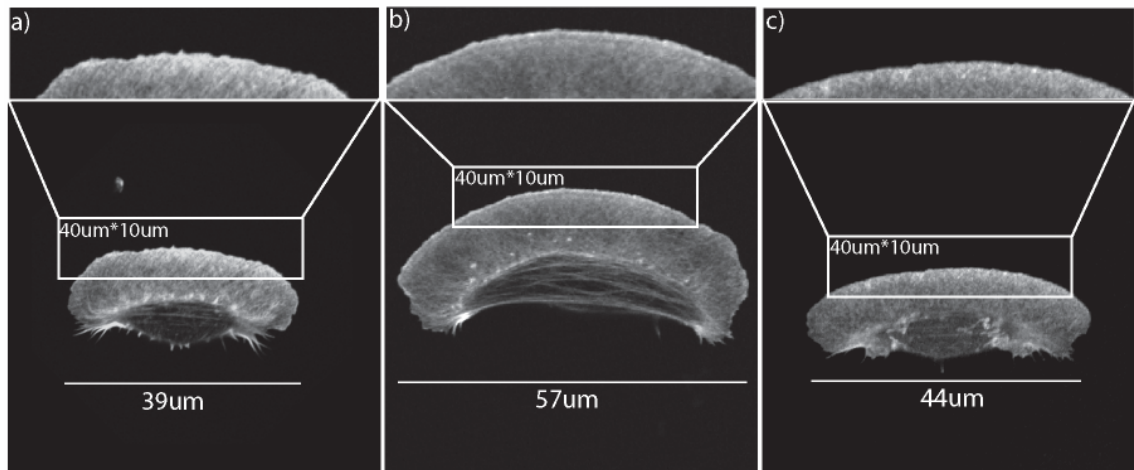


**Figure 3-2: size and leading edge comparison of fish keratocytes**

Fish keratocytes (a) swordtail, b) rainbow trout, c) zebra fish) were fixed and their actin-cytoskeleton stained with Alexa488 Phalloidin. Keratocytes differ in their size, as seen on scalebars. A close-up reveals differences in leading edge smoothness. Swordtail cells possess a very rough, uneven leading edge, in contrast to rainbow trout and zebra fish.

Phalloidin staining allowed the comparison of features of the actin cytoskeleton in all three cell types. The majority of rainbow trout keratocytes displayed a very fine meshed and homogeneous looking actin network. The actin meshwork of zebra fish keratocytes was similar, but in contrast, swordtail cells showed a slightly less homogeneous and more coarsely meshed network. Another obvious difference was the shape of the leading edge. Whereas the leading edges of rainbow trout and zebra fish cells were very smooth and continuous (Figure 3-2b+c), very rough and uneven leading edges could be observed in swordtail cells (Figure 3-2a). Overall, the actin cytoskeleton of swordtail keratocytes was less favourable compared to zebra fish and trout.

Although swordtail was the first choice according to preparation criteria (section 3.1.1), keratocytes gained from this fish-type did not possess the desired leading edge shape and therefore zebra fish was chosen for all future experiments (see summary and conclusions, section 3.3).

## 3.2 Protein expression in fish keratocytes

In order to expand the utility of fish keratocytes for further experiments related to the leading edge lipid diffusion barrier, it would be desirable to have

fluorescently tagged proteins expressed in these cells. Although fish keratocytes are a good model system for cell migration, the difficulty to transfect these terminally differentiated cells is often a limiting factor for possible experiments. This subchapter shows the results of my attempts to express fluorescent protein conjugates in zebra-fish keratocytes.

The first method tested was transfection, a commonly used method to bring plasmid DNA into cells for protein expression. Transfections are based on lipid reagents which form a complex with the DNA and fuse with the membrane to allow their cargo to enter the cell. The DNA then has to enter the cell nucleus, which mostly happens during cell division. Terminally differentiated cells do not divide any more and are therefore generally harder to transfect. It has been shown that transfection of fish keratocytes is possible, albeit only with a low efficiency of around 3.5% (Jurado et al., 2005). We tested three commercially available transfection reagents for their ability to transfect the used zebra-fish keratocytes: Superfect (Quiagen), GeneJammer (Stratagene) and Fugene (Roche). DNA Plasmids encoding GFP-actin were transfected according to manufacturer's guidelines, involving a reagent-DNA complex formation phase followed by an incubation phase of several hours to allow the cells to translate the introduced DNA. Parameters such as temperature, serum presence and incubation times were altered to optimise transfection protocols. In order to minimise variations, all fish keratocytes were obtained from one fish and were transfected on the same day after initial preparation. Figure 3-3 shows representative fluorescence images of the transfected cells obtained from some of the eight performed protocol variations. The results from the other transfection protocols, where no pictures are shown, are similar to the ones shown in Figure 3-3.

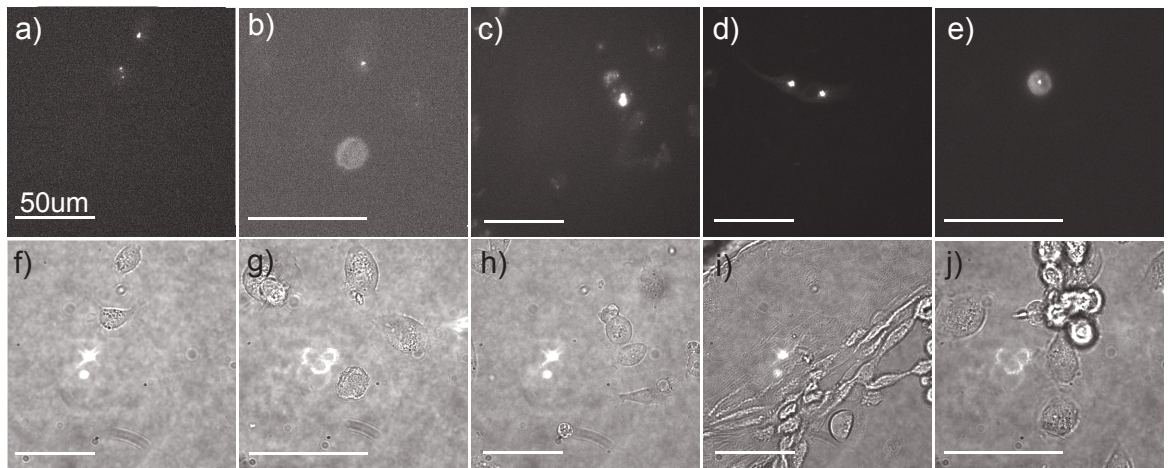


**Figure 3-3: transfection of fish keratocytes**

a-e) show representative images in the green fluorescent channel several hours after transfection, f-j) show the correlating transmitted light images; different protocols were used: a) Fugene reagent at 38°C without serum, b) Fugene reagent at room temperature with serum, c) Genejammer reagent with no serum, d) Superfect reagent without serum, e) untransfected cell; scalebar always 50µm.

Unfortunately, transfections were not successful, as we failed to see GFP-actin positive cells (Figure 3-3). Although some fluorescence could be detected, its subcellular localisation did not show any resemblance to the actin cytoskeleton and was quite possibly autofluorescence. The highest intensities were seen in puncta in the region of the cell body. Using only fluorescence, it was not possible to visualise the lamellipodium, which should be easily visible if the cells expressed GFP-actin. Quite often, bigger areas of fluorescence corresponded to dead cells or clustering of dirt. The fluorescence detected is therefore probably caused by autofluorescence, possibly due to the phenolred in the media. This explanation is supported by the fact that similar fluorescence was detected in untransfected control cells (Figure 3-3e). None of the 8 used protocols resulted in a single GFP-actin expressing keratocytes, and on the basis of these results this approach was abandoned.

Thoughts were given to try nucleofection as an alternative way to deliver plasmid DNA directly into the nucleus. The nucleofection protocol requires suspension and reattachment of the cells, but unfortunately we could not reattach previously suspended keratocytes. Nucleofection could have been tried with the suspended cell, but without the reattachment no control of transfection or execution of following experiments was possible.

Another method tested was microinjection of plasmid DNA. It was previously shown that fish keratocytes can be successfully microinjected with in-vitro produced fluorescently labelled proteins (Kaverina et al., 2002) or fluorescently labelled phalloidin (Vallotton et al., 2005). Previous work in our group revealed that it is also possible to inject plasmid DNA and we therefore attempted to optimise DNA microinjection in zebrafish keratocytes. Several microinjection sessions were performed, to try different DNA concentrations, injection pressures and become familiar with this technique. We injected plasmids encoding either GFP-actin or GFP-F, being in both cases familiar with the localisation of the expressed proteins. In order to be able to mark and therefore recognise injected cells, Alexa 594 Dextran was mixed with the plasmid DNA prior to injection.

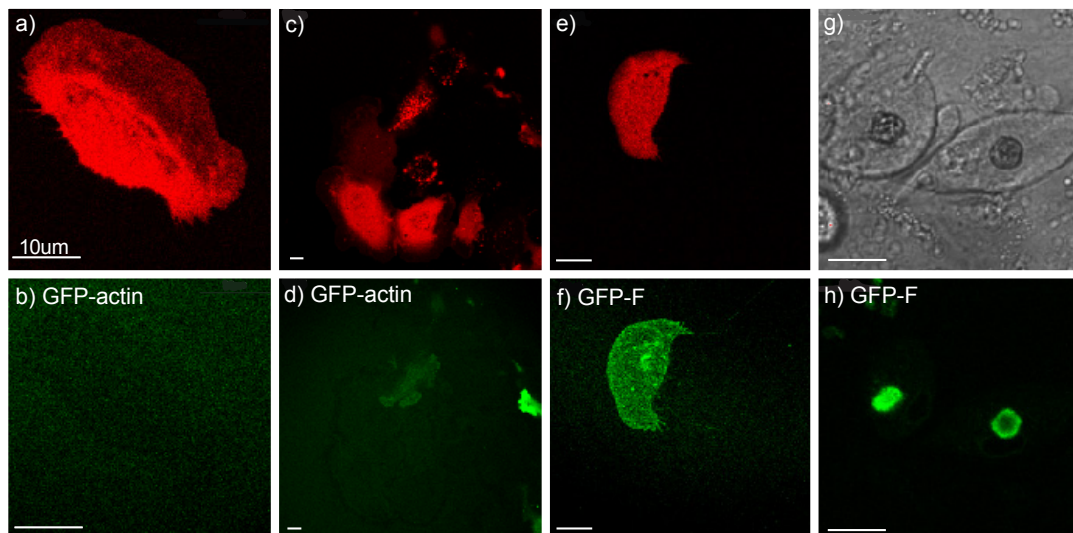


**Figure 3-4: microinjection of GFP-F and GFP-actin into zebra fish keratocytes**

The upper panel (except g) shows Alexa 594 Dextran intensities, the lower panel represents green fluorescence of either GFP-actin or GFP-F (membrane linked GFP), g) shows the transmitted light image corresponding to h; the cell represented in a+b) has red emission but no green which refers to successful injection but unsuccessful expression of the protein; the low protein expression rate is demonstrated in c+d; e+f) are images of one cell which expressed GFP-F after injection of DNA; g+h) images also represent GFP-F expression but the localisation is comprised to the nucleus, the fluorescent intensity was rather high, making it unlikely to be autofluorescence; the scalebar always represents 10µm.

Following injection and an approximate 5 hours incubation time for protein expression, many cells exhibited red fluorescence, resulting from the presence of Alexa 594 Dextran. Some were dead as a result of damage incurred during the injection process. Nevertheless, in every dish a useful number of keratocytes appeared to survive the injection and displayed normal morphology.

Unfortunately, only very few cells also displayed green fluorescence (Figure 3-4). In some cases, green expression could only be observed in the nucleus (Figure 3-4h), which is hard to explain, as translation should happen in the cytoplasm and GFP-F should be located at the cell membrane. Because of its rather high intensity, it is unlikely to represent previously experienced autofluorescence. A comparable microinjection protocol was carried out in P1 benign papilloma cells, resulting in many GFP-expressing cells. This indicates that the rather unsuccessful protein expression following injection of plasmid DNA in fish keratocytes is cell-type specific. Although it was possible to obtain some expression in fish keratocytes, the efficiency was too low for our experimental purposes.

### 3.3 Summary and conclusions

Fish keratocytes have previously been used to show that the interaction between the polymerising actin meshwork and the plasma membrane causes a reduction in the mobility of membrane dyes at the leading edge (Weisswange et al., 2005). To further study this diffusion barrier as a readout for actin-membrane interactions, we needed a suitable source of fish keratocytes. The purpose of this chapter was to establish whether keratocytes from rainbow trout, swordtail and a new source of zebra fish were suitable for the diffusion barrier experiments. Swordtail keratocytes were easy to obtain in large amounts, but their uneven, rough leading edge made them unusable. Indentations along the leading edge indicate that the actin polymerisation is not equal along the leading edge and therefore the actin-membrane interaction could be altered from one region of the leading edge to the next. As actin polymerisation is such a dynamic process, it would be impossible to predict where the resulting protrusion is active at the time of the FLOID measurement. In contrast, keratocytes obtained from rainbow trout possessed a smooth, even leading edge, which indicates similar instantaneous protrusion rates along the whole edge. Judging by this criterion, the rainbow trout keratocytes would be acceptable, but their preparation yielded in very low numbers of unstable cells, resulting in the necessity to have several fish preparations for each set of experiments. This

would normally be tolerable, if there was an easy access to the fish source, but the closest scientifically approved source for trout was over an hour away. Zebra fish keratocytes were easier to prepare than rainbow trout cells and they were suitable in their quality. Their leading edge was smooth and they lasted longer in culture. An initial problem was the lack of a scientifically approved source for this fish-type. But as a result of the keratocytes comparison, it was decided that the start of a zebra fish supply at the university would be the least problematic solution. Therefore, all subsequent experiments were performed with keratocytes obtained from zebrafish held for us at Glasgow University.

The expression of fluorescent protein chimeras for further investigation of the leading edge diffusion barrier was unsuccessful. Our goal was to introduce plasmid DNA into the cells to allow transcription and translation into the desired protein. Transfection did not result in any cells expressing GFP-fused proteins and was therefore discarded as not useful. It is not clear whether the DNA did not enter the cells or whether the cells did not express the protein due to transcriptional or translational reasons. Nucleofection tests had to be abandoned due to preparation problems. Microinjection resulted in some GFP-actin and GFP-F expressing fish keratocytes. Unfortunately the success rate was again too low for further use. Using Alexa 594 dextran as an indicator for successful introduction of the DNA solution into the cell, it could be shown that many cells contained the injected mixture but did not express the proteins. Another indication that keratocytes have a problem translating introduced plasmid DNA into proteins is that microinjection of another cell type using the same microinjection protocol yielded in a high expression rate. The question whether this relates to the use of a mammalian expression vector was raised, but not pursued further.

In short, zebra fish keratocytes were evaluated to be suitable in their quality, but transfection difficulties limit their experimental use.

## **4 The diffusion barrier at the leading edge is a universal feature of protrusion**

Prior to my thesis work, the presence of a lipid diffusion barrier at the leading edge had only been shown in fish keratocytes ((Weisswange et al., 2005), introduction section 1.2.3.3), leaving open the question whether it is a unique property of these highly specialised cells. A main goal of this thesis was to investigate if it could be found in other cell types, which would indicate that the disturbance of membrane diffusion through polymerising actin filaments at the leading edge is potentially a general feature of protrusion. The following chapter presents three different approaches to establish whether B16 F1 mouse melanoma cells exhibit decreased membrane diffusion around the leading edge: FLOID, selective photo-bleaching and photo-activation in TIRF, and FRAP.

### **4.1 FLOID**

My previous experience with the FLOID method in fish keratocytes allowed me to directly apply this method to the new cell type, knowing that the execution would be accurate. The only adaption of the method was a change in the choice of needle used to apply the dye to the cell surface. This was due to different equipment in Glasgow. Preliminary labelling tests with B16 cells showed that it was nearly impossible to stain the cells by touching them locally with a dye-coated needle. Although there was enough dye present on the needle and there was clear contact between the needle and the cell, no spreading of the dye within the cell membrane could be observed. One critical factor in the labelling part of the FLOID method is the formation of dye microcrystals, which attach to the cell surface and allow individual dye molecules to enter into the membrane and cause the labelling. The formation of these crystals depends on properties of the surrounding solution. In ethanol, the dye is completely soluble and forms no crystals, whereas it precipitates in water. The crystal-forming ability of the dye in aqueous solution is influenced by ionic strength (i.e. salt) and other supplementary, soluble components. The next step was therefore to test the

labelling efficiency of the dye on B16 cells in different cell culture media. F12-Ham, Microscope medium (F12-Ham + additives + Serum) and PBS were tested (Figure 4-1).

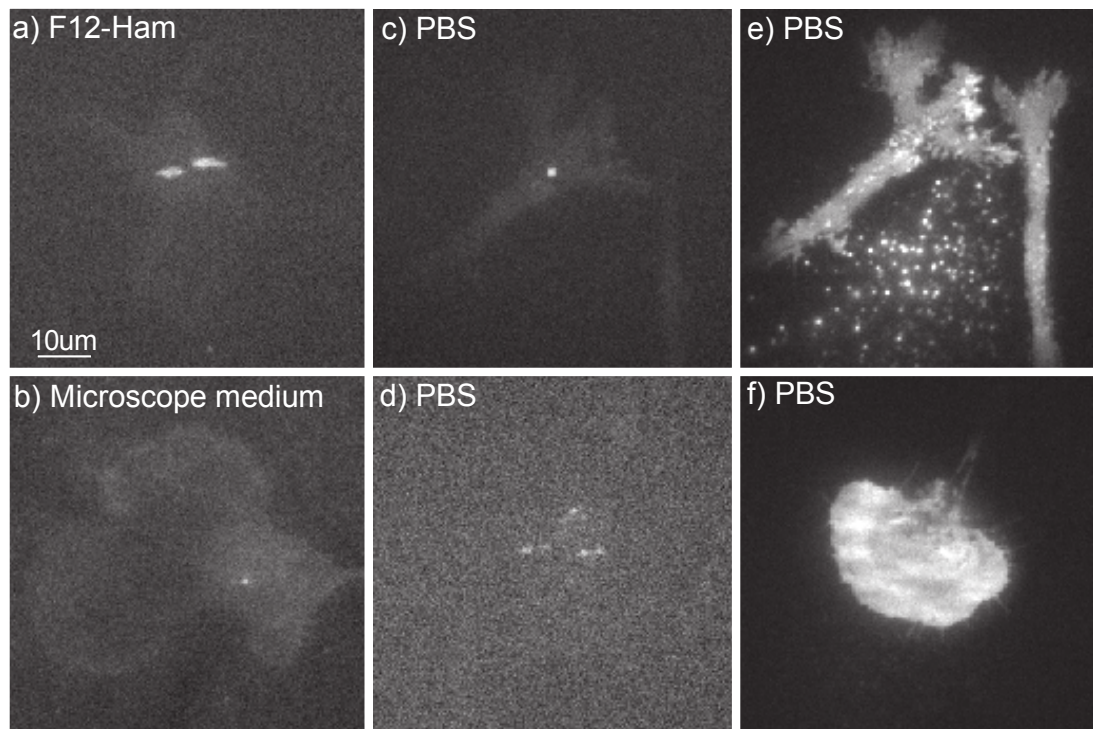


**Figure 4-1: Plasma membrane labelling of B16 cell using DiIc12 dye.**

In a-d a needle with DiIc12 carbocyanine dye microcrystals on the tip was brought into contact with the cell surface of cells surrounded by different solutions. No obvious spreading of the dye could be observed, but the initial contact point was visible, indicating successful touching of the cells. Pictures e and f show the same cells as in c and d (respectively) after squirting the dye out of the needle directly above the cells. In these cases, the dye spread around the whole cell membrane, resulting in a high fluorescent intensity. The shown scale bar applies to all images.

The presence of serum did not change the overall outcome. In the cases of F12-Ham as well as the microscope medium, the dye mainly remained at the point of initial contact and did not spread within the membrane (Figure 4-1a+b+c+d). It seemed that the dye was forming clumps, making it impossible to enter the membrane. In contrast, although it was still unusually difficult, some cells in PBS could be successfully labelled (Figure 4-2). It was often necessary to bring the needle into contact with the cell surface several times. This is not favourable for the cells, because each contact with the needle provides a potential source of damage for the cell. Overall, the labelling efficiency of B16 cells in all tested solutions was much weaker than in fish keratocytes, and successful labelling after the first contact could only be observed in a very small fraction. In addition, when labelling was successful, the resulting intensity was generally too

weak for analysis. Interestingly, when the dye was squinted out of the needle over the cells, nearly all cells were labelled with high intensity, even those which could not be labelled by touching with a dye-filled needle previously (Figure 4-1e+f). This suggests that the formation of dye microcrystals around the needle tip was impaired, which then led to unsuccessful transfer of the dye into the cell membrane.

The few successfully labelled cells with high enough intensity were analysed to see if diffusion was inhibited around the leading edge, completing all steps required for the FLOID method. Briefly, sequential TIRF and epi-fluorescent images were acquired to observe the manner in which the dye diffused from the dorsal to the ventral cell membrane.

Intensity analysis was performed on a straight line from the back to the front of the cell for epi and TIRF image sequences. The shape of keratocytes guaranteed that dye travelling to the leading edge on the dorsal cell surface reached the leading edge first (Figure 4-2a, blue path). This is an important requirement for analysis (see introduction section 1.2.3.3). In case of a single peak profile, where the dye only reached the ventral surface by diffusing around the back of the cell, it is crucial to know that the dye reached the leading edge in the dorsal surface, but was not able to diffuse to the ventral surface due to the lipid diffusion barrier. An accumulation of dye (step function, see introduction Figure 1-15f) in epi images indicated that the dye reached the leading edge. Due to the path length difference between dye travelling on the dorsal (Figure 4-2a brown path) or ventral (blue path) surface, the requirement for dye reaching the leading edge first via the dorsal membrane, was always fulfilled in fish keratocytes. In keratocytes, the intensity of the first TIRF image was therefore very low (Figure 4-2 b), as not much dye was able to spread to the ventral surface within the short time between labelling and first image acquisition.

In contrast, in B16 cells the first TIRF image already showed a high intensity of dye fluorescence (Figure 4-2d). The different cell shape of B16 cells (Figure 4-2 c) compared to fish keratocytes allowed dye to rapidly travel from the dorsal to the ventral surface. This led to a similar path length on both surfaces in order to reach the leading edge (Figure 4-2c, blue and brown paths). The dye in the basal membrane could therefore sometimes reach the leading edge before the

majority of dye visualised in epi (Figure 4-2e arrows in graphs). Although epi fluorescence records dye on both surfaces, the fact that intensity at the leading edge increases at a later stage than the TIRF intensity indicated that the dye in the dorsal membrane reached the leading edge later. The use of the FLOID methods to detect a lipid diffusion barrier at the leading edge critically depends on knowing that dye reaching the edge first comes from the dorsal surface. This was not possible in the case of B16 cells.

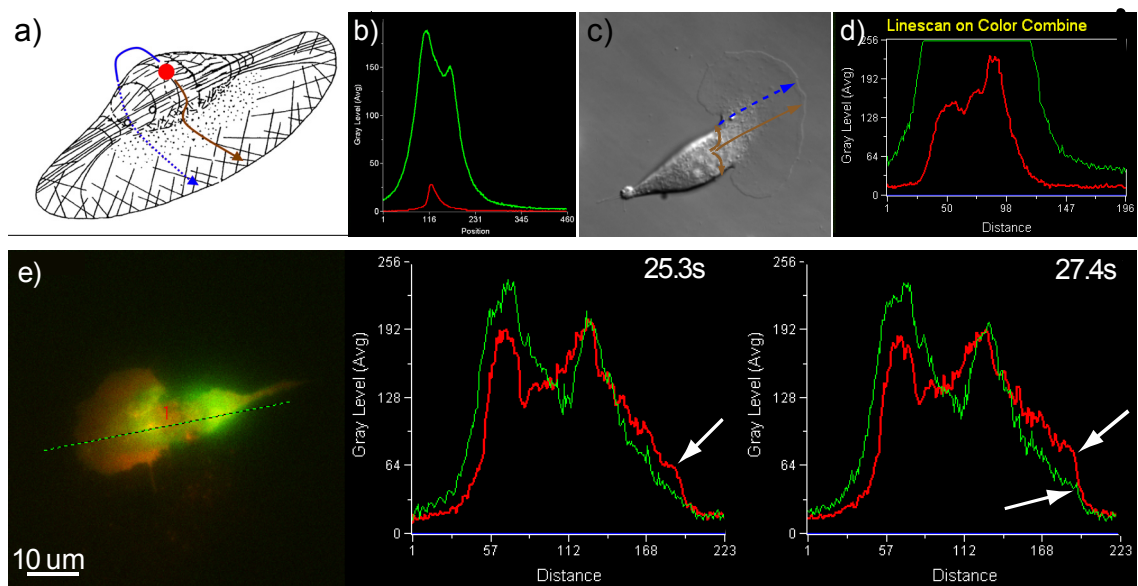


**Figure 4-2: Analysis of dye spreading**

In fish keratocytes the path length from the labelling location to the leading edge is slightly shorter via the dorsal membrane (brown path) compared to the basal membrane (blue path) (a). In contrast, in B16 cells the dye can go around the sides of the rather thin cell body, resulting in a similar distance to the leading edge in both membrane layers (c). Typically, the first TIRF image shows no or very little intensity (b (red curve), for fish keratocytes) but in B16 cells a huge amount of fluorescent intensity can be detected in the first TIRF image (d). In d it can be seen that the dye reaches the leading edge in TIRF before the majority of dye is visible in epi. At  $t=25.3s$  the arrow indicates the leading edge as identified by the accumulated intensity in TIRF (red curve) and at  $t=25.4s$  this accumulation is also visible in the green (epi) curve

Another surprising finding was that the linescan graph revealed that in B16 cells the arrival of dye at the leading edge takes around 25sec (Figure 4-2e, first graph). In contrast, in keratocytes this occurred within 2-4 sec. I cannot explain why the dye diffuses so slowly, as FRAP experiments later revealed a rather fast spreading (see section 4.3.3.)

In summary, the FLOID method could not be successfully applied on B16 F1 mouse melanoma cells. Cell shape and, even more importantly, the difficulty of labelling the cells with the membrane dye made this method unsuitable to determine the presence of a diffusion barrier around the leading edge in these cells.

## 4.2 Photo-bleaching and Photo-activation in TIRF

One major advantage of the B16 F1 mouse melanoma cells compared to fish keratocytes is that they can be easily transfected with fluorescent proteins. The expression of fluorescent membrane markers offered the potential to avoid damage induced by cell labelling through needle contact. FLOID analysis relies on imaging the initial diffusion of locally applied dye; however, transfected cells already display fully labelled cell membranes. In order to visualise the spreading of a membrane marker around the leading edge new approaches and techniques had to be tried. The first approach involved photo-bleaching of the ventral surface using evanescent field illumination followed by time lapse imaging in TIRF to observe dye diffusion around the edges. The customised TIRF system described in section 2.4 was constructed to provide the possibility of the following sequence: pre-image in TIRF using the 473 laser, bleaching of the ventral surface with the 405 laser in TIRF and start of a time-lapse of with the 473 laser in TIRF. Unfortunately we quickly realised, that the intensity of the 405 laser was not sufficient to effectively bleach the ventral membrane. Figure 4-3 shows pre-bleach and post-bleach images of GFP-F transfected B16 cells in TIRF.

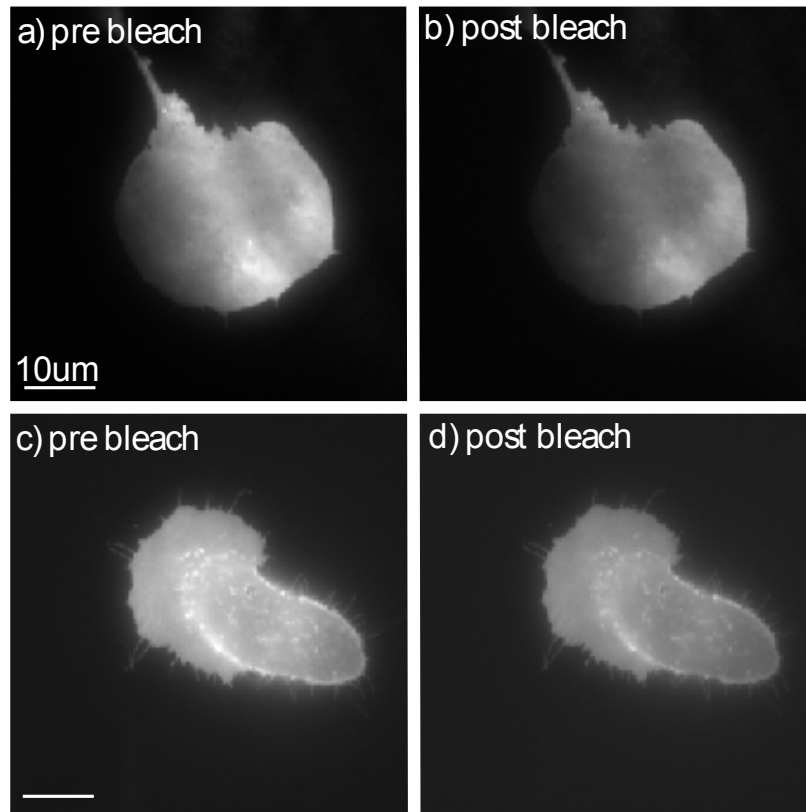


**Figure 4-3: photo-bleaching in TIRF**

Two examples of photo-bleaching using a 405 laser adjusted to TIRF are shown. Pre- and Post-bleach images were acquired with a 473 laser in TIRF to assess the quantity of decreased intensity after photo-bleaching. The first cell (a and b) resulted in 12.1% reduction, the second example (c and d) 7.8%. Both decreases are barely visible (images in same intensity scale).

Long bleaching times of 5sec resulted only in 2-13% reduction in GFP-F intensity. As membrane diffusion is a very fast process, it would be ideal to bleach on a timescale of milliseconds. Longer bleaching times would gradually result in the overall reduction in intensity, as non bleached molecules diffuse from the dorsal cell surface into the reach of the evanescent field, where they will also be bleached. As it was not possible to effectively bleach the ventral membrane enough after several seconds exposure, it would be impossible to achieve effective bleaching in a matter of milliseconds. Although the laser power of the 405 laser is with 55mW comparable to a confocal scanning microscope, the beam is expanded to illuminate an entire field, whereas in a confocal the beam is focussed to a very small area, resulting in a higher power per  $\mu\text{m}^2$ . Another factor could be a poor transmission of the TIRF objectives at 405nm. Ultimately, the power of our 405 laser is not enough to bleach the entire ventral surface in a short time and therefore, this approach had to be abandoned.

An alternative approach to photo-bleaching is photo-activation. In our experience photo-activation requires less laser power than photo-bleaching. We therefore decided to try photo-activation in TIRF as a second approach to replace the FLOID method. PA-GFP is a variant of GFP normally in a very low fluorescent state. After stimulation with 405 nm light, it switches to a high fluorescent state, emitting normal GFP emission at around 525nm (Patterson and Lippincott-Schwartz, 2002). Using the same TIRF setup as for the photo-bleaching, several datasets have been acquired. Instead of the previously used linescan analysis we analysed the intensity of small regions of interest at either protrusions sites or non-protrusion sites. After photo-activation of membrane bound PA-GFP (PA-GFP-F) through evanescent field illumination, the intensity signal at the bottom of the cell is predicted to decrease over time, as activated molecules diffuse away to the dorsal cell surface and are replaced by non-activated (non)-fluorescent molecules. If diffusion around the leading edge were inhibited, we would expect the intensity at the protrusion sites to decrease more slowly than at non-protrusion sites. Figure 4-4 shows a graph of the average of 25 individual regions for both situations.

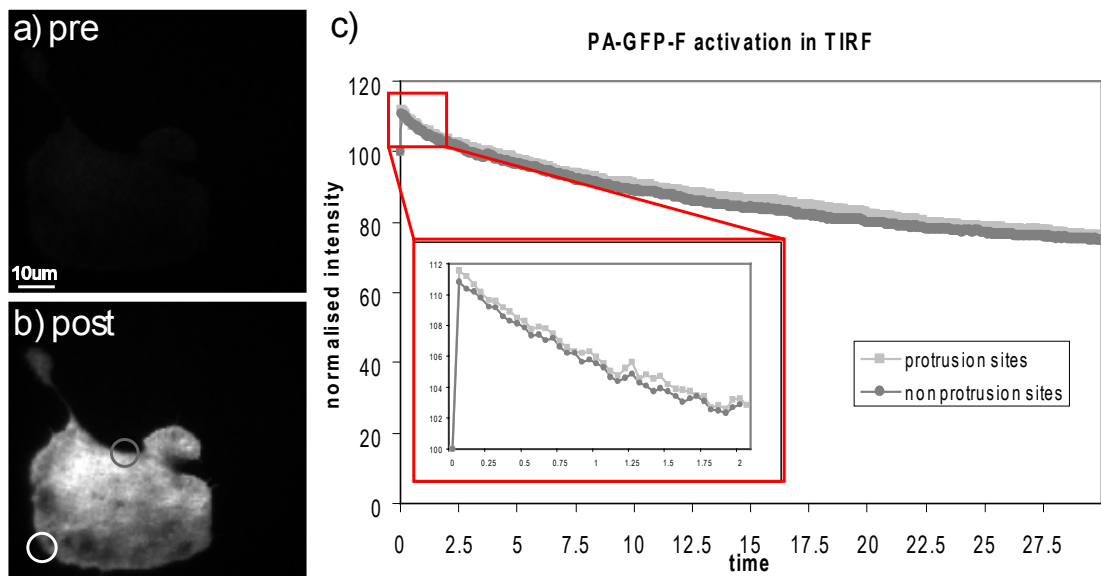


**Figure 4-4: analysis of photo-activation in TIRF**

Images a and b show the intensity of PA-GFP acquired with 473 laser in TIRF before and after activation with 405 laser in TIRF. For analysis, regions at different locations of the cell edge (light grey – leading edge = protrusion sites, dark grey – non protrusion sites) have been analysed over time and an intensity vs time graph is shown in c. No differences between the intensity curves could be observed for the different regions.

The graph demonstrates that the measured fluorescence intensity decreases over time in both regions, and there was no significant difference in the rate or amount of fluorescence loss at protrusions or non-protrusion sites. Both curves show an equal progression, meaning that the diffusion behaviour around the leading edge and cell body are similar. Another set of experiments (different day, fewer cells, data not shown) showed a slight decrease in intensity for non-protrusion sites and a stable intensity for protrusion sites (for at least 60 seconds). Although there is a difference between the two situations, it can not be concluded that a diffusion barrier was found. A stable intensity is surprising, as our previous data suggests that the leading edge diffusion barrier normally only hinders dye in its diffusion, but does not stop it completely. One possible reason could lie in the setup of the TIRF microscope. Evanescent field illumination excites molecules within 100-200nm of the glass surface. A lamellipodium is only around 70-180nm thick (including both membrane layers) (Koestler et al., 2009) and it is therefore possible that the evanescent wave excites both membrane layers and not just the ventral membrane. If this is the case, the intensity measured in regions at the leading edge would not decrease much after evanescent field activation, as activated molecules diffusing away would be replaced by also activated molecules from the dorsal lamellipodial surface.

This different result obtained from a separate experiment than the result shown in Figure 4-4, also indicates that this photo-activation method is highly variable. We cannot obtain the exact depth of evanescent field for different experiments, making it hard to compare datasets with each other.

In summary, the use of evanescent field photo-bleaching and photo-activation to determine the existence of a diffusion barrier at the leading edge of B16 cells was not successful. Although it was possible to acquire datasets with photo-activation, the analysis was inconclusive due to uncertainties in technical factors such as depth of the evanescent field illumination.

## 4.3 FRAP of membrane probes

After the unsuccessful use of different TIRF-based approaches to test B16 cells for the presence of a leading edge diffusion barrier, we decided to try Fluorescence Recovery after Photo-bleaching (FRAP) to compare the diffusion constant of membrane markers at the leading edge and further back within the lamellipodium. If the membrane diffusion barrier hinders membrane components in their diffusion around the leading edge, this should be detectable by a slower diffusion rate of the probes at this location compared to areas where their diffusion is not influenced by the leading edge diffusion barrier. Based on these expectations, I decided to perform membrane FRAP analysis at different places within the cell surface and compare their diffusion constants.

The following sections describe the method and its analysis as well as results for fish keratocytes and B16 cells.

### 4.3.1 *FRAP acquisition and analysis*

Diffusion within the membrane is a very rapid process and the expected difference in diffusion rate between the leading edge and lamellar regions is small. It is therefore crucial to have appropriate acquisition settings and analysis methods in order to be confident of the results. All FRAP experiments described have been performed on an Olympus FV1000 confocal. Preliminary FRAP experiments using Dil labelled fish keratocytes indicated that I had to sacrifice image quality to achieve the scan speed required to capture the quick recovery of membrane diffusion process. Preliminary analysis of the recovery of a circular region showed that the halftime of dye recovery to the bleached area was less than 150ms. To image several time-points within this short initial period, the scan speed had to be set to 0.065s per frame, the fastest possible for the FV1000. Due to microscope specific restrictions, this scan speed is only allowed for acquisition of images with a size of 256 by 256 pixels. As no averaging of lines or frames is possible at this acquisition speed, the resulting image sequences are very noisy. To achieve a reliable results, it was decided to take

more than 20 (generally around 40-80) measurements for each experimental condition. An additional important feature of the FV1000 is the separate SIM scanner, which allows acquisition with the 488 laser and simultaneous bleaching with the 405 laser, without interrupting the imaging scan. It became clear that the timing of the bleach (405) in relation to the imaging scan (488) was crucial and the diffusion constant changed if both parameters were not correlated. Ideally, the bleaching event (405 laser) has to be timed in a way that it occurs just before the position (ROI) is imaged with the 488 laser. Acquisition of the transmitted light channel allowed visualisation of exact time of the targeted photo-bleaching event (Figure 4-5).

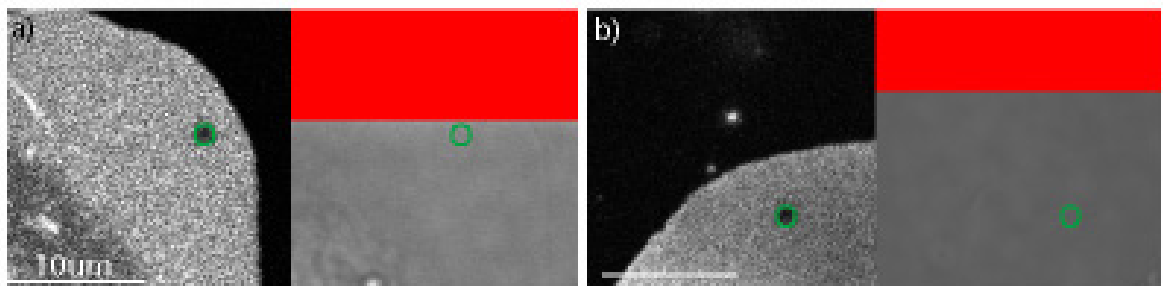


**Figure 4-5: positioning of the region for targeted bleaching (ROI)**

a) The ROI for the targeted bleach (green circle) was positioned at a place which would be imaged directly after the end of the bleach event, which is visualised in the transmitted light channel (red area, oversaturated detection due to the additional 405 laser excitation). In b, the ROI is further away, leading to half-a-frame-time-loss between bleaching and imaging.

By placing the region of interest (ROI) at a position which will be scanned by the imaging 488 laser just after the end of the bleaching event, the initial time point of the recorded timelapse will be equal to the starting point of the recovery (Figure 4-5a). If the ROI is positioned further away from the end of the stimulation (Figure 4-5b), the first timepoint will in reality already have partly recovered, leading to false results. In the example shown in Figure 4-5b, the distance between the end of the bleach event and the position of the region is roughly half a frame, corresponding to nearly 35ms. For a half-time of recovery of 150ms this time loss equals 20%. For all experiments the optimal y-position for the targeted photo-bleaching was therefore determined at the beginning of each session and its position within the 256x256 Pixel image preview was kept stable to the best of our ability. To position the cells, the stage was moved manually during a short live imaging period until the region of the cell which was chosen for targeted bleaching overlapped with the fixed ROI position. Movement

of the ROI along the x-axis of the image was allowed, as this does not affect the timing between imaging and bleach event.

After optimising the acquisition parameters, an appropriate analysis method had to be chosen. The two different approaches tested were: Mullineaux fit and exponential curve fit (both described in section 1.3.3).

For the calculation of Diffusion constants, the Mullineaux method has the advantage that no manual selection of a ROI is necessary for analysis. A FRAP timelapse was opened in Image J and the intensity profile along a straight line through the bleached area was plotted. This was repeated for several frames after the bleach.

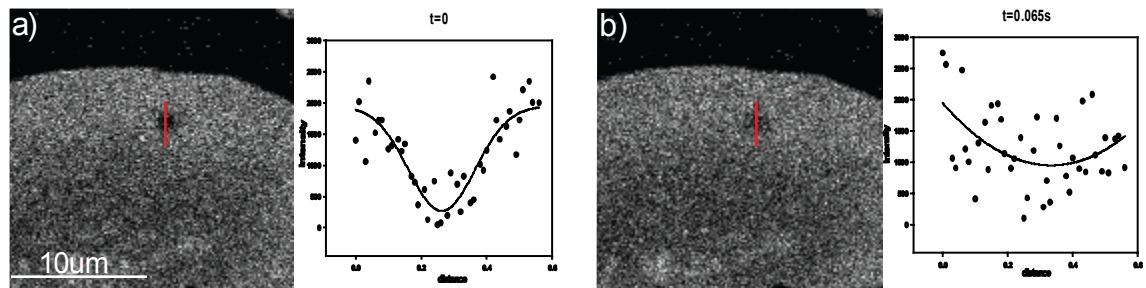


**Figure 4-6: Mullineaux analysis**

Intensity linescans across the bleached regions are performed at different time points after the targeted bleach event. In both images, the bleached area is visible per eye (a, c images). A Gaussian curve could be fitted into the intensity plot data from the first image (a), but for the image in b, SigmaPlot was not able to recognise a Gaussian profile.

The normal procedure of the method would be to fit a Gaussian profile in each of the intensity profiles, create a graph using the curve fit parameter and extract the diffusion constant using the slope of the fitted regression line. Unfortunately, the fluctuations in intensity in our data were too high (Figure 4-6). At  $t=0$ , the first image after stimulation, a Gaussian profile can be obtained. But by the next image (Figure 4-6b), the noise levels in non-bleached areas are in the same magnitude as the recovered intensity of the bleached area. Although a bleached area is still visible by eye, SigmaPlot was unable to fit a Gaussian profile. The Mullineaux method requires at least three points to fit a representative straight line and obtain a result. However, beside the first time point, the data were too noisy and the method could not be completed due to a lack of timepoints for the final extraction of the diffusion constant.

The second choice of analysis, exponential curve fit, only depends on the intensity in the bleached area. Preliminary analysis in the FV1000 software indicated that a good recovery curve could be obtained from the acquired data. For a more detailed analysis the image sequence was opened in Image J and intensity values of a region matching the bleached region were extracted. These data were then fitted using the “Exponential rise to maximum” equations in SigmaPlot. (Figure 4-7).

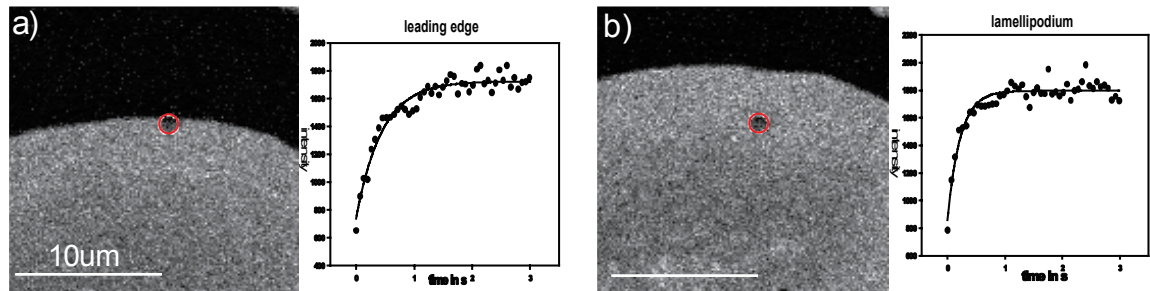


**Figure 4-7: exponential curve fit analysis**

A circular analysis region was overlaid with the bleach area (a and b images) and an intensity vs time plot was created and an “exponential rise to maximum” curve fit was performed using SigmaPlot. In a, an example of recovery at the leading edge is shown, in b, inside the lamellipodium. It can be seen from the graphs, that the dye has a faster recovery in lamellar regions compared to the leading edge.

In order to determine whether a single or double exponential equation would better represent the data, test data sets were fit using both functions. Several tests on initial FRAP data using the membrane dye DiI showed that the fit did not improve by the application of double exponential fits. The quality of a fit was judged by comparing the  $R^2$  values associated with different curve fits. If  $R^2$  did not increase significantly by the use of a double exponential equation, it was concluded that the data represent only a single exponential nature. As the membrane dye recovers only through diffusion within the membrane, this was the expected result. Most of the data shown in the following sections and chapters were analysed using the following equation to fit the data:

$y = y_0 + a(1 - e^{-bx})$ , with  $y$  representing the changing intensities at different time points ( $x$ ) and  $y_0$  being the intensity at  $t=0$ , the lowest intensity value and  $b$  the parameter used to determine the diffusion constant.

In some cases it was observed that the curve fit did not start close to the initial intensity value. In these cases  $y_0$  was set equal to this value, forcing the curve

fit to start at this point. If this increased the quality of the fit ( $R^2$ ) the result was changed. If  $R^2$  decreased, either the non-forced curve fit result was taken or this particular dataset was excluded from the final results.  $R^2$  values were normally around or above 0.9, but for some datasets numbers as low as 0.6 were obtained. This was not due to a bad curve fit itself, but rather to the high fluctuations in intensity of the measurement, leading to a very broad intensity range within the plateau of the recovery curve. Averaging the individual data sets may solve this problem. Before data sets could be averaged they had to be normalised, which can be done according to the normalisation procedure described by Axelrod (Axelrod et al., 1976). However, I decided not to average the curves, for the following reasons: Firstly, by averaging several fluorescence recovery curves into one, it was less apparent if one of individual curves behaved strangely and should have been excluded from the analysis set. Using the individual curve fit, outliers were recognised clearly and could be withdrawn from further analysis. A second disadvantage of the averaging method was the lack of means of error estimations. In order to compare diffusion rate at leading edge and lamellar regions, we performed a t-test to check whether the datasets obtained from the two regions were statistically different. The student t-test only functions using all individual data points (b from the curve fits or calculated Ds), as it needs the average as well as the standard deviation of the whole set. No standard deviation was obtained from the curve fit of the averaged data (i.e. one resulting b or D for each region), and therefore, it would not be possible to statistically compare the two situations.

The final procedure to analyse the FRAP data was as followed:

- 1) the image sequence acquired on the FV 1000 was imported into image J
- 2) a suitable region of interest was chosen manually (same region diameter for all datasets of one experiment)
- 3) an intensity vs time analysis was done using a plugin in Image J and resulting values were exported to Excel
- 4) unnecessary data (pre-bleach) were deleted and the Image J frame numbers were changed to time values by knowing the acquisition intervals

- 5) the data were transferred to SigmaPlot and each recovery curve datasets was fitted with an exponential rise to maximum curve fit resulting in a b value for each curve, which was transferred to Excel.
- 6) the diffusion constant was calculated from each b using the following equation:  $D = \frac{w^2 * b}{4 \ln 2}$  w= radius of analysis circle; b=curve fit parameter
- 7) the average of all D's of each region (leading edge and lamellipodium) was calculated and a two tailed, paired Student t-test was performed to test for significance

It has to be stated that the calculated diffusion constants do not represent absolute values. To measure absolute diffusion rates, a factor  $\gamma_D$  has to be calculated and multiplied with the above calculated D. This factor depends on the shape of the laser beam used for the targeting bleach and on the amount of bleach. Parameters were kept similar for all experiments and the multiplication with  $\gamma$  would only change the absolute values but not the comparison (t-test result) between two situations.

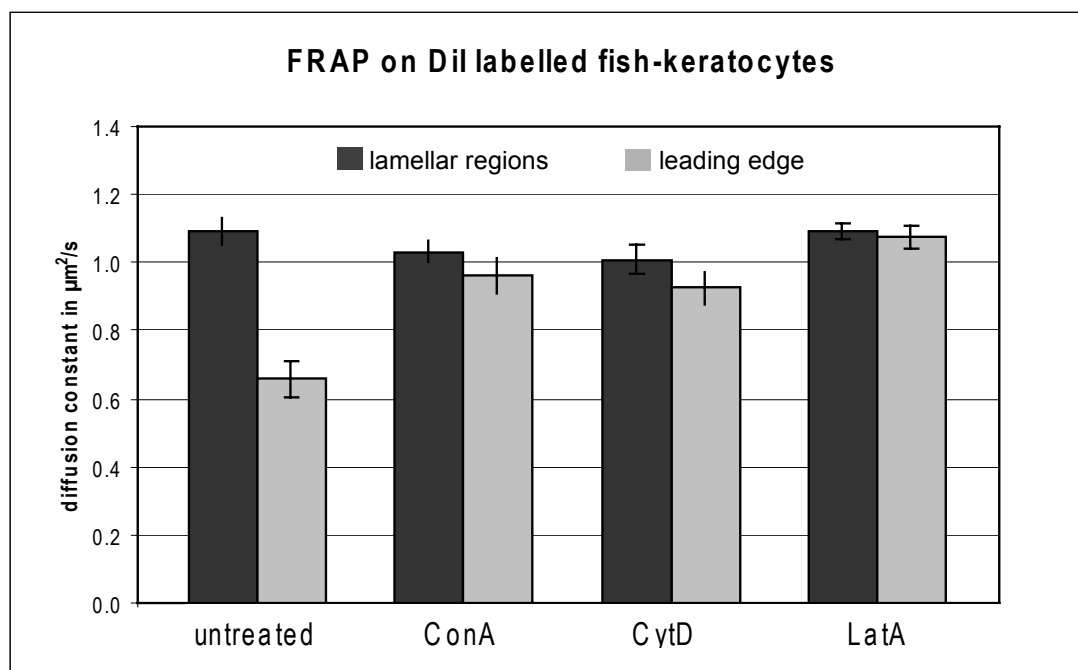
In my analysis, a circular region of interest is applied to the leading edge, resulting in half of the circle corresponding to an area outside the cell. Suggestions had been made that this may influence the analysis, as the circle would only be partly filled with intensity. Theoretically, the use of an only half-filled circle should not influence the analysis. Although this part of the analysed region will never recover, it did not possess any intensity to start with. The calculation of  $t_{1/2}$ , would be influenced by any slow recovering component, but not by a non recovering fraction. The only situation where the circular shape of the analysis region can influence the result is by movement of the cell, which steadily increases the intensity within the region. As membrane diffusion is very rapid, we only need a very short time to reach a clear plateau in the recovery curve. I used approximately 2sec of each dataset for the curve fit and within this time not even the fast moving fish keratocytes showed any measurable movement. Membrane diffusion rates are much higher than cell movement and the latter are therefore not influencing our results. Nevertheless, I compared circle and half-circle analysis for some data and realised that practical

difficulties and variances with the creation of half-circle regions made the latter method inappropriate.

A more problematic influence on the analysis of FRAP data is the intensity loss due to imaging. If fluorescent molecules are bleached by the imaging laser during their movement into the area of the targeted bleach, it will change the measured intensity during recovery and therefore incorrectly influence  $t_{1/2}$ . Data sets have to be normalised against the imaging dependent intensity loss. This imaging dependent bleaching was only problematic in the case of dictyostelium FRAP experiments and a correction was not needed for other datasets. The correction method is therefore explained further in the appropriate section (5.1.3).

### ***4.3.2 FRAP of Dil labelled fish keratocytes***

To identify whether the FRAP approach would be usable for the detection of a diffusion barrier at the leading edge, experiments were performed on fish keratocytes labelled with Dil C12 membrane dye. The same cells and dye were used for the initial discovery of the leading edge diffusion barrier with the FLOID method (Weisswange et al., 2005). The results of several independent experiments are shown in Figure 4-8.



	D in $\mu\text{m}^2/\text{s}$	s.e.m	n	$\Delta D$	P (t-test)	conclusion
untreated lam pod	1.09	0.04	44	0.43	<0.0001	different
untreated l. edge	0.66	0.05	41			
ConA lam pod	1.03	0.03	25	0.07	0.256	not different
ConA leading edge	0.96	0.05	25			
CytD lam pod	1.01	0.04	45	0.08	0.212	not different
CytD l. edge	0.93	0.05	45			
LatA lam pod	1.09	0.02	50	0.02	0.69	not different
LatA l. edge	1.08	0.03	50			

**Figure 4-8: FRAP on Dil labelled fish keratocytes**

Results of FRAP experiments on Dil labelled fish keratocytes. The graph shows the diffusion constants in lamellar regions (black) and at the leading edge (grey) of untreated, CytD treated and LatA treated keratocytes. The diffusion at the leading edge of untreated cells is much smaller than in lamellar regions. After drug treatment, this difference was abolished. The table shows all diffusion constants, their error (s.e.m.), the total number of FRAP experiments per situation (n) and the result of a t-test to compare lamellar and leading edge diffusion rates.

The diffusion coefficient of Dil C12 within an untreated lamellar region was  $1.09\mu\text{m}^2/\text{s}$ . In contrast, diffusion at the leading edge was 38.4% lower ( $0.66\mu\text{m}^2/\text{s}$ ). It can therefore clearly be stated that the diffusion of the Dil C12 membrane dye was hindered at the leading edge of untreated, protruding fish keratocytes.

To test the dependence of the lipid diffusion barrier on actin, cells were treated with CytD or LatA to disrupt their actin cytoskeleton. These treatments were preceded by ConA treatment to conserve the cell shape and the lamellipodium.

Surprisingly, FRAP experiments on only ConA treated cells revealed that ConA increased the diffusion of Dil in leading edge regions (Figure 4-8). The diffusion coefficient at the leading edge of ConA treated cells was  $0.96\mu\text{m}^2/\text{s}$ , compared to  $0.66\mu\text{m}^2/\text{s}$  at the leading edge of untreated cells. In lamellar regions the diffusion coefficient of Dil was statistically equal in ConA treated ( $1.03\mu\text{m}^2/\text{s}$ ) or untreated ( $1.09\mu\text{m}^2/\text{s}$ ) keratocytes ( $P(\text{t-test})=0.28$ ). Previous results using ConA treated keratocytes and the FLOID method showed that 50% of cells possessed a diffusion barrier and 50% did not (Weisswange et al, 2005). This result was explained by the through ConA treatment introduced centripetal flow, which pulls the actin filaments away from the leading edge membrane. This 50/50 situation may not be visible with the FRAP method, as we always get a valid diffusion rate only the magnitude changes, whereas the FLOID method gave diffusion barrier or no diffusion barrier as an answer. Being more quantitative, the FRAP method provides a range of different diffusion constants, but does not distinguish between the two extreme cases, which in the ConA situation probably leads to a less informative result.

Cells treated with CytD or LatA (both preceded by ConA treatment) did not show a difference in diffusion rates between the leading edge and the lamellipodium. Treatment with either drug combination resulted in statistically equal diffusion coefficients of Dil C12 in both regions (Figure 4-8). However, these results can not be used to conclude that the diffusion barrier was abolished through the destruction of the actin cytoskeleton, as ConA treatment alone had the same effect.

Besides the elimination of diffusion difference between leading edge and lamellar regions, ConA (alone and in conjunction with CytD) also reduced the lamellar diffusion rate of the Dil C12 membrane dye. The reduction of around 7.5% in both cases is not significant ( $P(\text{t-test, ConA+CytD vs untreated})=0.17$ ). It can not be concluded at this stage whether this is a coincidental data fluctuation or the result of a biological effect of the drugs, but results in section 4.3.3 and 4.3.4 suggest a biological cause. The result that ConA treatment alone alters

membrane diffusion means that the actin-dependency of the diffusion barrier could not be concluded using the presented FRAP data. But as these data do not disprove an actin dependency either, they are not in disagreement with the previously published results that DiI C12 dye is hindered in its diffusion around the leading edge of fish keratocytes in an actin dependent manner (Weisswange et al., 2005). In fact, my data agree with the from Weisswange et al found leading edge lipid diffusion barrier. The newly used FRAP approach not only confirms a diffusion rate difference between leading edge and lamellar regions, but it also provides quantitative details of the reduction at the leading edge (38%). Although the drug treatment results can not be interpreted biologically, the equal diffusion rates in lamellar as well as leading edge regions show that the FRAP approach is able to distinguish between the presence and the absence of a lipid diffusion barrier at the leading edge. This also eliminates causes such as membrane curvature as the reason for the slower diffusion at the leading edge, as the curvature is still present in the drug treated cells which do not show a diffusion barrier. It can therefore be concluded that the FRAP approach can be used to detect this diffusion barrier and is a suitable approach for further experiments. However, other ways have to be found to show or test for an actin dependency of this diffusion barrier, as the drug treatments gave misleading results.

### ***4.3.3 FRAP of DiI labelled B16 F1 cells***

Following the successful use of FRAP to show the membrane diffusion barrier at the leading edge of DiI C12 labelled fish keratocytes, we performed similar experiments on DiI labelled B16 F1 cells in order to test for the existence of a leading edge diffusion barrier in these cells. If a lipid diffusion barrier is present, we would expect a difference in diffusion rates between leading edge and lamellar regions. This difference should disappear after LatA or CytD treatment. Figure 4-9 shows the obtained diffusion rates.

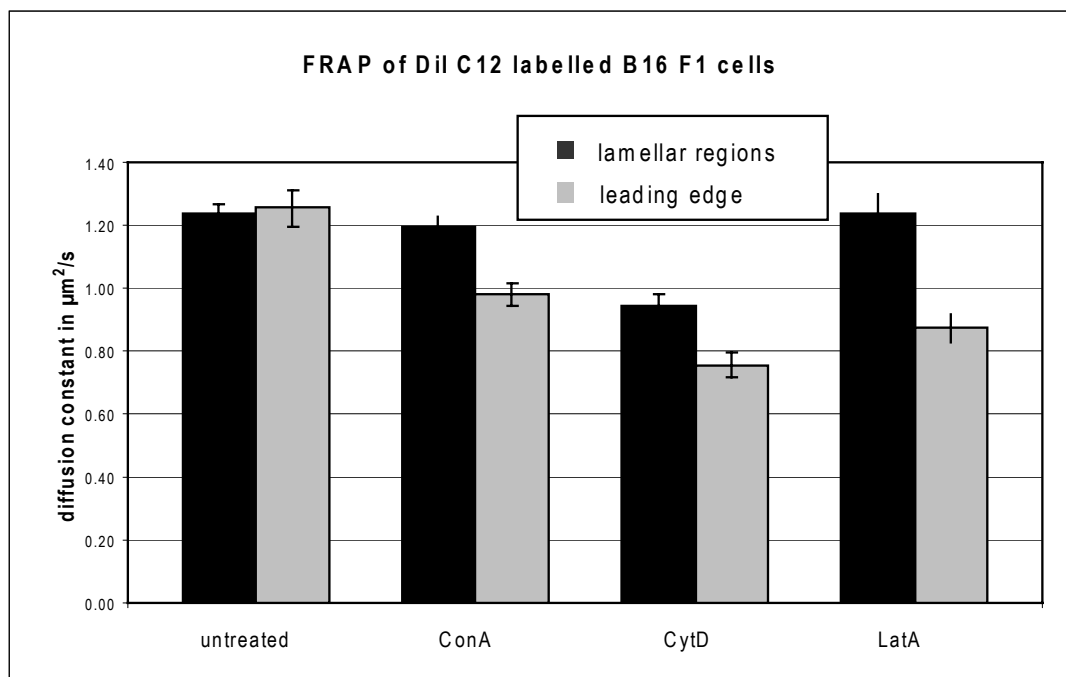


**Figure 4-9: FRAP of Dil C12 labelled B16 F1 cells**

Results of FRAP experiments on Dil labelled B16-F1 cells. The graph shows the diffusion constants in lamellar regions (black) and at the leading edge (grey) of untreated, CytD, LatA and ConA treated cells. No difference in diffusion rate between lamellar regions and the leading edge could be observed in untreated cells, whereas differences were present after drug treatments. The table shows all diffusion constants, their error (s.e.m.), the total number of FRAP experiments per situation (n) and the result of a t-test to compare lamellar and leading edge diffusion rates.

The obtained results were not in agreement with our expectations, they were in fact the complete opposite. The according to these data apparent findings are inconclusive and inconsistent with previous results from fish keratocytes.

First, no difference in diffusion rates between the leading edge and lamellar region could be detected in untreated cells. The diffusion constants were  $1.24\mu\text{m}^2/\text{s}$  for lamellar regions and  $1.25\mu\text{m}^2/\text{s}$  at the leading edge. Therefore, Dil C12 dye does not appear to be hindered in its diffusion around the leading edge

of B16 F1 cells. One possible explanation may be that the Dil dye is too small to be hindered by effects of actin polymerisation at the leading edge of B16-F1 cells. Although the dye was slowed down at the leading edge of fish keratocytes, it may be that the strength of the membrane diffusion inhibition depends on cell type specific factors. A major difference between B16 cells and fish keratocytes is their protrusion velocity. Less protrusion indicates that actin polymerisation is generating less force against the leading edge membrane of B16 cells. Perhaps this weaker force on the membrane means that the lipid diffusion barrier is less efficient in these cells and is not able to block diffusion of Dil dye in the outer membrane leaflet of the leading edge. This are only speculations at this stage, as the performed FRAP experiments do not provide evidence for the cause of the diffusion barrier or its strength. This problem will be addressed in chapter 5.

The second surprising result was that all drug treatments (ConA alone and ConA followed by CytD or LatA) significantly reduced the diffusion rates at the leading edge but not within lamellar regions (Figure 4-9). As mentioned before, ConA treatment was needed to prevent the lamellipodium from collapsing due to the destruction of the actin cytoskeleton following LatA or CytD treatment. FRAP on ConA treated cells was performed as a control to ensure this drug treatment would not influence later results. However, it seems like ConA is changing the mobility of the Dil dye in B16 cells. Lamellar regions showed a diffusion rate statistically equal to untreated cells, but the diffusion rate of ConA treated cells at the leading edge was 21.6% lower than the rate at the same location in untreated cells. The lectin ConA is a very non-specific drug, interacting with many targets, such as sugars, glycoproteins, glycolipids (Sharon and Lis, 1972) and MMPs (Yu et al., 1995). Having so many binding partners on the cell surface can greatly influence membrane dynamics. Already in Dil labelled keratocytes ConA influenced the diffusion behaviour at the leading edge. Confusingly, in this case ConA increased Dil diffusion at the leading edge (section 6.3.2). As a consequence of these results, I conclude that ConA is not a good drug to use in conjunction with diffusion rate measurements of membrane probes and it would be ideal to avoid its use for further membrane diffusion experiments. Unfortunately we could not treat the cells with CytD or LatA alone, as this destroyed the lamellipodium. But, due to the influence of ConA on membrane diffusion, the in Figure 4-9 shown results for CytD and LatA can not be used for

interpretation, as it can not be distinguished between the effect of ConA and the actin-disrupting drugs.

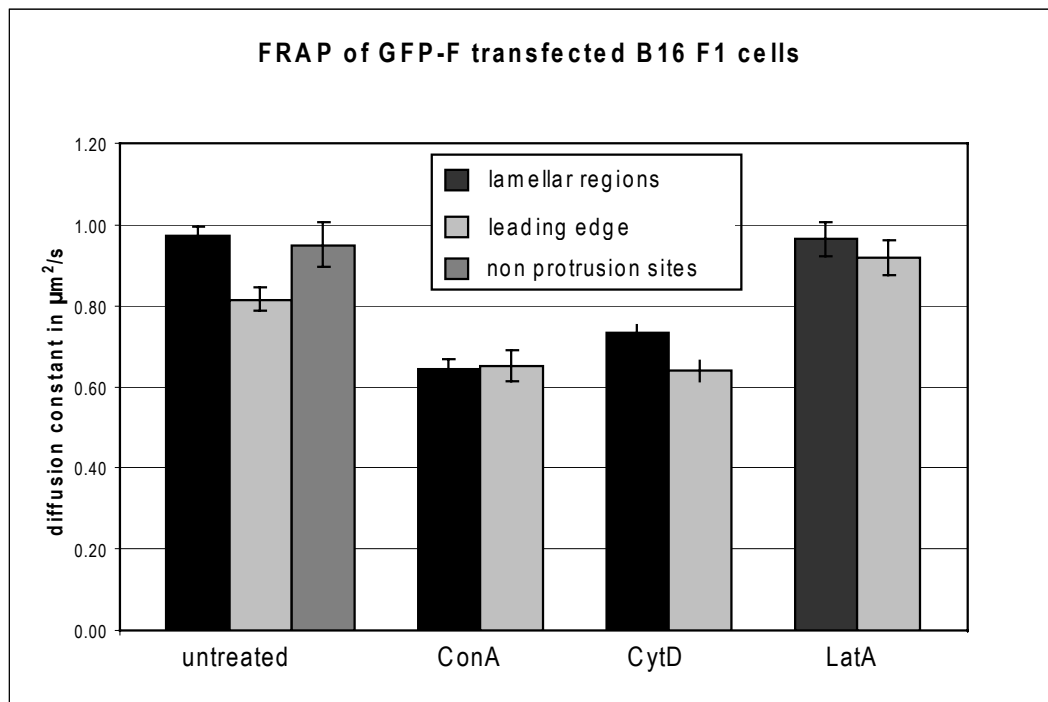
One interesting aspect of the data is that CytD treatment of B16 cells reduced the diffusion rate in lamellar regions compared to untreated cells. A similar effect was also observed in Dil labelled keratocytes (section 4.3.2), but in contrast to keratocytes, in the B16 cells this difference was clearly significant ( $P(t\text{-test}) < 0.0001$ ). Possible explanations will be given in section 4.3.4.

Another general observation was that both cell types showed a dissimilar rate of diffusion of DilC12 within the lamellipodium. The difference in diffusion rates in lamellar regions of both cell types equals  $0.15\mu\text{m}^2/\text{s}$  and is significant ( $P(t\text{-test}) = 0.004$ ). This may be due to cell-type specific composition (lipids as well as proteins) of the membrane.

In summary, diffusion rates for Dil treated B16 cells were confusing and inconclusive in regards to the diffusion barrier. Drug treatment greatly influences the mobility of the membrane dye and should, if possible, be avoided. Other approaches to test for an actin dependency of the lipid diffusion barrier have to be considered, one will be explained in the following section.

#### **4.3.4 FRAP of GFP-F transfected B16 F1 cells**

Following the confusing results with the Dil membrane dye, which was inhibited at the leading edge of keratocytes but not B16 cells, I wanted to test another membrane marker and see if its diffusion behaves differently and maybe indicates the existence of a leading edge diffusion barrier in B16 cells. In comparison to the fish keratocytes, B16 cells are easily transfectable, which allows a much wider choice of membrane markers. I chose GFP-F, a GFP linked to the membrane via an added farnesylation sequence from H-Ras (Hancock et al., 1991). Preliminary transfection tests showed a very uniform expression at the plasma membrane. The results of the FRAP experiments using GFP-F are shown in the graph and the table below.



	D in $\mu\text{m}^2/\text{s}$	s.e.m	n	$\Delta D$	t-test	conclusion
untreated lampod	0.97	0.02	111	0.157	3.03E-05	different
untreated l. edge	0.82	0.03	80			
non-protrusion sites	0.95	0.06	31			
ConA lampod	0.65	0.02	30	-0.01	0.87	not different
ConA l.edge	0.65	0.04	30			
CytD lampod	0.73	0.02	40	0.09	0.006	different
CytD l.edge	0.64	0.03	40			
LatA lampod	0.96	0.04	39	0.05	0.43	not different
LatA l.edge	0.92	0.04	40			

**Figure 4-10: FRAP of GFP-F transfected B16 F1 cells**

Results of FRAP experiments on GFP-F labelled B16-F1 cells. The graph shows the diffusion constants in lamellar regions (black) and at the leading edge (grey) of untreated, CytD and LatA treated cells. The diffusion at the leading edge of untreated cells is significantly smaller than in lamellar regions. this difference was abolished after drug treatment and no difference could be observed between lamellar regions and non-protrusion sites. The table shows all diffusion constants, their error (s.e.m.), the total number of FRAP experiments per situation (n) and the result of a t-test to compare lamellar and leading edge diffusion rates. The table also includes data from ConA treated cells, which are not shown in the graph.

The first aspect of these data was that the diffusion of GFP-F was significantly slower ( $P(\text{t-test}) < 0.001$ ) than the diffusion of Dil C12 in the same cell type. In lamellar regions, GFP-F showed a diffusion constant of  $0.97\mu\text{m}^2/\text{s}$ , compared to  $1.24\mu\text{m}^2/\text{s}$  for Dil labelled lamellar regions. This may be explained by the different size of these two membrane markers, in conjunction with their location within the membrane bilayer. Whereas the small, lipid-size Dil sits in

the outer membrane surface, the rather big GFP part of GFP-F sticks out from the inner membrane layer. The GFP-F may therefore be more influenced by membrane bound proteins and its diffusion might also be hindered by the actin cytoskeleton. The influence of the cortical actin meshwork on membrane diffusion has been described in the membrane fence model (Sako and Kusumi, 1995) and could explain the lower diffusion rate of GFP-F.

The second, more important result of the FRAP experiments on GFP-F labelled B16 cells was the lower diffusion rate at the leading edge compared to lamellar regions. The decrease of  $0.16\mu\text{m}^2/\text{s}$  (16.2%) is not as big as it was in Dil labelled fish keratocytes (38.4%), but is clearly significant ( $P(\text{t-test}) < 0.0001$ ) and suggests the existence of a leading edge membrane diffusion barrier in B16 cells.

Treatments with drugs in order to test for actin dependency resulted again in very confusing results, which cannot be used for final conclusions. As seen with Dil labelled B16 cells (and Dil labelled keratocytes) ConA also changed the behaviour of GFP-F membrane diffusion. ConA treatment alone significantly reduced the general, lamellar diffusion rate compared to untreated cells ( $0.65\mu\text{m}^2/\text{s}$  vs  $0.97\mu\text{m}^2/\text{s}$ ). ConA clusters carbohydrate-containing receptors which may lead to a tighter association with the underlying actin cytoskeleton as well as a more rigid membrane. Membrane diffusion could therefore be slower than in untreated cells. A possible explanation why there is no difference in diffusion rates at the leading edge and inside the lamellipodium could be the effect of ConA on the lamellipodial actin meshwork (not the cytoskeleton, but the network of actin filaments responsible for protrusion). If somehow ConA would decouple this normally in respect to the substrate stationary filament meshwork from its anchors, this network could then be retracted by myosins. This retraction of the actin meshwork is also called retrograde or centripetal flow and could be observed in ConA treated keratocytes (Weisswange et al, 2005). The distinction between the effect of ConA on the cytoskeletal or the lamellipodial actin meshwork might explain the different results using CytD or LatA after ConA treatment. ConA+LatA treated cells show similar diffusion rates as untreated cells, but no difference between lamellar or leading edge regions, whereas ConA+CytD treated cells maintain the slower membrane diffusion caused by ConA but show a small difference between the two regions (Figure 4-10).

Destruction of the actin cytoskeleton as well as the lamellipodial meshwork by LatA might disrupt the tight membrane-cytoskeleton association caused by ConA and allow membrane components to move more freely, explaining the faster, in comparison to untreated cells similar, diffusion rate. The reason why CytD treatment does not have the same effect could lie in the different working mechanism of both drug. As LatA binds actin monomers, the G-actin concentration within the cell is near 0 and the treadmilling equilibrium of actin will be shifted towards depolymerisation, resulting in the destruction of a very high percentage of actin filaments. CytD binds to the +ends (barbed ends) of actin filaments and impedes the addition of new actin monomers. But it also induces the formation of actin-dimers (Goddette and Frieden, 1986). Through the depolymerisation of CytD blocked actin filaments, the amount of actin monomers (G-actin) within the cell increases rapidly, which leads to enlarged actin polymerisation. CytD treated cells might therefore have many short actin filaments left, whereas in LatA treated cells no filaments are left at all, as this drug sequesters monomers, preventing any polymerisation. If all the actin-oligomere-clusters of the CytD treated cells are in contact with the membrane, they could form a less efficient but still existent cytoskeleton fence to hinder membrane diffusion. It has also been shown that CytD influences the membrane impedance (Ravdin et al., 1985), which could also affect diffusion within the membrane. As there are normally more +ends concentrated at the leading edge it may well be that the effect of CytD-actin-membrane clustering is stronger there, explaining the reduced diffusion rate at this location of CytD treated cells in comparison with lamellar regions of the same cells.

The FRAP data of GFP-F transfected B16 cells can be used to conclude that the leading edge of B16 F1 cells acts as a diffusion barrier for membrane components. However, due to the high influence of the used drugs on membrane diffusion, an actin dependency of this leading edge diffusion barrier could not be shown. We therefore looked for another way to show the dependence on actin polymerisation without the use of ConA, CytD or LatA.

In contrast to fish keratocytes, protrusion in B16 cells is less robust. Not all regions of the leading edge actively protrude at all times and when the cell changes direction, a previously active region can cease its protrusion. It is in general easy to find regions which appear to have reduced or stopped actin

polymerisation. The same FRAP experiments as for the seemingly protruding leading edges were performed on non-protruding cell edges (figure 4-11)

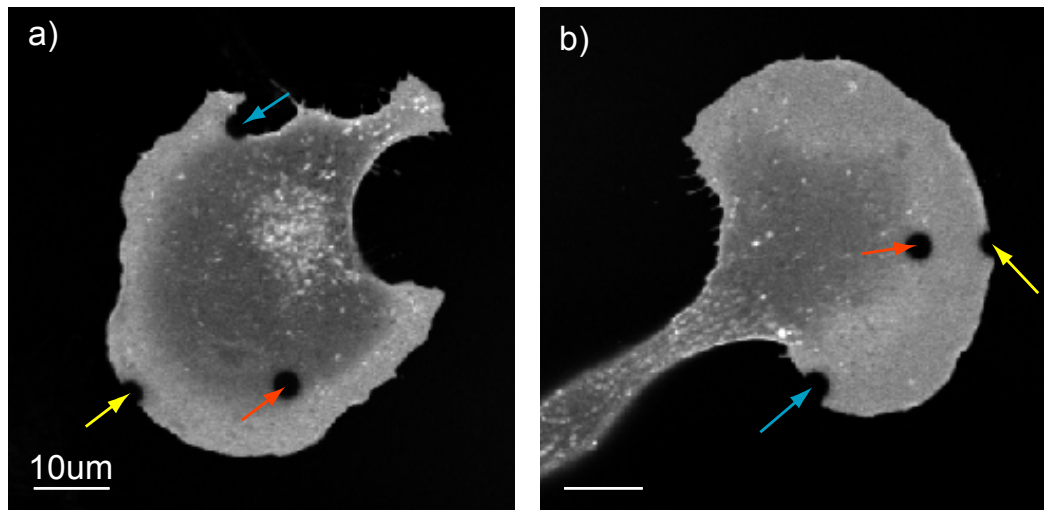


**Figure 4-11: FRAP positions**

The two images show fixed GFP-F transfected B16-F1 cells, where typical examples of regions for the FRAP analysis were bleached. The red arrows show lamellar regions, the yellow arrows indicate regions at the protruding leading edge and the blue arrows point towards regions at non-protrusion sites.

The diffusion constant at non-protruding cell edges was statistically equal to lamellar regions ( $3.80\mu\text{m}^2/\text{s}$  vs  $3.89\mu\text{m}^2/\text{s}$ ; Figure 4-10). This result was achieved on untreated cells, without the use of actin-drugs which may have secondary effects. These results show that in the absence of active protrusion no membrane diffusion barrier can be detected. This supports the idea that actin polymerisation is needed to hinder membrane components in their diffusion around the cell edge.

Diffusion measurements at the leading edge and inside the lamellipodium were also performed on GFP-PH-PLC and GFP-MEM transfected B16 cells. These constructs (described in Material and Methods) have different membrane anchors compared to GFP-F and were tested as a control that the leading edge diffusion barrier in B16 cells can be seen as a membrane feature and not a GFP-F specific property. GFP-PH-PLC diffusion was significantly ( $P=0.013$ ) lower at the leading edge, with a diffusion constant of  $0.63\mu\text{m}^2/\text{s}$  compared to  $0.79\mu\text{m}^2/\text{s}$  in lamellar regions. This indicates that the diffusion barrier seems to influence membrane anchored proteins in general. Oddly, the rate of GFP-MEM diffusion was much faster than the other membrane anchored GFPs tested, resulting in  $D=1.83\mu\text{m}^2/\text{s}$

in lamellar regions. Furthermore, its diffusion was not reduced at the leading edge ( $D=1.89\mu\text{m}^2/\text{s}$ ). I cannot explain these results. It has been shown that MEM-fused fluorophores tightly interact with each other within the membrane (Konig et al., 2008), suggesting a localisation within membrane subdomains. However, this would result in a slower rather than a faster diffusion. But, as this probe clearly behaves differently than both other tested membrane markers (GFP-F and GFP-PH-PLC), I consider the GFP-MEM result as irrelevant.

In summary, it could be shown that B16 F1 cells possess a hindered diffusion of membrane markers at the leading edge. Without the use of any drug treatment it could be shown that this leading edge diffusion barrier depends on active protrusion.

#### 4.3.4.1 FRAP of cytoplasmic GFP in B16 cells

As a control, another set of experiments was done using non membrane bound GFP. One purpose of this experiment was to show that the observed difference in membrane diffusion is not due to analysis errors or due to a tight packing of cytoplasmic components within the thin lamellipodium. Another reason was to demonstrate the specificity of the found decrease in membrane diffusion.

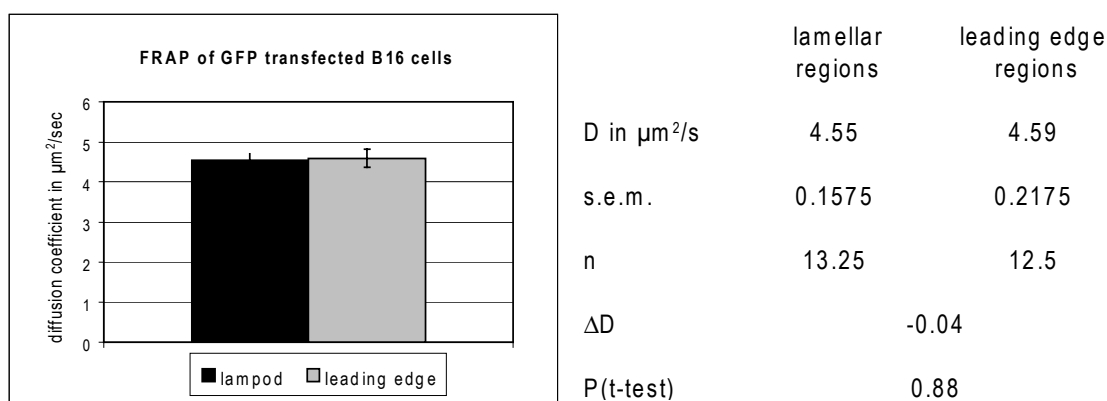


**Figure 4-12: FRAP of GFP transfected B16 cells**

Diffusion of non-targeted GFP was equally fast in lamellar regions as well as at the leading edge (graph). The table shows the detailed results, including a t-test.

The diffusion rate of cytoplasmic GFP is higher than of GFP-F, with an increase of more than 3 times to  $4.55\mu\text{m}^2/\text{s}$  in lamellar regions. At the leading edge an

equally fast recovery could be observed ( $4.59\mu\text{m}^2/\text{s}$ ). Both results are expected. Since GFP is not linked to anything, it can freely diffuse within the cell and should not be hindered by participation in any biological processes or incorporation to specific structures. This result also shows that the FRAP approach can distinguish between two cases: a similar diffusion rate in lamellar and leading edge regions or a slower rate at the leading edge. The only uncertainty in the cytoplasmic GFP results is the actual magnitude of the diffusion coefficient. Due to the limitations of microscope scan speed, it could well be that the real diffusion coefficient is even higher than I was able to measure. However, it is not necessary to know the exact diffusion rate. This probe serves as a control to show that inhibition of membrane bound probes at the leading edge is specific.

## 4.4 Summary and conclusions

This chapter presented several approaches to determine the existence of a membrane diffusion barrier around the leading edge. Photo-activation and -bleaching of the ventral cell membrane did not result in clear data and technical uncertainties made these techniques unsuitable. The FLOID method, which had previously been used on keratocytes, was not applicable to B16 F1 cells due to labelling difficulties as well as unsuitable cell shape. Using a FRAP approach, I could reproduce previously published data (Weisswange et al., 2005), showing that the membrane diffusion around the leading edge of fish keratocytes is hindered.

Compared to the FLOID method, FRAP measurements not only give the same conclusions, but they also provide quantitative information about the difference in membrane diffusion. In fish keratocytes the diffusion of DiI C12 membrane dye around the leading edge was decreased by 38.5%. No reduction in DiI diffusion around the leading edge of B16 cells could be found, but the diffusion of membrane anchored GFP (GFP-F) was decreased by 15.98%. This smaller reduction in the B16 cells compared to fish keratocytes could be the reason why no barrier was found with DiI C12 dye in B16 cells. The smaller decrease of

diffusion suggests a weaker influence of actin polymerisation on the membrane at the leading edge of B16 cells. Whereas the rather big GFP-F is hindered in its diffusion, the actin-membrane interaction is not strong enough to impede the diffusion of the small lipid dye.

The use of drug treatments to test for a dependency of the leading edge diffusion barrier was not successful, as the drugs interfered with the general membrane diffusion and the obtained FRAP results could therefore not be used for clear conclusions. An important result was therefore the absence of a membrane diffusion barrier at non-protruding areas of the lamellipodium edge, which was achieved without any drug treatment.

Theseresults demonstrates that the interaction between polymerising actin filaments and the plasma membrane reduces the mobility of membrane components at the leading edge. Having observed this phenomenon in two different cell types, using several different membrane probes suggests that it may be a general feature of protrusion.

The use of FRAP also indicated that the leading edge is not a diffusion barrier but rather a zone of restricted mobility. Diffusion within this zone is possible, but at a lower rate than in lamellar regions. This restricted mobility might be important for actin polymerisation at the leading edge, as it may trap actin-regulating proteins in this area and therefore influence actin regulation.

## 5 Investigations into the physical basis of the leading edge lipid diffusion barrier

After showing in the previous chapter that the membrane diffusion barrier around the leading edge may be a general feature of protrusion in cells, the next step was to investigate its cause. Previously discussed results indicated that the inhibition of membrane diffusion around the leading edge is dependent on actin polymerisation, which suggests that the interaction between the +ends of the actin filaments and the membrane is the reason for this diffusion barrier. There are two hypothetical models which could explain how this interaction can influence diffusion within the membrane: a) force-based model and b) density-based model. The force-based model is predicated on the force generated by actin polymerisation directly behind the leading edge membrane fold. As this force causes cell protrusions by pushing the membrane forward, it is not unreasonable to suppose that it might influence lipid diffusion within the membrane. By exerting force against the inner membrane layer, the lipids from both bilayers are squeezed together and their tangled acyl chains may form dense region within the membrane, leading to hindered diffusion for membrane components. It could also be that pushing against the membrane changes the composition of the inner membrane layer which then results in a rearrangement of the outer membrane layer as well. Although it was shown that the lipid diffusion barrier around the leading edge does not depend on lipid rafts (Weisswange et al., 2005), the involvement of other, perhaps temporary micro domains may not be excluded. The second hypothetical model is based on a high density of membrane associated proteins. It could be that such proteins occupy so much space at the leading edge that other membrane components are hindered in their diffusion through this area. These proteins may also be linked to the polymerising actin filaments, creating a fence as described in other membrane fence models known to alter membrane diffusion ((Nakada et al., 2003), see introduction section 1.2.2).

The previously described experiments using the FLOID method and the FRAP approach (chapter 4) identified the leading edge as a region of hindered diffusion, but did not provide much indication of its cause. With now two cell lines (fish keratocytes and B16 F1 mouse melanoma cells) demonstrated to

possess a lipid diffusion barrier we were able to extend the range of experiments to characterise this phenomenon. B16 cells allow expression of fluorescently tagged proteins and are more easily available due to their immortality in culture. Keratocytes however have the advantage of more consistent movement and robust protrusion. In the previous chapter, I showed that the use of drugs to influence cell behaviour could lead to confusing results due to non-specific side effects of these drugs. A major criterion for experimental conditions was therefore not to use unnecessary drug treatment.

The following chapter will show different approaches to investigate the nature of the actin-membrane interaction at the leading edge in order to provide data which might distinguish between force-based and density-based mechanisms.

## **5.1 FRAP approaches**

Following the successful use of FRAP to measure a difference in diffusion rate between the leading edge and lamellar regions, I wanted to further use this in comparison to FLOID more flexible method to investigate the cause of the lipid diffusion barrier. Thus, more FRAP measurements were performed under different, carefully defined conditions.

### ***5.1.1 Influence of the speed of protrusion on the leading edge diffusion barrier***

As shown in chapter 4, the difference in magnitude of the diffusion impairment at the leading edge between Dil labelled fish keratocytes and GFP-F transfected B16 cells is significant. In B16 cells, diffusion of Dil membrane dye around the leading edge was not hindered. A major difference between the two cell types is velocity and robustness of their migration. Fish keratocytes are much faster than B16 cells. This led to the idea that the strength of the diffusion barrier could

depend on the protrusion rate of the cell. To verify this hypothesis, FRAP measurements at the leading edge were combined with measurements of the leading edge protrusion velocity. Figure 5-1 shows the result for one dataset of DiI labelled fish keratocytes. The prediction was to obtain smaller diffusion rates with increased cell velocity.

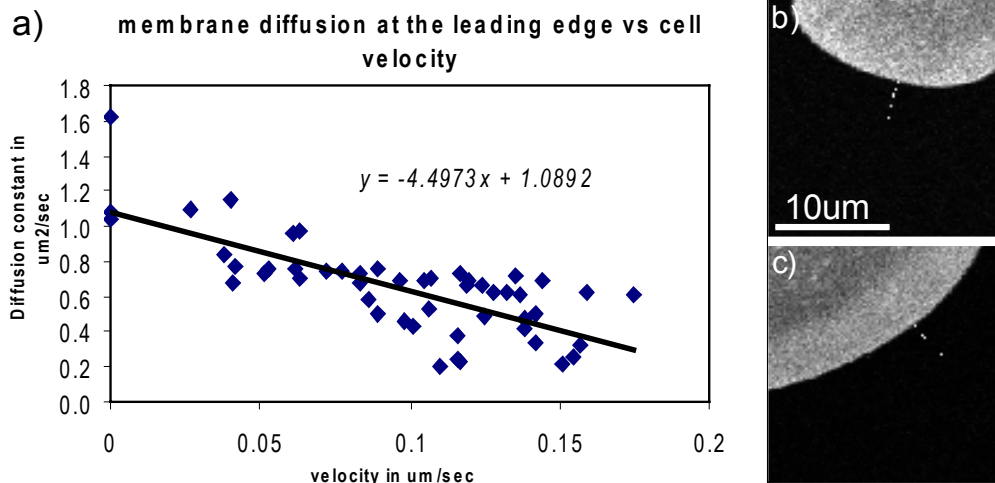


**Figure 5-1: protrusion rate influences lipid diffusion around the leading edge.**

A 6sec time-lapse was taken to determine the protrusion rate of the leading edge. The first 2 sec included a targeted bleaching event and its recovery. The velocity was then determined at the location of the targeted bleach in order to minimise the influence of local differences in protrusion. In a, a set of 50 measurements (i.e. cells) is represented, taken during one experimental session. A linear regression shows an obvious decline of diffusion rate (represented by the Diffusion constant in  $\mu\text{m}^2/\text{s}$ ) at higher cell velocities (in  $\mu\text{m}/\text{s}$ ). Pictures b and c represent two examples of cells at the beginning of the measurement and the white lines show the path the cell will have accomplished till the end of the time-lapse.

The velocity of protrusion was measured by acquiring a short timelapse (6sec) just after the targeted bleaching event. Analysis was done using Image J manual tracking of the leading edge movement at the location of the stimulation event. Each pair of data (diffusion constant, velocity) was then entered into an Excel graph and a linear regression was performed on all data from each experiment. Measurements had been done on 5 different days and the total number of cells was 122. The average trend line slope was -3.29, a noticeable decline. These results show that the membrane diffusion around the leading edge decreases with higher protrusion rates. In other words, the diffusion barrier is stronger the faster the cell protrudes i.e. the more force is generated through actin polymerisation.

It is known that many proteins localise to the leading edge of a protruding cell, but only VASP has been shown to accumulate in proportion to the rate of protrusion (Rottner et al., 1999). This suggests that the concentration of the majority of actin regulating proteins, including membrane bound ones, does not significantly change at different protrusion rates. Dil C12, the membrane marker used in these experiments, labels only the outer layer of the membrane. Consequently, it might be assumed that only the increase of transmembrane proteins would be able to alter the diffusion of this lipid dye. But, as mentioned, it has not been shown that transmembrane proteins accumulate at the leading edge. This suggests that the reduced mobility of Dil C12 in rapidly protruding keratocytes is not caused by a high protein-density. The observed increasing difficulty of the dye to diffuse around the leading edge of faster protruding cells is therefore, in my opinion, due to the elevated pushing force associated with rapid diffusion.

### ***5.1.2 Membrane recovery in fixed cells***

One possible way to distinguish between force and density based mechanisms of diffusion inhibition is to measure the rate of membrane diffusion in fixed cells. If the pushing force against the membrane is causing the lipid diffusion barrier, we would expect that fixed cells would not show reduced diffusion at the leading edge, as no force can be generated after fixation. In contrast, membrane linked proteins would be fixed in their position and the membrane diffusion would be hindered. No indication of a leading edge diffusion barrier in fixed cells would therefore point towards the force-based model, whereas the existence of a membrane diffusion barrier would favour the density-based explanation. With both results being in agreement with one model, this experiment could provide important information on finding the physical cause of the lipid diffusion barrier.

First, several fixation and labelling procedures were tested and representative pictures are shown in Figure 5-2.

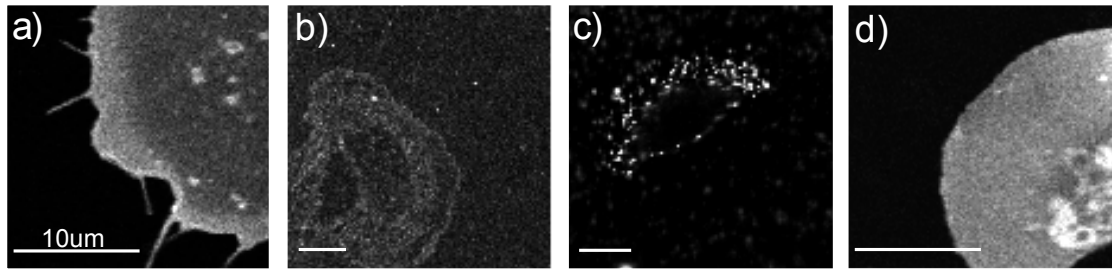


**Figure 5-2: fixation of membrane probes**

Different methods of fixation were tested in order to find the most suitable method to perform FRAP measurements on membrane labelled fixed cells. Picture a represents a B16 cell expressing GFP-F. A nice membrane labelling was observed, but the membrane marker did not recover after targeted bleaching, concluding its immobilisation through fixation. In b, DiI C12 labelled fish keratocytes have been fixed using  $-80^{\circ}\text{C}$  Methanol and in c the cells were fixed prior to addition of the membrane dye. Both methods did not result in a sufficient membrane staining, as the dye is soluble in Methanol and FRAP tests have shown that the dye is immobile. Picture d represents a fish keratocytes labelled with DiI C12 and fixed with Glutaraldehyde followed by Paraformaldehyde. Fixation did not alter the homogeneous membrane staining and the dye could still recover after targeted bleaching.

Our normally used fixation procedure is a combined treatment of Glutaraldehyde (GA) and Paraformaldehyde (PFA). But, these fixatives crosslink proteins and may influence membrane bound GFP. Indeed, fixed GFP-F transfected B16 cells (Figure 5-2a) could not be used because this membrane probe was completely immobilised by fixation. GFP-F can easily be crosslinked by GA and PFA, as they preferentially target lysine groups (Kiernan, 2000), an amino acid which can be found over 20 times in GFP-F. As DiI C12 dye is a lipid, it was not directly affected by the cross linking actions and its recovery following fixation and photo-bleaching could be observed.

Methanol fixations is an alternative to GA/PFA fixation, however, this approach did not result in a usable DiI staining. When pre-labelled cells were fixed with Methanol, the dye was probably dissolved and extracted from the membrane, resulting in a very weak remaining staining (Figure 5-2b). The label intensity was far too weak for FRAP measurements. When the dye was added after fixation (Figure 5-2c), no membrane staining was visible at all. The dye was visible only in intense punctae all over the cell. The bottom of the cell (found by transmitted light) did not show any labelling. This suggests that the dye is not able to enter the membrane. Some preliminary FRAP tests on pre-labelled and then Methanol fixed cells showed that the dye in these cells did not recover after bleaching. Methanol fixation could therefore not been used, as it appears to fix membrane lipids.

The best membrane staining result was achieved by Glutaraldehyde and Paraformaldehyde fixation of Dil C12 (Figure 5-2d). As B16 cells did not show a diffusion barrier with this dye (see section 4.3.3), they could not be used for these experiments and FRAP measurements therefore had to be performed on Dil labelled, fixed fish keratocytes. Initial observation of dye recovery by eye suggested that the recovery was much slower in fixed cells than in live cells. Indeed, the analysed diffusion rate in lamellar regions of fixed cells was only  $0.12\mu\text{m}^2/\text{s}$ , nearly 9 times slower than in live keratocytes ( $1.09\mu\text{m}^2/\text{s}$ ). The fixation of all proteins in the plasma membrane leads to stationary obstacles, which the mobile dye has to bypass. This results in global inhibition of diffusion. However, in contrast to live cells, the diffusion rate at the leading edge was equal to the rate in lamellar regions (see Figure 5-3), demonstrating that fixation abolished the difference in diffusion at the leading edge compared to lamellar regions.

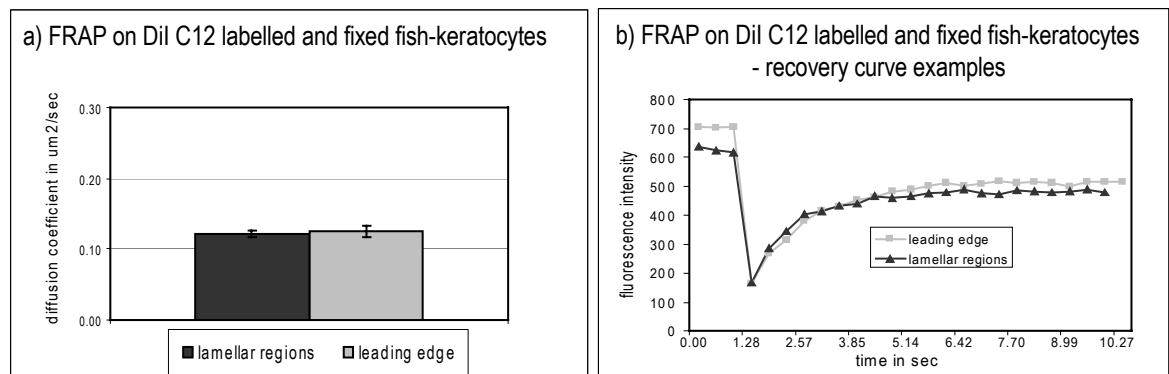


**Figure 5-3: FRAP on fixed Dil C12 labelled fish keratocytes**

The diffusion of Dil C12 in GA+PA fixed fish keratocytes was measured and graph a shows the final diffusion constants of lamellar regions (black) as well as at the leading edge (light grey) (28 measurements each). There is no statistical difference in both diffusion rates, which is also demonstrated in b, where a recovery curve of each region is presented. Time difference between each point of the recovery curves is 0.428s (compared to 0.065s in live cells).

This result indicates that the pushing force generated by actin polymerisation and applied to the leading edge membrane fold could cause the diffusion barrier. In fixed cells, no force is generated by actin polymerisation and the dye therefore diffuses around the leading edge and within lamellar regions at the same rate. If a high protein density within the leading edge membrane were the reason for the in live cells observed diffusion barrier, this slower diffusion should still be measurable in fixed cells. The proteins within or close to the membrane would be fixed in their position at the leading edge and the dye would have to

move around these stationary obstacles. Consequently, one would expect to see a hindered diffusion around the leading edge in fixed cells if the diffusion barrier were dependent on a density-based mechanism. Even a membrane-skeleton-fence-type mechanism without associated proteins does not seem to be causing the slower diffusion of membrane dye at the leading edge. Assuming the fixation preserved the actin-meshwork, this fence should still hinder membrane diffusion if it were the cause. For me, the absence of a diffusion barrier in fixed cells therefore suggests that direct pushing might cause the decreased dye mobility at the leading edge of live and protruding cells.

### **5.1.3 Membrane diffusion under “actin-waves”**

In most situations, actin polymerisation occurs behind a membrane fold such as the leading edge, which is pushed by the elongation of the actin filaments. But it has been shown that *dictyostelium discoideum* cells can form dynamic actin meshworks in the absence of a membrane fold ((Bretschneider et al., 2004), see introduction section 1.1.1.1 *dictyostelium discoideum*). The so called actin wave grows parallel to the membrane, and dye-exclusion data show that these waves do not push against the basal cell membrane (Gerisch 2004). If the polymerising front of the actin wave is physically linked to the membrane underneath via membrane bound actin regulators, the expectation would be to observe an impaired diffusion of membrane components underneath the front of the actin waves. I therefore sought to perform membrane FRAP experiments beneath the front of polymerising actin waves.

The first challenge was to find an appropriate membrane dye to use in the determination of membrane diffusion in dictyostelium cells. FM 4-64 is a commonly used membrane dye, but was not well tolerated under the conditions of our experiment. The cells changed shape and behaviour after addition of the dye. Once cells were labelled, FM 4-64 as well as DiI C12 showed a very non-homogeneous membrane labelling, due to rapid endocytosis. This was problematic over the one hour timescale needed to complete a FRAP experiment session. After unsuccessful labelling with external dyes, I considered using a membrane-linked GFP similar to GFP-F previously used in B16 cells. No suitable

construct was available, and personal communication with Douwe Veltman suggested that such constructs are not well tolerated by Dictyostelium cells. A commonly used membrane marker in dictyostelium is GFP-CAR; GFP fused to cAMP receptor cAR1. The resulting membrane labelling was very homogeneous and no obvious labelling of internal membranes could be observed. GFP-CAR cells were cotransfected with mRFP $\Delta$ Lim, a marker for F-actin needed to locate the actin waves. Control measurements of membrane diffusion in the absence of actin waves were performed in untreated cells. After that, the formation of actin waves was stimulated using Latrunculin A treatment, as described in Materials and Methods section 2.1.3, and FRAP measurements were performed (Figure 5-4).

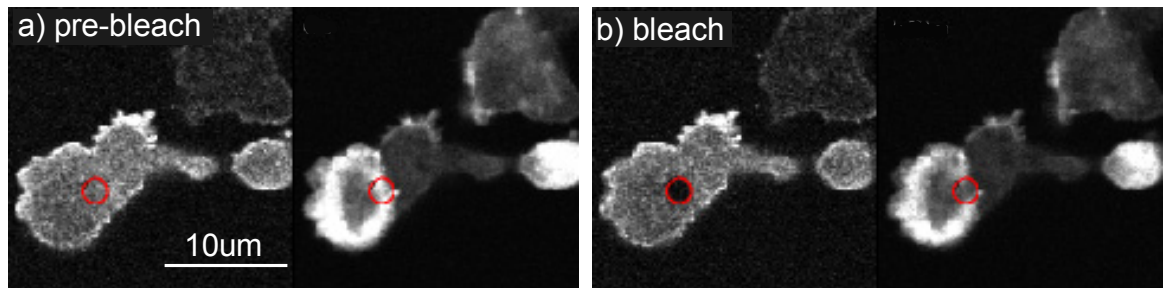


**Figure 5-4: membrane FRAP beneath a polymerising actin wave**

FRAP was performed on dictyostelium cells expressing GFP-CAR as a membrane and RFP $\Delta$ Lim as an F-actin marker. The position of the targeted bleach (ROI) was chosen to be beneath a polymerising actin wave, which is not close to the membrane at the edge of the cell (a). Both markers (GFP-CAR and RFP $\Delta$ Lim) were bleached by the 405 laser (b). For analysis, only cells were taken where the actin wave continued to travel or at least stayed stationary.

Several complications occurred during these experiments. First, positioning of the targeted bleach region of interest (ROI) was less straight forward, as the goal was to bleach underneath the front of a polymerising actin wave, but the exact speed and direction of travel was hard to predict. It often occurred that after positioning the ROI, switching to bleach and time-lapse mode, the wave front had already passed the ROI area, or changed direction and therefore did not enter the predicted ROI at all. A second problem was the influence of the laser light. The waves were very fragile and often collapsed during imaging or after the bleaching event. For analysis, only image sequences where the bleach was underneath a wave front which lasted until the end of GFP-F recovery were taken. Another problem was the imaging dependent decrease of intensity of the GFP-CAR channel; i.e. general, non-targeted bleaching of the probe (Figure 5-5a). Measurements of control regions outside the region of the targeted bleach

ROI showed a high intensity loss during the timelapse. Thus, the raw recovery data had to be corrected for general photo-bleaching of the probe during imaging. This was achieved by normalising the intensity of a control region to 1 for each image of the acquired time series and applying the same factor to the intensity measurements made within the bleach ROI. The corrected data are shown in Figure 5-5b.

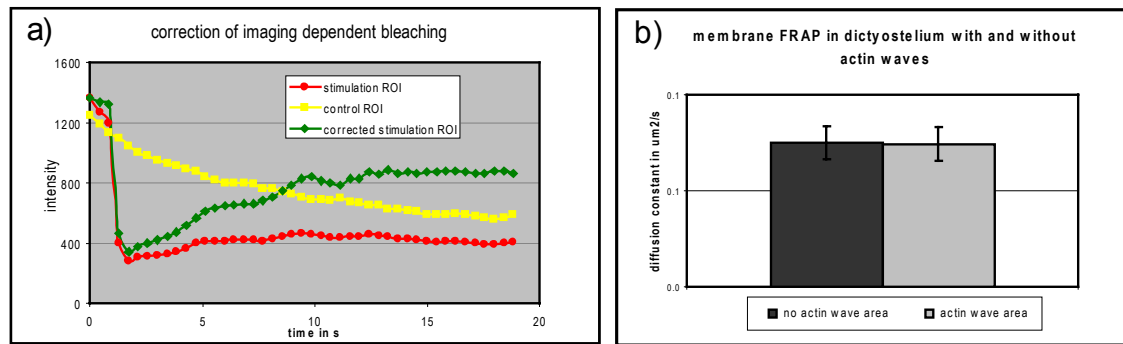


**Figure 5-5: Dictyostelium membrane FRAP corrections and results**

The measured FRAP recovery curves of GFP-CAR in Dictyostelium had to be corrected for a high general, non-targeted bleaching during imaging (a). A control region (yellow) outside the targeted bleach area was normalised to represent a non-bleached timelapse, i.e. normalised to initial intensity values for all time points. The actual recovery curve (red) was then multiplied with the resulting correction factor to achieve a corrected recovery curve (green). No correction would result in false  $t_{1/2}$  values. Graph b shows the average of all corrected curves for membrane areas (black, 36 cells) and membrane areas beneath an actin wave (grey, 18 cells). No difference between the two situations could be observed.

The diffusion constant of GFP-CAR within control membrane areas was  $0.075\mu\text{m}^2/\text{s}$ . This value is comparable with data published by de Keijzer et al, who used single molecule tracking to determine a diffusion constant of the cAMP-receptor of  $D=0.17\mu\text{m}^2/\text{s}$  (de Keijzer et al., 2008). Achieving a similar diffusion constant with a different technical approach (FRAP vs single molecule microscopy) suggests that our measurements are reliable and accurate. The rate of membrane diffusion beneath actin waves was equal ( $0.074\mu\text{m}^2/\text{s}$ ) to control membrane areas. No diffusion barrier could be found.

The first implication of this result is to conclude that no membrane-bound actin regulating proteins are hindering membrane diffusion underneath the polymerising front of an actin meshwork. This suggests that the diffusion barrier (found in keratocytes and B16 cells) is instead caused by the actin filaments pushing against the leading edge membrane. In the actin wave situation, actin polymerisation is directed parallel to the membrane and therefore, no force is

applied to the membrane. Consequently, the through actin polymerisation generated force can not alter the diffusion of membrane components within the underlying, basal cell membrane. One problem with this interpretation of the data could be the use of GFP-CAR itself. As mentioned earlier, the probe is a receptor and its diffusion might not represent normal membrane diffusion. This idea may also be supported by the low diffusion constant ( $0.075\mu\text{m}^2/\text{s}$ ) compared to other membrane probes in other cell types ( $D_{\text{GFP-F}}$  in B16 cells equals  $0.97\mu\text{m}^2/\text{s}$ ). It might be that normal membrane diffusion underneath the actin waves is hindered, but we cannot detect it using the GFP-CAR. Experiments to verify the result further were abandoned due to lack of time. However, even if GFP-CAR does not represent normal membrane diffusion, it can still be seen as a valid probe for diffusion under actin waves if we assume that the cAMP-receptor is not active during the short experiment. Inactive receptor would also represent membrane diffusion, which could then be influenced by the actin waves.

Altogether the equal diffusion rates of GFP-CAR within membranes underneath a polymerising actin wave and control membranes without these actin meshworks support the idea of a force-based mechanism for the membrane diffusion barrier at the leading edge.

## 5.2 FLIM-FRET approaches

Fluorescence Lifetime Imaging to measure Fluorescence Resonance Energy transfer (FLIM-FRET) is a widely used method to investigate close interactions between cell components. To investigate the mechanism of the lipid diffusion barrier, we wanted to use FLIM-FRET to characterise the contact between the lamellipodial actin meshwork and the leading edge plasma membrane. A direct interaction between actin filaments and the plasma membrane at the leading edge may point towards a force-based mechanism. Or, finding an actin-regulating protein mediating between the membrane and the actin meshwork, would suggest a protein-density mechanism. The data shown were acquired using a time-correlated single photon counting (TCSPC) approach with multiphoton excitation (see introduction section 1.3.4).

Some data described in this chapter were published in König et al (König et al., 2008).

### **5.2.1 Influences on lifetime measurements**

A positive FRET situation can be concluded if the lifetime of the donor fluorophore decreases in the presence of a suitable acceptor. It is therefore necessary to be confident of the donor lifetime measured without the acceptor and to understand the influence of acquisition parameters. The following subchapters present some control FLIM experiments and show potential pitfalls in the determination of lifetime shifts.

#### **5.2.1.1 Fluorophore environment**

Each fluorophore has a unique fluorescence lifetime, but this value can be altered by changes in the environment of the fluorophore (Lakowicz, 2006). Indeed, changes in fluorescence lifetime can be used to study cellular parameters, such as pH, oxygen levels and calcium concentrations. Alternatively, however, changes in the local environment of a fluorophore can complicate the measurements and interpretation of a FRET experiment. To understand the magnitude of lifetime changes resulting from small environmental modifications, we measured the lifetime of GFP fused to different targeting domains or proteins. The targeting domains or proteins themselves do not possess an individual lifetime, but can influence the fluorescence lifetime of GFP in several ways. First, they may create alterations in the structure of the fluorophore, leading to a different GFP lifetime. A secondary effect which may influence the GFP-lifetime is that each fusion probe will localise to specific areas of the cell. GFP-actin will be incorporated within the actin cytoskeleton of the cell, whereas the membrane targeting domains are supposed to confine the GFP to certain membrane domains (F -> disordered domains; MEM -> ordered domains, PH-Akt -> PIP<sub>3</sub>; PH-PLC -> PIP<sub>2</sub>; references see (König et al., 2008)). If the local environment of these locations differs from

the general cytoplasmic milieu, than the lifetime of the fused GFP may be altered. By comparing the lifetime of the GFP-fusions to GFP alone, a lifetime shift caused by the fusion can be calculated. The following figure shows lifetimes, shifts and the result of t-test analysis for 5 GFP-fusions and GFP.

Probe	$\tau$ (ps)	n	s.e.m	$\Delta \tau$	P
<b>GFP</b>	<b>2406</b>	42	12	0	-
GFP-actin	2369	47	7	-36	0.0101
GFP-F	2320	17	11	-86	0.0001
GFP-PH-PLC	2352	25	14	-53	0.0076
GFP-PH-Akt	2390	28	11	-16	0.3714
GFP-MEM	2448	33	5	42	0.0059

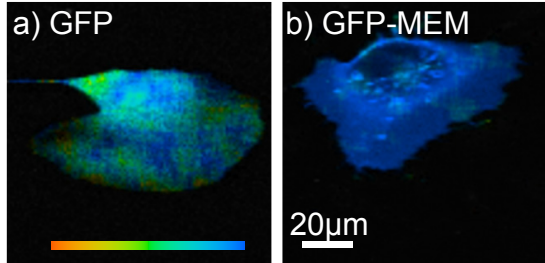


**Figure 5-6: environmental influence of GFP lifetime**

The lifetime of cytoplasmic, non targeted GFP was measured to be 2406ps and the different lifetimes for GFP-fusions are shown in the table. According to a student t-test all except GFP-PH-Akt are statistically different. Picture a shows a colour coded lifetime image of one cell expressing GFP, whereas b represents a cell expressing GFP-MEM. Both images are scaled to the same colour range (2000ps to 2500ps – red to blue). It can be seen that the lifetime of GFP-MEM is higher (more blue) than  $\tau_{\text{GFP}}$ . This shift is due to non-specific, not FRET related changes of the GFP fluorophore or its environment.

The data show that fusion of GFP to different targeting domains or proteins can cause significant lifetime changes. GFP-actin, GFP-F and GFP-PH-PLC all show a significant lifetime reduction, which could be falsely interpreted as a positive FLIM-FRET result. In contrast, GFP-MEM has a higher lifetime than GFP and although this shift is in the wrong direction for a FLIM-FRET result, it is still a significant difference. Only the GFP-PH-Akt lifetime is tested equal to GFP, suggesting that the fusion of Akt leads to the smallest changes in GFP conformation or environment. The average lifetime shift caused by these different fusions is 47ps (absolute value). These results show the magnitude of lifetime changes which are not due to a FRET situation, but rather small differences in the local environment of the fluorophore. During a real FRET experiment such lifetime changes may unintentionally occur through factors such as a slight change of pH due to the lack of CO<sub>2</sub> or a temperature change during the measurement. To know the magnitude of these non-FRET lifetime changes might prevent the false interpretation of future FLIM-FRET results, as it indicates a basal limit for FLIM-FRET shifts.

### 5.2.1.2 Photo-bleaching

FLIM-FRET experiments on our Becker&Hickl TCSPC system required around 30sec exposure time for each measurements. For control purposes, we recorded the image intensity at the beginning of the 30sec acquisition as well as at the end. During analysis it became apparent that a large decrease in intensity due to photo-bleaching could be associated with a shorter lifetime of these cells compared to cells with less intensity loss. A separate experiment was performed to test whether this change was coincidental or an effect of reduced intensity. Figure 5-7 shows 3 lifetime images, obtained by sequential measurements of the same cell.

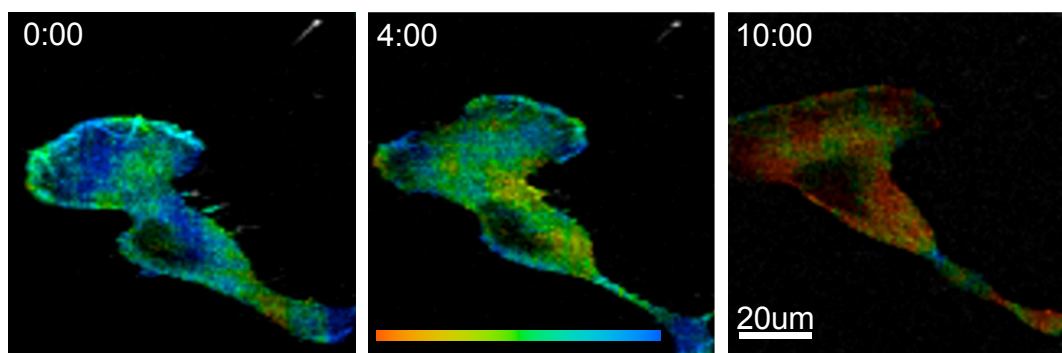


**Figure 5-7: effect of photo-bleaching on GFP lifetime**

A fluorescence lifetime time-lapse sequence was performed with GFP-actin expressing B16 cells. The three images represent 3 time points and show the decrease of GFP lifetime during the time course (colour scale from 200ps in red to 2500ps in blue). At  $t=0$  the calculated lifetime was 2371ps, at  $t=4\text{min}$  2303ps and at  $t=10\text{min}$  2109ps. The multiple acquisitions therefore decreased the lifetime significantly and this shift is probably caused by a decrease in intensity due to photo-bleaching.

It can clearly be seen that the lifetime of this GFP-actin B16 cell is reduced during this time series. The initial lifetime value at  $t=0\text{min}$  is 2371ps, and is reduced to 2303ps at 4min and 2109ps at 10min, resulting in a final lifetime reduction of  $\sim 260\text{ps}$ . Although Tramier et al have shown that the lifetime of CFP was changed by photo-bleaching, they did not observe an influence on the lifetime of GFP (Tramier et al., 2006). However, their bleaching was performed using prolonged 405 illumination in-between life time measurements. In contrast, our photo-bleaching was part of the actual lifetime measurement and a GFP multi-photon wavelength was used (843nm). This influence of prolonged illumination on the GFP lifetime can lead to false-positive FLIM-FRET results. For

all subsequent measurements care was taken to minimise photo-bleaching and to exclude data from cells with high intensity loss (typically > 30%).

### ***5.2.2 Interaction between actin and the plasma membrane***

The next question to address was whether actin filaments directly interact with the leading edge membrane. An interaction would indicate direct pushing of actin filaments against the membrane. If no interaction were found, it would suggest that the via actin polymerisation generated force is transmitted via intermediate components such as proteins between the plasma membrane and the actin filament +ends.

To estimate the magnitude of lifetime reduction in FRET situations, we compared the lifetime of GFP ( $\tau_{\text{GFP}}$ ) with  $\tau_{\text{GFP-RFP}}$ . GFP-RFP is a fusion between the donor and the acceptor fluorophore, creating an obligatory FRET situation which leads to a lifetime reduction. The lifetime of GFP-RFP was 2111ps, which, compared to  $\tau_{\text{GFP}}=2406\text{ps}$ , is a shift of nearly -300ps (Figure 5-8). Co-expression of GFP and RFP resulted in a lifetime of 2411ps, statistically equal to  $\tau_{\text{GFP}}$ . A second, less artificial, control was a co-transfection of GFP-MEM and RFP-MEM. MEM-targeted fluorescent proteins have previously been shown to localise tightly to ordered membrane subdomains and be able of FRET (Zacharias et al., 2002). The lifetime of GFP-MEM was significantly shortened in co-transfected cells (by 156ps). Although this is half the magnitude of the GFP-RFP reduction, it is still a clear positive FLIM-FRET result, proving that we can measure biological FRET situations. The next step was to address our questions for interaction between the actin filament and the plasma membrane.

Probe	$\tau$ (ps)	n	s.e.m	$\Delta \tau$	P
<b>GFP</b>	<b>2406</b>	<b>42</b>	<b>12</b>	0	-
GFP + RFP	2411	28	5	5	0.7391
GFP-RFP	2111	45	6	-295	<0.0001
<b>GFP-actin</b>	<b>2369</b>	<b>47</b>	<b>7</b>	0	-
GFP-actin + LatA	2344	21	12	-26	0.0548
GFP-actin + CytD	2330	34	6	-40	0.0001
GFP-actin + ds red-F	2414	32	5	44	<0.0001
<b>GFP-F</b>	<b>2320</b>	<b>17</b>	<b>11</b>	0	-
GFP-F + RFP-actin	2332	12	7	13	0.3784
<b>GFP-PH-PLC</b>	<b>2352</b>	<b>25</b>	<b>14</b>	0	-
GFP-PH-PLC + RFP-actin	2366	24	6	14	0.3674
<b>GFP-PH-Akt</b>	<b>2390</b>	<b>28</b>	<b>11</b>	0	-
GFP-PH-Akt + RFP-actin	2348	25	9	-42	0.0042
<b>GFP-mem</b>	<b>2448</b>	<b>33</b>	<b>5</b>	0	-
GFP-mem + RFP-actin	2426	28	5	-22	0.0048
GFP-mem + RFP-mem	2292	29	10	-156	<0.0001
GFP-mem + dsRed-mem	2342	27	8	-105	<0.0001

**Figure 5-8: lifetime measurements, - shifts and their statistical significance**

Data in this table represent average lifetime values for different fluorophores, - fusions and combinations. In each group, the reference lifetime (donor alone) is marked in bold and all other lifetime values within each group are compared to the reference, leading to the calculated lifetime shift (3<sup>rd</sup> column). The last column shows the P-value of a student's t-test to evaluate the significance of the lifetime shift.

As a first step, B16-F1 cells were co-transfected with GFP- $\beta$ -actin and DsRed-F as a membrane marker. A small but statistically significant lifetime shift of 44ps was observed (Figure 5-8), but unexpectedly, it was a lifetime increase rather than a decrease. This increase in  $\tau_{\text{GFP}}$  may be caused by a second GFP lifetime, which is formed during the maturation of DsRed (Baird et al., 2000). For further FLIM-FRET measurements we therefore decided to use RFP as an acceptor.

Another limitation of our labelling strategy (green actin and red membrane) is the proportion of donor expected to interact with the acceptor. Even if the tips of the actin filaments interact with the leading edge membrane, the resulting lifetime shift could be masked by a much larger proportion of GFP-actin molecules not in close contact with the acceptor. The multilayer structure of the actin meshwork will increase this problem, as without any further sectioning methods, multiple GFP lifetimes from different z-levels will mix in one image of

the lamellipodium. An alternative labelling strategy combining membrane linked FRET donors with actin linked FRET acceptor might improve the detection. In this case the proportion of membrane interacting with actin filaments at the leading edge may be increased.

The lifetimes of GFP-F and GFP-PH-PLC were not significantly changed in the presence of RFP-actin (Figure 5-8; shifts of 13 and 14ps respectively) and it can be concluded that there is no FRET situation between either of these probes and actin. In contrast, co-transfection with RFP-actin reduced the lifetime of GFP-PH-Akt and GFP-MEM. Both reductions were small (42ps and 22ps, respectively) but tested as significant (Figure 5-8). In light of the magnitude of possible lifetime changes caused by non-specific environmental changes, the 22ps decrease for the GFP-MEM/RFP-actin pair is in our view too small to be reliably attributed to FRET. Although 42ps is not comparable with lifetime decreases we obtained for our positive controls, it can be seen as indication that PH-Akt and actin are in close proximity, causing a FRET situation between their fused fluorophores. Unfortunately, we did not see any lifetime decrease concentration at the leading edge, where we wanted to investigate the actin-membrane interaction. We therefore conclude that although the cortical actin meshwork seems to be most closely associated with PIP3-rich membrane compartments, there is no evidence for a direct interaction between the actin filament +ends and the leading edge membrane fold. However, whereas FRET strongly indicates a interaction, no-FRET does not necessarily means there is no interaction. Besides the close proximity FRET also requires the right fluorophore orientation. We can therefore not exclude an interaction between actin filament +ends and the plasma membrane at the leading edge.

### ***5.2.3 Investigation of the involvement of actin regulating proteins in linking the actin to the membrane***

Initially we hoped to use FLIM-FRET to show direct pushing of actin filaments against the membrane. However, FLIM results described in the previous section

(section 5.2.2) suggested that actin is not directly pushing the leading edge membrane. This may be due to sensitivity or orientation issues, but it might also be possible that actin is only indirectly pushing against the membrane. We therefore wanted to investigate whether proteins lie in between the actin filament +ends and the membrane. An overview of proteins involved in the regulation of actin polymerisation at the leading edge is given in the introduction section 1.1.1.2 (Figure 1-6). Some of these actin-regulating proteins are obviously further away from the membrane, such as ADF/cofilin, but many proteins localise to the leading edge (WAVE2, CP, VASP; Lai et al, 2008) and some have been shown to interact with the membrane (IRSp53, Mattila et al, 2007). The following chapter will show FLIM results of two chosen actin-regulating proteins to test whether they would lie between the actin filaments and the leading edge membrane.

One obvious candidate is IRSp53. This ubiquitous regulator of the actin cytoskeleton has all necessary functional properties to link actin to the leading edge membrane fold (see introduction section 1.1.1.2 IRSp53). The expression of GFP-IRSp53 did not alter the behaviour of B16 cells markedly. Some very high expressing cells showed an increased number of filopodia, but normal and lower expressing cells possessed nice lamellipodia. The following figure shows results from FLIM-FRET measurements between GFP-IRSp53 and cherry-F as a membrane marker.

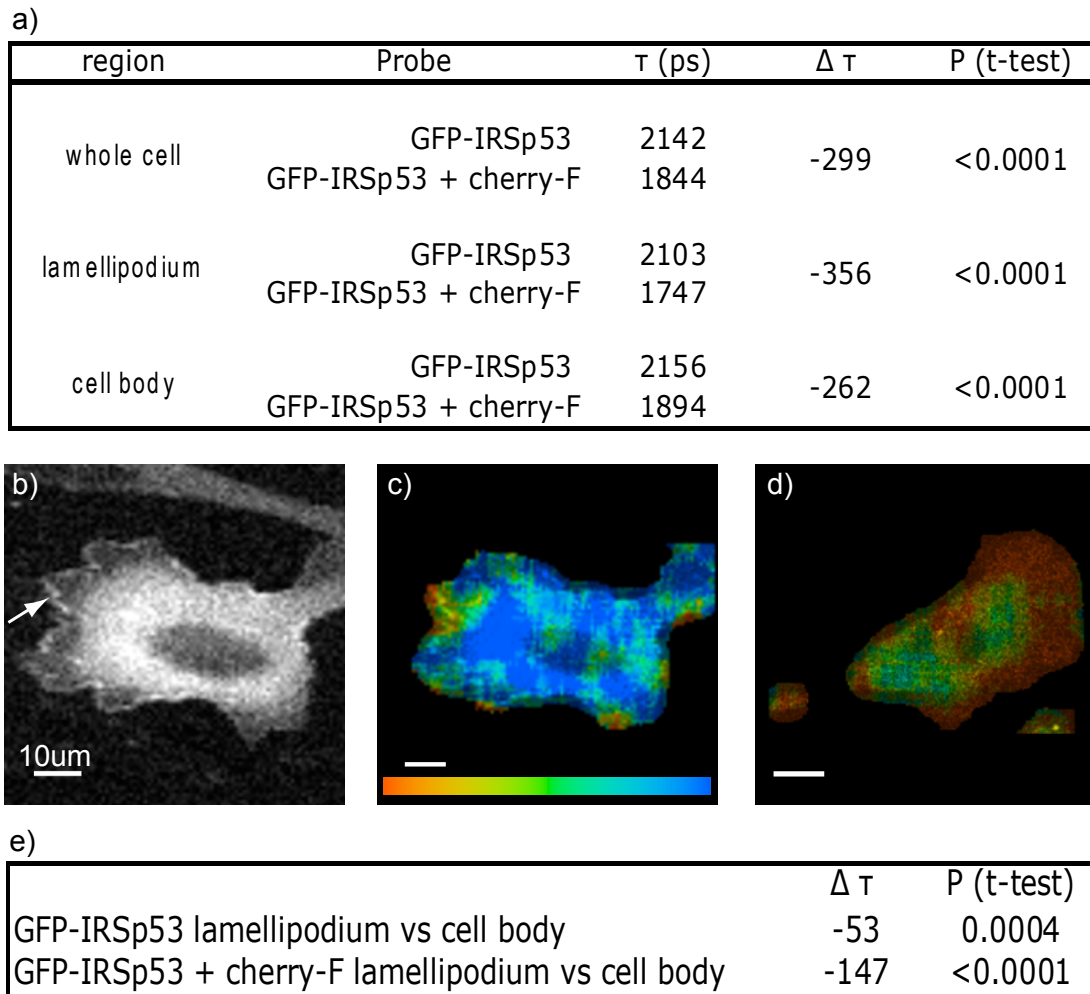


**Figure 5-9: FLIM results of IRSp53 and membrane**

Table a) shows the lifetimes measured for GFP-IRSp53 with (n=28) or without (n=27) cherry-F as a membrane marker. Average lifetimes are shown for the whole cell as well as lamellipodium and cell body, analysed with the use of the masking function in the Becker and Hickl analysis software (SPCImage). In all cases, the presence of an acceptor (cherry-F) results in a clear lifetime decrease. S.e.m values are as followed: 9,19,11,25,8,20 (from top to bottom). An intensity image of GFP-IRSp53 is shown in b. A bright rim can be observed at the leading edge, suggesting the localisation at the leading edge. C and d show fluorescence lifetime images of GFP-IRSp53 (c) and GFP-IRSp53+cherry-F (d). The lifetime bar represents lifetime values from 1750ps (red) to 2250ps (blue). In d it can be seen that the lamellipodium shows a shorter lifetime than the cell body and the differences between these two regions are shown in e (for donor alone and donor+acceptor).

The first encouraging observation was the visualisation of the intense GFP-IRSp53 band at the lamellipodial edge (Figure 5-9b), which was not possible using a wide-field frequency domain FLIM system (not shown). Unexpectedly, the control lifetime of GFP-IRSp53 was much lower than previous GFP lifetimes acquired on the B&H system (see previous subchapter). However, as the calculation for a FRET situation is always done with the relevant donor, this difference can be ignored. The initial GFP-IRSp53 lifetime shifted from 2142ps to 1844ps in the presence of cherry-F (Figure 5-9a). This is a decrease of nearly 300ps, around the magnitude we observed in the artificial positive control (GFP-

RFP, see previous subchapter) and can clearly be seen in the lifetime images (Figure 5-9c+d). Our expectations predicted stronger FRET interactions at the leading edge, but the intense GFP-IRSp53 band at the leading edge (Figure 5-9b arrow) did not overlap with any obvious lifetime changes. Interestingly, it could be observed that the lamellipodium showed a lower lifetime than the cell body. Comparison of the average lifetimes within cell body and lamellar regions revealed that in the GFP-IRSp53/cherry-F situation the lifetime was 147ps shorter in the lamellipodium. This suggests that IRSp53 is more closely associated to the plasma membrane in the lamellipodium compared to the cell body. Surprisingly, cells expressing GFP-IRSp53 alone also showed a small but significant lifetime difference between the lamellipodium and the cell body (53ps). This difference could be due to some intensity changes of GFP-IRSp53 expression within the cell. It can be seen in Figure 5-9b, that the lamellipodium shows a lower intensity than the cell body. (Note that a lower intensity can also be observed underneath the cell nucleus.) The fluorescence intensity is not known to influence FLIM measurements (Lakowicz, 2006), but the analysis depends on the number of photon counts. Lower intensity results in less counts and the curve fit to extract the lifetime will be less reliable due to more noise. Knowing that there is no acceptor present this shift does not represent the investigated FRET situation (IRSp53+membrane), but shows once again how easily environmental changes as well as system and acquisition parameters can influence lifetime measurements. However, the observed decrease of GFP-IRSp53 lifetime within the whole cell (-299ps) and especially within the lamellipodium (356ps) are clearly outwith the range of unspecific lifetime changes and indicate a strong interaction between IRSp53 and the membrane.

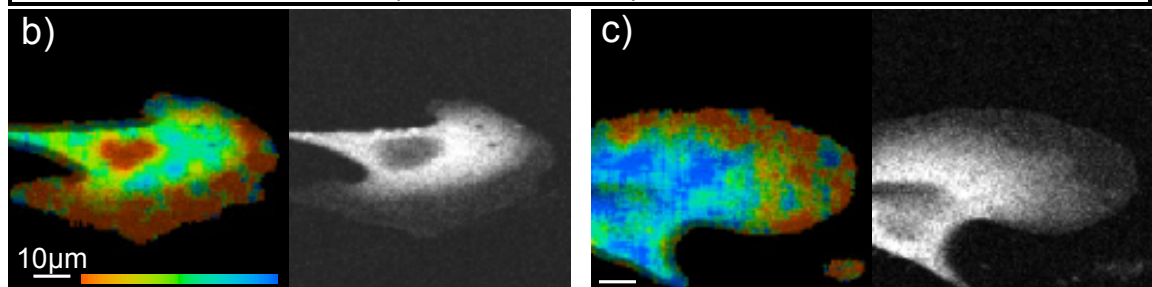
The next set of FLIM measurements was made using mutated versions of IRSp53, starting with IRSp53-IMDmut (described in introduction section 1.1.1.2 IRSp53). Briefly, IRSp53-IMDmut possesses reduced membrane binding ability and F-actin bundling activity. Due to the reduced membrane binding, our expectation would be that no FRET occurs between GFP-IRSp53-IMDmut and cherry-F. Surprisingly, the fluorescence lifetime of GFP-IRSp53-IMDmut decreased by 195ps in the presence of cherry-F (Figure 5-10). This shift was less pronounced than the lifetime shift between GFP-IRSp53 (WT) and cherry-F (299ps) but still suggested a strong interaction. As seen with the wild-type IRSp53 probe, differences could

be observed between lamellipodial regions and the cell body. The differences are of similar magnitude as seen in the wild-type case, suggesting that the difference in the donor alone case (GFP-IRSp53-IMDmut; -59ps) is due to intensity changes whereas the -112ps in the donor+acceptor case (GFP-IRSp53-IMDmut + cherry-F) shows a slightly tighter association with the membrane within the lamellipodium. Nevertheless, data from all regions indicate the existence of an interaction between the membrane-binding mutant of IRSp53 and the membrane, which is at first glance surprising. However, this observation makes more sense when seen with the results of the GFP-IRSp53- $\Delta$ SH3/cherry-F FLIM experiment discussed in the next paragraph. Other possible explanation for the indication that IMD-mutated IRSp53 still possesses close associations with the plasma membrane may be due to the fact that the mutation was not intended to abolish all membrane binding (see introduction section 1.1.1.2 IRSp53) or possible dimerisation with endogenous wild-type IRSp53. However, FRAP data described in the following chapter (6.2) indicate that dimerisation does not seem to influence the mutant behavior, probably due to the rather low percentage of mutant-wild-type dimmers compared to mutant-mutant dimmers.

In my opinion, the lifetime data of GFP-IRSp53-IMDmut with and without cherry-labeled membrane suggest that there is still an interaction between this membrane-binding mutant and the membrane. Comparing the lifetime shift of GFP-IRSp53-IMDmut/cherry-F with the previous measured GFP-IRSp53/cherry-F, it can be shown that the lifetime reduction is of a smaller magnitude than in the first case (-195ps vs -299ps), suggesting a weaker, but still existent membrane association.

a)

region	Probe	$\tau$ (ps)	$\Delta \tau$	P (t-test)
whole cell	GFP-IRSp53-IMDmut	2094	-195	<0.0001
	GFP-IRSp53-IMDmut + cherry-F	1899		
lamellipodium	GFP-IRSp53-IMDmut	2039	-209	<0.0001
	GFP-IRSp53-IMDmut + cherry-F	1830		
cell body	GFP-IRSp53-IMDmut	2098	-156	<0.0001
	GFP-IRSp53-IMDmut + cherry-F	1942		
whole cell	GFP-IRSp53- $\Delta$ SH3	2132	-39	0.16
	GFP-IRSp53- $\Delta$ SH3 + cherry-F	2093		
lamellipodium	GFP-IRSp53- $\Delta$ SH3	2110	-179	<0.0001
	GFP-IRSp53- $\Delta$ SH3 + cherry-F	1931		
cell body	GFP-IRSp53- $\Delta$ SH3	2147	-19	0.45
	GFP-IRSp53- $\Delta$ SH3 + cherry-F	2128		



d)

Probe	$\Delta \tau$	P (t-test)
GFP-IRSp53-IMDmut lamellipodium vs cell body	-59	0.01
GFP-IRSp53-IMDmut + cherry-F lamellipodium vs cell body	-112	0.0008
GFP-IRSp53- $\Delta$ SH3 lamellipodium vs cell body	-37	0.09
GFP-IRSp53- $\Delta$ SH3 + cherry-F lamellipodium vs cell body	-197	<0.0001

**Figure 5-10: FLIM results of IRSp53-IMDmut and IRSp53- $\Delta$ SH3 and membrane**

Lifetime results for donor (GFP fusions) and donor+acceptor (GFP fusions + cherry-F) for the whole cell as well as lamellipodial and cell body regions are shown in a. The lifetime difference for each donor/acceptor pair in each region is displayed, as well as the result of a student's t-test. 35 cells have been measured for GFP-IRSp53-IMDmut, 32 for the same probe with cherry-F and 20 each for GFP-IRSp53- $\Delta$ SH3 with or without cherry-F. The corresponding s.e.m. values are: 13, 21, 17, 25, 13, 20, 14, 24, 18, 36, 13 and 21 (from top to bottom in table). Pictures b and c show the lifetime map and an intensity image of GFP-IRSp53-IMDmut+cherry-F (b) and GFP-IRSp53- $\Delta$ SH3+cherry-F (c) with a color scale from 1750 (red) to 2250 (blue). Lifetime differences between the lamellipodium and the cell body can be observed in both cases. In d) these differences are shown in numbers with their respective t-test result.

The second mutation tested was IRSP53- $\Delta$ SH3, which is described in detail in introduction section 1.1.1.2 IRSp53. Briefly, deletion of the SH3 domain abolishes binding to actin regulators such as WAVE2, resulting in little to no association to the actin meshwork. As the membrane-binding domain (IMD) is not affected by this mutation, our expectation is that a similar interaction with the membrane should be observed with this mutant as seen with wild-type GFP-

IRSp53. But, the overall lifetime of cells expressing GFP-IRSp53- $\Delta$ SH3 co-transfected with cherry-F was only 39ps smaller than the lifetime of GFP-IRSp53- $\Delta$ SH3 alone, a difference which is not statistically significant. It seems like the interaction between IRSp53 and the membrane was abolished through the deletion of the SH3 domain. A closer analysis of the GFP-IRSp53- $\Delta$ SH3 with and without cherry-F lifetimes by cell region showed no FRET within the cell body (19ps difference) but a significant lifetime reduction in the lamellipodium. This lifetime decrease of 179ps was around half of the decrease observed in the lamellipodium of GFP-IRSp53 (WT) cells cotransfected with cherry-F (365ps). However, the magnitude of the lamellar shift in GFP-IRSp53- $\Delta$ SH3 + cherry-F cells was clearly outside the range of non-specific, environmental influences observed previously (chapter 5.2.1). These results suggest that although the membrane binding ability of this mutant is intact, an association with the actin meshwork is needed to push the protein close enough against the membrane to create a FRET interaction. The mutation lost its actin regulating function and is therefore not associated with the actin cytoskeleton, which in the cell body results in a non altered lifetime of the donor even in the presence of an acceptor. One possible explanation why there is still a lifetime shift associated with a FRET situation in the lamellipodium (between GFP-IRSp53- $\Delta$ SH3 and cherry-F) might be the very high density of polymerising actin filaments inside the rather thin lamellipodium, which might push against the mutated protein even if it is not regulating the polymerisation. Although an actin cytoskeleton is also present in other cell regions (cell body), only the lamellipodial actin meshwork is generating force against the membrane. The result that the cell body regions do not show a FRET interaction between GFP-IRSp53 $\Delta$ SH3 and cherry-F indicate that this force is needed to push IRSp53 against the membrane.

The conclusions from the GFP-IRSp53- $\Delta$ SH3 FLIM data open up a new explanation for the GFP-IRSp53-IMDmut data. Against our expectations there was still a FRET situation between IRSp53-IMDmut and cherry-F, indicating an interaction between the membrane-binding mutant (IRSp53-IMDmut) and the membrane. This FRET was measured in lamellar as well as cell body regions. With the indications of the GFP-IRSp53- $\Delta$ SH3 data that the association with actin is needed to establish IRSp53 interactions with the membrane, I suggest that the measured FRET between GFP-IRSp53-IMDmut and cherry-F is due to its functional

actin-regulating function. Although its membrane binding is disrupted, the actin cytoskeleton seems to push this mutant close enough to membrane in order to make FRET possible. The FRET associated lifetime decrease within the lamellipodium was 356ps for GFP-IRSp53, 209ps for GFP-IRSp53-IMDmut and 179ps for GFP-IRSp53- $\Delta$ SH3. Comparison of these data suggest that the strong interaction of GFP-IRSp53 with the membrane is partly due to its membrane binding through the IMD domain and partly due to the proteins interaction with the actin cytoskeleton through its SH3 domain. According to the amounts of lifetime decrease, both domains seem to contribute roughly the same magnitude.

Work from Soheil Ahmeds group shows a positive FRET interaction between IRSp53 and actin (Lim et al., 2008), which is not due to the actin binding ability of the IMD domain. My FLIM results of GFP-IRSp53 (WT) and cherry-F (representing the membrane) combined with these data suggest that IRSp53 may bridge the actin filaments to the plasma membrane. Furthermore, based on my results with the mutations of IRSp53, I propose that the close interaction with the membrane is weaker in the absence of normal actin association.

The second candidate choice for bridging actin and the plasma membrane was Capping Protein (CP). The obvious interaction is with the tip of the actin filaments (see introduction section 1.1.1.2 CP), and the first step was therefore to perform FLIM measurements between GFP-CP and mRFP-actin (Figure 5-11).

a)

region	Probe	$\tau$ (ps)	$\Delta \tau$	P (t-test)
whole cell	GFP-CP	2012	-1	0.96
	GFP-CP + mRFP-actin	2013		
lamellipodium	GFP-CP	1946	11	0.72
	GFP-CP + mRFP-actin	1935		
cell body	GFP-CP	2054	-11	0.63
	GFP-CP + mRFP-actin	2065		

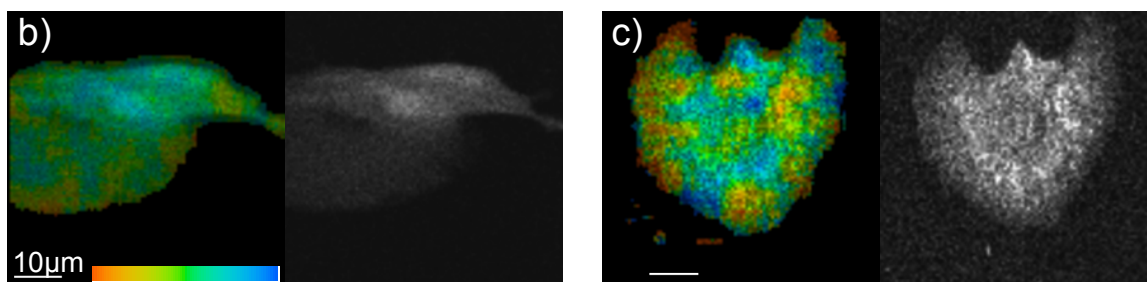


**Figure 5-11: FLIM results of CP and actin**

No lifetime shift associated with a FRET interaction could be observed between GFP-CP and mRFP-actin. Table a) shows the averages of the donor lifetimes with or without acceptor, the calculated differences for this pair in different regions of the cell as well as the result of a student's t-test to assess their significance. 15 cells were analysed for each condition and the s.e.m was calculated at: 13, 17, 17, 24, 15 and 17 (from top to bottom). The colour images of GFP-CP (b) and GFP-CP+mRFP-actin (c) display these results in a lifetime colour range from 1500 (red) to 2500 (blue). Next to the lifetime maps a corresponding intensity image is shown. Although the donor+acceptor situation shows a less homogeneous lifetime distribution, no global difference was observed between the two situations (donor alone and donor+acceptor).

Surprisingly, no positive result could be achieved. The lifetime of GFP-CP ( $\tau_{\text{GFP-CP}}=2012\text{ps}$ ) did not change in the presence of mRFP-actin ( $\tau_{\text{GFP-CP/RFP-actin}}=2013\text{ps}$ ). Even regional analysis did not show any FRET situation. As the interaction between CP and actin is known (Wear and Cooper, 2004), these results are probably due to orientation of the donor and acceptor fluorophore rather than their distance.

A wrong orientation of fluorophores was also suggested as a possible explanation for no FRET between actin filament tips and the membrane (section 5.2.2). The helical structure of the actin filaments may be problematic for FRET detection. Several control experiments to test if we can detect an interaction with actin filaments were performed but none showed positive FLIM-FRET results. Co-transfection of GFP-actin and RFP-actin cells resulted in a 23ps lifetime increase, GFP-actin in conjunction with Alexa 555 Phalloidin showed a 15ps decrease, combination of Alexa 488 and Alexa 555 Phalloidin decreased the

donor lifetime by 34ps and GF-actin co-transfected with SM22-Ds-RED did not change the lifetime. These combinations are all expected to show FRET and the fact that none did leads to the conclusion that actin filaments may force an orientation of fluorophore orientation which is unfavourable for FRET measurements.

Based on the negative result using GFP-CP and actin, further experiments with mutations of capping protein were abandoned.

### 5.3 Summary

Two possible explanations have been hypothesised to be the cause for the actin dependent diffusion barrier at the leading edge. Either the pushing force generated by actin polymerisation hinders membrane components in their diffusion around the leading edge (force-based model). Alternatively, the space requirement of membrane-bound proteins with or without a possible association with the actin cytoskeleton (density-based model) is thought to cause the lipid diffusion barrier. Several different approaches were undertaken to differentiate between these two possibilities. Membrane FRAP analysis in fixed cells, as well as under actin-waves in dictyostelium cells favour the force-based model. The same was concluded from experiments correlating the protrusion speed with the strength of the diffusion barrier. Using FLIM-FRET measurements, no direct actin-membrane interaction, which is thought to be needed for the pushing model could be shown. But, a dependency of the strength of the interaction of IRSp53 with the membrane on the presence of an association with a lamellipodial actin meshwork was indicated. This could mean that the diffusion barrier is caused by the force generated from actin polymerisation which is applied to the membrane indirectly via other proteins such as IRSp53.

## **6 Consequence of the diffusion barrier for the actin polymerisation at the leading edge**

As shown in the previous chapters, the interaction between polymerising actin filaments and the leading edge membrane fold is strong enough to hinder lipid dye and membrane bound proteins in their diffusion. The next question to address is whether this interaction plays a role in the regulation and localisation of actin polymerisation. One hypothesis is that actin polymerisation creates a diffusion barrier, which traps membrane associated actin regulating proteins at this specific leading edge location. In this case, the diffusion barrier could be seen as a positive feedback loop for promoting robust actin polymerisation. The expectation would therefore be to find a slower diffusion rate of actin regulating proteins at the leading edge, compared to other cell regions. In theory, diffusion rate comparisons between different proteins should also help to identify proteins which are affected by the diffusion barrier and those which are not. The following chapter tries to assess the influence of the diffusion barrier on the mobility of actin regulating proteins by measuring their diffusion.

### **6.1 Localisation and diffusion of actin-regulating proteins**

Many proteins have been shown to localise to the leading edge of migrating cells (for example: WAVE2, CP, VASP in B-16 cells (Lai et al., 2008). Members of the WASP family are partly regulated by phosphoinositides (Takenawa and Suetsugu, 2007) and IRSp53 is able to deform membranes for protrusions (Mattila et al., 2007), making them candidates to be involved in linking the actin filaments to the membrane. I chose the following proteins as representatives to study whether they are affected by the leading edge diffusion barrier: IRSp53, CP, N-WASP and WAVE2. For all of these, GFP fusions were transiently transfected into B16 F1 cells. Figure 6-1 shows their intracellular localisation in these cells.

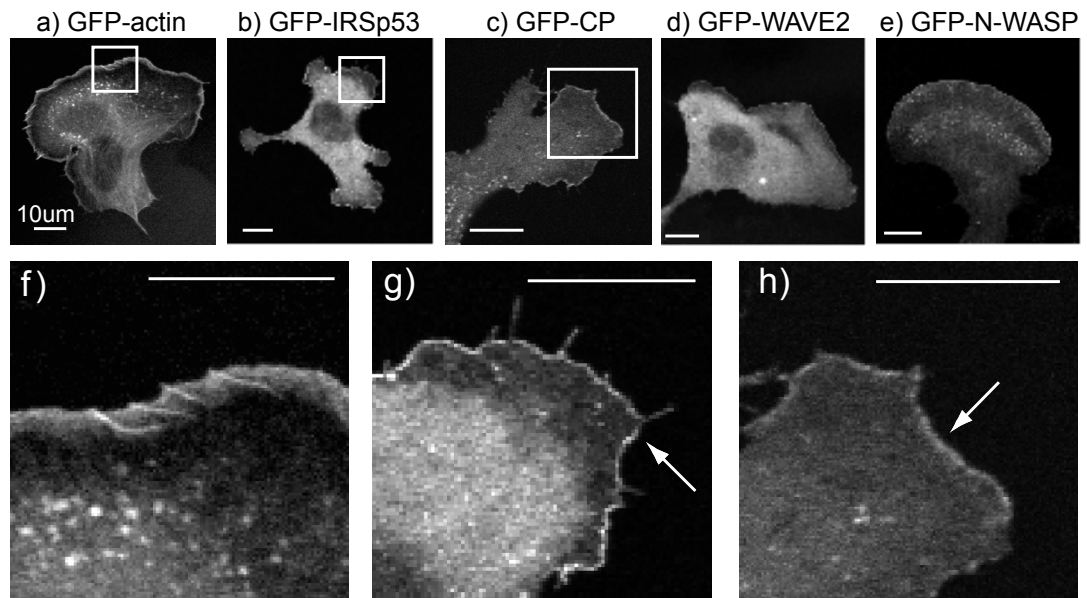


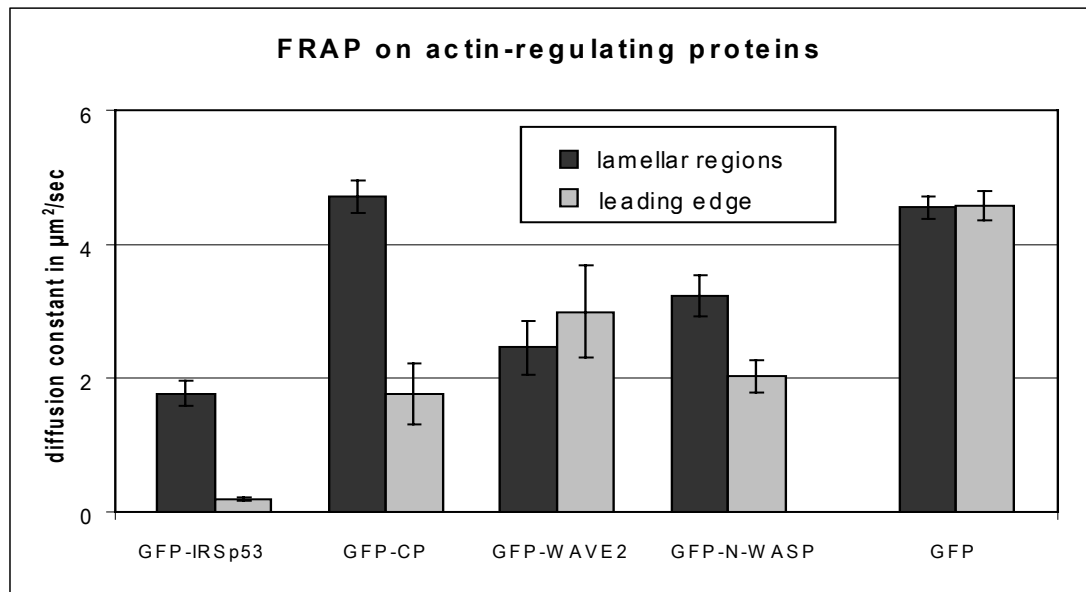
**Figure 6-1: localisation of actin regulating proteins**

Localisation of GFP-actin (a and f), GFP-IRSp53 (b and g), GFP-CP (c and h), GFP-WAVE2 (d) and GFP-N-WASP (e) in B16 F1 cells. IRSp53 and CP showed a clear and narrow localisation at the leading edge (arrows). GFP-actin occupies a broader area. GFP-WAVE2 and GFP-N-WASP do have a very weak localisation at the leading edge, which cannot clearly be seen on these images due to the high scan speed of the microscope and the resulting poor quality.

First, it can be stated that the expression of these GFP constructs at moderate levels did not alter previously observed cell shape or behaviour. In contrast to reports in the literature (Millard et al., 2005, Krugmann et al., 2001), only extreme overexpression of GFP-IRSp53 resulted in an increase of filopodia, whereas the majority of cells still displayed large lamellipodia. For IRSp53 and CP constructs, a very distinct localisation along the leading edge could be observed (Figure 6-1 g, h arrows). These locations corresponded with sites of expected actin polymerisation. In TIRF microscopy GFP-IRSp53 was also found in distinct punctae at the basal membrane (not shown), possibly sites of clathrin mediated endocytosis. WAVE2 and N-WASP GFP fusions also showed a higher intensity at the leading edge, but it was less pronounced and often very temporary and therefore hard to image (Figure 6-1 d and e). Local punctae inside the lamellipodium could be observed mainly in GFP-N-WASP transfected cells. These punctae resemble structures seen in GFP-actin cells (figure 6-1a), where they probably represent a pool of actin available for polymerisation. It has to be noted that N-WASP is not normally associated with lamellipodial actin protrusions (Pollitt and Insall, 2009), but could be observed at the leading edge in my experiments. In comparison with the stripe formed by the actin regulating proteins, the actin-rich band at the lamellipodium front is much broader,

consistent with the different roles in the actin machinery. Actin itself is incorporated into filaments, which are disassembled further away from the leading edge. In contrast, IRSp53 is involved in the activation of the Arp2/3 complex via WAVE2 and therefore only recruited to acute activation sites, i.e. the leading edge. Its possible role in membrane deformation also consists with its localisation. CP caps growing filaments at the leading edge in order to accelerate the polymerisation of remaining free barbed ends. Blocked filaments are possibly severed rapidly, which would explain the lower GFP-CP intensity behind the leading edge.

Next, I investigated the diffusion of these proteins by comparing their diffusion rate at the leading edge and inside the lamellipodium. Figure 6-2 shows lamellar and leading edge diffusion constants of GFP fusions of IRSp53, CP, N-WASP, WAVE2.



	D in μm <sup>2</sup> /s	s.e.m.	n	ΔD	P (t-test)	conclusion
GFP-IRSp53 lamellar regions	1.77	0.19	21	1.57	<0.0001	different
GFP-IRSp53 leading edge	0.2	0.02	27			
GFP-CP lamellar regions	4.72	0.24	28	2.95	<0.0001	different
GFP-CP leading edge	1.77	0.46	22			
GFP-WAVE2 lamellar regions	2.46	0.4	8	-0.54	0.51	not different
GFP-WAVE2 leading edge	3	0.7	8			
GFP-N-WASP lamellar regions	3.23	0.31	19	1.21	0.003	different
GFP-N-WASP leading edge	2.02	0.24	21			

**Figure 6-2: diffusion constants of actin regulating proteins**

The graph shows obtained diffusion constants for GFP-IRSp53, GFP-CP, GFP-WAVE, GFP-N-WASP and GFP (as comparison). Black bars indicate the diffusion rate in lamellar regions and grey bars at the leading edge. A difference in diffusion rate between both locations can be seen for GFP-IRSp53, GFP-CP and GFP-N-WASP.

The diffusion of GFP-IRSp53, GFP-CP and GFP-N-WASP was significantly reduced at the leading edge (Figure 6-2). The reduction of diffusion rate in GFP-N-WASP ( $3.23\mu\text{m}^2/\text{s}$  to  $2.02\mu\text{m}^2/\text{s}$ ) was 37%; much smaller than for GFP-IRSp53 (89%; from  $1.77\mu\text{m}^2/\text{s}$  to  $0.2\mu\text{m}^2/\text{s}$ ) and GFP-CP (63%; from  $4.72\mu\text{m}^2/\text{s}$  to  $1.77\mu\text{m}^2/\text{s}$ ). These data correlate with the observed distinctiveness of intense localisation at the leading edge. The constructs with the more obvious and sharper band (IRSp53 and CP) show a bigger reduction in diffusion at the leading edge compared to GFP-N-WASP, whose band was less obvious and more variable. In my opinion, the leading edge diffusion barrier cannot be solely responsible for this decrease in motility of the actin-regulating proteins, as the magnitude of the decrease is much higher for the actin-regulating proteins (up to 89% for IRSp53) compared to membrane bound GFP (GFP-F), which is hindered in its diffusion by the leading edge diffusion barrier ( $D_{\text{GFP-F}}$  decrease at the leading edge = 16.2%, see chapter 4.3.4). The main reason for the slower diffusion rate at the leading edge of these actin-regulating proteins is therefore probably their practical involvement in the actin machinery, as the reduction in diffusion occurred at the location of function of these proteins. However, these data do not clarify whether this reduction is at least partly caused solely by the diffusion barrier at the leading edge or if the slower diffusion at the leading edge is solely the result of the direct or indirect association of these proteins with the actin meshwork.

The diffusion rates of GFP-WAVE2 are statistically considered equal in lamellar and leading edge regions (Figure 6-2,  $P(\text{t-test})=0.51$ ). This result is possibly due to a highly dynamic involvement of WAVE2 in the activation process of Arp2/3. As no stable localisation at the leading edge could be observed, the measurement was probably done on the same population as in the lamellar regions. It may also be that the GFP fusion influences the characteristics of the probe. WAVE2 is part of a 5-member-complex and although GFP-WAVE2 has been used in B16 cells (Lai et al., 2008), it may be that the cell favours complex formation with endogenous WAVE2 and does not fully incorporate our GFP-WAVE2. The measured diffusion rates would then not represent the mobility of endogenous WAVE2. It has to be mentioned that the GFP-WAVE2 data were not acquired in high number ( $n=8$ ), as priority was given to IRSp53 and CP (see following chapters). It could be possible that a more detailed investigation of

GFP-WAVE2 diffusion with a higher number of measured cells would lead to a different result.

Looking at the raw data, I had the impression that for some proteins, the diffusion constant values indicated a possible separation into a slow and a fast recovering group. A Lilliefors test for non-normal distribution confirmed this presumption, suggesting that more than one population of diffusion rates was present at the time of the measurement. A bi-modal distribution could be shown most clearly in the case of GFP-CP, where the data from the leading edge could be split into two distinct populations (fast  $> 1.5\mu\text{m}^2/\text{s}$ , slow  $< 1\mu\text{m}^2/\text{s}$ ). The faster fraction showed an average diffusion rate of  $4.44\mu\text{m}^2/\text{s}$ , similar to the rate of GFP-CP found in lamellar regions ( $4.72\mu\text{m}^2/\text{s}$ ). The average of the second, slower population was around  $0.49\mu\text{m}^2/\text{s}$ . This suggests that for GFP-CP, but also for the other measured actin-regulating proteins, the obtained diffusion rate at the leading edge does include a faster fraction, from a lamellar protein population. The sole diffusion rate of the leading edge population is therefore most likely smaller than measured.

Another interesting observation is the difference in diffusion rates inside the lamellipodium between the different constructs. GFP-CP was with  $4.72\mu\text{m}^2/\text{s}$  the fastest of the four tested proteins. This diffusion rate is comparable with the one obtained from GFP alone ( $4.55\mu\text{m}^2/\text{s}$ ) (see Figure 6-2). This suggests a rather free diffusion of GFP-CP in areas where it is not needed for actin filament capping. GFP-IRSp53 showed a much slower rate of diffusion in lamellar regions ( $1.77\mu\text{m}^2/\text{s}$ ), which is closer to previously measured membrane diffusion ( $D_{\text{GFP-F}}=0.97\mu\text{m}^2/\text{s}$ ) than to cytoplasmic movement ( $D_{\text{GFP}}=4.55\mu\text{m}^2/\text{s}$ ). This correlates with the membrane binding ability of IRSp53 and shows that this protein probably travels at least partly within the membrane to reach the leading edge. This makes it a very obvious candidate to be affected by the diffusion barrier.

Unfortunately, I cannot conclude that the diffusion of any of the tested proteins is solely or partly hindered by the leading edge membrane diffusion barrier on the basis of the present data. Two possible reasons for the slower diffusion rates of GFP-IRSP53, GFP-CP and GFP-N-WASP at the leading edge compared to their rates in lamellar regions may be their association with the actin meshwork or the lipid diffusion barrier. Their functional role within actin regulation makes is

likely that these proteins are temporarily slower at the leading edge compared to lamellar regions. IRSp53 mediates arriving Rac1 signals to WAVE2 and thereby activates the latter, which, in the form of a five-membered complex, is then activating the Arp2/3 complex. As the WAVE-complex is thought to be activated through a conformational change upon IRSp53 mediated Rac1 stimulation (Ismail et al., 2009), it is likely that IRSp53 has to be present until WAVE fulfilled its function, resulting in a prolonged stay of IRSp53 at the leading edge. CP caps the +ends of actin filaments and stays there until uncapping or depolymerisation of the filament. The leading edge diffusion barrier may influence the mobility of these proteins when they are not performing their actin-regulating role, increasing dwell time for these proteins at the leading edge and therefore increase the probability for the proteins to act again. The here presented FRAP data do not allow discrimination between the influence of the diffusion barrier or the association with actin machinery, and therefore, more experiments are needed to be able to distinguish between the two possibilities.

## 6.2 FRAP on IRSp53 mutants

In order to investigate a possible influence of the leading edge diffusion barrier on the diffusion of IRSp53, we decided to compare the diffusion of wild type IRSp53 with mutants. FRAP on wild-type GFP-IRSp53 showed a 89% lower diffusion constant at the leading edge compared to lamellar regions (6.1). This decrease might be caused by two possibilities: the association with the lamellipodial actin meshwork through the Rac1/WAVE2 mediating function of IRSp53 or the diffusion of the membrane bound IRSp53 is hindered at the leading edge by the membrane diffusion barrier. However, the GFP-IRSp53 FRAP data could not provide evidence for one or the other possibility to be the sole reason or identify their magnitude of contribution to the overall diffusion decrease at the leading edge. I hoped that analysis of the diffusion of different mutations would help us to distinguish between the leading edge diffusion barrier and the association to the actin machinery as cause for the slower leading edge diffusion of this protein. A membrane-binding mutant should not be influenced by the lipid diffusion barrier and its diffusion rate at the leading edge should therefore

only be controlled by its association with the actin meshwork. In contrast, the diffusion of a mutant with abolished actin meshwork association should show if the diffusion barrier is impairing its mobility at the leading edge or not.

The mutations (IRSp53-IMDmut and IRSp53- $\Delta$ SH3) were kindly provided by Laura Machesky and are described in the introduction section 1.1.1.2 IRSp53. In short, IRSp53-IMDmut inhibits the F-actin bundling function as well as binding to PIP<sub>2</sub>, and IRSp53- $\Delta$ SH3 abolishes interaction with actin regulators such as WAVE2. Localisation of GFP-fusions of these mutants in B16 F1 cells is shown in Figure 6-3 below.

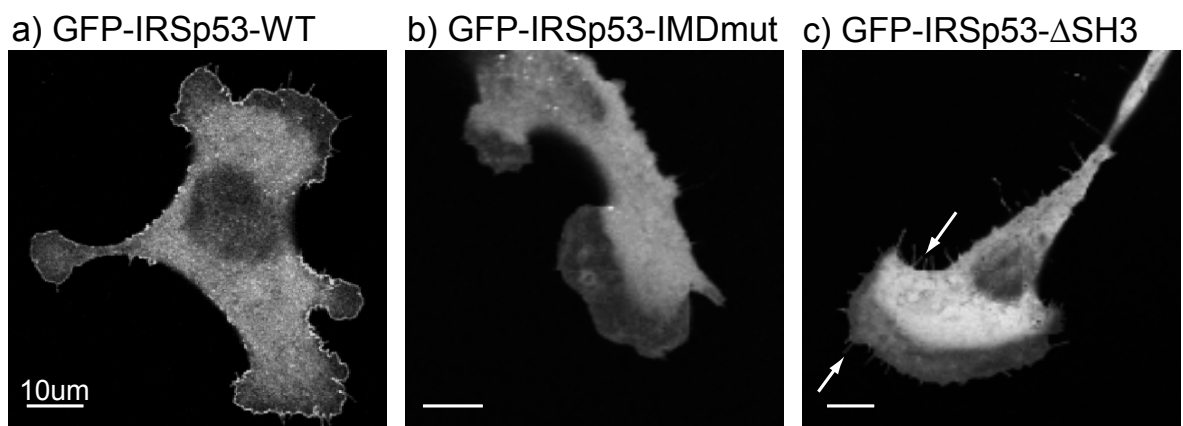
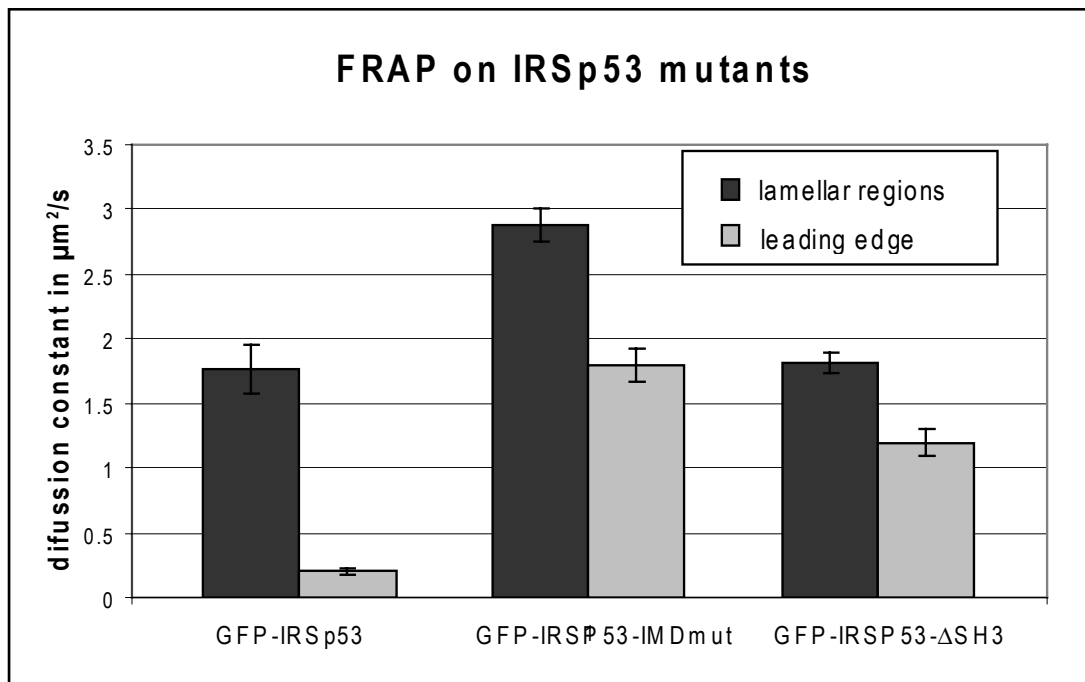


**Figure 6-3: Localisation of wild-type and mutants GFP-IRSp53**

While GFP-IRSp53-WT (a) show a clear localisation at the leading edge, both mutants (GFP-IRSp53-IMDmut (b) and GFP-IRSp53- $\Delta$ SH3 (c)) lack this intense rim. GFP-IRSp53-IMDmut resembles a cytoplasmic expression. Very few to no filopodia can be seen with this probe, in contrast to GFP-IRSp53- $\Delta$ SH3 (arrows).

Localisation of all overexpressed proteins was as expected: GFP-IRSp53-WT could be seen in an intense rim at the leading edge, which was absent in both mutants. GFP-IRSp53-IMDmut showed a rather cytoplasmic expression, with sometimes a very faint, wider rim at the leading edge. This mutant probe was not observed in filopodia, which could be due either to its loss of membrane binding or the absence of its F-actin bundling function. The latter function is mainly used to form the parallel actin filament structure of filopodia. In contrast, GFP-IRSp53- $\Delta$ SH3 was clearly visible in filopodia, but again, no intense rim at the leading edge could be observed in cells expressing this mutant.

FRAP experiments were performed on cells transfected with these mutations and compared to previously acquired GFP-IRSp53-WT data. The following graph and table shows the resulting diffusion constants.



	D in $\mu\text{m}^2/\text{s}$	s.e.m.	n	$\Delta D$	P (t-test)	conclusion
GFP-IRSp53-WT lamellar regions	1.77	0.19	21	1.57	<0.0001	different
GFP-IRSp53-WT leading edge	0.2	0.02	27			
GFP-IRSp53-IMDmut lamellar regions	2.88	0.12	35	1.08	<0.0001	different
GFP-IRSp53-IMDmut leading edge	1.8	0.13	36			
GFP-IRSp53- $\Delta$ SH3 lamellar regions	1.81	0.08	35	0.61	<0.0001	different
GFP-IRSp53- $\Delta$ SH3 leading edge	1.2	0.11	37			

**Figure 6-4: diffusion constants of GFP-IRSp53 wild-type and mutants**

Comparison of the diffusion constants for GFP-IRSp53 WT and mutants in lamellar (black) and leading edge (grey) regions (graph). The table shows the exact diffusion rates of GFP-IRSp53-WT, GFP-IRSp53-IMDmut and GFP-IRSp53- $\Delta$ SH3 as well as the respective errors (s.e.m.) and the results of a t-test between lamellipodium and leading edge rates of each construct.

Inside the lamellipodium, the recovery of the wild-type GFP-IRSp53 construct ( $D_{\text{GFP-IRSp53-WT}}=1.77\mu\text{m}^2/\text{s}$ ) is similar to membrane diffusion (see section 6.1). In contrast, GFP-IRSp53-IMDmut shows a significantly faster diffusion rate in lamellar regions ( $2.88\mu\text{m}^2/\text{s}$ ) compared to wild-type. This rapid diffusion could be due the loss of membrane binding and therefore more cytoplasmic behaviour. The lamellar diffusion of GFP-IRSp53- $\Delta$ SH3 is with  $1.81\mu\text{m}^2/\text{s}$  statistically equal to GFP-IRSp53 recovery in the lamellipodium ( $1.77\mu\text{m}^2/\text{s}$ ). The mutant which lacks the association with actin but has correct membrane binding behaves

equally to the wild-type inside the lamellipodium. This suggests that the association with the actin meshwork does not influence the diffusion of IRSp53 in lamellar regions.

As explained previously (section 6.1), the intense band of GFP-IRSp53 at the leading edge shows a very slow recovery compared to lamellar regions. Although the IRSp53-IMDmut is also significantly slower at the leading edge ( $1.80\mu\text{m}^2/\text{s}$ ), this diffusion rate is still much higher than the diffusion rate of the WT protein at this location. The same is true for the SH3-deletion mutant. Its diffusion rate at the leading edge is significantly slower than in lamellar region, but with  $D_{\text{GFP-IRSp53-}\Delta\text{SH3-leading edge}} = 1.19\mu\text{m}^2/\text{s}$  it recovers much faster than the WT version.

Assuming that the mobility of wild-type IRSp53 at the leading edge may be influenced by either the leading edge diffusion barrier or its actin-regulating function, we would (in theory) expect the IMDmut protein not to be influenced by the diffusion barrier, while still slowed down at the leading edge through its actin regulating ability. The difference in diffusion rate of GFP-IRSp53-IMDmut between lamellar and leading edge regions ( $2.88\mu\text{m}^2/\text{s}$  vs  $1.8\mu\text{m}^2/\text{s}$ ) therefore suggests that the association with the actin machinery restrains the mobility of IRSp53 at the leading edge. The magnitude of diffusion decrease of this membrane-binding mutant could also indicate how much the association with the actin machinery may be able to slow the protein down. Whereas WT-IRSp53 showed a 89% slower diffusion at the leading edge compared to lamellar regions, the recovery of IRSp53-IMDmut at the leading edge was only 37% slower than inside the lamellipodium. This difference in mobility decrease between WT and IMD mutant would suggest that the wild-type IRSp53 is slowed down at the leading edge by more than just its association with the actin machinery, suggesting an influence of the membrane diffusion barrier.

According to the expectations, the SH3-deletion mutant should not be delayed by association with the actin machinery, but could be hindered in its mobility around the leading edge by being trapped within a zone of restricted diffusion. The obtained difference in diffusion rates of IRSp53- $\Delta\text{SH3}$  between lamellar and leading edge regions ( $1.81\mu\text{m}^2/\text{s}$  vs  $1.2\mu\text{m}^2/\text{s}$ ) shows that membrane association alone reduces the mobility of this protein at the leading edge. As associations with the actin meshwork are abolished, they can be excluded as factor for the

limited diffusion of this mutant. This suggests an influence of the leading edge diffusion barrier on the mobility of GFP-IRSp53- $\Delta$ SH3 and therefore also of wild-type IRSP53.

Interpretation of these data may be influenced by the possible dimerisation (see introduction section 1.1.1.2 IRSp53) of the mutants. Dimerisation of one mutated IRSp53 molecule may take place with another mutated molecule, but can also occur with endogenous, non-mutated IRSp53. The latter situation can mask the real effect of the mutation on the diffusion rate, as the endogenous, functioning protein would slow the mutant down. In the lamellipodium the diffusion rates of GFP-IRSp53-WT and GFP-IRSP53- $\Delta$ SH3 are similar, suggesting that dimerisation does not affect the diffusion in lamellar regions. Abolishing the association with the actin meshwork had no effect on protein mobility away from the leading edge. The observation of a significantly faster diffusion rate of IRSp53-IMDmut in lamellar regions compared to wild-type IRSp53 supports the assumption that dimerisation with endogenous wild-type protein does not play a major role in the diffusion behaviour of the mutants. GFP-IRSp53-IMDmut is faster than wild-type because it lost its membrane binding and therefore behaves like a cytoplasmic protein. If the majority of mutant molecules would be associated with an endogeneous wild-type IRSp53, then we would expect the diffusion rate of GFP-IRSp53-IMDmut to be equal to GFP-IRSp53, as a dimerised mutant cannot move faster than its membrane-linked partner. Therefore, I consider the influence of dimerisation as neglectable and the conclusions described above as valid. The reduced mobility of wild-type IRSp53 at the leading edge seems to be partly caused by its actin association and partly by restricted diffusion at the leading edge.

In summary, I performed FRAP experiments on IRSp53 mutations in order to find out whether the leading edge diffusion barrier is involved in the reduction of wild-type GFP-IRSp53 diffusion rate at this location. Analysis of both actin and membrane binding mutants indicate that the lipid diffusion barrier is a contributing factor in decreasing the diffusion rate of IRSp53 at the leading edge compared to lamellar regions. The leading edge diffusion barrier may therefore play an important role in promotion of actin polymerisation, as it prolongs the dwell time of IRSp53 at the leading edge, giving this protein a higher chance to mediate Rac1 to WAVE2 binding and consequently result in a higher activation

rate of Arp2/3. More active Arp2/3 can lead to an increased number of polymerising actin filament +ends, allowing wider protrusion.

### 6.3 FRAP on CP mutants

Capping protein in its functional form has no obvious link to the membrane (Wear and Cooper, 2004) and our expectation was that its mobility at the leading edge should not be hindered by the leading edge diffusion barrier. But due to its actin filament capping activity in the leading edge region, the mobility of wild-type CP at this location is significantly slower than in lamellar regions (see subchapter 6.1). The diffusion analysis of mutated CP was expected to show a clear independence on the leading edge diffusion barrier of this protein and therefore function as a negative control for the interpretation of the IRSp53mutant FRAP results. Two mutations were made available to us: CP $\Delta$ 7 and CPmut (described in introduction section 1.1.1.2 CP). In short, they both affect binding to the actin filament tips. However, the effect is probably more pronounced for CP $\Delta$ 7, which possibly also affects heterodimerisation with the  $\alpha$  subunit.

Figure 6-5 shows the localisation of GFP-fusions of wild-type Cp and both mutants in B16 F1 cells.

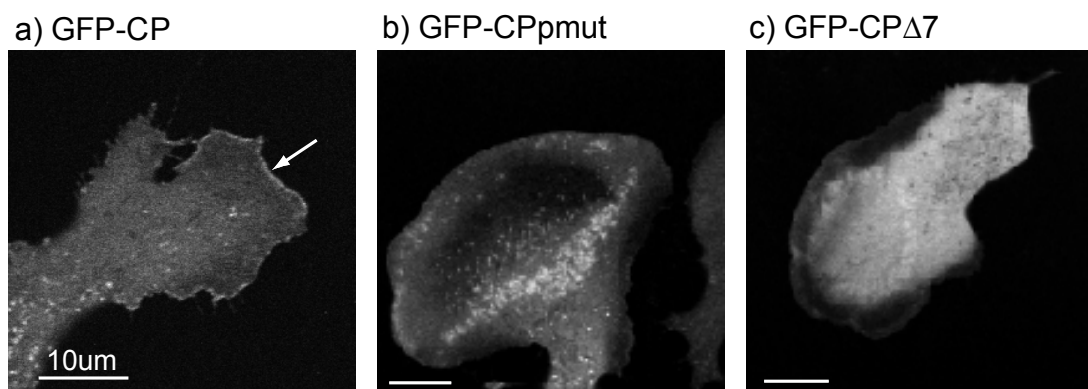
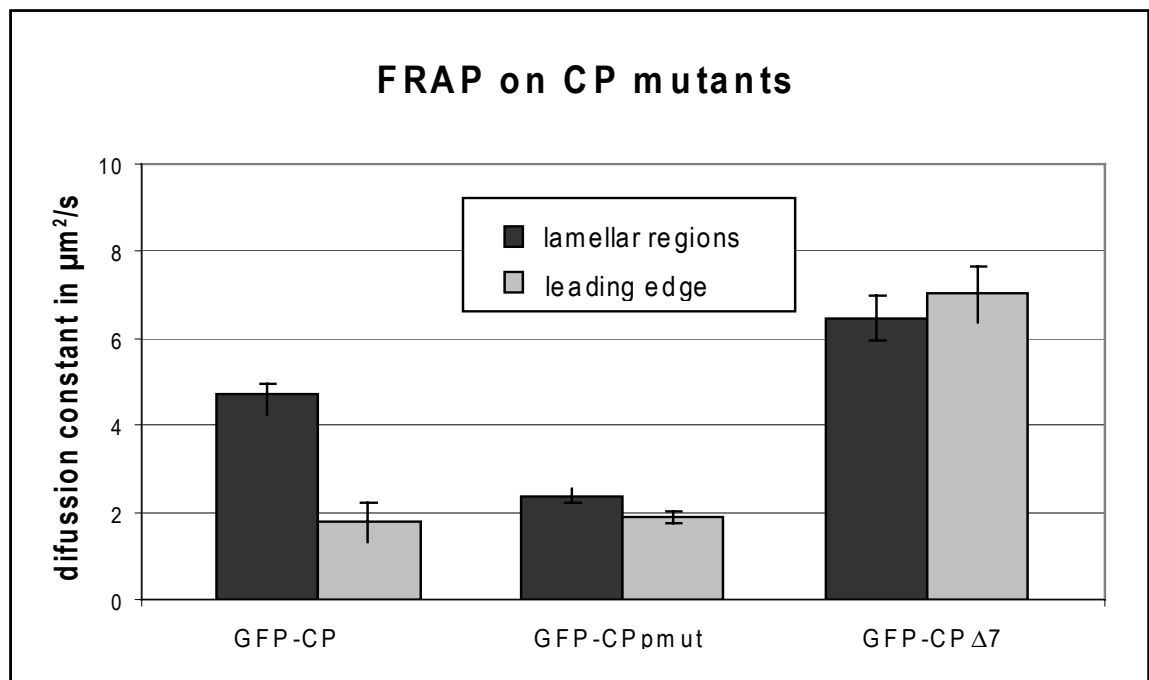


**Figure 6-5: localisation of GFP fusion of wild-type CP and two mutations**

Wild-type GFP-CP shows a distinct localisation at the leading edge (a, arrow), which is not seen in GFP-CPmut (b) and GFP-CP $\Delta$ 7 (c). GFP-CPmut localises to patches within the cell body, whereas GFP-CP $\Delta$ 7 has a rather cytoplasmic localisation.

In contrast to wild type GFP-CP, neither of the mutants showed a distinct localisation at the leading edge (Figure 6-5). In the case of GFP-CP<sub>pmut</sub>, localisation to a group of punctae could be observed, resembling patterns seen in GFP-actin transfected cells (Figure 6-1a). This suggests that there might still be a link to the actin machinery but not at the site of actin filament capping. Note that this localisation was not observed in all cells. In contrast, GFP-CP $\Delta$ 7 shows a rather cytoplasmic localisation with no specific accumulations. No punctate localisation could be observed with this mutation, suggesting less actin-binding activity than the CP<sub>mut</sub> construct. GFP-localisation therefore confirms that CP<sub>pmut</sub> retained some actin binding, whereas CP $\Delta$ 7 possesses no actin binding. The results of FRAP measurements are shown in Figure 6-6.



	D in $\mu\text{m}^2/\text{s}$	s.e.m.	n	$\Delta D$	P (t-test)	conclusion
GFP-CP lamellar regions	4.72	0.24	28	2.95	<0.0001	different
GFP-CP leading edge	1.77	0.46	22			
GFP-CP <sub>pmut</sub> lamellar regions	2.38	0.15	25	0.51	0.017	different
GFP-CP <sub>pmut</sub> leading edge	1.87	0.14	24			
GFP-CP $\Delta$ 7 lamellar regions	6.46	0.5	25	-0.55	0.49	not different
GFP-CP $\Delta$ 7 leading edge	7.01	0.63	22			

**Figure 6-6: diffusion rates of GFP-fusions of CP wild-type and mutants**

The graph shows a comparison of diffusion rates in lamellar regions and the leading edge of all GFP-fusions. The table shows the exact diffusion rates of GFP-CP, GFP-CP<sub>pmut</sub> and GFP-CP $\Delta$ 7 as well as the respective errors (s.e.m.) and the results of a t-test between lamellipodium and leading edge rates of each construct.

Interestingly, comparison of the diffusion rates within the lamellipodium of all three constructs showed that the rate of GFP-CPmut ( $2.38\mu\text{m}^2/\text{s}$ ) was approximately 50% lower and the rate of GFP-CP $\Delta$ 7 ( $6.46\mu\text{m}^2/\text{s}$ ) nearly 40% higher than wild-type GFP-CP ( $4.72\mu\text{m}^2/\text{s}$ ). This is surprising, as loss of actin-binding function was expected to influence only the diffusion at the leading edge but not inside the lamellipodium. It may suggest that CP is performing its function not only on the sites of obvious actin polymerisation (i.e. the leading edge) but also further behind. Still it is surprising, why the GFP-CPmut moves slower than wild-type CP. Loss of actin binding was expected to lead to faster diffusion rather than slower. And although this mutant may retain some actin-binding function, this would not explain why it is moving slower than wild-type. The faster lamellar diffusion rate of GFP-CP $\Delta$ 7 (compared to GFP-CP-WT), may be caused by its inability to dimerise. A CP molecule has to consist of one  $\alpha$  and one  $\beta$  subunit in order to function (Sizonenko et al., 1996). If the  $\Delta$ 7 mutant were not able to dimerise it may be that it is diffusing in the cytoplasm, without any specific function. I can not say at present why this diffusion constant is even higher than that measured for free GFP ( $4.55\mu\text{m}^2/\text{s}$ ). One possible explanation would be inaccuracy in measuring fast diffusions due to the acquisition limits of the microscope. As  $t_{1/2}$  for these fast constructs lies under the minimal scan time per frame ( $=65\text{ms}$ ), it may well be that the real diffusion constant is faster for both constructs. Small differences in positioning of the ROI could lead to changed results and normally equal diffusion rates may appear different

The leading edge diffusion of GFP-CP $\Delta$ 7 was with  $D=7.01\mu\text{m}^2/\text{s}$  statistically equal to the lamellar diffusion rate of this construct ( $6.46\mu\text{m}^2/\text{s}$ ). This result would correlate with a potential lack of function due to the mutant's inability to dimerise. This indicates that, as expected, the decreased mobility of wild-type CP at the leading edge is solely due to its actin-binding function and the leading edge membrane diffusion barrier is not involved in the motility of this non-membrane bound protein.

GFP-CPmut showed a significantly slower diffusion at the leading edge ( $1.87\mu\text{m}^2/\text{s}$ ) compared to lamellar regions ( $2.38\mu\text{m}^2/\text{s}$ ). Interestingly, this leading edge diffusion rate was comparable with wild type ( $1.77\mu\text{m}^2/\text{s}$ ;  $P(\text{t-test})=0.82$ ), indicating at first glance a non-altered function of the mutant at this location. But as explained in subchapter 6.1, the FRAP data of GFP-CP can

be divided into two populations, with the diffusion rate of the slower population ( $0.57\mu\text{m}^2/\text{s}$ ) most certainly reflecting molecules within the bright rim at the leading edge. In contrast, the Lilliefors test showed a normal distribution of the GFP-CPpmut data, leading to the conclusion that CPpmut at the leading edge turns over much faster than the slow recovering, “working” wild-type CP. The disruption in actin capping function of this construct explains this faster diffusion rate, as the mutated protein does not bind and therefore does not stay at the capped actin filament tips and can thus recover faster. Interestingly, the expectation that an actin-binding mutated CP should have an equal diffusion at the leading edge and inside the lamellipodium was not fulfilled with the CPpmut construct. There is still a small, but significant decrease in leading edge diffusion rate compared to lamellar regions (21.4%). There are two factors which may contribute to this result. First, CPpmut retain some actin-binding function, which means it may still partly bind actin filament +ends. Second, dimerisation with a functional  $\alpha$  subunit may have a similar effect of partial actin binding. This partial actin binding may explain why this mutant retains a slower diffusion at the leading edge compared to lamellar regions.

In summary, most of the FRAP results can be explained with the functional differences between wild type CP and the mutants. The results of CPpmut FRAP do not correlate with our expectation, but may be explained by only partial functional loss and dimerisation. However, the equal diffusion rates of GFP-CP $\Delta$ 7 in lamellar and leading edge regions correlate with our expectation and show that the slower diffusion of wild-type CP at the leading edge is only due to its actin-binding function. The diffusion barrier does not influence this non-membrane bound protein.

## 6.4 Summary and conclusions

In this chapter I wanted to identify whether actin regulating proteins are hindered in their mobility by the leading edge diffusion barrier. If so, this would support the idea that this area of restricted diffusion may be an important feature for actin polymerisation.

Initial FRAP experiments with different actin-regulating proteins did not lead to any conclusive results. It could be measured that IRSp53, CP and N-WASP are slower at the leading edge compared to lamellar regions. However, it was not possible to prove that the diffusion barrier is, at least partially, causing these reductions. A major reason for the slower leading edge recovery of these proteins is most likely their association with the actin machinery, be it by being bound to filament +ends (CP) or by their roles in Arp2/3 activation (IRSp53 and N-WASP). The challenge was to identify to what extent the membrane diffusion barrier is involved in the decreased mobility of these proteins at the leading edge.

This challenge was addressed through the use of mutated versions of IRSp53 and CP. The non-membrane bound CP acted as a control to see whether the loss of actin-binding function and therefore the loss of any association with the actin meshwork would lead to a complete abolishment of the in wild-type observed difference in diffusion rates between lamellar regions and the leading edge. Although this was not achieved with CPmut, a mutant with reduced actin-binding ability, this may be explained by its partial loss of function as well as its dimerisation with a functional  $\alpha$  subunit. In contrast, the CP $\Delta$ 7 mutant confirmed our expectations: an equal diffusion at the leading edge and inside the lamellipodium was observed. This shows that the diffusion barrier does not influence the diffusion of non-membrane bound proteins at the leading edge.

In the case of the membrane-associated IRSp53, the use of mutants indicated that the membrane diffusion barrier is reducing their diffusion rate at the leading edge. Wild-type IRSp53 showed a hugely (89%) slower diffusion at the leading edge compared to inside the lamellipodium, but it was not possible to identify how much of this reduction is caused by the diffusion barrier and how much by the protein's link to the actin machinery. A membrane-bound mutant with abolished association to the actin meshwork (IRSp53- $\Delta$ SH3) still showed a decreased diffusion rate at the leading edge as compared to lamellar regions, suggesting that at least a part of the in wild-type IRSp53 observed decrease is caused by the leading edge diffusion barrier. IRSp53-IMDmut, a mutant with disrupted membrane binding but intact function to mediate Rac1 and WAVE binding, showed a much lower decrease at the leading edge than the wild-type. The diffusion of the IMDmut at the leading edge was only 37% slower than in

lamellar regions, as compared to 89% seen in IRSp53-WT. The measured 37% decrease most likely corresponds to the reduction caused by association with the actin-machinery, leaving 52% unaccounted for. The membrane diffusion barrier is most likely to be responsible for this further decrease of leading edge diffusion in wild-type IRSp53. Although the involvement of IRSp53 in lamellipodia might be controversial, the localisation of GFP-IRSp53 observed within this thesis points towards a function outside of filopodia. Even if it might not be by linking Rac1 to WAVE2, the domain structure of IRSp53 (see introduction section 1.1.1.2) suggests an important association with the actin machinery and the interpretation of my results can therefore be seen as valid.

We can therefore propose that the leading edge diffusion barrier not only hinders membrane markers in their diffusion at the leading edge, but also affects membrane associated actin-regulating proteins. This suggests that this zone of restricted diffusion may be important for actin polymerisation at the leading edge by trapping necessary proteins at the location of polymerisation. Proteins which would normally rapidly diffuse around and maybe away from the leading edge, would be kept longer at the leading edge, making them easier available to be involved in the actin polymerisation machinery.

## 7 Summary and conclusions

This project investigated the interaction between actin filament tips and the plasma membrane at the leading edge. The biochemical process of actin polymerisation generates force against the leading edge membrane and drives cell protrusion. Many models explain how this polymerisation might generate and exert force, but due to the dynamic nature of this process and its spatially restricted location, experimental data are sparse. Investigation of membrane diffusion around the leading edge is one way to study the membrane-actin interaction without interfering in the protrusion process.

In chapter 4, I addressed the first aim of this thesis, which was to investigate whether the lipid diffusion barrier (Weisswange et al., 2005) can be found in other cell systems than fish keratocytes. Using a FRAP approach, I could show that the diffusion of membrane linked GFPs (GFP-F and GFP-PH-PLC) was slower at the leading edge of B16 F1 mouse melanoma cells compared to lamellar regions. Experiments with actin disrupting drugs such as CytD and LatA (following necessary pre-treatment with ConA) were inconclusive due to drug related side effects which altered the membrane diffusion. Investigation of diffusion at non-protruding sites of the cell edge demonstrated the actin-dependency of the restricted diffusion zone in a drug-free environment. Thus, the leading edge diffusion barrier seems to be a general feature of protrusion.

Chapter 5 describes investigations undertaken to characterise the nature of the actin-membrane interaction. FRAP experiments on cells with different protrusion velocities, fixed cells and polymerising actin waves were undertaken to examine the basis of the diffusion barrier. The results indicate that the force of the actin filaments pushing against the membrane might hinder membrane components in their mobility. A force-based mechanism would also explain why no diffusion barrier was found in Dil labelled B16 cells (chapter 4). This dye is hindered in its diffusion around the leading edge of fish keratocytes, but B16 cells show a slower protrusion rate than keratocytes and the force generated against the membrane in these mouse melanoma cells is probably not strong enough to hinder the small dye molecule in the outer membrane leaflet. These data support the theoretical force production model of Mogilner and Oster (“elastic

ratchet and tethered filament” model) which assumes the existence of free working filament exerting force against the membrane.

FLIM-FRET approaches to study the interaction between the actin filament tips and the membrane showed no direct contact. This might at first glance contradict the indication for a force-based mechanism, but FLIM results using IRSp53 suggest that this protein might be positioned between the filaments and the membrane, which may explain why no direct interaction between actin and the membrane could be detected. Interestingly, the close interaction of IRSp53 with the membrane was abolished through deletion of its actin association (SH3 domain) but not its membrane binding (IMDmut). This suggests that the force generated by actin polymerisation is pushing IRSp53 against the membrane and this force may therefore also be responsible for the hindered diffusion of membrane components at the leading edge.

In chapter 6, I could show that the membrane associated actin-regulating protein IRSp53 seems to be hindered in its mobility at the leading edge by the membrane diffusion barrier. The much slower diffusion of GFP-IRSp53 at the leading edge compared to lamellar regions is partly due to its association with the actin machinery, but partly also due to trapping within a membrane domain with restricted diffusion. In contrast, the mobility of non-membrane associate CP seems only to be restrained by its actin filament capping function. This influence of the diffusion barrier on actin-regulating proteins may be an important feature for actin polymerisation. By restricting their diffusion within the leading edge, the dwell time of affected proteins at this location would be increased, leading to a higher availability of these proteins for further actin polymerisation. The diffusion barrier might therefore act as a positive feed-back loop for actin polymerisation at the leading edge.

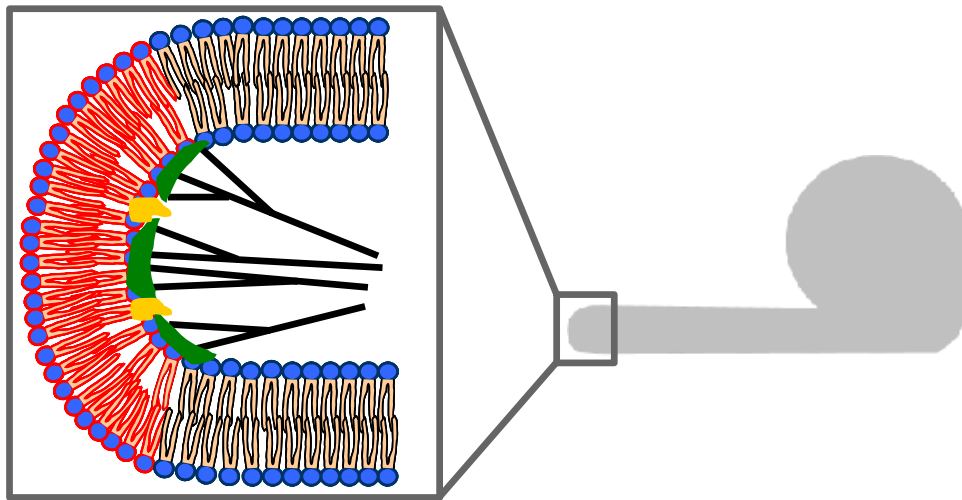


**Figure 7-1: model of the leading edge diffusion barrier**

This schematic shows a representation of the leading edge of a migrating cell, with actin filaments (black) pushing against proteins at the membrane (such as IRSp53 - green). The force generated by actin polymerisation changes the local membrane behaviour and a zone of restricted diffusion is created (red). This zone is thought to hinder membrane associated proteins (yellow and green) in their diffusion, causing increased actin polymerisation at this location.

Diffusion barriers such as tight junctions in epithelial cells or the axon initial segment in neurons have been shown to play a crucial role in maintaining polarity of cells and therefore separate specific functions (Dragsten et al., 1981, Winckler et al., 1999). Although the leading edge membrane diffusion barrier seems to be an area of restricted diffusion rather than a strict barrier, its presence could still be an important feature for cell polarisation needed for migration. By trapping certain actin-regulating proteins at the leading edge the diffusion barrier could increase their involvement in actin polymerisation and therefore maintain localised protrusion. The influence of membrane composition on cell migration has been shown by the group of Paul Fox. They found that the plasma membrane microviscosity is higher at the leading edge than in areas at the back of the cell (Vasanji et al., 2004). They suggest that the change of microviscosity within the membrane may increase actin polymerisation and therefore cell velocity. One open question in regards to their findings combined with results shown in this thesis is whether membrane composition changes first and influences actin polymerisation or if actin polymerisation changes the membrane composition to create a positive feed-back loop for itself. Regardless of which case may be true, it can be said that restricted diffusion within the membrane may be an important feature for localisation and maintenance of actin polymerisation in migrating cells.

## References

- Abercrombie, M., Heaysman, J. E. and Pegrum, S. M. (1970a), The locomotion of fibroblasts in culture. I. Movements of the leading edge, *Exp Cell Res*, 59, 393-8.
- Abercrombie, M., Heaysman, J. E. and Pegrum, S. M. (1970b), The locomotion of fibroblasts in culture. II. "Ruffling", *Exp Cell Res*, 60, 437-44.
- Abou-Kheir, W., Isaac, B., Yamaguchi, H. and Cox, D. (2008), Membrane targeting of WAVE2 is not sufficient for WAVE2-dependent actin polymerization: a role for IRSp53 in mediating the interaction between Rac and WAVE2, *J Cell Sci*, 121, 379-90.
- Abraham, V. C., Krishnamurthi, V., Taylor, D. L. and Lanni, F. (1999), The actin-based nanomachine at the leading edge of migrating cells, *Biophys J*, 77, 1721-32.
- Alberts, B., Johnson, A., Lewis, J., Raff, M., Roberts, K. and Walter, P. (2008) *Molecular Biology of the cell*, 5, Garland Science, Taylor & Francis Group.
- Amann, K. J. and Pollard, T. D. (2001), The Arp2/3 complex nucleates actin filament branches from the sides of pre-existing filaments, *Nat Cell Biol*, 3, 306-10.
- Ambrose, E. J. (1956), A surface contact microscope for the study of cell movements, *Nature*, 178, 1194.
- Anderson, K. I. and Cross, R. (2000), Contact dynamics during keratocyte motility, *Curr Biol*, 10, 253-60.
- Anderson, K. I. and Small, J. V. (1998) In *Cell Biology: A laboratory Handbook*, Vol. 2 (Ed, Celis, J. E.) Academic Press, London, pp. 372-376.
- Anderson, K. I., Wang, Y. L. and Small, J. V. (1996), Coordination of protrusion and translocation of the keratocyte involves rolling of the cell body, *J Cell Biol*, 134, 1209-18.
- Axelrod, D. (1981), Cell-substrate contacts illuminated by total internal reflection fluorescence, *J Cell Biol*, 89, 141-5.
- Axelrod, D., Koppel, D. E., Schlessinger, J., Elson, E. and Webb, W. W. (1976), Mobility measurement by analysis of fluorescence photobleaching recovery kinetics, *Biophys J*, 16, 1055-69.
- Axelrod, D., Thompson, N. L. and Burghardt, T. P. (1983), Total internal reflection fluorescent microscopy, *J Microsc*, 129, 19-28.
- Baird, G. S., Zacharias, D. A. and Tsien, R. Y. (2000), Biochemistry, mutagenesis, and oligomerization of DsRed, a red fluorescent protein from coral, *Proc Natl Acad Sci U S A*, 97, 11984-9.
- Balda, M. S., Whitney, J. A., Flores, C., Gonzalez, S., Cereijido, M. and Matter, K. (1996), Functional dissociation of paracellular permeability and transepithelial electrical resistance and disruption of the apical-basolateral intramembrane diffusion barrier by expression of a mutant tight junction membrane protein, *J Cell Biol*, 134, 1031-49.
- Ballestrem, C., Wehrle-Haller, B., Hinz, B. and Imhof, B. A. (2000), Actin-dependent lamellipodia formation and microtubule-dependent tail retraction control-directed cell migration, *Mol Biol Cell*, 11, 2999-3012.
- Barron-Casella, E. A., Torres, M. A., Scherer, S. W., Heng, H. H., Tsui, L. C. and Casella, J. F. (1995), Sequence analysis and chromosomal localization of human Cap Z. Conserved residues within the actin-binding domain may link Cap Z to gelsolin/severin and profilin protein families, *J Biol Chem*, 270, 21472-9.

- Benesch, S., Polo, S., Lai, F. P., Anderson, K. I., Stradal, T. E., Wehland, J. and Rottner, K. (2005), N-WASP deficiency impairs EGF internalization and actin assembly at clathrin-coated pits, *J Cell Sci*, 118, 3103-15.
- Berney, C. and Danuser, G. (2003), FRET or no FRET: a quantitative comparison, *Biophys J*, 84, 3992-4010.
- Berro, J., Michelot, A., Blanchoin, L., Kovar, D. R. and Martiel, J. L. (2007), Attachment conditions control actin filament buckling and the production of forces, *Biophys J*, 92, 2546-58.
- Boczkowska, M., Rebowski, G., Petoukhov, M. V., Hayes, D. B., Svergun, D. I. and Dominguez, R. (2008), X-ray scattering study of activated Arp2/3 complex with bound actin-WCA, *Structure*, 16, 695-704.
- Bretscher, M. S. (1973), Membrane structure: some general principles, *Science*, 181, 622-9.
- Bretscher, M. S. (1985), The molecules of the cell membrane, *Sci Am*, 253, 100-8.
- Bretschneider, T., Diez, S., Anderson, K., Heuser, J., Clarke, M., Muller-Taubenberger, A., Kohler, J. and Gerisch, G. (2004), Dynamic actin patterns and Arp2/3 assembly at the substrate-attached surface of motile cells, *Curr Biol*, 14, 1-10.
- Buckley, I. K. and Porter, K. R. (1967), Cytoplasmic fibrils in living cultured cells. A light and electron microscope study, *Protoplasma*, 64, 349-80.
- Campellone, K. G., Webb, N. J., Znameroski, E. A. and Welch, M. D. (2008), WHAMM is an Arp2/3 complex activator that binds microtubules and functions in ER to Golgi transport, *Cell*, 134, 148-61.
- Carlier, M. F., Wiesner, S., Le Clainche, C. and Pantaloni, D. (2003), Actin-based motility as a self-organized system: mechanism and reconstitution in vitro, *C R Biol*, 326, 161-70.
- Casella, J. F. and Torres, M. A. (1994), Interaction of Cap Z with actin. The NH2-terminal domains of the alpha 1 and beta subunits are not required for actin capping, and alpha 1 beta and alpha 2 beta heterodimers bind differentially to actin, *J Biol Chem*, 269, 6992-8.
- Chalfie, M., Tu, Y., Euskirchen, G., Ward, W. W. and Prasher, D. C. (1994), Green fluorescent protein as a marker for gene expression, *Science*, 263, 802-5.
- Connolly, B. A., Rice, J., Feig, L. A. and Buchsbaum, R. J. (2005), Tiam1-IRSp53 complex formation directs specificity of rac-mediated actin cytoskeleton regulation, *Mol Cell Biol*, 25, 4602-14.
- Dai, J. and Sheetz, M. P. (1999), Membrane tether formation from blebbing cells, *Biophys J*, 77, 3363-70.
- De Bruyn, P. P. H. (1947), Theories of amoeboid movement, *The Quarterly Review of Biology*, 22, 1-24.
- de Keijzer, S., Serge, A., van Hemert, F., Lommerse, P. H., Lamers, G. E., Spaink, H. P., Schmidt, T. and Snaar-Jagalska, B. E. (2008), A spatially restricted increase in receptor mobility is involved in directional sensing during Dictyostelium discoideum chemotaxis, *J Cell Sci*, 121, 1750-7.
- De La Cruz, E. M. and Pollard, T. D. (1995), Nucleotide-free actin: stabilization by sucrose and nucleotide binding kinetics, *Biochemistry*, 34, 5452-61.
- Dederer, P. H. (1921), The behaviour of cells in tissue cultures of fundulus heteroclitus with special reference to the ectoderm, *Connecticut College London*.
- Dickinson, R. B. and Purich, D. L. (2002), Clamped-filament elongation model for actin-based motors, *Biophys J*, 82, 605-17.

- Downey, G. P., Chan, C. K., Lea, P., Takai, A. and Grinstein, S. (1992), Phorbol ester-induced actin assembly in neutrophils: role of protein kinase C, *J Cell Biol*, 116, 695-706.
- Dragsten, P. R., Blumenthal, R. and Handler, J. S. (1981), Membrane asymmetry in epithelia: is the tight junction a barrier to diffusion in the plasma membrane?, *Nature*, 294, 718-22.
- Fidler, I. J. (1975), Biological behavior of malignant melanoma cells correlated to their survival in vivo, *Cancer Res*, 35, 218-24.
- Forscher, P. and Smith, S. J. (1988), Actions of cytochalasins on the organization of actin filaments and microtubules in a neuronal growth cone, *J Cell Biol*, 107, 1505-16.
- Fujiwara, T., Mammoto, A., Kim, Y. and Takai, Y. (2000), Rho small G-protein-dependent binding of mDia to an Src homology 3 domain-containing IRSp53/BAIAP2, *Biochem Biophys Res Commun*, 271, 626-9.
- Funato, Y., Terabayashi, T., Suenaga, N., Seiki, M., Takenawa, T. and Miki, H. (2004), IRSp53/Eps8 complex is important for positive regulation of Rac and cancer cell motility/invasiveness, *Cancer Res*, 64, 5237-44.
- Futerman, A. H., Khanin, R. and Segel, L. A. (1993), Lipid diffusion in neurons, *Nature*, 362, 119.
- Gerbal, F., Chaikin, P., Rabin, Y. and Prost, J. (2000a), An elastic analysis of *Listeria monocytogenes* propulsion, *Biophys J*, 79, 2259-75.
- Gerbal, F., Laurent, V., Ott, A., Carlier, M. F., Chaikin, P. and Prost, J. (2000b), Measurement of the elasticity of the actin tail of *Listeria monocytogenes*, *Eur Biophys J*, 29, 134-40.
- Gerisch, G., Bretschneider, T., Muller-Taubenberger, A., Simmeth, E., Ecke, M., Diez, S. and Anderson, K. (2004), Mobile actin clusters and traveling waves in cells recovering from actin depolymerization, *Biophys J*, 87, 3493-503.
- Gingell, D. and Owens, N. (1992), How do cells sense and respond to adhesive contacts? Diffusion-trapping of laterally mobile membrane proteins at maturing adhesions may initiate signals leading to local cytoskeletal assembly response and lamella formation, *J Cell Sci*, 101 ( Pt 2), 255-66.
- Goddette, D. W. and Frieden, C. (1986), Actin polymerization. The mechanism of action of cytochalasin D, *J Biol Chem*, 261, 15974-80.
- Goldberg, M. B. and Theriot, J. A. (1995), *Shigella flexneri* surface protein IcsA is sufficient to direct actin-based motility, *Proc Natl Acad Sci U S A*, 92, 6572-6.
- Goodrich, H. B. (1924), Cell behavior in tissue cultures, *Biological Bulletin*, 46, 252-262.
- Gouin, E., Gantelet, H., Egile, C., Lasa, I., Ohayon, H., Villiers, V., Gounon, P., Sansonetti, P. J. and Cossart, P. (1999), A comparative study of the actin-based motilities of the pathogenic bacteria *Listeria monocytogenes*, *Shigella flexneri* and *Rickettsia conorii*, *J Cell Sci*, 112 ( Pt 11), 1697-708.
- Hahne, P., Sechi, A., Benesch, S. and Small, J. V. (2001), Scar/WAVE is localised at the tips of protruding lamellipodia in living cells, *FEBS Lett*, 492, 215-20.
- Hancock, J. F., Cadwallader, K., Paterson, H. and Marshall, C. J. (1991), A CAAX or a CAAL motif and a second signal are sufficient for plasma membrane targeting of ras proteins, *Embo J*, 10, 4033-9.
- Harder, T., Scheiffele, P., Verkade, P. and Simons, K. (1998), Lipid domain structure of the plasma membrane revealed by patching of membrane components, *J Cell Biol*, 141, 929-42.

- Heung, M. Y., Visegrady, B., Futterer, K. and Machesky, L. M. (2008), Identification of the insulin-responsive tyrosine phosphorylation sites on IRSp53, *Eur J Cell Biol*, 87, 699-708.
- Huang, S., Gao, L., Blanchoin, L. and Staiger, C. J. (2006), Heterodimeric capping protein from Arabidopsis is regulated by phosphatidic acid, *Mol Biol Cell*, 17, 1946-58.
- Hubbell, W. L. (1990), Transbilayer coupling mechanism for the formation of lipid asymmetry in biological membranes. Application to the photoreceptor disc membrane, *Biophys J*, 57, 99-108.
- Hug, C., Miller, T. M., Torres, M. A., Casella, J. F. and Cooper, J. A. (1992), Identification and characterization of an actin-binding site of CapZ, *J Cell Biol*, 116, 923-31.
- Ilsley, J. L., Sudol, M. and Winder, S. J. (2002), The WW domain: linking cell signalling to the membrane cytoskeleton, *Cell Signal*, 14, 183-9.
- Ishikawa, H., Bischoff, R. and Holtzer, H. (1969), Formation of arrowhead complexes with heavy meromyosin in a variety of cell types, *J Cell Biol*, 43, 312-28.
- Ismail, A. M., Padrick, S. B., Chen, B., Umetani, J. and Rosen, M. K. (2009), The WAVE regulatory complex is inhibited, *Nat Struct Mol Biol*, 16, 561-3.
- James, P. S., Hennessy, C., Berge, T. and Jones, R. (2004), Compartmentalisation of the sperm plasma membrane: a FRAP, FLIP and SPFI analysis of putative diffusion barriers on the sperm head, *J Cell Sci*, 117, 6485-95.
- Jurado, C., Haserick, J. R. and Lee, J. (2005), Slipping or gripping? Fluorescent speckle microscopy in fish keratocytes reveals two different mechanisms for generating a retrograde flow of actin, *Mol Biol Cell*, 16, 507-18.
- Kandel, E. R., Schwartz, J. H. and Jessel, T. M. (2000) *Principles of neural science*, 4, New York McGraw-Hill.
- Kasai, M., Nakano, E. and Oosawa, F. (1965), Polymerization of Actin Free from Nucleotides and Divalent Cations, *Biochim Biophys Acta*, 94, 494-503.
- Kaverina, I., Krylyshkina, O., Beningo, K., Anderson, K., Wang, Y. L. and Small, J. V. (2002), Tensile stress stimulates microtubule outgrowth in living cells, *J Cell Sci*, 115, 2283-91.
- Kiernan, J. (2000), Formaldehyde, formalin, paraformaldehyde and glutaraldehyde: What they are and what they do., *Microscopy Today*, 00-1, 8-12.
- Kim, A. S., Kakalis, L. T., Abdul-Manan, N., Liu, G. A. and Rosen, M. K. (2000), Autoinhibition and activation mechanisms of the Wiskott-Aldrich syndrome protein, *Nature*, 404, 151-8.
- Kim, K., McCully, M. E., Bhattacharya, N., Butler, B., Sept, D. and Cooper, J. A. (2007), Structure/function analysis of the interaction of phosphatidylinositol 4,5-bisphosphate with actin-capping protein: implications for how capping protein binds the actin filament, *J Biol Chem*, 282, 5871-9.
- Kiselar, J. G., Mahaffy, R., Pollard, T. D., Almo, S. C. and Chance, M. R. (2007), Visualizing Arp2/3 complex activation mediated by binding of ATP and WASp using structural mass spectrometry, *Proc Natl Acad Sci U S A*, 104, 1552-7.
- Kobayashi, K., Kuroda, S., Fukata, M., Nakamura, T., Nagase, T., Nomura, N., Matsuura, Y., Yoshida-Kubomura, N., Iwamatsu, A. and Kaibuchi, K. (1998), p140Sra-1 (specifically Rac1-associated protein) is a novel specific target for Rac1 small GTPase, *J Biol Chem*, 273, 291-5.

- Kobayashi, T., Storrie, B., Simons, K. and Dotti, C. G. (1992), A functional barrier to movement of lipids in polarized neurons, *Nature*, 359, 647-50.
- Koestler, S. A., Rottner, K., Lai, F., Block, J., Vinzenz, M. and Small, J. V. (2009), F- and G-actin concentrations in lamellipodia of moving cells, *PLoS One*, 4, e4810.
- Kolega, J., Shure, M. S., Chen, W. T. and Young, N. D. (1982), Rapid cellular translocation is related to close contacts formed between various cultured cells and their substrata, *J Cell Sci*, 54, 23-34.
- Kondo, H. and Ishiwata, S. (1976), Uni-directional growth of F-actin, *J Biochem*, 79, 159-71.
- Konig, I., Schwarz, J. P. and Anderson, K. I. (2008), Fluorescence lifetime imaging: association of cortical actin with a PIP3-rich membrane compartment, *Eur J Cell Biol*, 87, 735-41.
- Krugmann, S., Jordens, I., Gevaert, K., Driessens, M., Vandekerckhove, J. and Hall, A. (2001), Cdc42 induces filopodia by promoting the formation of an IRSp53:Mena complex, *Curr Biol*, 11, 1645-55.
- Kunda, P., Craig, G., Dominguez, V. and Baum, B. (2003), Abi, Sra1, and Kette control the stability and localization of SCAR/WAVE to regulate the formation of actin-based protrusions, *Curr Biol*, 13, 1867-75.
- Kuo, S. C. and McGrath, J. L. (2000), Steps and fluctuations of *Listeria monocytogenes* during actin-based motility, *Nature*, 407, 1026-9.
- Kusumi, A. and Sako, Y. (1996), Cell surface organization by the membrane skeleton, *Curr Opin Cell Biol*, 8, 566-74.
- Lai, F. P., Szczodrak, M., Block, J., Faix, J., Breitsprecher, D., Mannherz, H. G., Stradal, T. E., Dunn, G. A., Small, J. V. and Rottner, K. (2008), Arp2/3 complex interactions and actin network turnover in lamellipodia, *Embo J*, 27, 982-92.
- Lakowicz, J. (2006) *Principles of Fluorescence Spectroscopy*, 3rd, Springer.
- Laurent, V., Loisel, T. P., Harbeck, B., Wehman, A., Grobe, L., Jockusch, B. M., Wehland, J., Gertler, F. B. and Carlier, M. F. (1999), Role of proteins of the Ena/VASP family in actin-based motility of *Listeria monocytogenes*, *J Cell Biol*, 144, 1245-58.
- Le Clainche, C. and Carlier, M. F. (2008), Regulation of actin assembly associated with protrusion and adhesion in cell migration, *Physiol Rev*, 88, 489-513.
- Lim, K. B., Bu, W., Goh, W. I., Koh, E., Ong, S. H., Pawson, T., Sudhakaran, T. and Ahmed, S. (2008), The Cdc42 effector IRSp53 generates filopodia by coupling membrane protrusion with actin dynamics, *J Biol Chem*, 283, 20454-72.
- Linardopoulou, E. V., Parghi, S. S., Friedman, C., Osborn, G. E., Parkhurst, S. M. and Trask, B. J. (2007), Human subtelomeric WASH genes encode a new subclass of the WASP family, *PLoS Genet*, 3, e237.
- Liu, A. P. and Fletcher, D. A. (2006), Actin polymerization serves as a membrane domain switch in model lipid bilayers, *Biophys J*, 91, 4064-70.
- Loisel, T. P., Boujemaa, R., Pantaloni, D. and Carlier, M. F. (1999), Reconstitution of actin-based motility of *Listeria* and *Shigella* using pure proteins, *Nature*, 401, 613-6.
- Machesky, L. M., Atkinson, S. J., Ampe, C., Vandekerckhove, J. and Pollard, T. D. (1994), Purification of a cortical complex containing two unconventional actins from *Acanthamoeba* by affinity chromatography on profilin-agarose, *J Cell Biol*, 127, 107-15.

- Machesky, L. M. and Insall, R. H. (1998), Scar1 and the related Wiskott-Aldrich syndrome protein, WASP, regulate the actin cytoskeleton through the Arp2/3 complex, *Curr Biol*, 8, 1347-56.
- Machesky, L. M., Mullins, R. D., Higgs, H. N., Kaiser, D. A., Blanchoin, L., May, R. C., Hall, M. E. and Pollard, T. D. (1999), Scar, a WASP-related protein, activates nucleation of actin filaments by the Arp2/3 complex, *Proc Natl Acad Sci U S A*, 96, 3739-44.
- Mahadevan, L. and Matsudaira, P. (2000), Motility powered by supramolecular springs and ratchets, *Science*, 288, 95-100.
- Mattila, P. K., Pykalainen, A., Saarikangas, J., Paavilainen, V. O., Vihinen, H., Jokitalo, E. and Lappalainen, P. (2007), Missing-in-metastasis and IRSp53 deform PI(4,5)P2-rich membranes by an inverse BAR domain-like mechanism, *J Cell Biol*, 176, 953-64.
- Miki, H. and Takenawa, T. (1998), Direct binding of the verprolin-homology domain in N-WASP to actin is essential for cytoskeletal reorganization, *Biochem Biophys Res Commun*, 243, 73-8.
- Miki, H. and Takenawa, T. (2002), WAVE2 serves a functional partner of IRSp53 by regulating its interaction with Rac, *Biochem Biophys Res Commun*, 293, 93-9.
- Miki, H., Yamaguchi, H., Suetsugu, S. and Takenawa, T. (2000), IRSp53 is an essential intermediate between Rac and WAVE in the regulation of membrane ruffling, *Nature*, 408, 732-5.
- Millard, T. H., Bompard, G., Heung, M. Y., Dafforn, T. R., Scott, D. J., Machesky, L. M. and Futterer, K. (2005), Structural basis of filopodia formation induced by the IRSp53/MIM homology domain of human IRSp53, *Embo J*, 24, 240-50.
- Mizutani, K., Miki, H., He, H., Maruta, H. and Takenawa, T. (2002), Essential role of neural Wiskott-Aldrich syndrome protein in podosome formation and degradation of extracellular matrix in src-transformed fibroblasts, *Cancer Res*, 62, 669-74.
- Mogilner, A. and Oster, G. (1996), Cell motility driven by actin polymerization, *Biophys J*, 71, 3030-45.
- Mogilner, A. and Oster, G. (2003), Force generation by actin polymerization II: the elastic ratchet and tethered filaments, *Biophys J*, 84, 1591-605.
- Mullineaux, C. W. (2004), FRAP analysis of photosynthetic membranes, *J Exp Bot*, 55, 1207-11.
- Mullineaux, C. W., Tobin, M. J. and Jones, G. R. (1997), Mobility of photosynthetic complexes in thylakoid membranes, *nature*, 390.
- Nakada, C., Ritchie, K., Oba, Y., Nakamura, M., Hotta, Y., Iino, R., Kasai, R. S., Yamaguchi, K., Fujiwara, T. and Kusumi, A. (2003), Accumulation of anchored proteins forms membrane diffusion barriers during neuronal polarization, *Nat Cell Biol*, 5, 626-32.
- Nakamura, K., Yoshikawa, N., Yamaguchi, Y., Kagota, S., Shinozuka, K. and Kunitomo, M. (2002), Characterization of mouse melanoma cell lines by their mortal malignancy using an experimental metastatic model, *Life Sci*, 70, 791-8.
- Nolen, B. J. and Pollard, T. D. (2008), Structure and biochemical properties of fission yeast Arp2/3 complex lacking the Arp2 subunit, *J Biol Chem*, 283, 26490-8.
- Nourry, C., Grant, S. G. and Borg, J. P. (2003), PDZ domain proteins: plug and play!, *Sci STKE*, 2003, RE7.

- Okamura-Oho, Y., Miyashita, T. and Yamada, M. (2001), Distinctive tissue distribution and phosphorylation of IRSp53 isoforms, *Biochem Biophys Res Commun*, 289, 957-60.
- Oowski, H.-E. (1914), Ober aktive Zellbewegungen im Explantat von Wirbeltierembryonen, *Anatomisches Institut zu Halle*.
- Pacholsky, D., Vakeel, P., Himmel, M., Lowe, T., Stradal, T., Rottner, K., Furst, D. O. and van der Ven, P. F. (2004), Xin repeats define a novel actin-binding motif, *J Cell Sci*, 117, 5257-68.
- Pantaloni, D., Boujemaa, R., Didry, D., Gounon, P. and Carlier, M. F. (2000), The Arp2/3 complex branches filament barbed ends: functional antagonism with capping proteins, *Nat Cell Biol*, 2, 385-91.
- Pantaloni, D., Le Clainche, C. and Carlier, M. F. (2001), Mechanism of actin-based motility, *Science*, 292, 1502-6.
- Patel, H., Konig, I., Tsujioka, M., Frame, M. C., Anderson, K. I. and Brunton, V. G. (2008), The multi-FERM-domain-containing protein FrmA is required for turnover of paxillin-adhesion sites during cell migration of Dictyostelium, *J Cell Sci*, 121, 1159-64.
- Patterson, G. H. and Lippincott-Schwartz, J. (2002), A photoactivatable GFP for selective photolabeling of proteins and cells, *Science*, 297, 1873-7.
- Paunola, E., Mattila, P. K. and Lappalainen, P. (2002), WH2 domain: a small, versatile adapter for actin monomers, *FEBS Lett*, 513, 92-7.
- Peskin, C. S., Odell, G. M. and Oster, G. F. (1993), Cellular motions and thermal fluctuations: the Brownian ratchet, *Biophys J*, 65, 316-24.
- Pollard, T. D. (2007), Regulation of actin filament assembly by Arp2/3 complex and formins, *Annu Rev Biophys Biomol Struct*, 36, 451-77.
- Pollard, T. D. and Borisy, G. G. (2003), Cellular motility driven by assembly and disassembly of actin filaments, *Cell*, 112, 453-65.
- Pollard, T. D. and Mooseker, M. S. (1981), Direct measurement of actin polymerization rate constants by electron microscopy of actin filaments nucleated by isolated microvillus cores, *J Cell Biol*, 88, 654-9.
- Pollitt, A. Y. and Insall, R. H. (2009), WASP and SCAR/WAVE proteins: the drivers of actin assembly, *J Cell Sci*, 122, 2575-8.
- Prass, M., Jacobson, K., Mogilner, A. and Radmacher, M. (2006), Direct measurement of the lamellipodial protrusive force in a migrating cell, *J Cell Biol*, 174, 767-72.
- Pyenta, P. S., Holowka, D. and Baird, B. (2001), Cross-correlation analysis of inner-leaflet-anchored green fluorescent protein co-redistributed with IgE receptors and outer leaflet lipid raft components, *Biophys J*, 80, 2120-32.
- Rajendran, L. and Simons, K. (2005), Lipid rafts and membrane dynamics, *J Cell Sci*, 118, 1099-102.
- Ravdin, J. I., Guerrant, R. L. and Sperelakis, N. (1985), Entamoeba histolytica: impedance measurements and cytotoxicity in the presence of bepridil, verapamil, and cytochalasin D, *Exp Parasitol*, 60, 63-72.
- Rios, J. C., Rubin, M., St Martin, M., Downey, R. T., Einheber, S., Rosenbluth, J., Levinson, S. R., Bhat, M. and Salzer, J. L. (2003), Paranodal interactions regulate expression of sodium channel subtypes and provide a diffusion barrier for the node of Ranvier, *J Neurosci*, 23, 7001-11.
- Rohatgi, R., Ho, H. Y. and Kirschner, M. W. (2000), Mechanism of N-WASP activation by CDC42 and phosphatidylinositol 4, 5-bisphosphate, *J Cell Biol*, 150, 1299-310.
- Rohatgi, R., Ma, L., Miki, H., Lopez, M., Kirchhausen, T., Takenawa, T. and Kirschner, M. W. (1999), The interaction between N-WASP and the Arp2/3

- complex links Cdc42-dependent signals to actin assembly, *Cell*, 97, 221-31.
- Rottner, K., Behrendt, B., Small, J. V. and Wehland, J. (1999), VASP dynamics during lamellipodia protrusion, *Nat Cell Biol*, 1, 321-2.
- Sako, Y. and Kusumi, A. (1994), Compartmentalized structure of the plasma membrane for receptor movements as revealed by a nanometer-level motion analysis, *J Cell Biol*, 125, 1251-64.
- Sako, Y. and Kusumi, A. (1995), Barriers for lateral diffusion of transferrin receptor in the plasma membrane as characterized by receptor dragging by laser tweezers: fence versus tether, *J Cell Biol*, 129, 1559-74.
- Salih, H., Al-Amri, M. and Gomati, M. E. (2005), The miracle of light, *A world of science*, 3.
- Schafer, D. A., Jennings, P. B. and Cooper, J. A. (1996), Dynamics of capping protein and actin assembly in vitro: uncapping barbed ends by polyphosphoinositides, *J Cell Biol*, 135, 169-79.
- Schaus, T. E., Taylor, E. W. and Borisy, G. G. (2007), Self-organization of actin filament orientation in the dendritic-nucleation/array-treadmilling model, *Proc Natl Acad Sci U S A*, 104, 7086-91.
- Schliwa, M., Nakamura, T., Porter, K. R. and Euteneuer, U. (1984), A tumor promoter induces rapid and coordinated reorganization of actin and vinculin in cultured cells, *J Cell Biol*, 99, 1045-59.
- Scita, G., Confalonieri, S., Lappalainen, P. and Suetsugu, S. (2008), IRSp53: crossing the road of membrane and actin dynamics in the formation of membrane protrusions, *Trends Cell Biol*, 18, 52-60.
- Sharon, N. and Lis, H. (1972), Lectins: cell-agglutinating and sugar-specific proteins, *Science*, 177, 949-59.
- Shimomura, O., Johnson, F. H. and Saiga, Y. (1962), Extraction, purification and properties of aequorin, a bioluminescent protein from the luminous hydromedusan, *Aequorea*, *J Cell Comp Physiol*, 59, 223-39.
- Simons, K. and Ikonen, E. (1997), Functional rafts in cell membranes, *Nature*, 387, 569-72.
- Singer, S. J. and Nicolson, G. L. (1972), The fluid mosaic model of the structure of cell membranes, *Science*, 175, 720-31.
- Sizonenko, G. I., Karpova, T. S., Gattermeir, D. J. and Cooper, J. A. (1996), Mutational analysis of capping protein function in *Saccharomyces cerevisiae*, *Mol Biol Cell*, 7, 1-15.
- Small, J. V., Anderson, K. and Rottner, K. (1996), Actin and the coordination of protrusion, attachment and retraction in cell crawling, *Biosci Rep*, 16, 351-68.
- Small, J. V., Herzog, M. and Anderson, K. (1995), Actin filament organization in the fish keratocyte lamellipodium, *J Cell Biol*, 129, 1275-86.
- Small, J. V., Isenberg, G. and Celis, J. E. (1978), Polarity of actin at the leading edge of cultured cells, *Nature*, 272, 638-9.
- Spooner, B. S., Yamada, K. M. and Wessells, N. K. (1971), Microfilaments and cell locomotion, *J Cell Biol*, 49, 595-613.
- Stradal, T. E., Rottner, K., Dianza, A., Confalonieri, S., Innocenti, M. and Scita, G. (2004), Regulation of actin dynamics by WASP and WAVE family proteins, *Trends Cell Biol*, 14, 303-11.
- Suetsugu, S., Kurisu, S., Oikawa, T., Yamazaki, D., Oda, A. and Takenawa, T. (2006), Optimization of WAVE2 complex-induced actin polymerization by membrane-bound IRSp53, PIP(3), and Rac, *J Cell Biol*, 173, 571-85.

- Suzuki, T., Miki, H., Takenawa, T. and Sasakawa, C. (1998), Neural Wiskott-Aldrich syndrome protein is implicated in the actin-based motility of *Shigella flexneri*, *Embo J*, 17, 2767-76.
- Szent-Gyorgyi, A. G. (2004), The early history of the biochemistry of muscle contraction, *J Gen Physiol*, 123, 631-41.
- Takenawa, T. and Suetsugu, S. (2007), The WASP-WAVE protein network: connecting the membrane to the cytoskeleton, *Nat Rev Mol Cell Biol*, 8, 37-48.
- Takizawa, P. A., DeRisi, J. L., Wilhelm, J. E. and Vale, R. D. (2000), Plasma membrane compartmentalization in yeast by messenger RNA transport and a septin diffusion barrier, *Science*, 290, 341-4.
- Taunton, J., Rowning, B. A., Coughlin, M. L., Wu, M., Moon, R. T., Mitchison, T. J. and Larabell, C. A. (2000), Actin-dependent propulsion of endosomes and lysosomes by recruitment of N-WASP, *J Cell Biol*, 148, 519-30.
- Tilney, L. G. (1975), The role of actin in nonmuscle cell motility, *Soc Gen Physiol Ser*, 30, 339-88.
- Tramier, M., Zahid, M., Mevel, J. C., Masse, M. J. and Coppey-Moisan, M. (2006), Sensitivity of CFP/YFP and GFP/mCherry pairs to donor photobleaching on FRET determination by fluorescence lifetime imaging microscopy in living cells, *Microsc Res Tech*, 69, 933-9.
- Upadhyaya, A., Chabot, J. R., Andreeva, A., Samadani, A. and van Oudenaarden, A. (2003), Probing polymerization forces by using actin-propelled lipid vesicles, *Proc Natl Acad Sci U S A*, 100, 4521-6.
- Valdembri, D., Caswell, P. T., Anderson, K. I., Schwarz, J. P., Konig, I., Astanina, E., Caccavari, F., Norman, J. C., Humphries, M. J., Bussolino, F. and Serini, G. (2009), Neuropilin-1/GIPC1 signaling regulates  $\alpha 5 \beta 1$  integrin traffic and function in endothelial cells, *PLoS Biol*, 7, e25.
- Vallotton, P., Danuser, G., Bohnet, S., Meister, J. J. and Verkhovskiy, A. B. (2005), Tracking retrograde flow in keratocytes: news from the front, *Mol Biol Cell*, 16, 1223-31.
- Varnai, P., Bodeva, T., Tamas, P., Toth, B., Buday, L., Hunyady, L. and Balla, T. (2005), Selective cellular effects of overexpressed pleckstrin-homology domains that recognize PtdIns(3,4,5)P<sub>3</sub> suggest their interaction with protein binding partners, *J Cell Sci*, 118, 4879-88.
- Vasanji, A., Ghosh, P. K., Graham, L. M., Eppell, S. J. and Fox, P. L. (2004), Polarization of plasma membrane microviscosity during endothelial cell migration, *Dev Cell*, 6, 29-41.
- Wear, M. A. and Cooper, J. A. (2004), Capping protein: new insights into mechanism and regulation, *Trends Biochem Sci*, 29, 418-28.
- Weisswange, I., Bretschneider, T. and Anderson, K. I. (2005), The leading edge is a lipid diffusion barrier, *J Cell Sci*, 118, 4375-80.
- Welch, M. D., Rosenblatt, J., Skoble, J., Portnoy, D. A. and Mitchison, T. J. (1998), Interaction of human Arp2/3 complex and the *Listeria monocytogenes* ActA protein in actin filament nucleation, *Science*, 281, 105-8.
- Winckler, B., Forscher, P. and Mellman, I. (1999), A diffusion barrier maintains distribution of membrane proteins in polarized neurons, *Nature*, 397, 698-701.
- Winckler, B. and Mellman, I. (1999), Neuronal polarity: controlling the sorting and diffusion of membrane components, *Neuron*, 23, 637-40.
- Winckler, B. and Poo, M. M. (1996), No diffusion barrier at axon hillock, *Nature*, 379, 213.

- Wouters, F. S., Verveer, P. J. and Bastiaens, P. I. (2001), Imaging biochemistry inside cells, *Trends Cell Biol*, 11, 203-11.
- Yamagishi, A., Masuda, M., Ohki, T., Onishi, H. and Mochizuki, N. (2004), A novel actin bundling/filopodium-forming domain conserved in insulin receptor tyrosine kinase substrate p53 and missing in metastasis protein, *J Biol Chem*, 279, 14929-36.
- Yamaguchi, H., Miki, H., Suetsugu, S., Ma, L., Kirschner, M. W. and Takenawa, T. (2000), Two tandem verprolin homology domains are necessary for a strong activation of Arp2/3 complex-induced actin polymerization and induction of microspike formation by N-WASP, *Proc Natl Acad Sci U S A*, 97, 12631-6.
- Yamashita, A., Maeda, K. and Maeda, Y. (2003), Crystal structure of CapZ: structural basis for actin filament barbed end capping, *Embo J*, 22, 1529-38.
- Yamazaki, D., Oikawa, T. and Takenawa, T. (2007), Rac-WAVE-mediated actin reorganization is required for organization and maintenance of cell-cell adhesion, *J Cell Sci*, 120, 86-100.
- Yang, C., Czech, L., Gerboth, S., Kojima, S., Scita, G. and Svitkina, T. (2007), Novel roles of formin mDia2 in lamellipodia and filopodia formation in motile cells, *PLoS Biol*, 5, e317.
- Yarar, D., To, W., Abo, A. and Welch, M. D. (1999), The Wiskott-Aldrich syndrome protein directs actin-based motility by stimulating actin nucleation with the Arp2/3 complex, *Curr Biol*, 9, 555-8.
- Yarmola, E. G., Somasundaram, T., Boring, T. A., Spector, I. and Bubb, M. R. (2000), Actin-latrunculin A structure and function. Differential modulation of actin-binding protein function by latrunculin A, *J Biol Chem*, 275, 28120-7.
- Yeh, T. C., Ogawa, W., Danielsen, A. G. and Roth, R. A. (1996), Characterization and cloning of a 58/53-kDa substrate of the insulin receptor tyrosine kinase, *J Biol Chem*, 271, 2921-8.
- Yu, M., Sato, H., Seiki, M. and Thompson, E. W. (1995), Complex regulation of membrane-type matrix metalloproteinase expression and matrix metalloproteinase-2 activation by concanavalin A in MDA-MB-231 human breast cancer cells, *Cancer Res*, 55, 3272-7.
- Zacharias, D. A., Violin, J. D., Newton, A. C. and Tsien, R. Y. (2002), Partitioning of lipid-modified monomeric GFPs into membrane microdomains of live cells, *Science*, 296, 913-6.
- Zimmermann, P., Meerschaert, K., Reekmans, G., Leenaerts, I., Small, J. V., Vandekerckhove, J., David, G. and Gettemans, J. (2002), PIP(2)-PDZ domain binding controls the association of syntenin with the plasma membrane, *Mol Cell*, 9, 1215-25.
- Zuchero, J. B., Coutts, A. S., Quinlan, M. E., Thangue, N. B. and Mullins, R. D. (2009), p53-cofactor JMY is a multifunctional actin nucleation factor, *Nat Cell Biol*, 11, 451-9.

# Appendices